Grant No. AFOSR-87-0129

MODELLING OF THE IMPACT RESPONSE OF FIBRE-REINFORCED COMPOSITES

Y. L. Li, J. Harding and C. Ruiz
Department of Engineering Science
University of Oxford
Parks Road
Oxford OX1 3PJ
United Kingdom

30 September 1990

Final Report, 15th. November 1986 - 14th. November 1989

Approved for Public Release; distribution unlimited

Prepared for:

AFOSR/NA
Building 410
Bolling AFB
D. C. 20332

and

European Office of Aerospace
Research and Development
London
ENGLAND

SECURITY CLASSIFICATION OF THIS PAGE (4)

REPORT DOCUMENTATION PAGE

1a. REPORT SECURITY CLASSIFICATION	1b. RESTRICTIVE MARKINGS
2a. SECURITY CLASSIFICATION AUTHORITY	3. DISTRIBUTION/AVAILABILITY OF REPORT Approval for public release: distribution unlimited.
2b. DECLASSIFICATION/DOWNGRADING SCHEDULE	
4. PERFORMING ORGANIZATION REPORT NUMBER(S)	5. MONITORING ORGANIZATION REPORT NUMBER(S)
6a. NAME OF PERFORMING ORGANIZATION Department of Engineering Science, University of Oxford 6b. OFFICE SYMBOL (If applicable) MIC	7a. NAME OF MONITORING ORGANIZATION European Office of Aerospace Research and Development/LTS
6c. ADDRESS (City, State and ZIP Code) Parks Road Oxford OX1-3PJ U.K.	7b. ADDRESS (City, State and ZIP Code) AFOSR/NA [redacted]
8a. NAME OF FUNDING/SPONSORING ORGANIZATION AFOSR/NA 8b. OFFICE SYMBOL (If applicable) NA	9. PROCUREMENT INSTRUMENT IDENTIFICATION NUMBER AFOSR 87-0129
8c. ADDRESS (City, State and ZIP Code) Bolling AFB AFOSR/NA Washington DC 203 Bolling AFB DC 20332-6448	10. SOURCE OF FUNDING NOS. PROGRAM ELEMENT NO. 61102F; PROJECT NO. 2302; TASK NO. B1; WORK UNIT NO.
11. TITLE (Include Security Classification) Modelling of the Impact Response of Fibre-Reinforced Composites (U)	
12. PERSONAL AUTHOR(S) Y.L. Li, J. Harding and C. Ruiz	
13a. TYPE OF REPORT Final 13b. TIME COVERED FROM 15 Nov 88 TO 14 Nov 89	14. DATE OF REPORT (Yr., Mo., Day) 1990 September 30 15. PAGE COUNT 16 + Appendices
16. SUPPLEMENTARY NOTATION	

17 COSATI CODES			18. SUBJECT TERMS (Continue on reverse if necessary and identify by block number)
FIELD	GROUP	SUB. GR	
			Fibre-reinforced composites; Finite elements; Tensile impact testing; Laminate theory; Hopkinson-bar

19. ABSTRACT (Continue on reverse if necessary and identify by block number)

This Final Report on a three-year programme with the above title summarises the work that has been done over this period in three different areas - i) the development of experimental techniques for determining the impact mechanical properties of fibre reinforced epoxy laminates, ii) the experimental results obtained for the tensile, compressive and interlaminar shear properties of woven reinforced carbon/epoxy, glass/epoxy, Kevlar/epoxy, and hybrid carbon-glass/epoxy laminates and iii) the attempts that have been made to model the experimentally observed behaviour using a) a simple laminate theory approach and b) the method of finite elements. The present position regarding the modelling of the response of composite materials to impact loading is then critically assessed and suggestions are made for future work required in this area.

Publications arising form this work are listed and further details of particular aspects of the work are described in a series of appendices which are attached to the main report.

20. DISTRIBUTION/AVAILABILITY OF ABSTRACT UNCLASSIFIED/UNLIMITED ☒ SAME AS RPT. ☐ DTIC USERS ☐	21. ABSTRACT SECURITY CLASSIFICATION unclassified
22a. NAME OF RESPONSIBLE INDIVIDUAL SPENCER T. WU	22b. TELEPHONE NUMBER (Include Area Code) (202) 767-6962 22c. OFFICE SYMBOL AFOSR/NA

DD FORM 1473, 83 APR EDITION OF 1 JAN 73 IS OBSOLETE.

SECURITY CLASSIFICATION OF THIS PAGE

(4)

Fig. 3 Tensile impact test on unidirectional glass/epoxy specimen
(a) pull-out of fibre layer in grip region

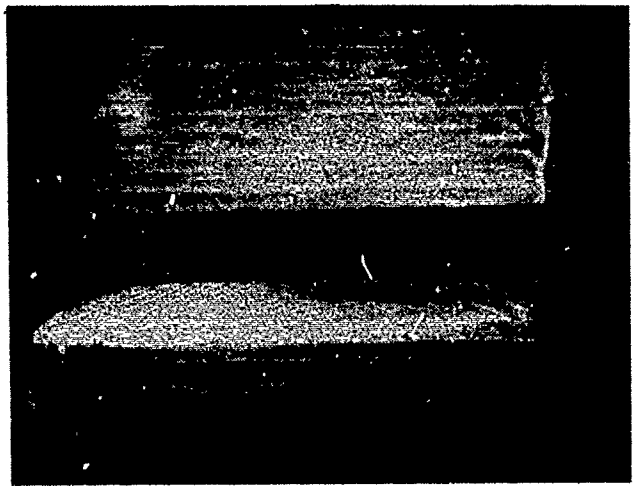

(b) unbroken gauge section showing debonding around matrix cracks

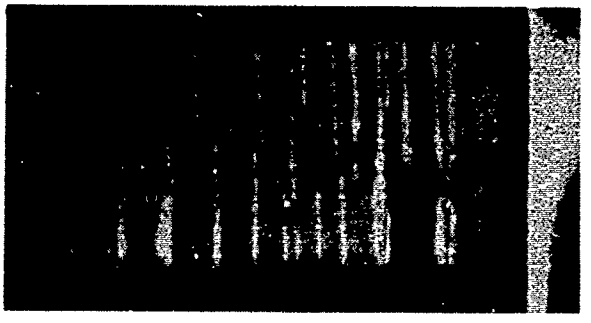

Fig. 4 Effect of strain rate on the tensile properties of a satin-weave glass/polyester composite at mean strain rates of (i) 0.0022/s; (ii) 22/s; (iii) 1260/s
(a) stress-strain curves

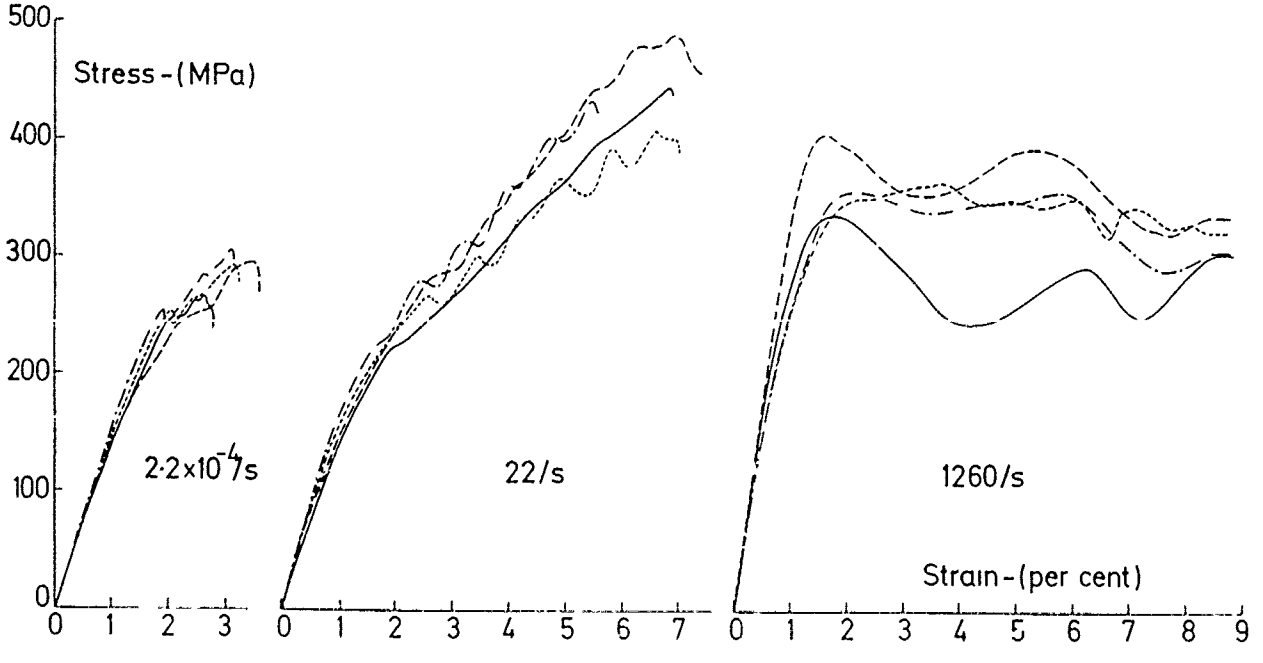

(b) fracture appearance

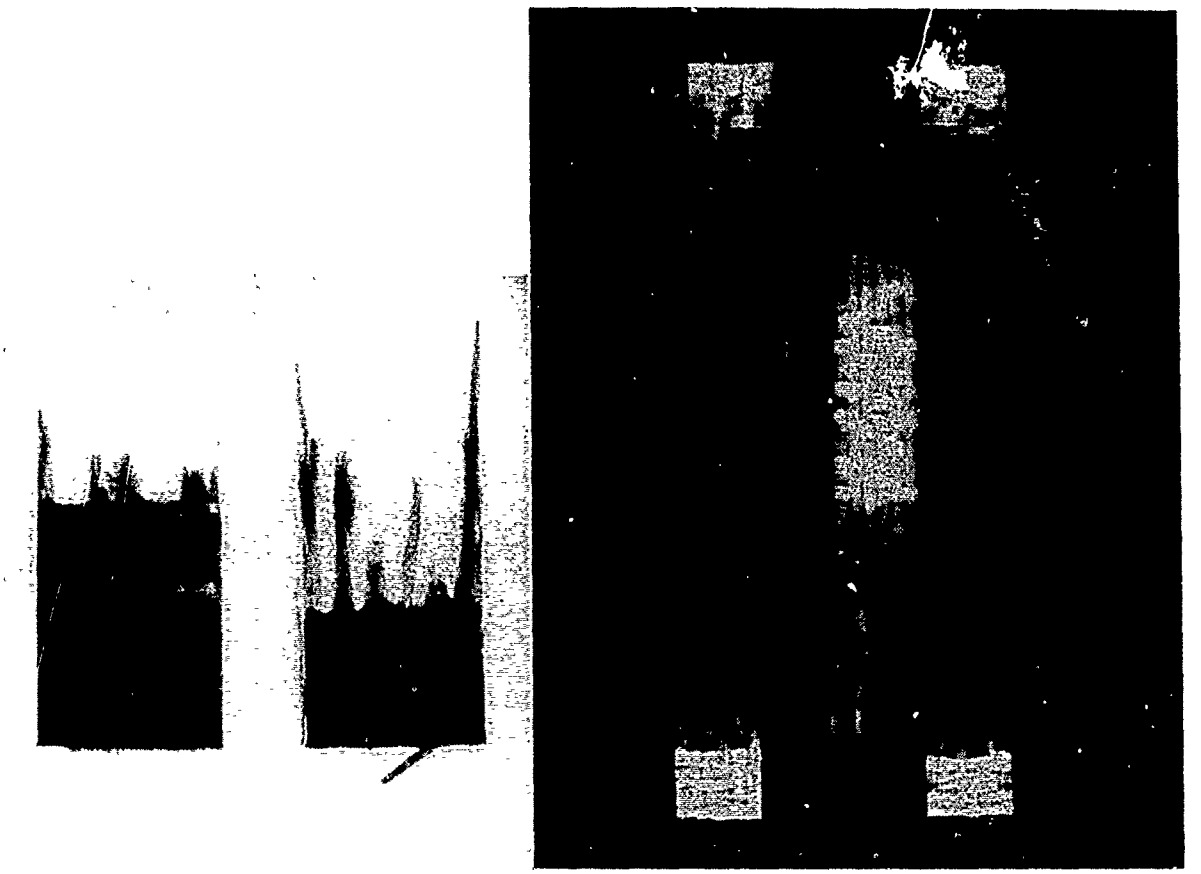

b(i) *b(ii)* *b(iii)*

Fig. 5 Interlaminar shear test
(a) specimen design

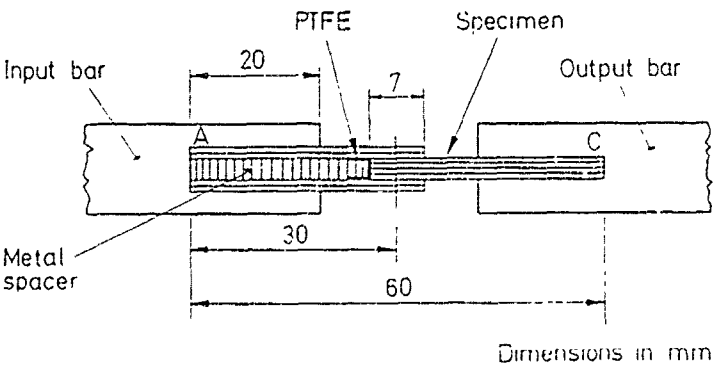

(b) fracture appearance

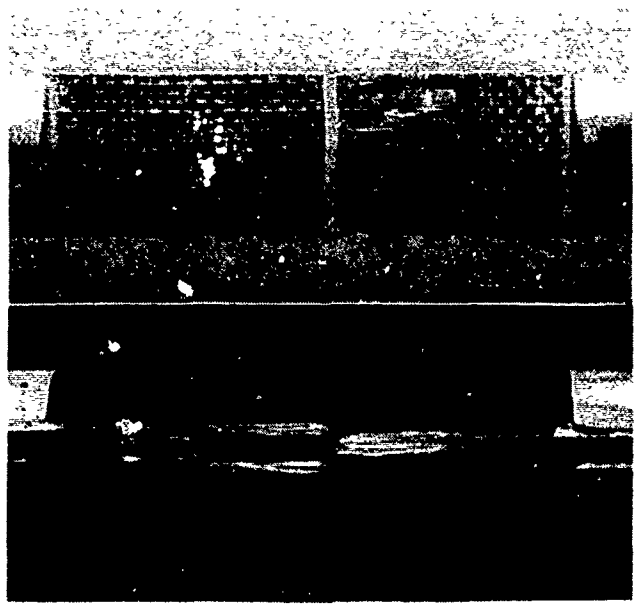

(c) strain distribution on failure plane

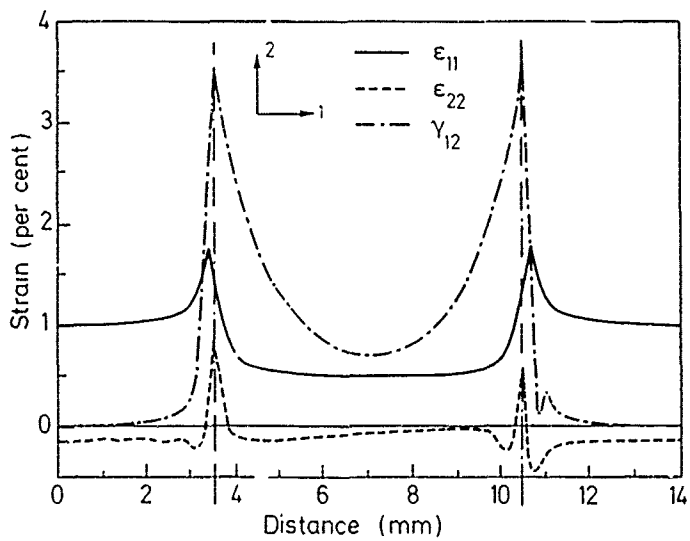

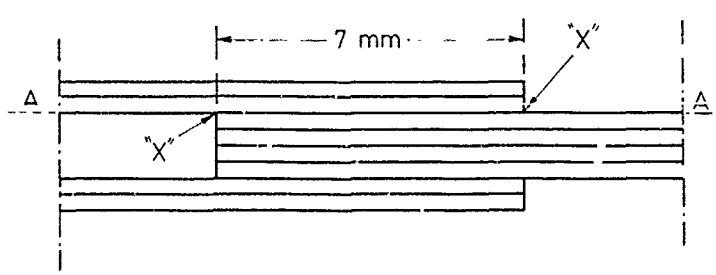

Fig. 6 Effect of strain rate and specimen geometry on compressive behaviour of woven glass/epoxy
(a) ultimate compressive strength

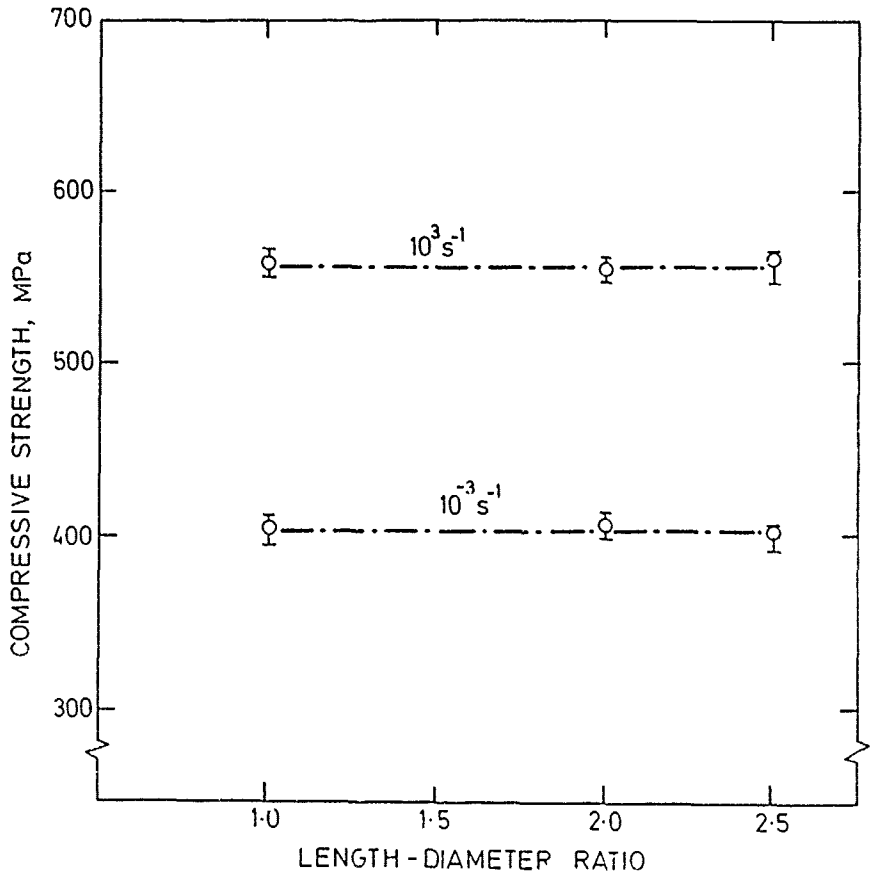

(b) quasi-static failure mode

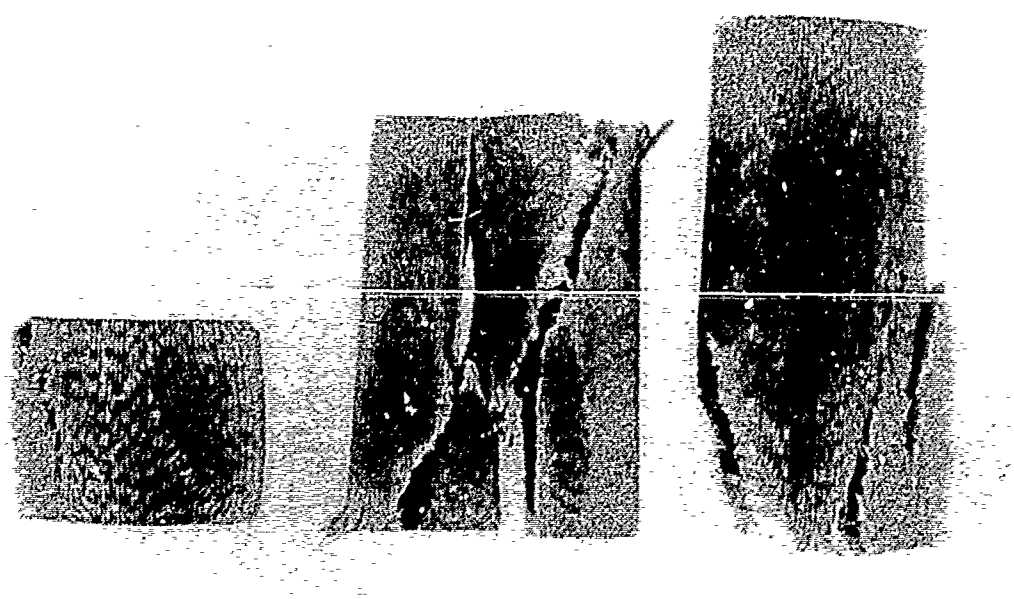

Fig. 7 Initial compressive failure in single-layer reinforced glass/epoxy specimens

(a) stress-strain curves *(b) shear failure across axially-aligned roving*

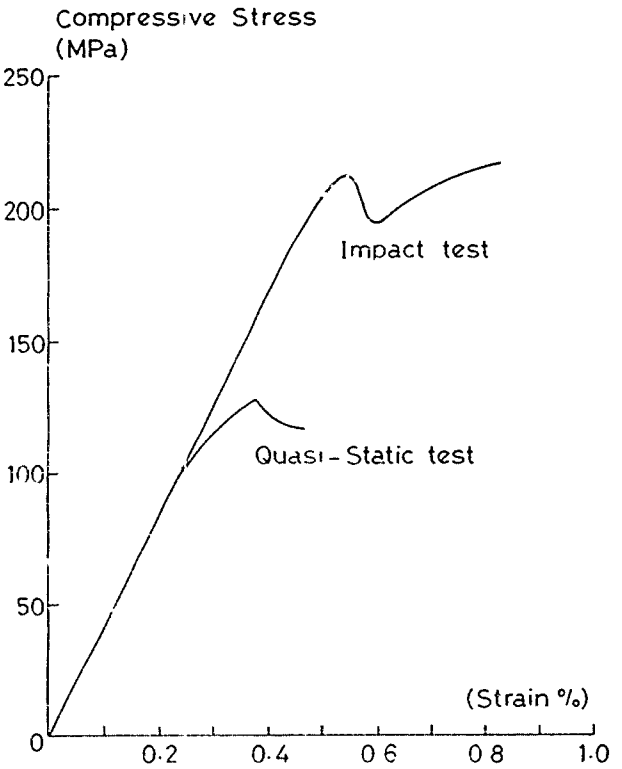

MODELLING OF THE IMPACT RESPONSE OF FIBRE-REINFORCED COMPOSITES

Y. L. Li, J. Harding and C. Ruiz

PREFACE

This final report gives a short summary of the work that has been done over the three years of the present grant, No. AFOSR-87-0129. (Reference is also made to work performed under earlier grants, in which some of the experimental techniques used here were developed). Some general conclusions are drawn and possible directions for further research are discussed. Fuller details of individual parts of the current three year programme have either been given in earlier reports on this programme, issued in May 1988 and July 1989, or are attached to this report in the form of appendices.

CONTENTS

APPENDICES

APPENDIX I - Effect of Strain Rate on the Through-Thickness Elastic Properties of Woven Laminates

APPENDIX II - A New Type of Shear Specimen for Measuring the Interlaminar Shear Strength under Impact Loading

APPENDIX III - The Interlaminar Shear Strength of Woven Carbon, Woven Glass and Woven Carbon/Glass Hybrid Laminates under Static and Impact Loading

APPENDIX IV - Analysis of Failure in Woven Carbon/Epoxy Laminates under Quasi-Static and Impact Loading

APPENDIX V - Stress Wave Propagation in Hybrid Composite Laminates

APPENDIX VI - Mechanical Behaviour of Composite Materials under Impact Loading

1. INTRODUCTION

The three-year programme under Grant No. AFOSR-87-0129, for which this is the Final Report, was preceeded by two separate one-year programmes, under Grant Nos. AFOSR-82-396 and AFOSR-84-092, and a one-year programme which was subsequently extended to a period of 18 months, under Grant No, AFOSR-85-218. Scientifically, however, these four programmes represent a single progressive development of work on the impact mechanical properties of woven-reinforced epoxy matrix laminates and it seems appropriate, therefore, to take this opportunity to overview the whole of this work.

The objective of the initial stages of the work was limited to obtaining dynamic tensile stress-strain curves for woven-reinforced hybrid carbon/glass and carbon/Kevlar laminates so as to allow a study of the effect of hybrid composition on their impact resistance. This required the introduction of an extended version of the standard tensile Hopkinson-bar apparatus and the construction of a gas-gun to accelerate the projectile. Subsequently the tensile impact loading technique was modified to use a cylindrical projectile so as to minimise the problems associated with the insertion of the specimen into the test equipment and to allow free access to the specimen during the course of the test.

Using these techniques tensile stress-strain curves were obtained at an impact strain rate of about 1000/s for three woven carbon/glass epoxy laminates having different hybrid compositions loaded in both the warp and the weft directions. Comparative results were also obtained at a quasi-static rate of about 10^{-3}/s and an intermediate rate of about 10/s. The effect of strain rate on the elastic and tensile strength properties of the two types of reinforcing ply was also obtained from quasi-static and impact tests on non-hybrid laminates reinforced with either woven carbon or woven glass and loaded in the warp and the weft directions and also in a direction at 45° to the warp and weft directions so as to allow a determination of the in-plane shear modulus. The two-dimensional stiffness matrix was found to be rate dependent for both the all-carbon and the all-glass laminates.

It became apparent at an early stage that even in hybrid lay-ups with a carbon weight fraction as low as 40% there was a drastic reduction in the tensile strain to failure over that for the all-glass laminate and hence a corresponding reduction in the ability to absorb impact energy. This was assumed to be related to the tensile loading configuration in which both fibre types nominally support the same strain at all times. Some work was undertaken, therefore, on the transverse impact loading of laminated hybrid plates for which different tensile strains will apply in different reinforcing plies. Plates with different stacking sequences and weight fractions of woven carbon to woven glass reinforcement were tested and load-displacement curves at the central point of impact were successfully obtained. However, while a measure of the effect of lay-up and hybrid composition on the impact energy absorbed could be made the transverse impact configuration is essentially a structural rather than a materials test and a more detailed analysis which attempts to model the observed impact response has so far not proved possible.

Following a detailed literature survey on strength and stiffness theories for composite laminates initial attempts to model the hybrid tensile impact response were based on the laminate theory approach and the Tsai-Wu failure

criterion. At both quasi-static and impact rates the hybrid stiffness could be predicted from the stiffness matrices of the non-hybrid laminates simply by the use of the rule of mixtures. Predictions of the tensile strengths of the hybrid laminates required, in principle, knowledge of the compressive as well as the tensile strengths of the non-hybrid laminates and a test technique was developed to obtain this information.

Using the laminate theory approach predictions of the quasi-static and the impact tensile strengths of the three hybrid lay-ups were obtained and found to show reasonable general agreement with those determined experimentally. The failure strains, however, were very significantly overestimated, particularly for the impact tests, and the bilinear stress-strain curve which was inherent in this approach, while showing the "knee" effect characteristic of woven laminates, was only a rough approximation to that obtained experimentally. It is also interesting to note that while, as predicted by the laminate theory approach, the experimental strength levels lay slightly above those that would have been predicted by the rule of mixtures, they also showed some dependence on the stacking sequence separate from their dependence on the hybrid composition. Since out-of-plane stresses are not considered this could not be predicted by a laminate theory approach.

In the light of this experience with the laminate theory approach it became clear that a more detailed modelling of the hybrid impact strength required a method which allowed a study of the progressive development of failure, i.e. of the damage accumulation process. Following a second literature survey, on the statistical and numerical methods which have been used to predict the quasi-static strengths of composite materials in general and hybrids in particular, a major effort has been made to apply the finite element method to the analysis of failure in woven hybrid laminates. This has required, in addition to information on the effect of strain rate on the tensile strengths of the two types of reinforcing ply, also a knowledge both of the effect of strain rate on the interlaminar shear strengths at the various possible interfaces, i.e. between two glass reinforced plies, two carbon reinforced plies and two plies one reinforced with carbon and the other with glass and a knowledge of the effect of strain rate on the strength and stiffness of the different laminates in the through-thickness direction.

To obtain this information a new interlaminar shear test technique has been developed which can be used at impact as well as quasi-static rates of strain. Although the far from uniform stress distribution on the interlaminar failure plane in this test does not allow the determination of a precise value of interlaminar shear strength at any given loading rate it does reveal a very significant increase in the interlaminar shear strength at impact rates of strain. An improved version of interlaminar shear test for impact testing has been designed and built but no tests have yet been performed using it. While successful attempts have also been made to determine the elastic properties in the through-thickness direction for the all-carbon and the all-glass laminates at both a quasi-static and an impact rate of strain, only a preliminary attempt has been at determining the strength properties normal to the three types of interface in the hybrid laminates.

With the various unforeseen developments in the work on the carbon/glass hybrids the study originally proposed on the carbon/Kevlar laminates has been greatly delayed. However a complete set of impact tests on a woven all-Kevlar laminate and on three different hybrid lay-ups of woven carbon and woven Kev-

lar has been completed, although there has only been time to analyse a limited amount of the test data so obtained.

Following this introductory survey subsequent sections of this report will summarise in rather more detail a) the work that has been done in developing experimental techniques, section 2, b) the range of experimental results that has been obtained, section 3, and c) the progress that has been made in attempting to model analytically and numerically the observed mechanical behaviour, section 4. These will be followed by a discussion section, section 5, in which an attempt is made to assess the present position, a conclusions section, section 6, a section which makes suggestions for future work, section 7, and a list of publications arising from the work of the present three-year programme.

2. SUMMARY OF EXPERIMENTAL TECHNIQUES

The principal experimental technique employed during the course of this investigation has been a modified version of the tensile Hopkinson-bar apparatus suitable for testing laminated composites. This has also involved the development of a new type of gas-gun in which a cylindrical projectile is used to set up a tensile loading wave in a long loading bar which lies along the axis of the gun barrel and extends into the region behind the gun [1]. Using this arrangement the split Hopkinson-bar assembly and the test specimen are accessible at all times, since they are not enclosed within a weighbar tube as in earlier versions of the tensile Hopkinson-bar apparatus. Experimental data from up to six separate strain gauge stations are stored in three dual-channel transient recorders and subsequently analysed on a microcomputer using software developed especially for the purpose [1].

The first attempts to predict the tensile impact strength of the various hybrid lay-ups from that of the all-glass and all-carbon laminates used a simple laminate theory approach. This required in addition a knowledge of the compressive strengths of the all-glass and all-carbon laminates. Most previous work on the compressive impact properties of composite materials has used a test specimen in the form of a short cylinder. This design was not possible in the present investigation as the laminate thickness was too small. Nor is the short cylinder an ideal design of specimen because of uncertainty as to the significance of end effects at the specimen loading-bar interfaces in masking the true material behaviour. In the present investigation, therefore, the same design of waisted strip specimen as was used in the tensile tests was also used in compression. This required the development of a special loading rig for use in the quasi-static tests [2] and the construction of a small air gun and compression Hopkinson-bar system for use in the impact tests [3].

During the course of the investigation it became apparent that even if attempts to model the composite impact behaviour were limited to that observed under *tensile* loading alone, the damage accumulation process following initial tensile fracture of a fibre tow somewhere within the test specimen would be very likely to involve failure mechanisms controlled by the distribution of both the shear stresses and possibly also the transverse tensile stresses close to this point of initial failure, the shear stresses favouring damage accumulation by delamination and the transverse tensile stresses favouring a deplying type process. It was necessary, therefore, to devise experimental techniques for assessing the effect of strain rate on the shear stress levels at which failure by interlaminar shear might be expected, and also, possibly,

---

1. K. Saka and J. Harding, "Behaviour of Fibre-Reinforced Composites under Dynamic Tension", Oxford University Engineering Laboratory Report No. OUEL 1602/85 (Final Report on Grant No. AFOSR-84-0092).

2. S. Shah, R. K. Y. Li and J. Harding, "Modelling of the Impact Response of Fibre-Reinforced Composites", Oxford University Engineering Laboratory Report No. OUEL 1730/88 (First interim report on Grant No. AFOSR-87-0129)

3. J. Harding, K. Saka and M. E. C. Taylor, "Behaviour of Fibre-Reinforced Composites under Dynamic Tension", Oxford University Engineering Laboratory Report No. OUEL 1654/86 (Interim Report on Grant No. AFOSR-85-0218)

the transverse stress levels at which failure by deplying might be expected, although this is unlikely to be an important part of the failure process when the tensile load is applied in one of the principal reinforcement directions except, possibly, for the case where initial tensile fracture of a fibre tow occurs at a site distant from the axis of loading, i.e. close to the specimen surface.

To provide data on the rate dependence of the critical interlaminar shear strength a special double-lap (or "tuning fork") type of shear specimen was devised [4]. This may be tested in the standard tensile Hopkinson-bar apparatus and gives an estimate of the average value of the shear stress on the interlaminar failure plane when fracture occurs. The interlaminar plane on which failure will occur is predetermined. This allows different types of interface to be studied. Thus all three types of interface present in hybrid carbon/glass specimens, i.e. carbon/carbon, glass/glass and carbon/glass, may be studied independently [5]. However, the major drawback of this test, in common with most other types of interlaminar shear test, is the far from uniform stress and strain distribution on the failure plane. The critical load at failure gives, therefore, only a general indication of the level of shear stress required to initiate interlaminar failure at the given strain rate. Finite element studies aimed at producing an improved design of interlaminar shear test were therefore undertaken. These are described and an improved design of test proposed in the report attached at Appendix II. Unfortunately there was insufficient time to build the proposed modified interlaminar shear test and to conduct experiments using it so this remains an area for future development.

Finite element studies were used both as a check on the stress and strain distribution within the various testing configurations and also in an attempt to model the failure process in the test specimens at different rates of loading. In both cases a knowledge of the elastic properties of each type of laminate was required. The bulk of the experimental work was concerned with the behaviour of three types of laminate, woven carbon, woven glass, and three different woven hybrid lay-ups of carbon and glass. By testing tensile specimens cut from both the woven carbon and the woven glass laminates with the tensile axis in either the warp or the weft directions or at 45° to the warp and weft directions and using strain gauge rosettes attached directly to the specimen test section, estimates were made of the two-dimensional in-plane stiffness matrix for each laminate at both a quasi-static [3] and an impact rate of loading [6]. Similar measurements in the through-thickness direction were not possible because the thickness of the available laminates was too small so estimated elastic properties had to be used in the finite element calculations.

---

4. J. Harding, Y. L. Li, K. Saka and M. E. C. Taylor, "Characterisation of the Impact Strength of Woven Carbon/Epoxy Laminates", in Proc. 4th. Oxford Int. Conf. on Mech. Props. Materials at High Rates of Strain, Institute of Physics Conf. Ser. No. 102, (Inst. of Physics, London and Bristol, 1989), pp. 403-410.

5. Y. L. Li, J. Harding and M. E. C. Taylor, "The Interlaminar Shear Strength of Woven Carbon, Woven Glass and Woven Carbon/Glass Hybrid Laminates under Static and Impact Loading", Oxford University Engineering Laboratory Report No. OUEL 1831/90

More recently, however, following the perceived need for an estimate to be made of the through-thickness strength properties and in view of the fact that the "tuning-fork" double-lap shear specimens could not be cut from existing laminates but had to be prepared specially, the opportunity was also taken to prepare thickner laminates from the same woven glass and carbon reinforcing mats and the same epoxy resin system as were used in the original laminates. Cylindrical specimens with the axis perpendicular to the plane of reinforcement were then cut from these thicker laminates, strain-gauged and loaded at either a quasi-static or an impact rate to give an estimate of the elastic properties in the through-thickness direction. Full details of this part of the work are given in the report attached at Appendix I.

Although these tests were generally taken through to failure, fracture was always on a plane adjacent to the specimen/loading-bar interface and was probably in most cases a measure of the strength of the adhesive. To give an estimate of the through-thickness tensile strength tests were performed on several designs of cylindrical specimen with a reduced diameter in the central section. Results obtained were quite promising but here again there was not sufficient time to complete these tests so this also remains a topic for some future development.

---

6. K. Saka, R. K. Y. Li and J. Harding, "Behaviour of Fibre-Reinforced Composites under Dynamic Tension", Oxford University Engineering Laboratory report No. OUEL 1714/87 (Final report on Grant No. AFOSR-85-0218)

3. SUMMARY OF EXPERIMENTAL RESULTS

Initially the experimental studies were concerned with the effect of strain rate on the tensile mechanical behaviour of five woven reinforced laminates, a coarse-weave carbon reinforced laminate, a fine-weave glass reinforced laminate and three different hybrid lay-ups of the woven carbon and woven glass reinforced plies. Tensile stress-strain curves were derived at impact rates of strain between 350 and 1100/s, depending on the hybrid weight fraction [7]. The tensile modulus and tensile strength both increased with an increasing weight fraction of carbon reinforcement while the strain to failure was very significantly reduced compared with that for the all-glass laminate. While it was clear that the very good tensile impact resistance of woven glass/epoxy laminates was not maintained when the glass reinforcement was combined in a hybrid lay-up with more than 40% by weight of carbon reinforcement, the strain to failure when glass reinforcing fibres were present was always greater than for the non-hybrid woven carbon reinforced laminate. It was also apparent that under tensile loading an optimum combination of hybrid strength and strain to failure was obtained at a weight fraction of carbon reinforcement of 70%.

Tensile stress-strain curves were also obtained at a quasi-static and an intermediate rate of strain, 0.001/s and 10/s respectively, for all five laminates [3] and a significant increase in the tensile strength with strain rate was observed in each case. A significant effect of strain rate was also seen on the elastic properties, as indicated by the various elements of the two-dimensional stiffness matrix, for both the carbon and the glass reinforced laminates, the effect being larger, in general, for the glass reinforced laminate [6].

Although the mechanical behaviour of the hybrid laminates under impact *tension* was the primary interest of this investigation, the use of a simple laminate theory approach to predict the hybrid tensile strength [3], under both quasi-static and impact loading rates, required a knowledge of the compressive strength of both the all-glass and the all-carbon laminates at each rate of loading. Compressive stress-strain curves for each laminate showed a very significant increase in both the failure strength and the strain to failure under impact loading [2]. This contrasts with the tensile behaviour where only the glass reinforced laminate showed an increased strain to failure under impact loading.

With the development of finite element techniques for modelling the failure process in hybrid laminates the need became apparent for data on the strain rate dependence of the interlaminar shear strength in such materials.

---

7. K. Saka and J. Harding, "The Deformation and Fracture of Hybrid Reinforced Composites under Tensile Impact", Proc. IUTAM Colloquium on Macro- and Micro- Mechanisms of High Velocity Deformation and Fracture, (Springer-Verlag, Berlin, 1988), pp. 97-111.

8. Y. L. Li, J. Harding and M. E. C. Taylor, "The Effect of Strain Rate on the Interlaminar Shear Strength of Woven Reinforced Laminates", to appear in Proc. ECCM-4, Fourth European Conference on Composite Materials, Stuttgart, September 1990.

A series of tests was performed, therefore, using the double-lap shear specimen, at both a quasi-static and an impact rate of loading, on specimens with different reinforcing ply lay-ups such that interlaminar failure took place at the interface between i) two carbon reinforced plies, ii) two glass reinforced plies and iii) one carbon and one glass reinforced ply. In each case the applied load at which interlaminar failure occurred was significantly higher under impact loading. While a direct experimental measure of the shear strain at the interface could not be made it was possible, by means of a finite element analysis, to relate the applied tensile strain to the average value of shear strain at the interface and hence to make an approximate estimate of the shear strain rate. Values obtained were 10^{-3}/s and 10^{3}/s in the quasi-static and the impact tests, respectively. Full details of this part of the work are given in the report attached at Appendix III. This work is to be published [8].

Originally it had been the intention to perform a parallel series of tensile impact tests to those described above but using a woven Kevlar reinforcement instead of the glass. A non-hybrid woven Kevlar laminate and three hybrid lay-ups of woven Kevlar with woven carbon were prepared. Full details of the Kevlar laminates were given in an earlier report [9]. However, as the work on the carbon/glass laminates expanded in unforeseen directions the tests on the Kevlar and Kevlar/Carbon laminates were delayed. These have now been completed and results for the non-hybrid Kevlar laminate loaded in the warp direction were given in the Second Interim Report [10].

The present report gives mean stress-strain curves and the corresponding strain rate-strain curves for several tests on the same all-Kevlar laminate loaded in the weft direction, fig. 1, and in the direction at 45° to the warp and weft directions, fig. 2. Strain gauges attached directly to the parallel section of specimens loaded in the warp and weft directions were used to measure the transverse as well as the longitudinal strains and so allowed an estimate of Poisson's ratio at impact rates of strain to be made. Strain gauge rosettes, 0°/45°/90°, attached similarly to the parallel section of the specimens loaded in the 45° direction allowed an estimate to be made of the in-plane shear modulus, giving the two-dimensional stiffness matrix quoted below for the Kevlar laminate at impact rates of strain. Unfortunately it has not proved possible in the limited time available to complete the analysis of the impact test data for the three hybrid Kevlar/Carbon laminates loaded in the warp, weft and 45° directions.

$$[Q_{ij}] = \begin{bmatrix} 40.6 & 3.75 & 0 \\ 3.75 & 39.1 & 0 \\ 0 & 0 & 2.8 \end{bmatrix} \text{ GPa}$$

---

9. K. Saka and J. Harding, "Behaviour of Fibre-Reinforced Composites under Dynamic Tension", Oxford University Engineering Laboratory Report No. OUEL 1543/84 (Final report on Grant No. AFOSR-82-0346)

10. Y. Li, C. Ruiz and J. Harding, "Modelling of the Impact Response of Fibre-Reinforced Composites", Oxford University Engineering Laboratory Report No. OUEL 1784/89 (Second interim report on Grant No. AFOSR-87-0129)

Fig. 1 TENSILE IMPACT TEST ON ALL-KEVLAR LAMINATE LOADED IN WEFT (B) DIRECTION

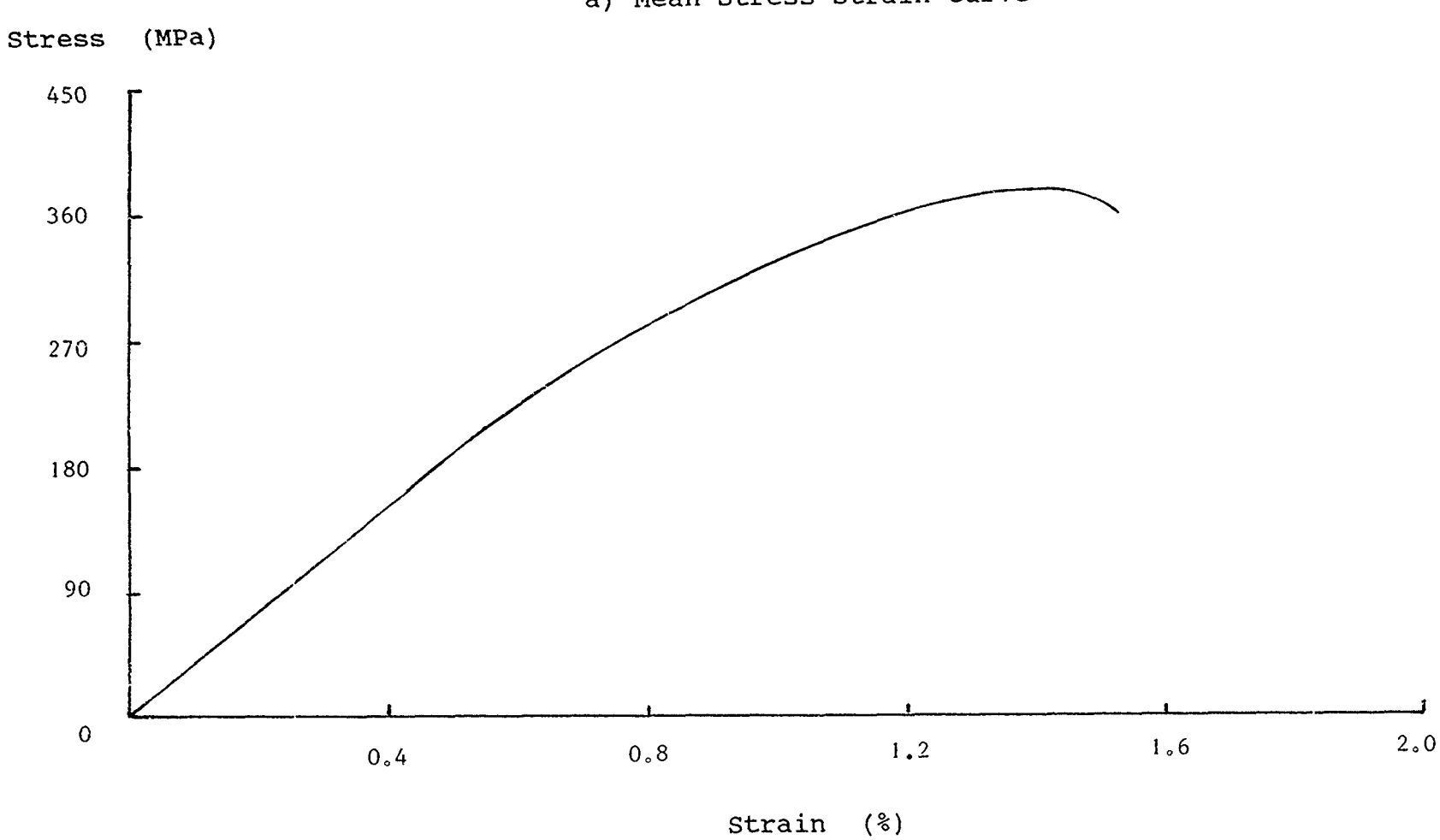

Fig. 1 TENSILE IMPACT TEST ON ALL-KEVLAR LAMINATE LOADED IN WEFT (B) DIRECTION

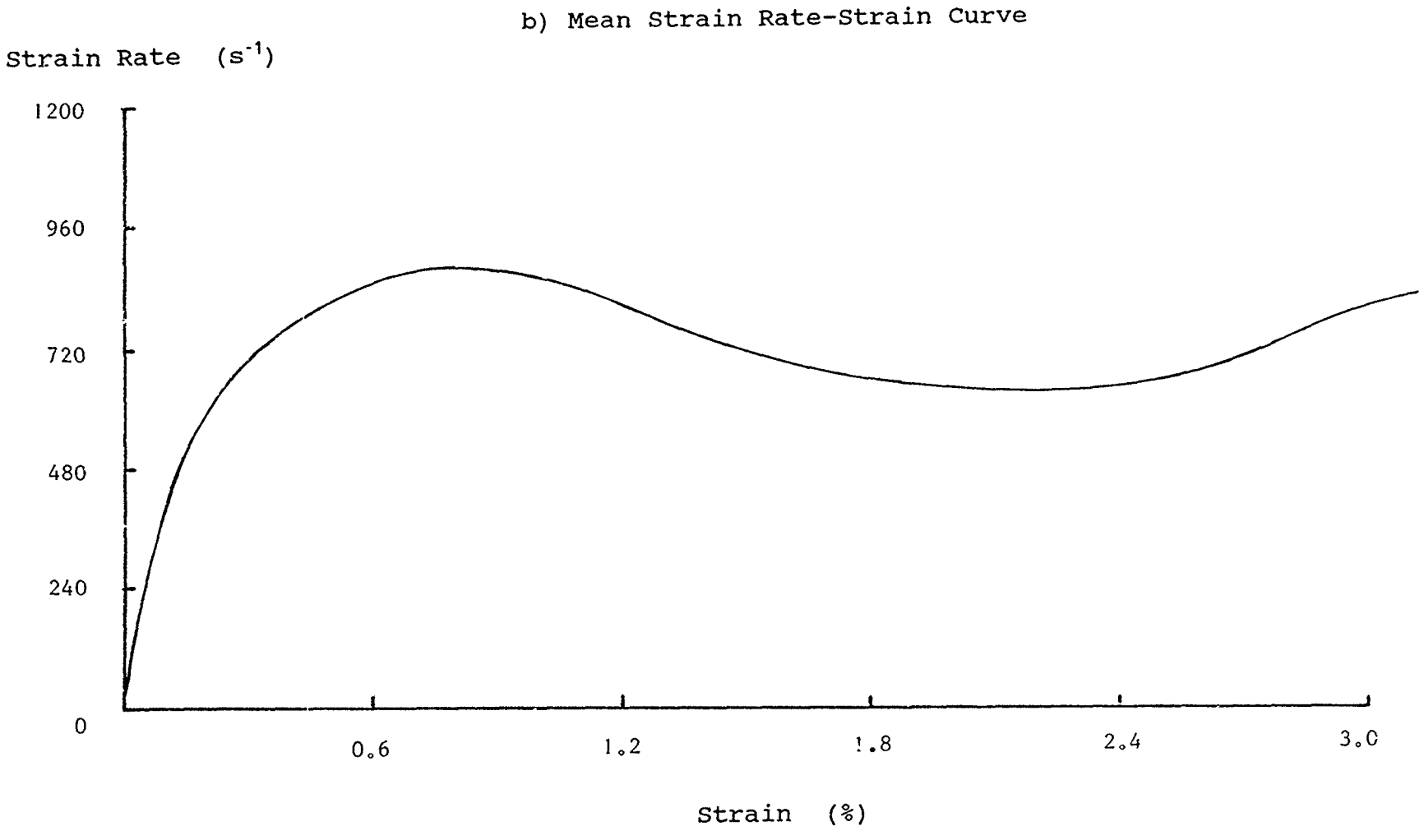

Fig. 2 TENSILE IMPACT TEST ON ALL-KEVLAR LAMINATE LOADED IN 45° (C) DIRECTION

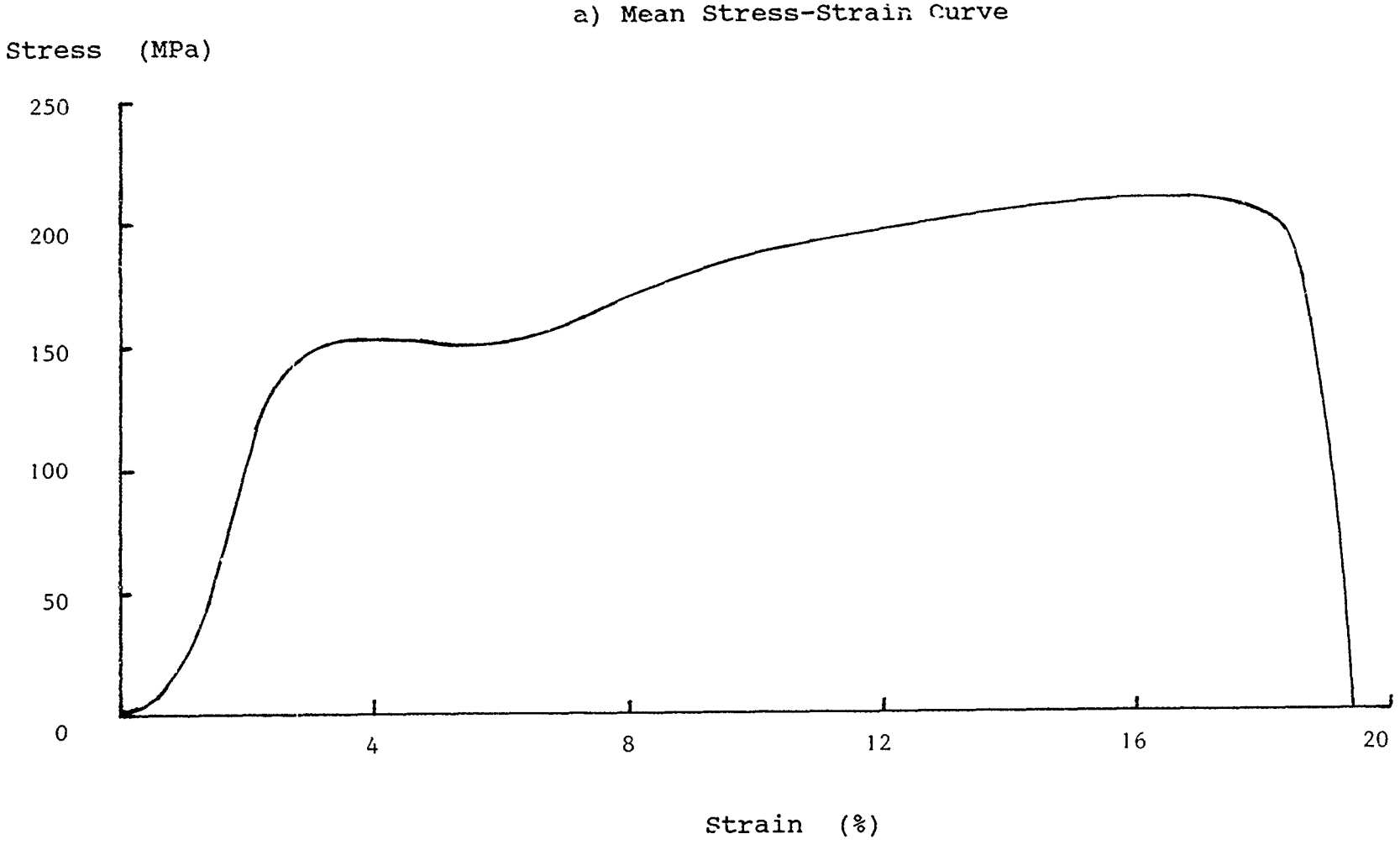

Fig. 2 TENSILE IMPACT TEST ON ALL-KEVLAR LAMINATE LOADED IN 45° (C) DIRECTION

b) Mean Strain Rate-Strain Curve

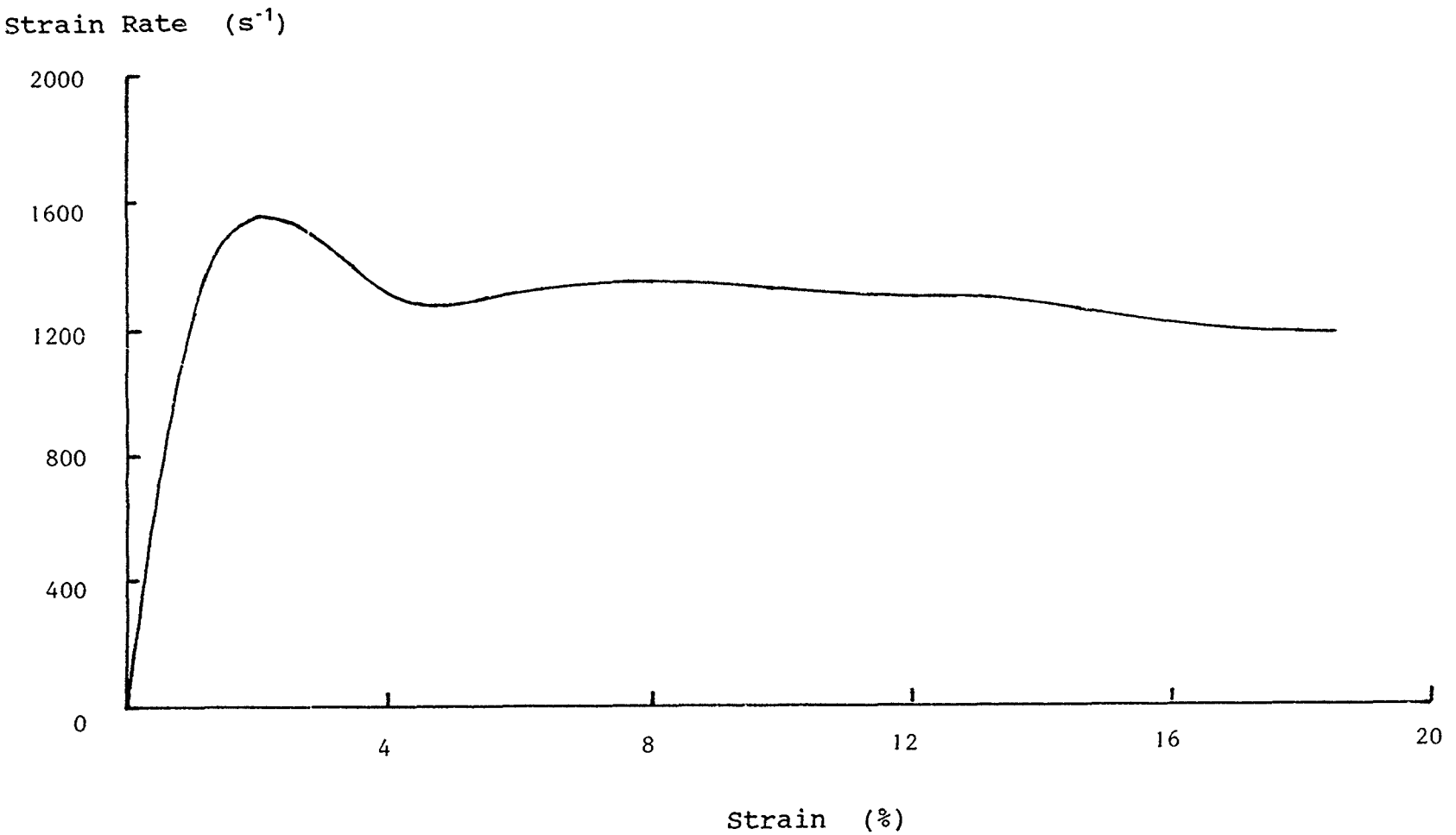

4. SUMMARY OF ANALYTICAL TECHNIQUES

Two techniques have been used in an attempt to model the experimentally observed tensile impact response of the hybrid woven-carbon/woven-glass epoxy laminates. In the first of these [11] a simple laminate theory approach was used to determine the in-plane two-dimensional stress system for each reinforcing ply of a given hybrid lay-up in terms of the experimentally determined elastic properties. The external loading is then increased until the resulting stress system reaches the critical level at which first failure is predicted to initiate in one of the two types of reinforcing ply. The prediction of first failure uses the Tsai-Wu failure criterion and the experimentally determined tensile and compressive failure strengths measured independantly for the two types of reinforcing ply from tests on the non-hybrid all-carbon and all-glass laminates.

In practice initial failure was always predicted in the low elongation carbon reinforced plies. Following initial ply failure a reduced tensile modulus is assumed for the failed carbon reinforced plies and the loading increased until the Tsai-Wu criterion is again satisfied, in this case for the glass reinforced plies, at which point final failure of the composite takes place. Thus a bilinear stress strain response is modelled, showing the "knee" effect often observed with woven reinforced composites. The failure strengths of the three hybrid lay-ups predicted in this way agreed reasonably well with the experimentally determined values at both a quasi-static and an impact rate of loading but the failure strains were significantly overestimated particularly in the impact tests. This is not surprising since there are several gross simplifications involved in the laminate theory approach. Two such simplifications are particularly significant. These are 1) cut-of-plane stresses are totally ignored and 2) when failure is predicted in a given type of reinforcing ply it is assumed to occur simultaneously throughout all plies of this type. The first of these simplifications means that the effects of different stacking sequences within the same overall hybrid composition cannot be taken into account while the second makes it impossible to model the damage accumulation process which clearly operates in composite materials generally and particularly so in woven reinforced composites.

In an attempt to deal with both of these drawbacks to the laminate theory approach a second technique was developed based on the finite element method [12]. Here the parallel region of the specimen is modelled in two dimensions by means of an array of elements with orthotropic elastic properties determined experimentally for each type of reinforcing ply. Initial tensile failure is assumed in an arbitrarily chosen element and modelled by a reduction in the tensile stiffness. The finite element analysis is then used to determine both the distribution of tensile strains in the neighbouring plies and the local shear stress distribution on the adjacent interlaminar planes of the given hybrid lay-up.

---

11. K. Saka and J. Harding, "A simple laminate theory approach to the prediction of the tensile impact strength of woven hybrid composites", Composites, Vol. 21, No. 5, September 1990, 439-447.

12. Y. L. Li, C. Ruiz and J. Harding, "Failure analysis of woven hybrid composites using a finite element method", (to appear in Composites Science and Technology).

Following initial tensile failure of a given element, subsequent steps in the failure/damage accumulation process might be expected to involve both the tensile failure of neighbouring elements, as a result of the increased local tensile strains, and a delamination on the adjacent interlaminar planes, under the high local interlaminar shear stresses induced by the initial tensile failure. Experimentally some delamination/fibre pull-out was found to be part of the failure process in tensile tests on each of the three hybrid lay-ups studied at both quasi-static and impact rates of loading. The finite element method was used, therefore, to determine the extent to which delamination on the interlaminar planes adjacent to the failed element was effective in reducing the local stress and strain concentrations and so allowing a further increase in the external loading before the next stage in the damage accumulation/failure process was initiated.

In its application to hybrid composites the main advantage of the finite element method over simple laminate theory is that it does give some account of the effect of different stacking sequences. Thus, for a given hybrid composition, changes in the hybrid lay-up were found to affect the amount of energy released both when a given carbon ply failed in tension and when there was subsequent delamination. The importance of the stacking sequence on the extent to which hybridisation might improve the composite mechanical performance was also clear from the way in which both the local tensile strain concentration and the local interlaminar shear stresses varied with the order in which tensile failure and delamination occurred.

One important drawback to the finite element method when applied to hybrid composites, however, derives from the discontinuity in the elastic properties at the interface between two different types of reinforcing ply, making accurate prediction of the stress levels in this region very difficult. In addition difficulties have also been experienced in determining experimentally a precise value of the interlaminar failure strength at each type of interface and each rate of loading. For these reasons, therefore, while the finite element method has been shown to highlight the general features found in the experimental work, a more detailed comparison between theory and experiment for hybrid composites has not been possible.

Where a non-hybrid lay-up is concerned, however, providing neighbouring reinforcing plies all have the same orientation, the first of these difficulties disappears. In a very recent report [13], see Appendix IV, the finite element method has been used to study the stress distribution in a woven carbon reinforced laminate following ply failure, either by break-up of the resin matrix and straightening of the fibres or by fibre fracture, both with and without subsequent delamination. The results of the finite element analysis were consistent with the experimentally observed behaviour of the given laminate at both a quasi-static and an impact rate of strain. In particular the reduced extent of anelastic deformation under impact loading was related to the much higher interlaminar shear strength at these rates of strain.

---

13. J. Harding and Y. L. Li, "Analysis of Failure in Woven Carbon/Epoxy Laminates under Quasi-Static and Impact Loading", Oxford University Engineering Laboratory Report No. OUEL 1846/90.

5. DISCUSSION

It is clear from previous sections of this report that if the impact mechanical response of composite materials is to be adequately modelled a technique has to be developed which allows successive stages in the damage accumulation process to be identified and taken into account. The finite element method has been used with considerable success in the modelling of impact induced deformations in metallic materials and structures, where the process is controlled by plastic flow and can be described by an empirical or semi-empirical form of constitutive relationship. Where composite materials are concerned, however, the deformations induced by impact are generally much smaller and are the result not of a single mechanism of plastic flow but of the combined effect of a wide variety of micro-fracturing processes, including, for example, matrix cracking, fracture of individual fibre tows, fibre pull-out, delaminatien induced by high local shear stresses and deplying resulting from high local normal stresses.

While, in theory, it is possible to treat the fibres and the matrix separately, analyses using this approach are generally only able to predict elastic properties [14], prediction of strength properties by this technique being very much more difficult. It is more usual, therefore, to combine the effects of the fibres and the matrix in each reinforcing ply by assigning to each ply characteristic bulk orthotropic elastic properties. In the present case the principal mechanisms associated with damage accumulation under tensile impact will be tensile fracture of the fibre tows and delamination between adjacent reinforcing plies although, if the loading becomes non-symmetrical during the fracturing process, the development of high normal stresses could lead to a deplying type failure as well.

If the damage accumulation during tensile impact is to be successfully modelled, therefore, several requirements must be met. A stress analysis technique must be available which adequately describes the state of stress in the laminate in terms of the applied loading and the appropriate elastic constants for the rate at which it is strained. Also the critical stress states must be known at which, also at the appropriate rate of straining, the various failure processes might be expected to operate. Finally, once damage has initiated at some point in the laminate an appropriate way of describing the properties of the damaged region must be available so as to allow the redistributed stress system to be determined and the next step in the failure process identified.

In the present investigation a finite element technique has been used to determine the stress distribution within the laminate both before initial failure and after each stage in the failure process. This technique suffers from the disadvantage that across interfaces where there is a discontinuity in the elastic properties as, for example, between glass-reinforced and carbon reinforced plies, there may be a significant loss in the accuracy with which the stress system is determined. This is likely to be particularly true in regions where delamination has or is expected to occur. It will also apply to laminates for which initially there are no such elastic discontinuities

---

14. Y. C. Zhang and J. Harding,"A numerical micromechanics analysis of the mechanical properties of a plain weave composite", Composites and Structures, Vol. 36, No. 5, 1990, 839-844

[13] but in which these develop after damage initiates.

With regard to the critical stress states required to initiate the different failure processes, although testing techniques have been developed in which the load, and hence a corresponding particular stress state, required to cause either tensile or interlaminar failure has been determined, it is not clear what feature of this stress state, i.e. whether, for example, it is the maximum value of the stress or the average value over a given minimum region, which is critical for failure to occur. In the absence of a specific failure criterion for each failure mechanism it may be of greater value to consider the amount of energy released when a given mechanism operates. Qualitative results have been obtained in this way [10,12] which highlight the effects of different stacking sequences and give a general indication as to which ply is likely to fail first.

In the present investigation, where it was tensile impact that was being studied, it has been assumed that initial failure was always either by the tensile fracture of a given fibre tow or by the break-up of the matrix in a given region allowing the woven fibre tows to straighten under the applied load. Both types of failure were modelled by a reduction in the tensile modulus in the loading direction, by an arbitrarily chosen factor of 1/100 or 1/1000, for tensile fracture, or 1/10, for matrix break-up. However, for the carbon reinforced plies in particular, the size of element over which this modulus reduction is applied is very much smaller than either the wavelength or the cross-sectional area of the woven carbon fibre tow. Clearly, therefore, there is no particular physical basis for the assumed reduction in modulus and its validity lies only in whether or not it allows results to be obtained which are not inconsistent with those observed experimentally. Similarly the delamination process is modelled assuming an arbitrary friction coefficient of 0.5 on the delamination crack surfaces because otherwise the finite element method would predict catastrophic delamination through to the ends of the specimen and experimentally this was known not to happen. Also the extent of delamination either side of the initial tensile failure was limited to about that observed in practice.

Nevertheless, despite all these various limitations and qualifications, it has proved possible using the finite element method to obtain a qualitative modelling of the early stages of damage accumulation in woven composites under tensile impact and to identify some of the effects of different hybrid stacking sequences. However, it is clear that much more work needs to be done before this method can be applied more generally to the prediction of impact damage in real composite structures.

6. CONCLUSIONS

Experimental techniques have been developed for obtaining reliable data on the mechanical properties of woven hybrid reinforced composite laminates under both tensile and compressive impact, although in compression some doubt remains regarding the effect of specimen geometry on the resulting failure mode. A technique has also been developed for studying the effect of loading rate on the interlaminar shear strength between woven plies reinforced with carbon or glass and suggestions have been made for improving the technique so as to reduce the variation of shear stress on the interlaminar plane prior to failure. Elastic properties in the through-thickness direction under tensile impact loading have also been determined but a method for determining the tensile strength normal to the reinforcing plies is only in the early stages of development.

Tensile stress strain curves have been obtained for woven carbon, woven glass and hybrid carbon/glass reinforced laminates at three loading rates from quasi-static to impact. The two-dimensional stiffness matrix for both the carbon and the glass reinforced laminates is found to be dependent on strain rate, particularly strongly for the glass reinforced laminate. A significant raising of the failure strength with strain rate was observed for the glass reinforced and the three hybrid laminates, for the latter by slightly more than would be predicted by the rule of mixtures. Similar results, but for a more limited range of conditions, have been obtained for a woven Kevlar and three hybrid woven Kevlar/carbon laminates.

Initial attempts using simple laminate theory and the Tsai-Wu failure criterion to predict the tensile impact strength of the woven carbon/glass hybrids in terms of the experimentally measured elastic and strength properties of the non hybrid carbon and glass laminates gave reasonably close estimates of failure strengths but significantly overestimated the corresponding failure strains. A possible effect of stacking sequence observed in the experimental results for hybrid tensile strength could not be modelled by the laminate theory approach.

A more detailed analysis of failure using the finite element method has been developed. This method, which improves on the laminate theory approach by allowing successive stages in the process of damage accumulation to be modelled, has been found to highlight many of the features observed experimentally and gives a qualitative indication of possible effects of different hybrid stacking sequences and of the likelihood of initial failure in different reinforcing plies.

7. FUTURE WORK

The long term aim must be to develop a technique for modelling the damage accumulation process up to final failure for a composite structure, e.g. the fan blade in an aero engine, when subjected to impact loading. The present report describes a possible approach to tackling this problem. A great deal of work, however, remains to be done on several fronts. Considerable refinement in the finite element technique is required if reliable estimates are to be made of the stress distributions close to damage zones and to interfaces between regions with different properties. Improvements are also required to the testing technique used to determine interlaminar shear strength while a technique for determining the through-thickness tensile strength needs to be fully developed. To check the validity of the methods used to model the damaged regions, for example, a reduction in tensile modulus, a detailed experimental study of the various stages in the failure process would be very valuable. This would require impact tests in which the specimen was unloaded after different degrees of damage before final failure and is not likely to be very easy to achieve.

As a test of its successful development the technique for modelling the damage accumulation process should be able to describe the experimentally observed behaviour in a well monitored simple test such as the tensile impact test. It should then be further tested by applying it to a simple structural problem, for example the transverse impact of a composite beam or plate, where again the external loading and the deformations occurring during the impact may be closely monitored but where the stress system is likely to be more complicated and where stress waves within the composite may need to be taken into account. If this is successfully achieved then the technique should be capable of application to real structural problems.

8. LIST OF PUBLICATIONS

The following papers, describing work performed under Grant No. AFOSR-87-0129, have been accepted for publication either in journals or in conference proceedings.

1. J. Harding and K. Saka, "The effect of strain rate on the tensile failure of woven reinforced carbon/glass hybrid composites", Proc. IMPACT 87 (DGM Informationsgesellschafft mbH, Oberursel, 1988), vol. 1, pp. 515-522.

2. J. Harding, Y. L. Li, K. Saka and M. E. C. Taylor, "Characterisation of the impact strength of woven carbon/epoxy laminates", Proc. 4th. Oxford Int. Conf. on Mech. Props of Materials at High Rates of Strain, Institute of Physics Conf. Ser. No. 102, (Inst. of Physics, London and Bristol, 1989), pp. 403-410.

3. K. Saka and J. Harding, "A simple laminate theory approach to the prediction of the tensile impact strength of woven hybrid composites", Composites, Vol. 21, No. 5, September 1990, 439-447.

4. Y. L. Li, C. Ruiz and J. Harding, "Failure analysis of woven hybrid composites using a finite element method", (to appear in Composites Science and Technology).

5. Y. L. Li, C. Ruiz and J. Harding, "Stress wave propagation in hybrid composite materials", (to appear in J. Plastics and Reinforced Composites).

6. Y. L. Li, J. Harding and M. E. C. Taylor, "The effect of strain rate on the interlaminar shear strength of woven reinforced laminates", (to appear in Proc. ECCM4, Fourth European Conference on Composite Materials, Stuttgart, September 1990).

7. Y. L. Li, C. Ruiz and J. Harding, "Failure analysis of woven hybrid composite using ABAQUS", Proc. 5th. ABAQUS User Group Conference, (ABAQUS User Group UK, 1989), pp. 115-124.

In addition two review papers in the general area of Impact Damage in Composite Materials which include results obtained during the course of the current programme have been prepared. One has been published in Science and Engineering of Composite Materials,

J. Harding, "Impact Damage in Composite Materials", Science and Engineering of Composite Materials", vol. 1, No.2, 1989, pp. 41-68.

and the other was an invited presentation at EXPLOMET 90 in San Diego, August 1990,

J. Harding, "Mechanical behaviour of composite materials under impact loading", to appear in Proc. EXPLOMET 90 (San Diego, August 1990).

9. ACKNOWLEDGMENT

This research was sponsored by the Air Force Office of Scientific Research , Air Force Systems Command, USAF, under Grant No. AFOSR-87-0129.

APPENDIX I

EFFECT OF STRAIN RATE ON THE THROUGH-THICKNESS ELASTIC PROPERTIES OF WOVEN LAMINATES

Y. L. Li, J. Harding and M. E. C. Taylor
Department of Engineering Science
University of Oxford
Parks Road
OXFORD OX1-3PJ, UK

ABSTRACT

Woven-carbon, woven-glass and hybrid woven carbon/woven glass epoxy laminates have been prepared and tested in tension at a quasi-static and an impact rate of strain. The tensile load was applied normal to the interlaminar plane and $0^{\circ}/90^{\circ}$ strain gauge rosettes were used to determine the corresponding strains in the loading and transverse directions. From the data obtained the effect of strain rate on the tensile elastic modulus in the through-thickness direction and on the values of Poisson's ratio for planes normal to the warp and weft reinforcing directions was determined.

INTRODUCTION

Previous investigations[1,2] have shown a significant effect of strain rate on the in-plane elastic properties, i.e. the tensile modulus, shear modulus and Poisson's ratio, for woven-reinforced glass/epoxy and carbon/epoxy laminates. Recently attempts to model the tensile failure of such laminates at different rates of strain using a finite element method[3,4] have required a knowledge of the elastic properties in both the in-plane and the through-thickness directions. In the absence of data for the through-thickness properties estimated values have had to be used. The present report describes an attempt to provide the missing data and hence to confirm or otherwise the validity of the previous finite element studies.

SPECIMEN MATERIALS AND DESIGN

In order to develop the experimental technique initial tests were performed on a laminate prepared from woven carbon pre-preg material. A 5-end satin-weave fabric was used, woven from 3000 filament fibre tows with, respectively, 70 and 72 yarns per 10cm in the warp and weft directions, and having a dry weight of 285g/m^2. The pre-preg was manufactured by Hexcel and Genin using a type ES.36 self-adhesive epoxy resin to give a fibre weight fraction of 52% and an uncured pre-preg weight of 548g/m^2. Twenty-four layers of fabric, each 75mm x 150mm, were laid up in a small externally heated pressure vessel (autoclave), see fig. 1, beween two layers of peel ply and two layers of breather felt on each side and covered by a neoprene rubber seal which separated the two halves of the autoclave. The base of the autoclave was covered with a PTFE coated fabric. An air pressure of 70 to 80 psi was applied above the neoprene seal and the region below was evacuated to 28 inches of mercury. The whole autoclave was placed inside a small oven, the temperature raised over a period of 1 hour to 125°C, held at this temperature for 1 hour and then allowed to cool to room temperature. The finished plate thickness was ~8.3mm.

The experimental technique having been established subsequent tests were performed on laminates prepared from dry plain-weave carbon and glass fabrics using the Ciba-Geigy XD-927 epoxy resin system. Although these laminates were more difficult to prepare they did allow a direct comparison to be made with previous experimental work in tension[5] and compression[6] and gave data which it was hoped would be useful in the finite element modelling of the results obtained in these earlier experimental studies[3]. When specimens are prepared from dry fabric the use of a vacuum and an external pressure are particularly important to minimise the void content in the final laminate. However this may lead to some resin loss during curing giving a higher fibre fraction than originally intended. To limit this effect a smaller autoclave was used for the dry fabric/epoxy resin laminates and a reduced vacuum of 25 inches of mercury was applied. The cure cycle required the temperature to be raised to 100°C over a period of one hour, to be held at this temperature for 16 hours and then to be cooled to room temperature at a rate of 8°C/hour.

For the plain-weave composites the carbon fabric was woven from Toray 3000 filament fibre tows, type T300-3000A. The resulting fabric had a weight of 189g/m^2 and an approximate thickness of 0.28mm. The fibres were supplied with a surface treatment suitable for use with epoxy resin systems. The

fabric had a relatively coarse weave geometry with only 47 ends and picks per 10cm. The plain-weave glass fabric had a designation 11 x 2EC5 and was woven from continuous E-glass fibres to give a weight of $96g/m^2$ and an approximate thickness of 0.10mm. With 252 ends and 173 picks per 10cm the weave was much finer than that for the carbon fabric. The fibre finish, type 205, was suitable for use with both epoxy and polyester resin systems.

As with the pre-preg material the all-carbon laminate was prepared from 24 layers of fabric, giving in this case a smaller finished laminate thickness of only ~7.7mm and a fibre weight fraction of ~43%. For the all-glass laminate, where the fabric was of a much finer weave, 60 layers were used, giving a final laminate thickness of ~6.15mm and a fibre weight fraction of ~59%. Several attempts were made at producing a hybrid laminate with alternating carbon and glass reinforced plies. In the final version 18 carbon layers and 19 glass layers were used, giving a final laminate thickness of ~8.4mm and a total fibre weight fraction of ~44% (carbon 65% to glass 35% by weight).

Cylindrical specimens, of 19mm nominal diameter, were cut from the finished plates with the axis perpendicular to the plane of reinforcement, taking care to minimise the resulting surface damage. Four $0^o/90^o$ strain gauge rosettes were fixed to the specimen cylindrical surface on planes normal to the warp and weft directions, see fig. 2, although in the all-carbon specimens it was not possible to distinguish between these two directions.

EXPERIMENTAL TECHNIQUES

a) Quasi-Static Tests

Quasi-static tests were performed on a standard screw-driven Instron testing machine at a crosshead speed of 0.2 in/min. The specimen was fixed between two 19mm diameter titanium alloy loading bars, using Chemlok type 204 epoxy adhesive, in series with a special strain-gauged load cell. To ensure axiality of loading a pair of ball-and-socket joints were used to attach the loading assembly to the testing machine, as shown in fig. 3a. The integrated output from a pair of linear variable differential transformers (LVDT's) in parallel with the specimen was used to monitor the overall displacement across the specimen. Signals from the load cell, the LVDT's and the four pairs of strain gauges attached to the specimen were recorded on channels 1, 2 and 3 to 6, respectively, of three dual-channel Datalabs type DL902 transient recorders, see fig. 3b, and subsequently transferred to floppy disc via an IBM PC. The specimen strain gauges were arranged as shown in fig. 4 so that transverse strains were recorded on channels 3 and 5 and longitudinal strains on channels 4 and 6. In general the strain gauges for channels 3 and 4 were fixed on the specimen surface normal to the weft direction while those for channels 5 and 6 were fixed on the specimen surface normal to the warp direction*.

*But note that for the all-glass specimens this arrangement was reversed while for the all carbon specimens the warp and weft directions could not be distinguished

A typical set of traces from the six transient recorder channels for a quasi-static test on the plain weave all-carbon laminate is given in fig. 5. These traces relate, respectively, to the applied load, the overall displacement and the signals from the four pairs of specimen strain gauges. The peak value on the load cell signal corresponds to tensile failure of the adhesive at the specimen/loading bar interface and is not a measure of the tensile strength of the laminate normal to the interlaminar plane. The two traces of negative sign, on channels 3 and 5, are a measure of the (compressive) transverse strains in the warp and weft directions due to the tensile strain applied in the through-thickness direction.

b) Impact Tests

At impact rates of strain the specimen was fixed in the same way between the input and output bars of a tensile Hopkinson bar apparatus. The test set-up, which is shown in fig. 6a, has been described previously[7]. The only differences in the present arrangement are i) that the 3m long titanium alloy loading bar which lies along the axis of the gas-gun also serves as the input bar of the split Hopkinson-bar assembly and ii) the limitation to only six recording channels meant that only one gauge station could be used on the input side of the specimen, gauge station I in fig. 6b. As a result it is not possible to use the Hopkinson-bar analysis to determine the specimen strain during the course of the test. However the signal from the input bar gauge station I does provide a check on the repeatability of the impact loading applied to the specimen from one test to the next.

Signals from the gauge stations on the input and output bars and from the four sets of strain gauges on the specimen were recorded in the same way as for the quasi-static tests except that Datalabs type 912 dual-channel transient recorders were used. These have the faster response time required for the impact tests. Again the data was stored on floppy discs and subsequently analysed using an IBM PC.

A typical set of traces from the six transient recorder channels for an impact test on the same plain weave all-carbon laminate is given in figs. 7. In this case these relate, respectively, to the input bar gauge station, the output bar gauge station, which gives a direct measure of the load supported by the specimen, and the four sets of specimen strain gauges. Here again the peak load observed on the trace from strain gauge station III is due to tensile failure in the adhesive layer between the specimen and the loading bar and the two traces of negative sign, on channels 3 and 5, are a measure of the (compressive) transverse strains in the warp and weft directions due to the tensile strain applied in the through-thickness direction.

RESULTS

a) Quasi-static tests

By cross-plotting the load cell data from fig. 5, corresponding to the applied stress, against the data from channels 4 and 6, corresponding to the specimen longitudinal strain, two estimates of the through-thickness tensile modulus, E_3, may be obtained. The stress-strain curves so determined are shown in figs. 8a and b. While neither is completely linear the mean slopes agree very closely, giving moduli of 6.87GPa and 6.58GPa respectively. Similarly by cross-plotting the data from channel 3 against that from channel 4, i.e. the transverse strain v. the longitudinal strain on the plane perpendicular to the weft direction, Poisson's ratio, ν_{23}, may be determined while cross-plotting data from channel 5 against that from channel 6 gives an estimate of ν_{13}. Results obtained in this way are shown in figs. 8c and d, the latter showing an almost totally linear response. The corresponding values for Poisson's ratio are found to be 0.091 and 0.123 respectively.

Similar sets of transient recorder traces and the corresponding stress-strain and transverse strain-longitudinal strain curves are given in Appendix I for the plain weave all-glass laminate, the hybrid laminate and the satin weave pre-preg carbon laminate. Collected data from all the quasi-static tests are listed in Table I below.

b) Impact Tests

In analysing the results of the impact tests allowance has to be made for the time delay between the arrival of the loading wave at the specimen strain gauges and its subsequent arrival at strain gauge position III on the output bar. The wave speed in the through-thickness direction of the specimen may be estimated with sufficient accuracy from the through-thickness tensile modulus determined in the quasi-static tests. Since the wave speed in the titanium bar and the distances the wave has to travel are known, the time delay may be estimated as shown in fig. 9. Although, strictly speaking, this time delay should be different for the various laminate lay-ups and specimen thicknesses, in practice the differences were very small and a single time delay was used, therefore, in all cases.

Apart from this allowance for the time delay the impact test data of fig. 7 are treated in exactly the same way as described above for the quasi-static data of fig. 5. Through-thickness stress-strain curves obtained by cross-plotting the data from gauge station III (channel 2) against those from channels 4 and 6 are shown in figs. 10a and b and give mean tensile moduli of 9.19GPa and 8.96GPa, respectively, significantly higher than the quasi-static values for the same material given above. Similarly, by cross-plotting the data from channel 3 against those from channel 4 and the data from channel 5 against those from channel 6, see figs. 10c and 10d, estimates for ν_{23}, of 0.111, and ν_{13}, of 0.114, are obtained. Collected data from all the impact tests are list-ed in Table II below.

TABLE I THROUGH-THICKNESS ELASTIC PROPERTIES QUASI-STATIC TESTS

Material	Test No.	Tensile Modulus (GPa)		Poisson's Ratio	
		$(E_3)_1$ (ch1/ch6)	$(E_3)_2$ (Ch1/ch4)	ν_{13} (ch5/ch6)	ν_{23} (ch3/ch4)
Hybrid (37 plies)	MT312	6.557	6.926	0.115	0.115
	MT313	6.413	6.637	0.134	0.128
	MT314	6.436	5.978	0.110	0.120
Mean		6.47±0.07	6.51±0.47	0.120±0.012	0.121±0.007
Carbon (24 plies)	MT316	6.461	6.684	0.081	0.108
	MT317	6.583	6.867	0.123	0.091
	MT318	---	6.941	0.112	0.113
	MT319	6.458	(9.002)*	0.106	0.136
Mean		6.50±0.06	6.83±0.13	0.106±0.021	0.112±0.022
Glass (60 plies)	MT308	5.971	6.253	0.138	0.174
	MT309	6.530	6.770	0.145	0.170
	MT310	6.212	5.719	0.152	0.189
	MT311	5.416	5.901	0.156	0.174
Mean		6.03±0.56	6.16±0.53	0.148±0.009	0.177±0.010
Pre-preg (24 plies)	MT302	9.699	(8.821)*	0.090	0.096
	MT304	9.885	9.773	0.092	0.097
	MT305	9.294	9.825	0.128	0.111
	MT306	9.605	9.847	0.104	0.091
	MT320	11.073	10.496	0.096	0.108
Mean		9.91±0.89	9.99±0.36	0.102±0.019	0.101±0.019

*(suspect result - ignore)

TABLE II THROUGH-THICKNESS ELASTIC PROPERTIES IMPACT TESTS

Material	Test No.	Tensile Modulus (Gpa)		Poisson's Ratio	
		$(E_3)_1$ (ch2/ch6)	$(E_3)_2$ (Ch2/ch4)	ν_{13} (ch5/ch6)	ν_{23} (ch3/ch4)
Hybrid	MT101	- --	8.97	0.108	0.105
(37 plies)	MT102	8.54	7.97	0.137	0.105
	MT103	8.85	8.85	0.113	0.110
Mean		8.40±0.14	8.60±0.50	0.119±0.015	0.107±0.003
Carbon	MT104	9.19	8.96	0.114	0.111
(24 plies)	MT105	8.60	8.80	0.079	0.105
	MT106	9.06	8.56	0.129	0.099
Mean		8.95±0.30	8.77±0.20	0.107±0.025	0.105±0.006
Glass	MT107	8.73	10.07	0.146	0.155
(60 plies)	MT108	8.21	9.10	0.135	0.156
	MT109	No stress signal		0.157	0.147
Mean		8.47±0.26	9.59±0.49	0.146±0.011	0.153±0.005
Pre-preg	MT111	Records on channels 5 and 6		0.080	---
(24 plies)	MT112	No stress signal		0.088	0.078
	MT113	12.64	12.00	0.113	0.086
Mean		12.64	12.00	0.094±0.017	0.082±0.004

DISCUSSION

From a comparison of the summarised results at the ends of Tables I and II it is apparent that at both the quasi-static and the impact rate of strain the value of the through-thickness tensile modulus, E_3, is very similar for the three plain-weave lay-ups. There is, however, a marked effect of strain rate, the average modulus for the three lay-ups increasing from ~6.42±0.77GPa at the quasi-static rate to ~8.81±0.97GPa at the impact rate, a rise of over 35%. The pre-preg material has a higher through-thickness modulus at both rates of strain but shows a smaller increase, from 9.94±0.89GPa at the quasi-static rate to 12.32±0.32GPa at the impact rate, a rise of slightly less than 25%. These results contrast with the behaviour previously observed[2] for the in-plane tensile moduli in the two reinforcing directions where, at the quasi-static rate, the modulus was much higher for the carbon than for the glass-reinforced laminate, ~44.3GPa as compared to ~15.2GPa. At the impact rate of loading these both increase, by about 36% to ~20.6GPa, for the glass-reinforced laminate, but by only 10%, to ~48.9GPa, for the carbon-reinforced laminate.

These differences in behaviour between the in-plane and through-thickness directions are not unexpected. Since the in-plane tensile moduli in the directions of reinforcement are likely to depend primarily on the stiffness of the reinforcing fibres it is not surprising that they are found to be higher in the carbon reinforced material. However the difference in rate-dependence suggests that the matrix properties also play a part, presumably by resisting more strongly the straightening of the fibres at the higher rate of strain. The issue is complicated by the difference in the weave geometries, the glass fabric being of a much finer weave than the carbon. This does allow the possiblity, however, that the higher rate dependence of the moduli for the glass-reinforced laminate is due to higher local strain rates in the resin associated with the finer weave geometry.

In contrast the through-thickness modulus is likely to depend primarily on the properties of the resin. Thus a previous estimate[3] of the quasi-static through-thickness modulus, based on the assumption that the fibres could be taken as effectively rigid and assuming a fibre volume fraction of 50%, gave a value of 6GPa. This is very close to the measured values reported here which support, therefore, the assumptions on which the earlier estimate was made. However, if the three plain-weave laminates are considered separately some differences in the rate dependence of E_3, similar to those for the in-plane moduli, are again apparent. As before the largest increase, by just under 50%, is shown by the glass-reinforced laminate while the carbon reinforced and the hybrid laminates show a smaller increase of just over 30% in each case. Again this may be due to the different weave geometries. In this case, however, a second factor may operate. Because of the problems experienced in accurately controlling the fibre volume fraction in the three plain-weave laminates differences in the rate dependence of the transverse modulus, E_3, could arise from differences in the resin content. This would be more likely, however, if the glass-reinforced laminate had the highest resin content whereas in practice it had the lowest.

CONCLUSIONS

Four woven reinforced epoxy laminates were prepared using respectively a plain-weave glass reinforcement, a plain-weave carbon reinforcement, a satin-weave carbon reinforcement and a hybrid lay-up of plain-weave carbon and plain-weave glass. The laminates were loaded in tension in a direction normal to the plane of reinforcement at a quasi-static and an impact rate and the elastic properties, transverse tensile modulus and Poisson's ratio, were determined, using strain gauges attached directly to the specimen. A significant increase in the tensile modulus with strain rate was observed in all cases. Only small changes were apparent in the measured values of Poisson's ratio. These showed no consistent effect of strain rate and were probably an indication of the accuracy of the experimental technique.

REFERENCES

1. K. Saka, R. K. Y. Li and J. Harding, Behaviour of Fibre-Reinforced Composites under Dynamic Tension (Fourth Progress Report), OUEL Report No. 1714/87.

2. J. Harding, K. Saka and M. E. C. Taylor, The Effect of Strain Rate on the Tensile Failure of Woven-Reinforced Carbon/Glass Hybrid Composites, in Proc. IMPACT 87, Impact Loading and Dynamic Behaviour of Materials, eds. C. Y. Chiem, H.-D. Kunze and L. W. Meyer, (DGM Informationsgesell-schafft mbH, Oberursel), 1988, vol. 1, pp. 515-522.

3. Y. L. Li, C. Ruiz and J. Harding, Failure Analysis of Woven Hybrid Composites using a Finite Element Method, Composites Science and Technology (in press).

4. Y. L. Li, C. Ruiz and J. Harding, Failure Analysis of Woven Hybrid Composite using a Finite Element Method, OUEL Report No. 1791/89.

5. K. Saka and J. Harding, The Deformation and Fracture of Hybrid Reinforced Composites under Tensile Impact, Proc. IUTAM Colloquium on Macro- and Micro- Mechanisms of High Velocity Deformation and Fracture, (Springer-Verlag, Berlin), 1988, pp. 97-111.

6. J. Harding, Y. L. Li, K. Saka and M. E. C. Taylor, Characterisation of the Impact Strength of Woven Carbon Fibre/Epoxy Laminates, Proc. 4th. Oxford Int. Conf. on Mechanical Behaviour of Materials at High Rates of Strain, ed. J. Harding, Inst. of Physics Conf. Ser. No. 102 (Inst. of Physics, London and Bristol), 1989, 403-410.

7. K. Saka and J. Harding, Behaviour of Fibre Reinforced Composites under Dynamic Tension, (Second Progress Report), OUEL Report No. 1602/85.

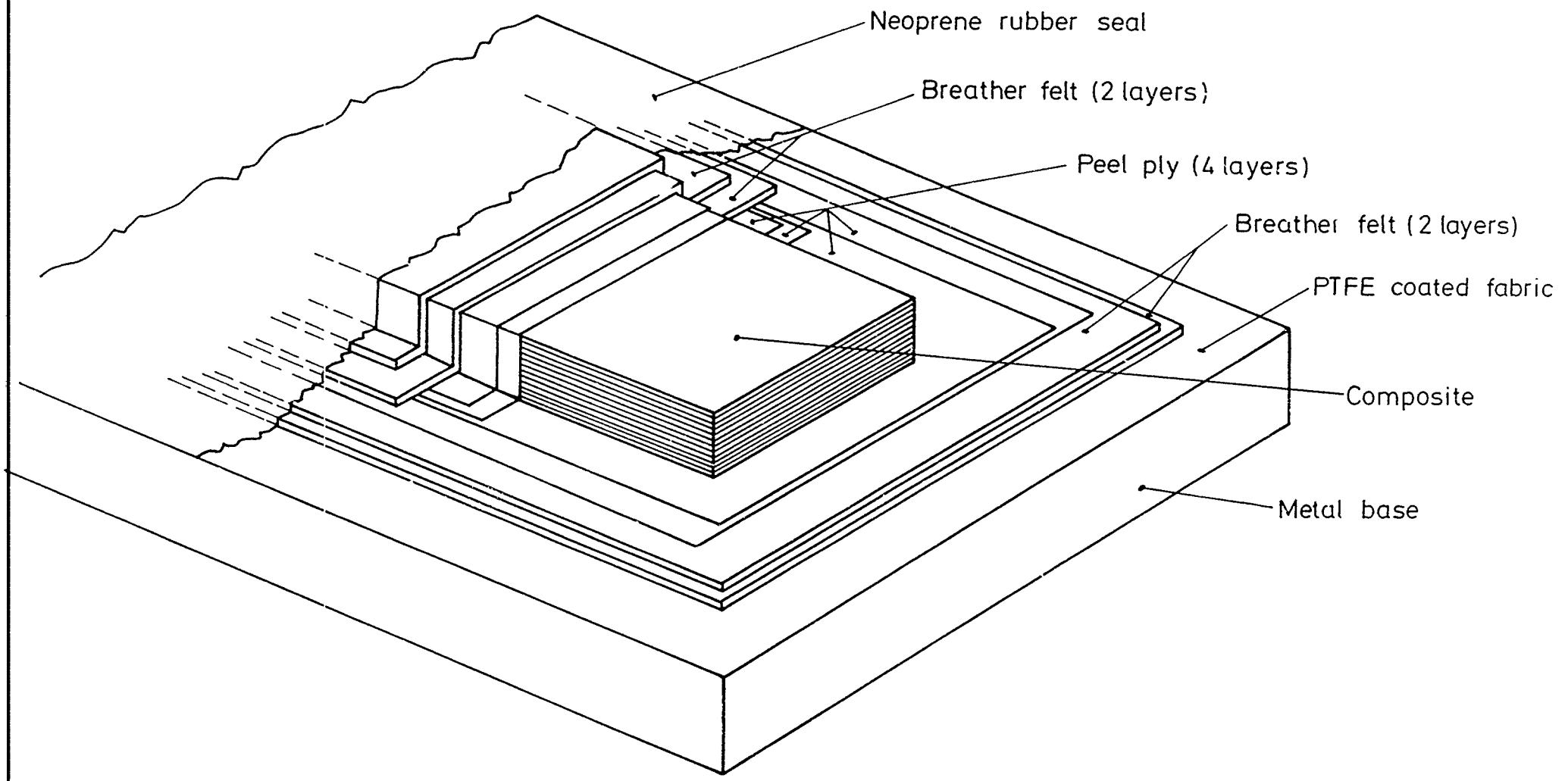

Fig. 1 ARRANGEMENT OF AUTOCLAVE

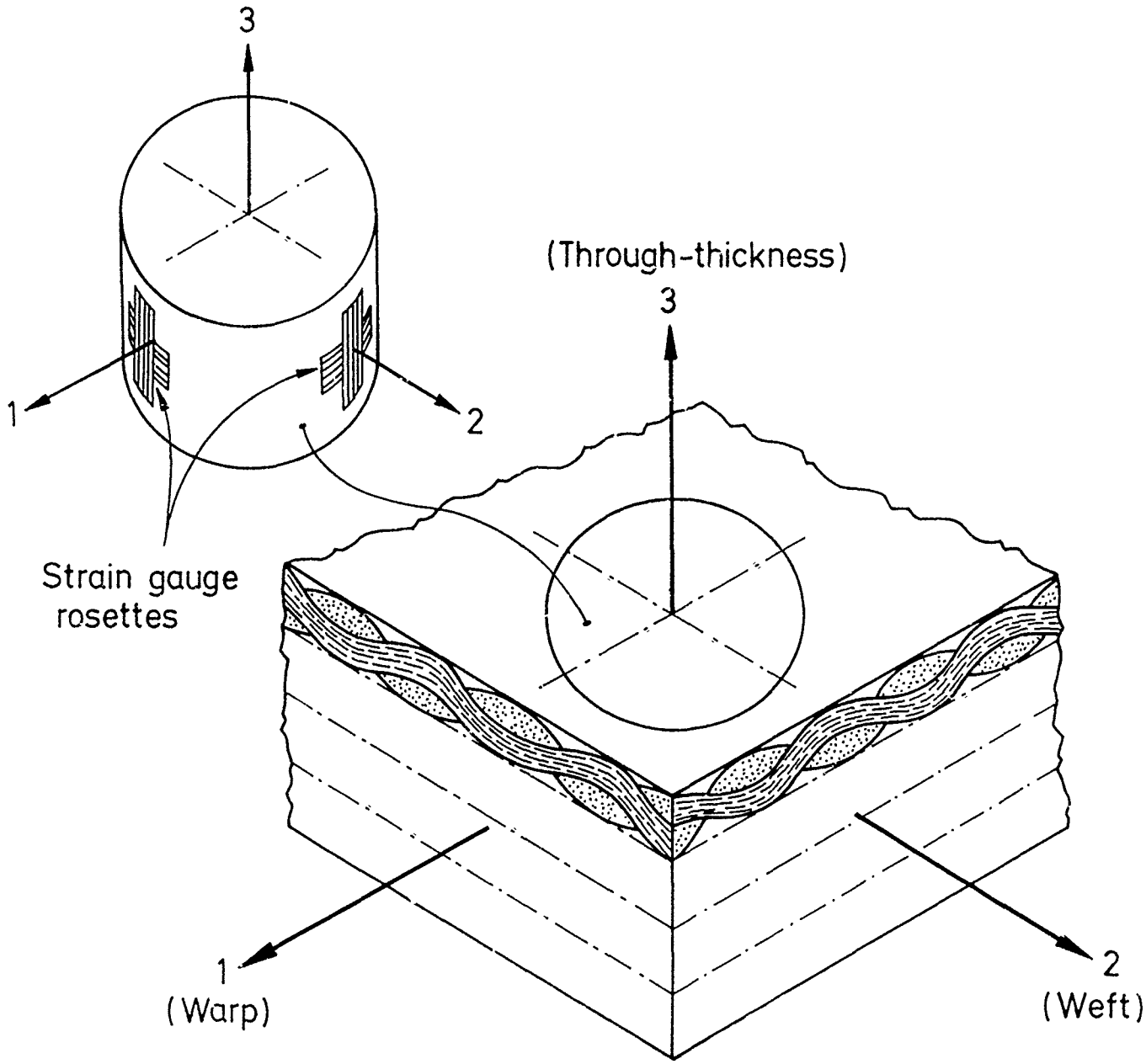

Fig. 2 DEFINITION OF DIRECTIONS IN COMPOSITE SPECIMENS

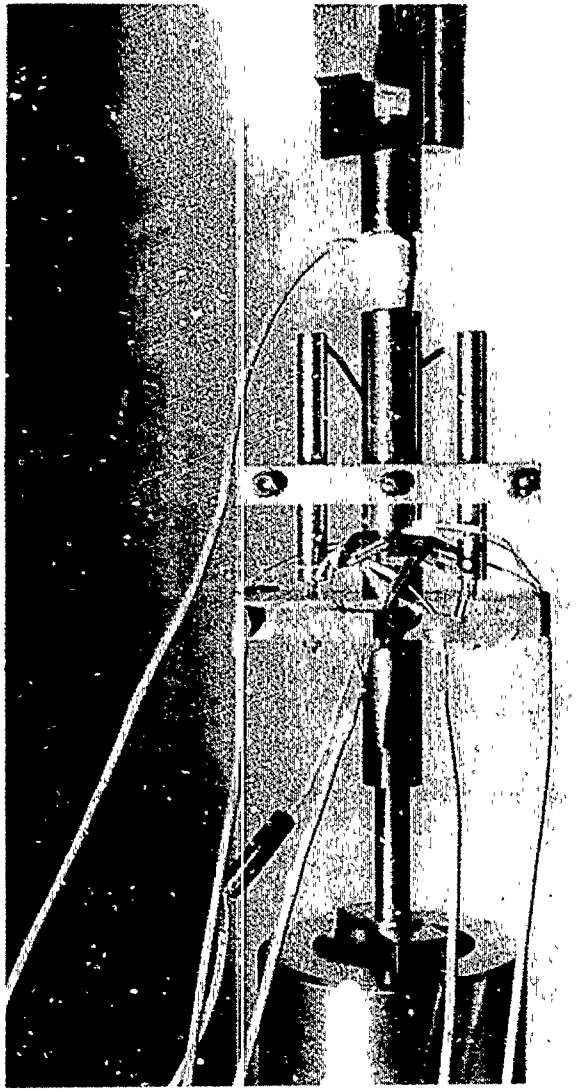

a) Loading Rig, Displacement Transducers and Specimen Gauges

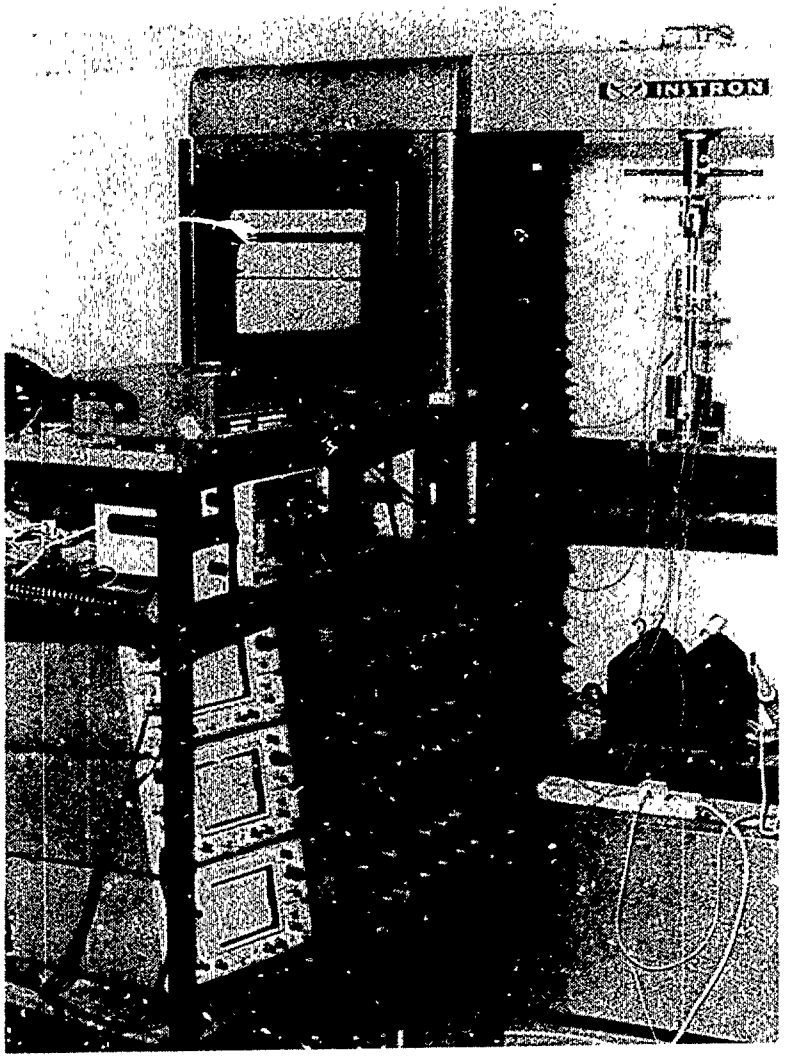

b) Electronic Instrumentation

Fig. 3 EXPERIMENTAL EQUIPMENT FOR QUASI-STATIC TESTING

Fig. 4 ARRANGEMENT OF STRAIN GAUGE ROSETTES ON TEST SPECIMEN

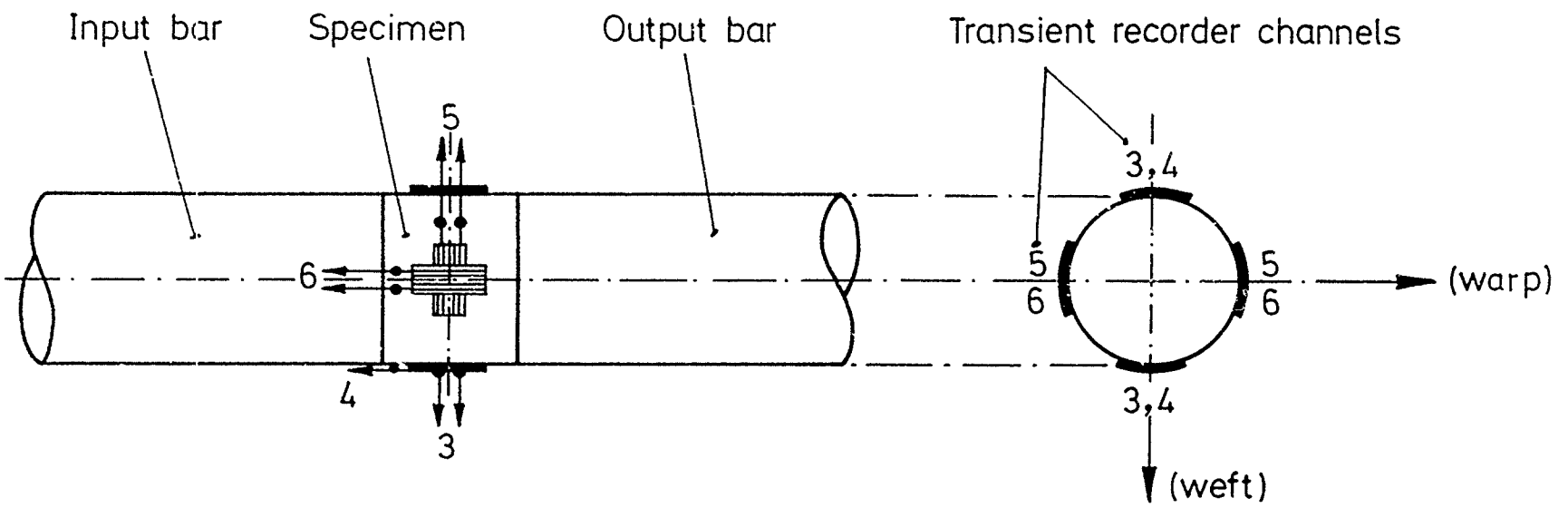

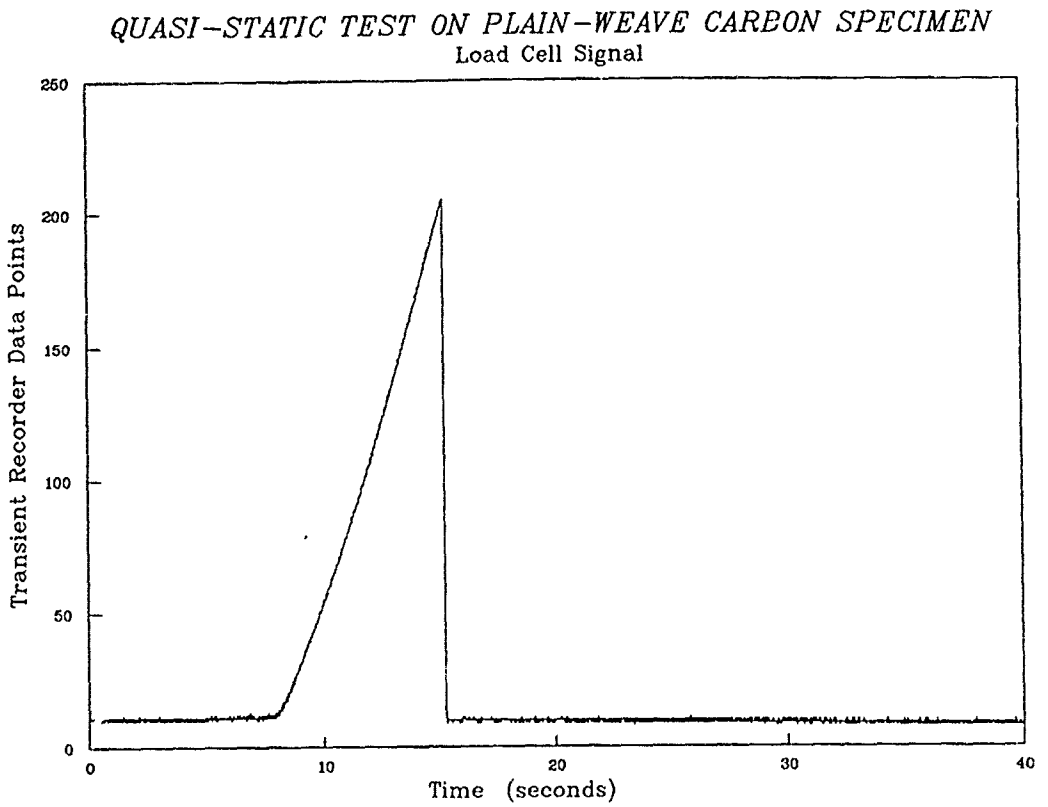

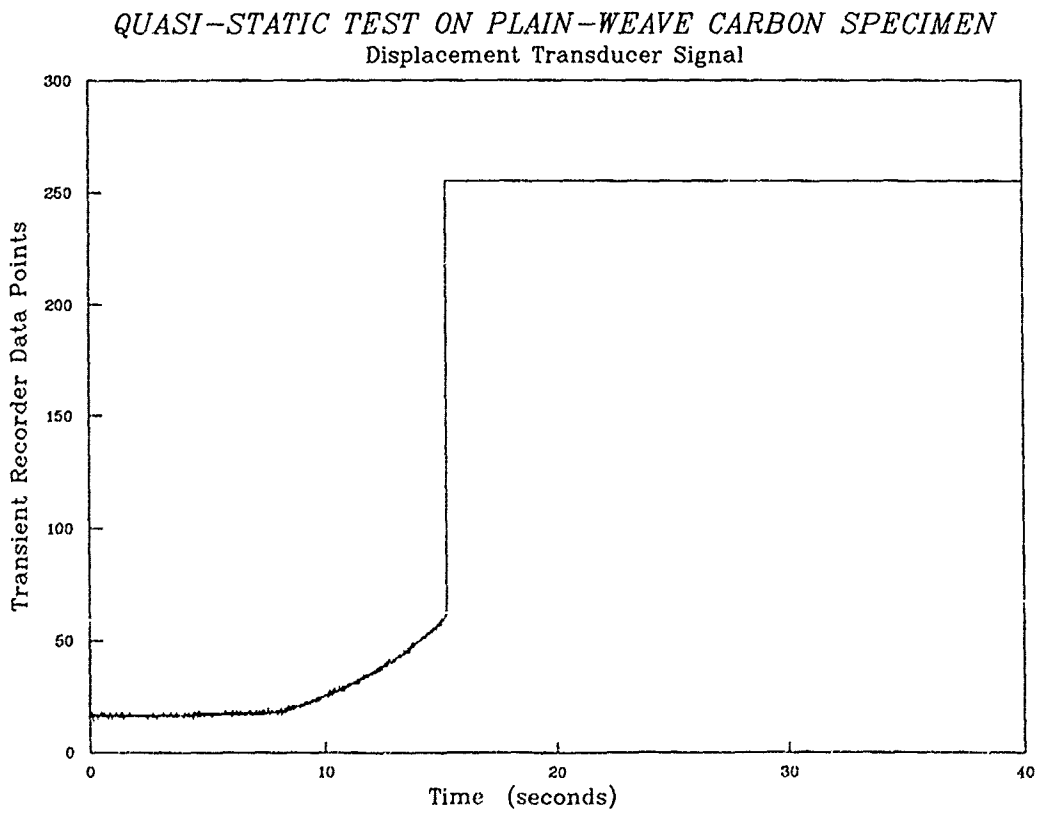

Fig. 5 TRANSIENT RECORDER TRACES FOR QUASI-STATIC TEST ON PLAIN-WEAVE CARBON SPECIMEN

a) Load Cell Signal b) Displacement Transducer Signal

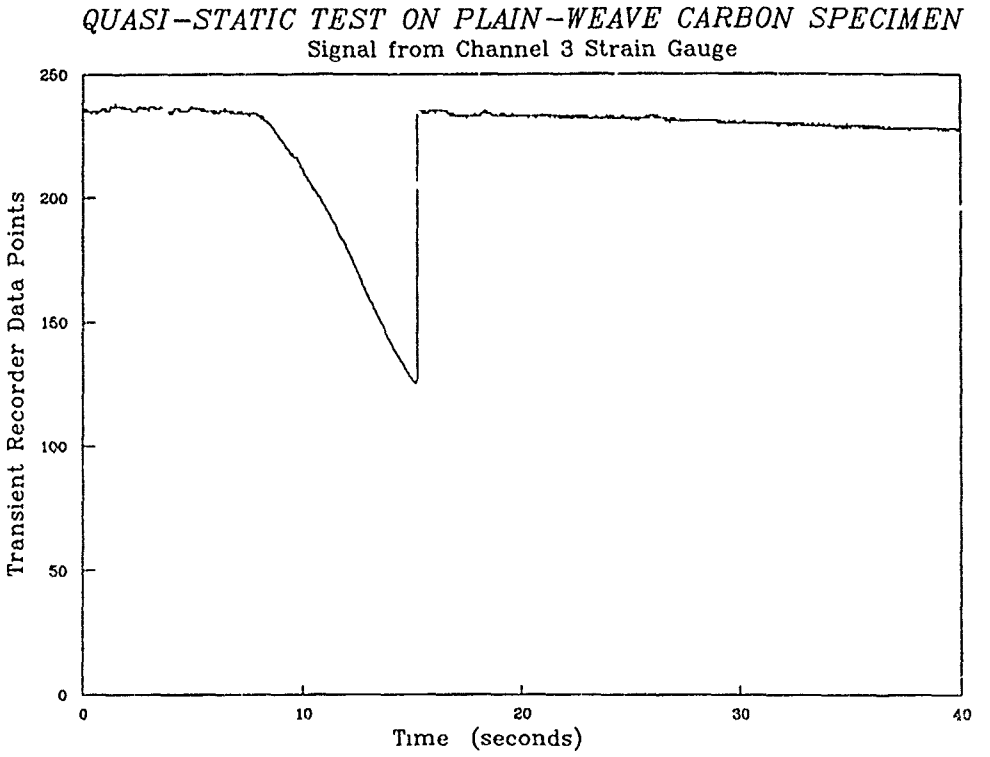

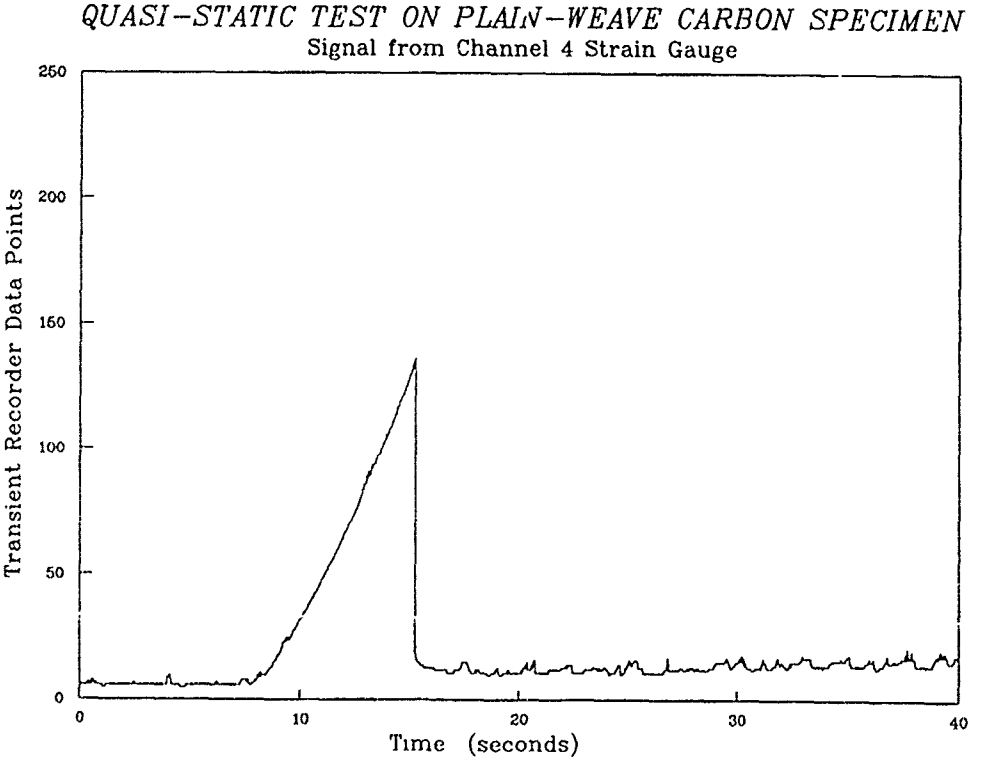

Fig. 5 TRANSIENT RECORDER TRACES FOR QUASI-STATIC TEST ON PLAIN-WEAVE CARBON SPECIMEN

c) Channel 3 Strain Gauge Signal d) Channel 4 Strain Gauge Signal

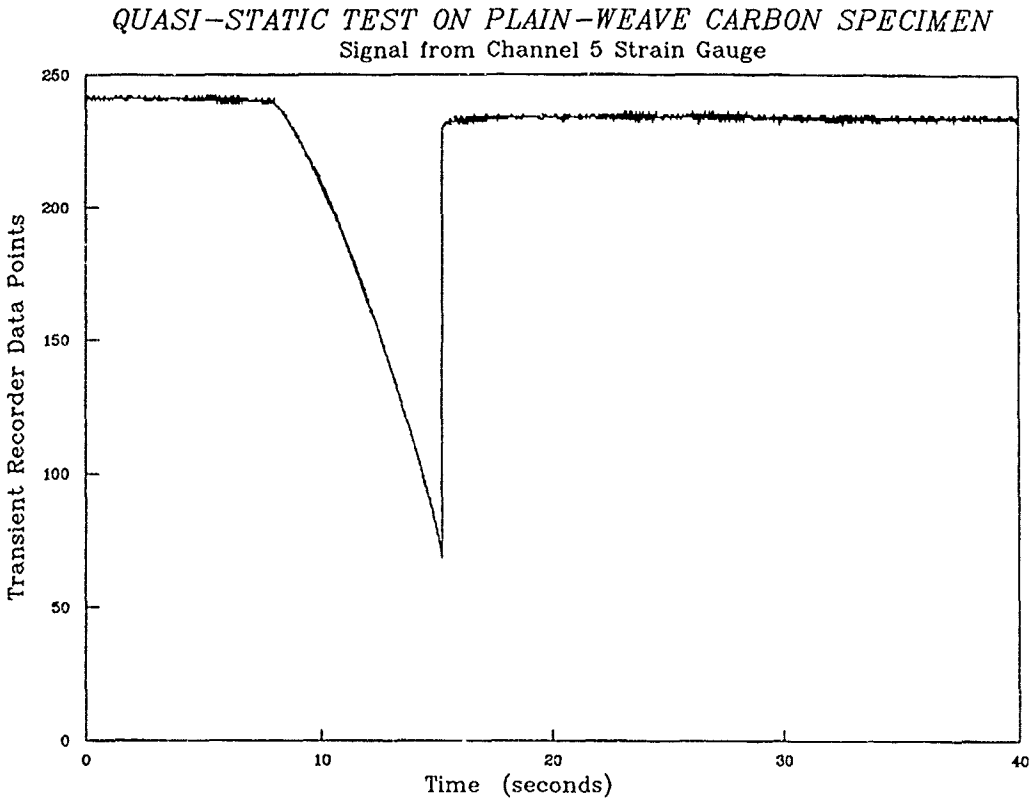

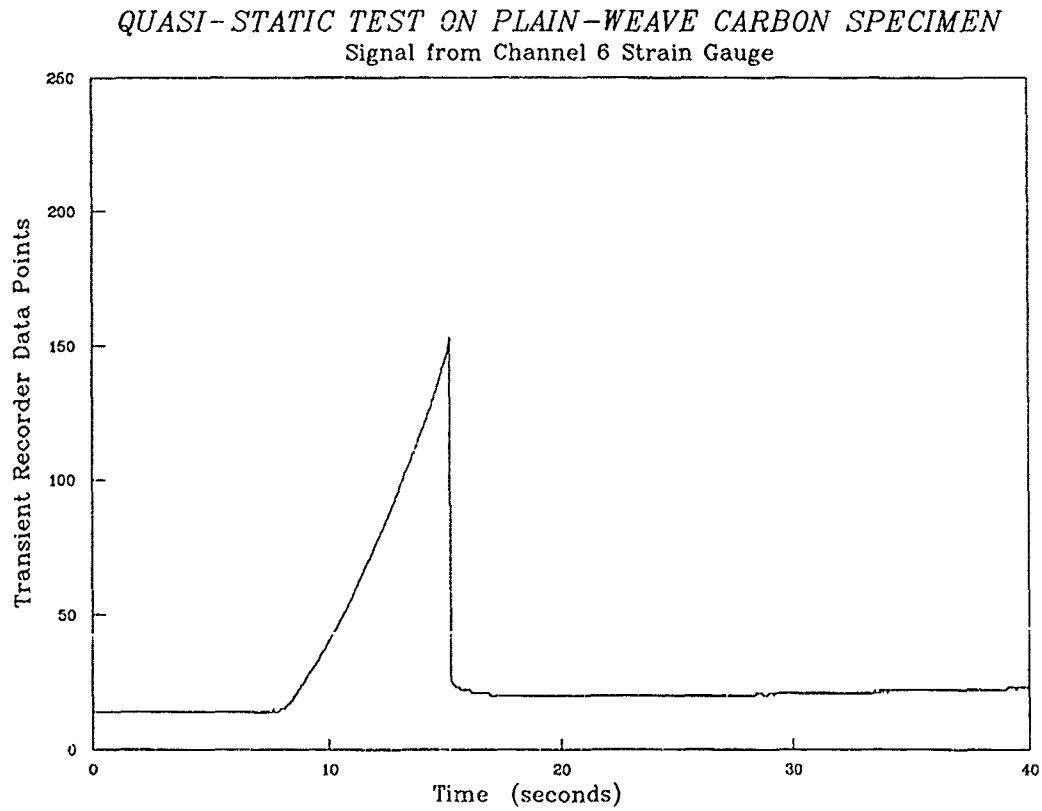

Fig. 5 TRANSIENT RECORDER TRACES FOR QUASI-STATIC TEST ON PLAIN-WEAVE CARBON SPECIMEN

e) Channel 5 Strain Gauge Signal f) Channel 6 Strain Gauge Signal

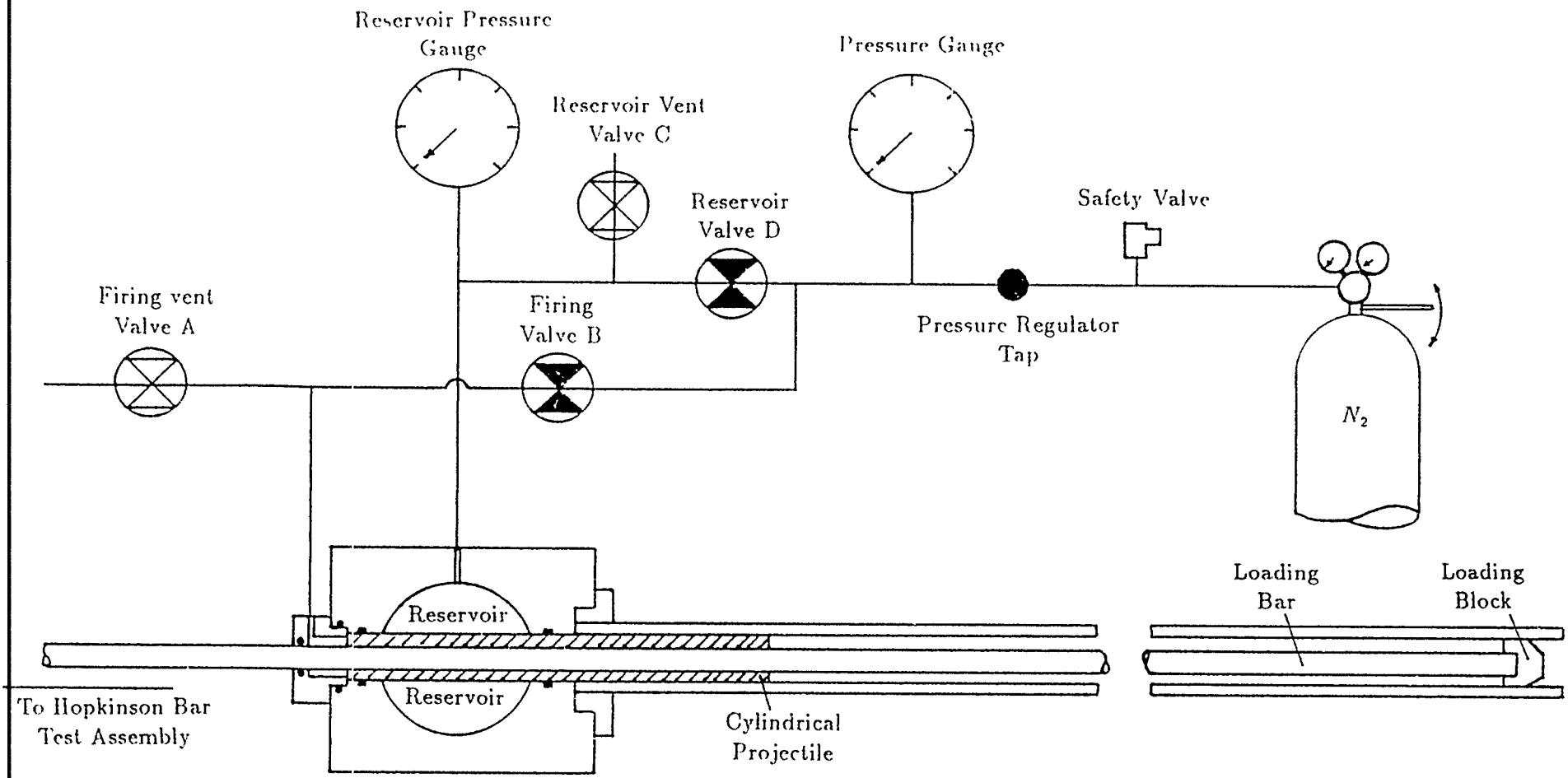

Fig. 6a TEST SET-UP FOR TENSILE IMPACT TESTS

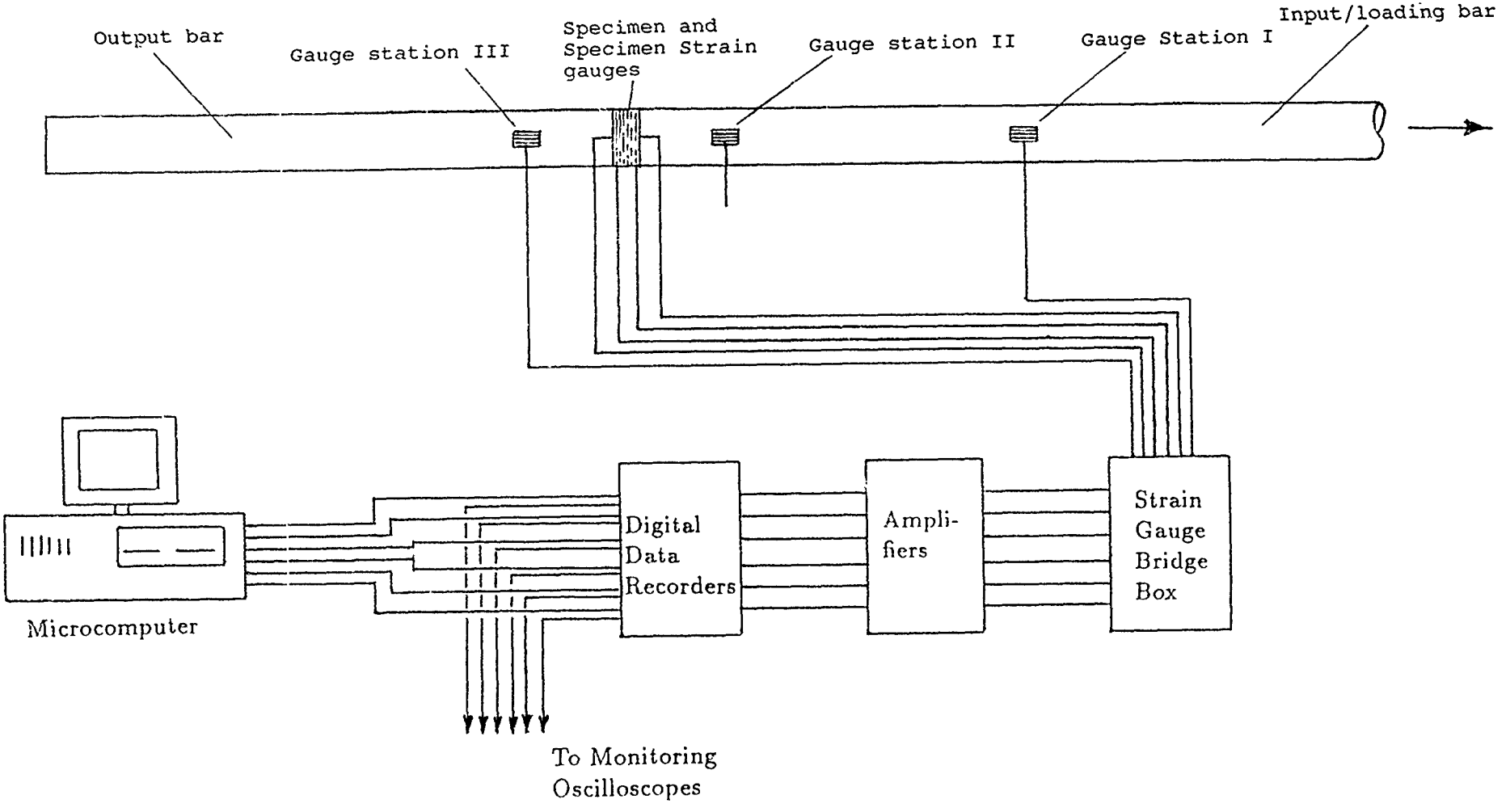

Fig. 6b HOPKINSON-BAR SET-UP FOR TENSILE IMPACT TESTS

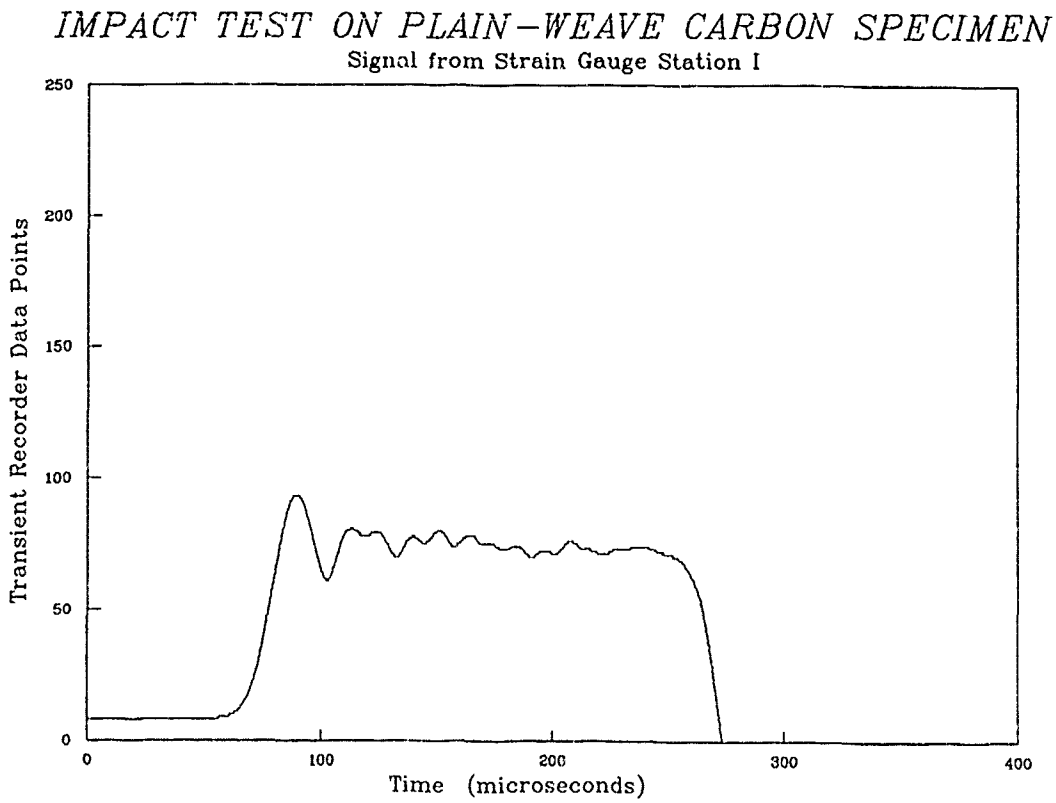

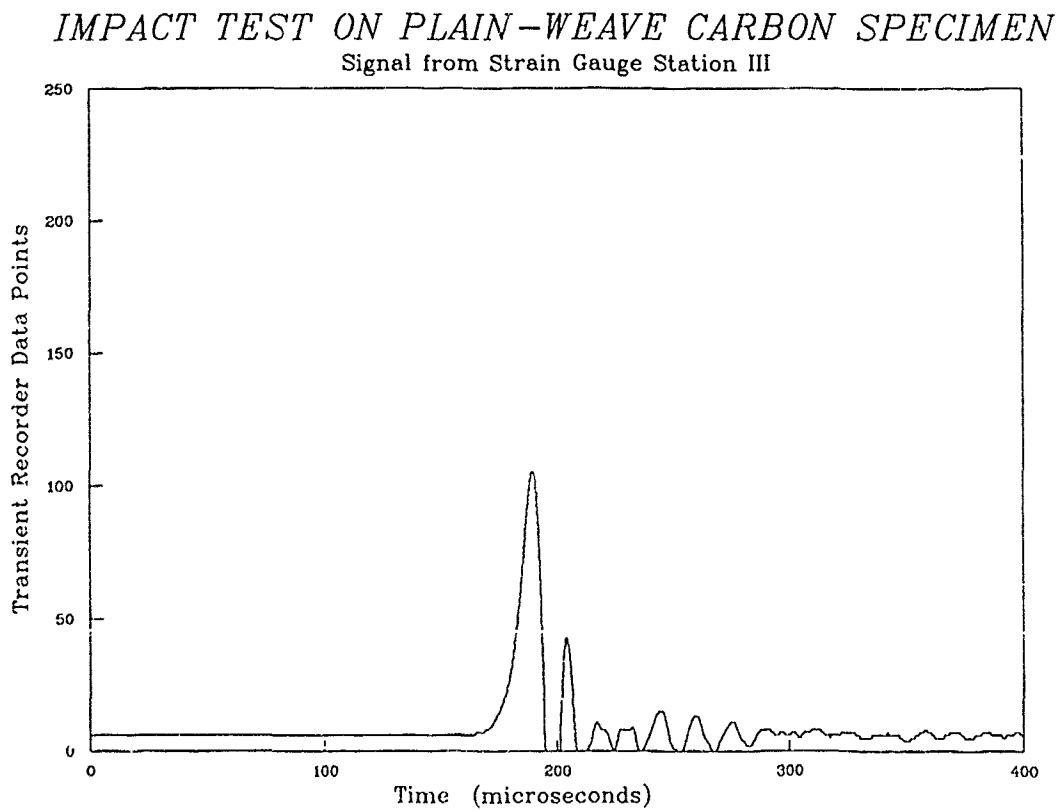

Fig. 7 TRANSIENT RECORDER TRACES FOR IMPACT TEST ON PLAIN-WEAVE CARBON SPECIMEN

a) Input bar Gauge Station I Signal b) Output bar Gauge Station III Signal

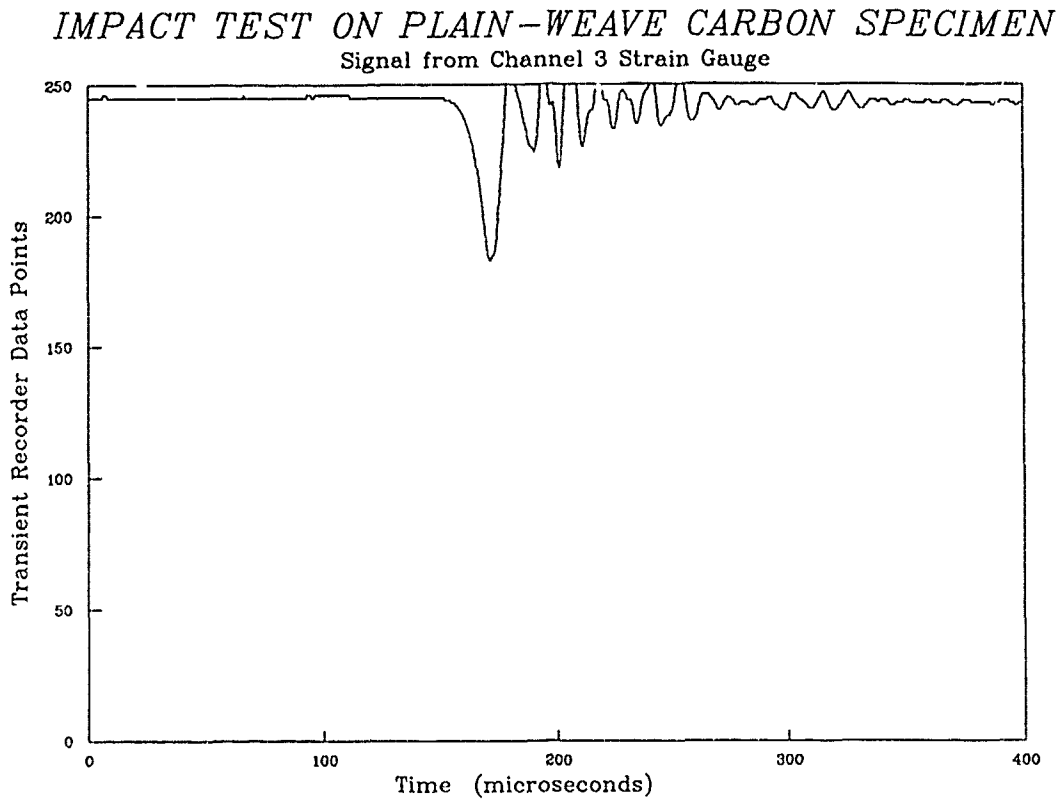

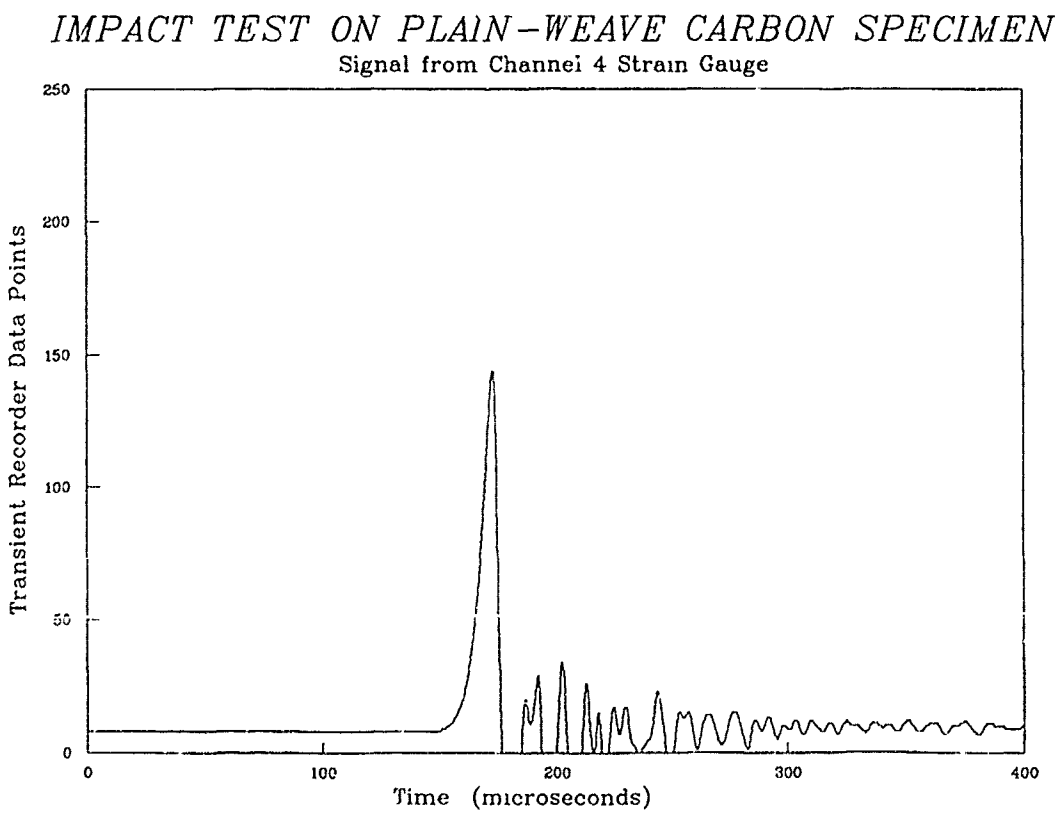

Fig. 7 TRANSIENT RECORDER TRACES FOR IMPACT TEST ON PLAIN-WEAVE CARBON SPECIMEN

c) Channel 3 Strain Gauge Signal d) Channel 4 Strain Gauge Signal

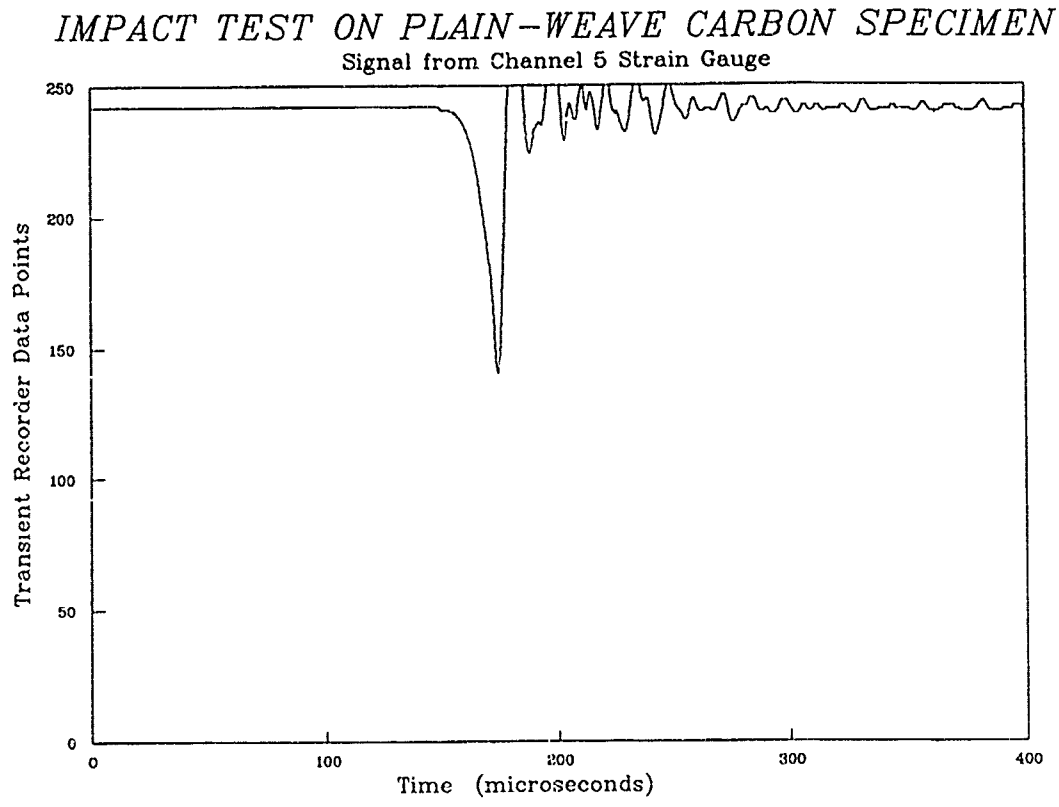

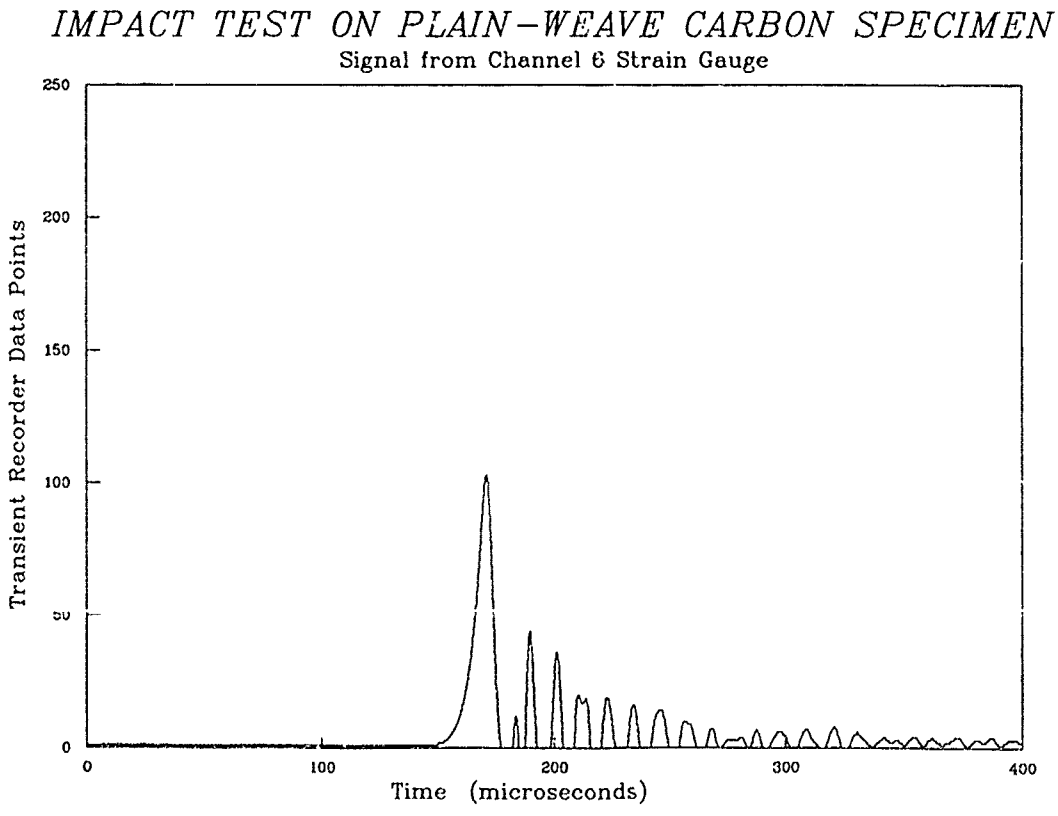

Fig. 7 TRANSIENT RECORDER TRACES FOR IMPACT TEST ON PLAIN-WEAVE CARBON SPECIMEN

e) Channel 5 Strain Gauge Signal f) Channel 6 Strain Gauge Signal

Fig. 8a STRESS v LONGITUDINAL STRAIN

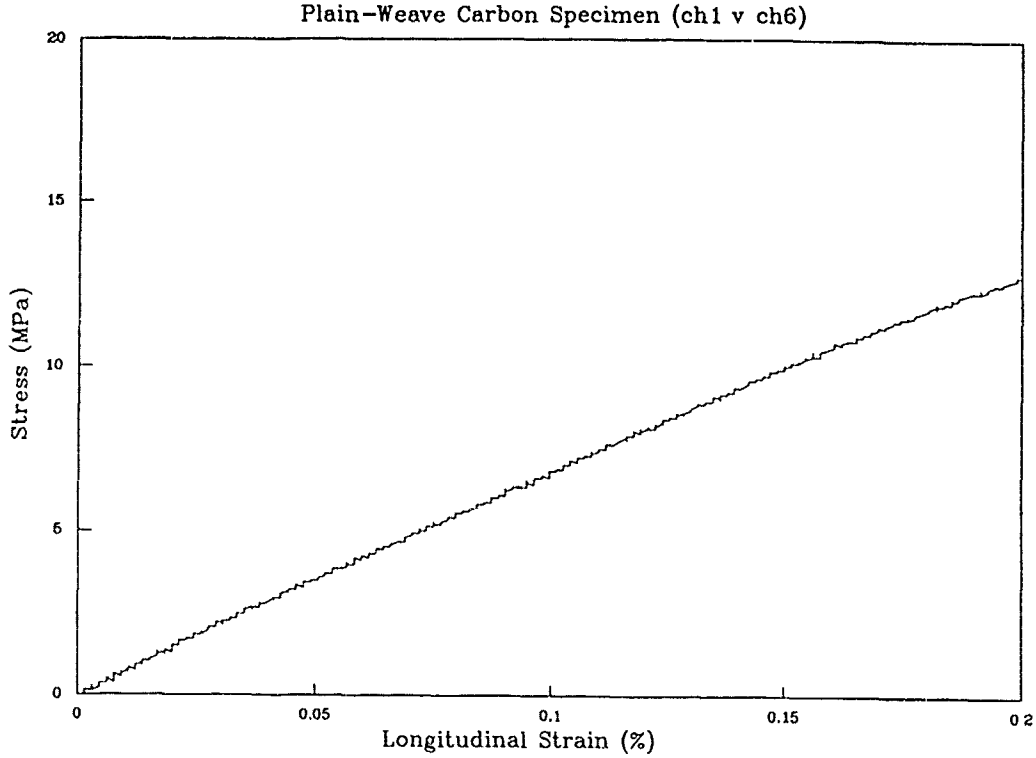

Fig. 8b STRESS v LONGITUDINAL STRAIN

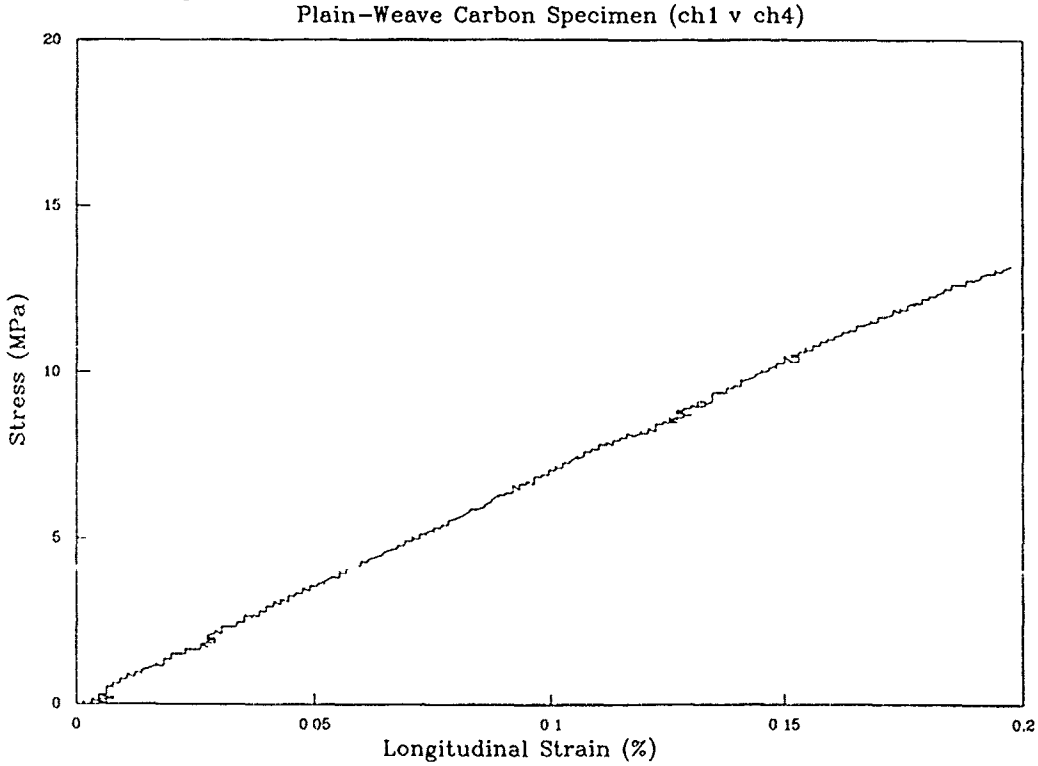

Fig. 8c TRANSVERSE STRAIN v LONGITUDINAL STRAIN

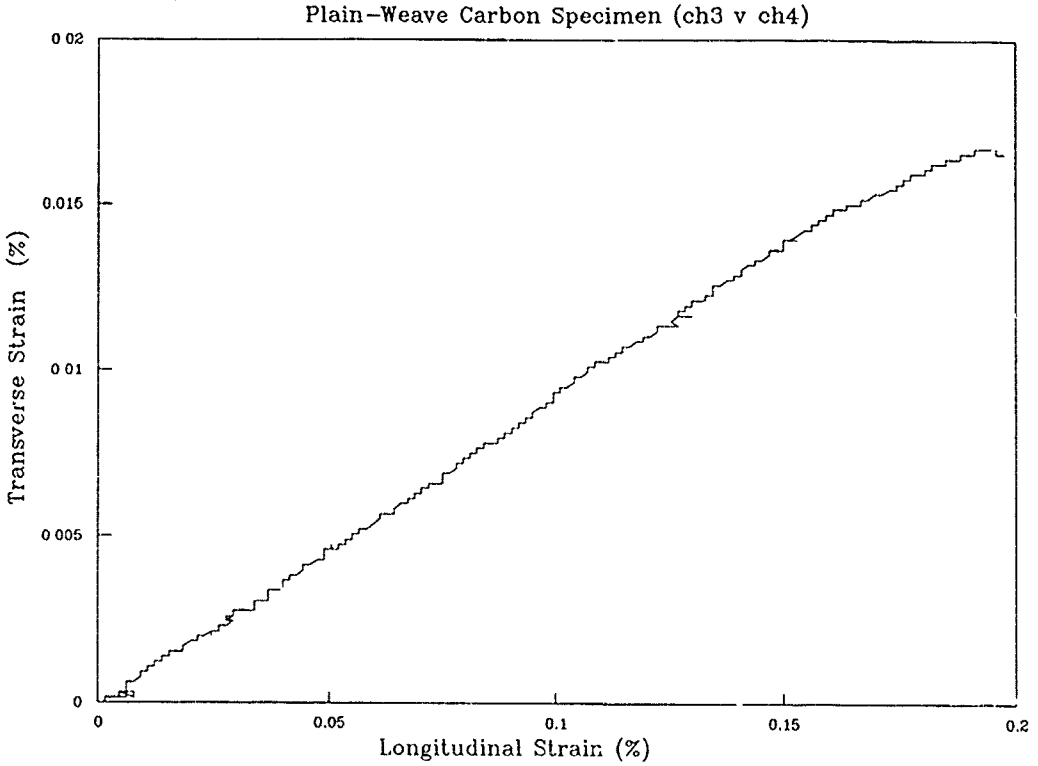

Fig. 8d TRANSVERSE STRAIN v LONGITUDINAL STRAIN

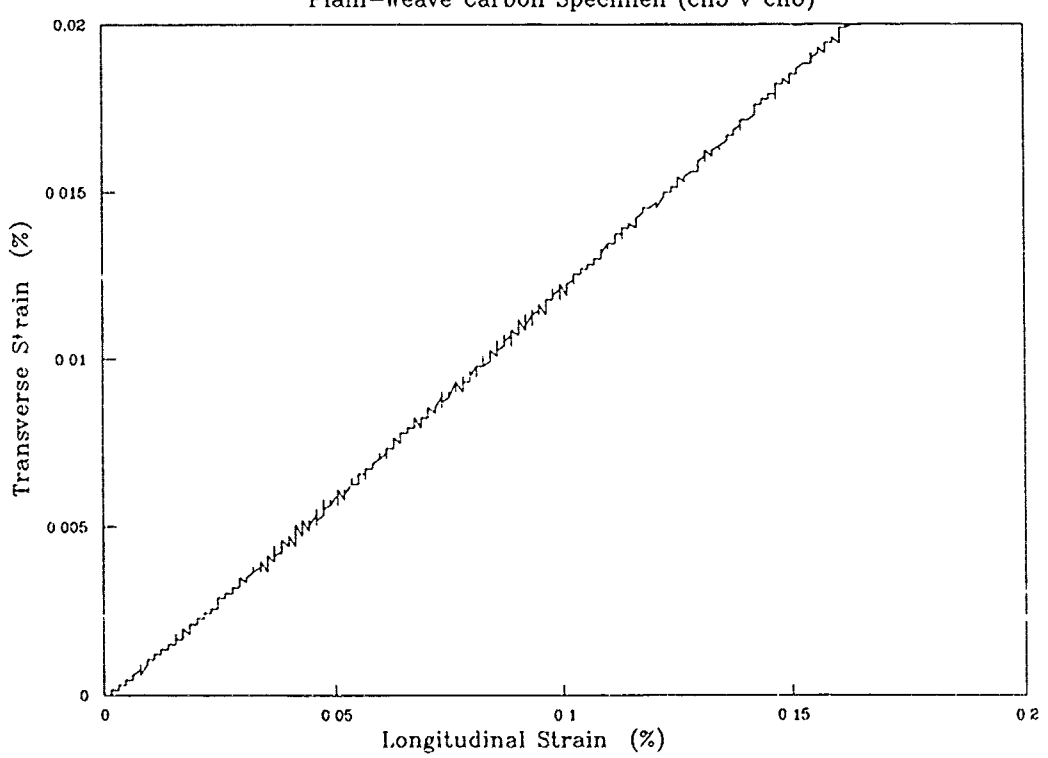

Fig. 9 TIME DELAY BETWEEN SPECIMEN STRAIN GAUGES AND OUTPUT BAR GAUGE STATION III

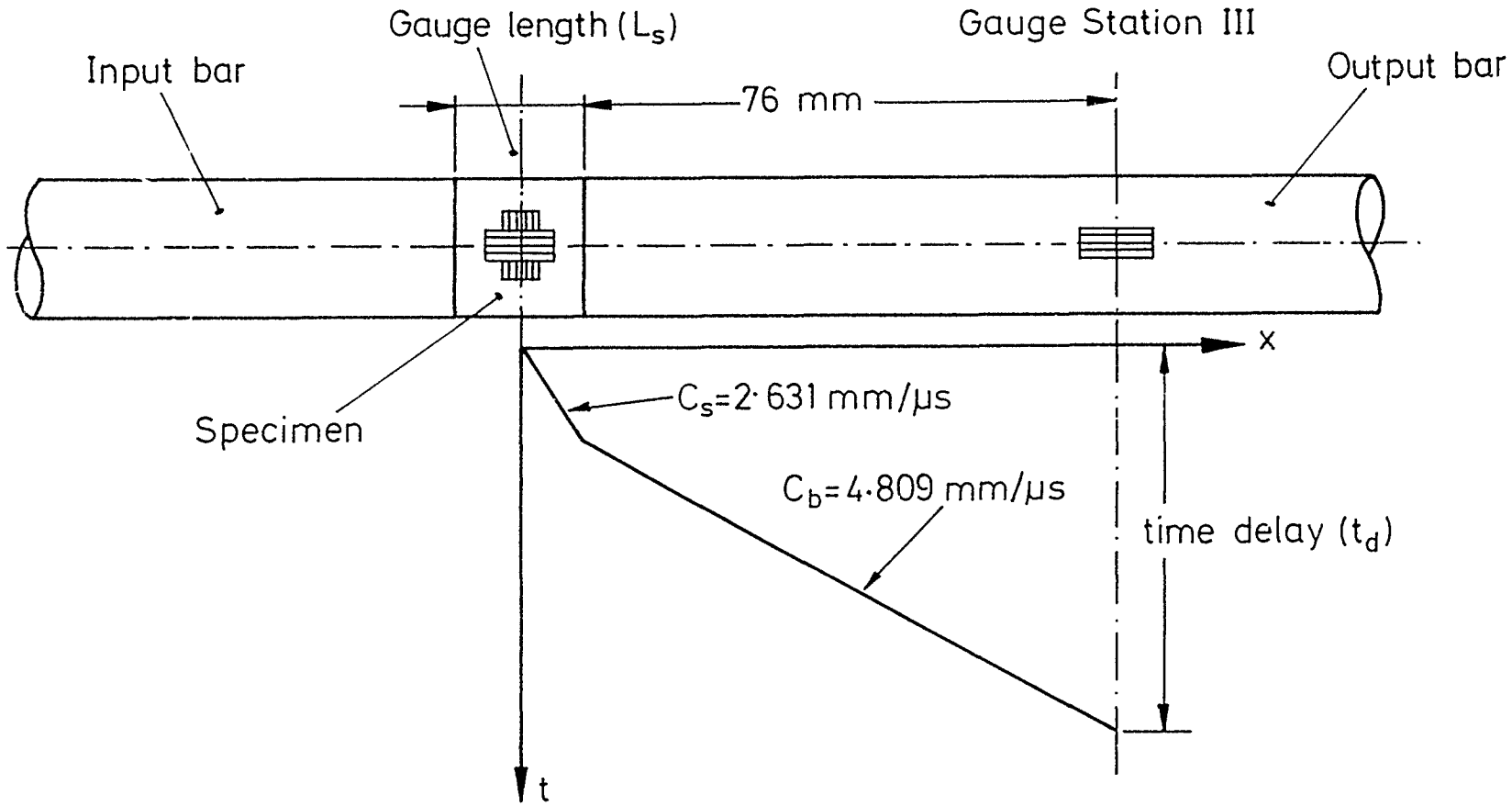

For L_s=7·5 mm, t_d=17·2 μs

Fig. 10a STRESS v LONGITUDINAL STRAIN

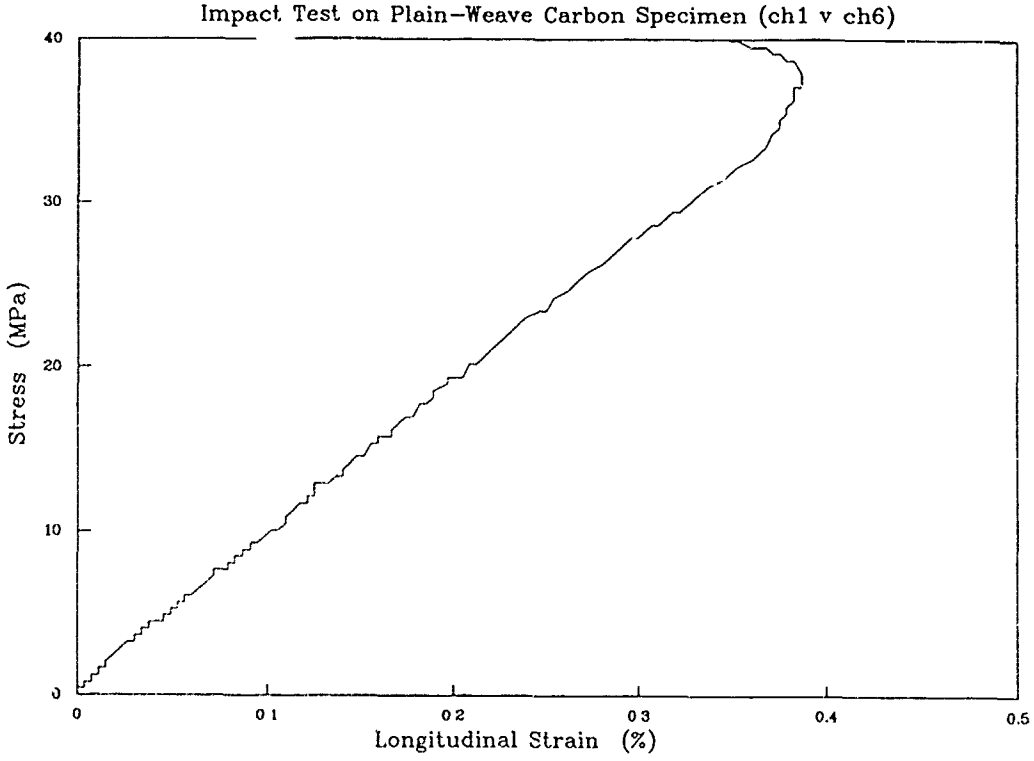

Fig. 10b STRESS v LONGITUDINAL STRAIN

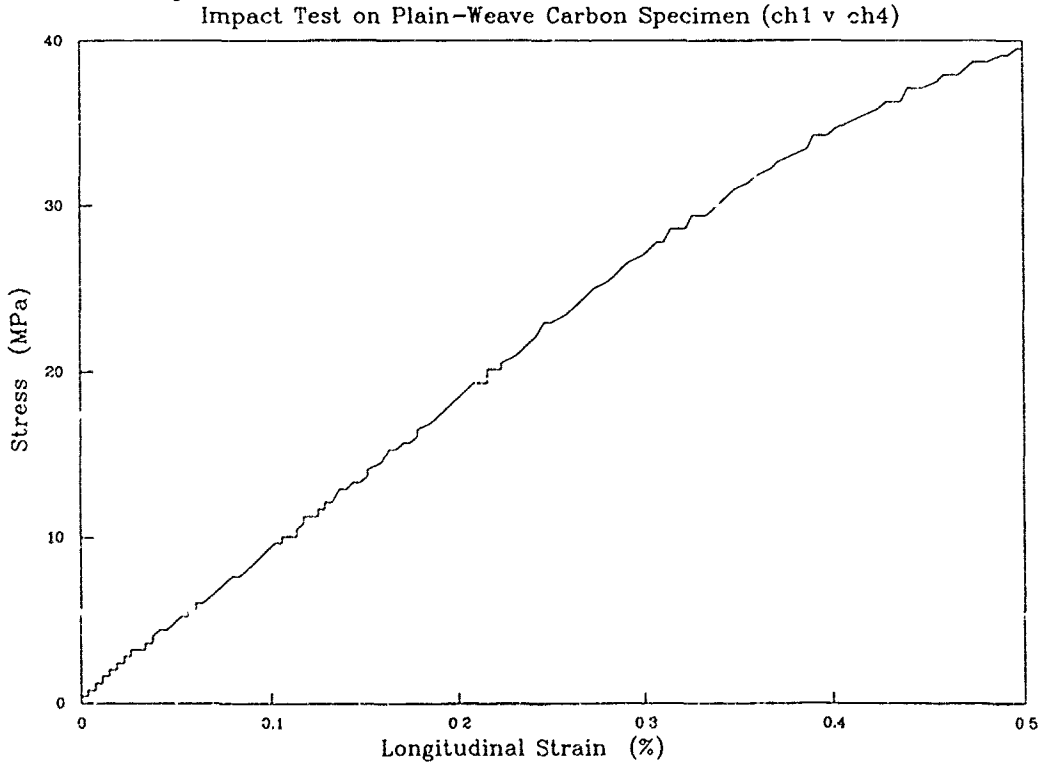

Fig. 10c TRANSVERSE STRAIN v LONGITUDINAL STRAIN

Impact Test on Plain-Weave Carbon Specimen (ch3 v ch4)

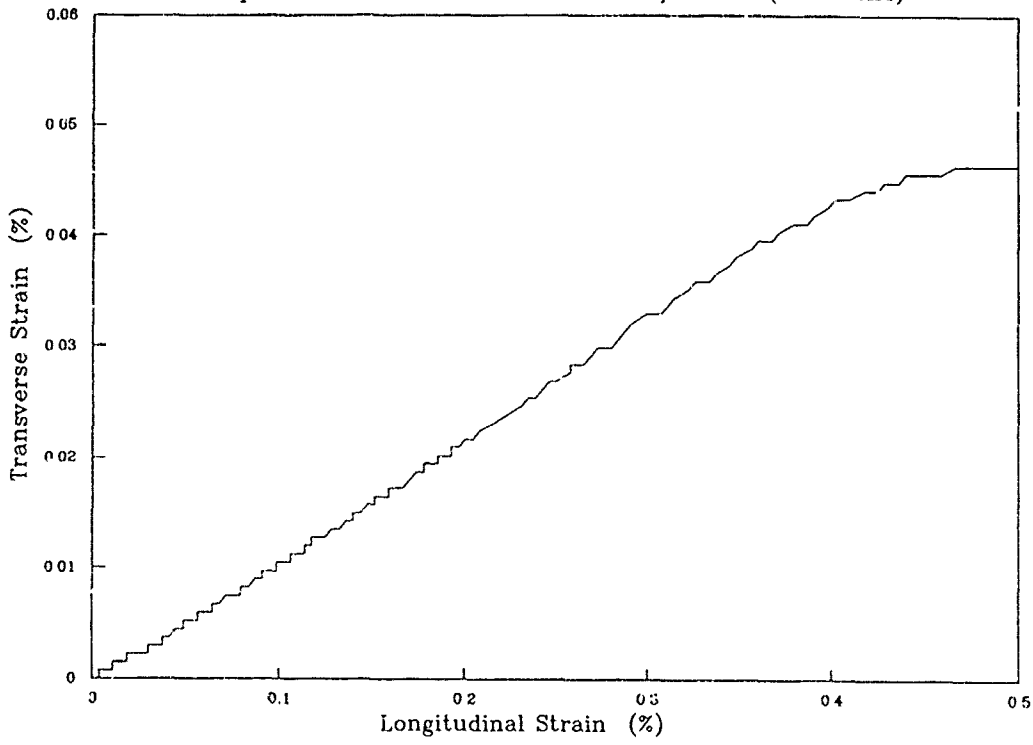

Fig. 10d TRANSVERSE STRAIN v LONGITUDINAL STRAIN

Impact Test on Plain-Weave Carbon Specimen (ch5 v ch6)

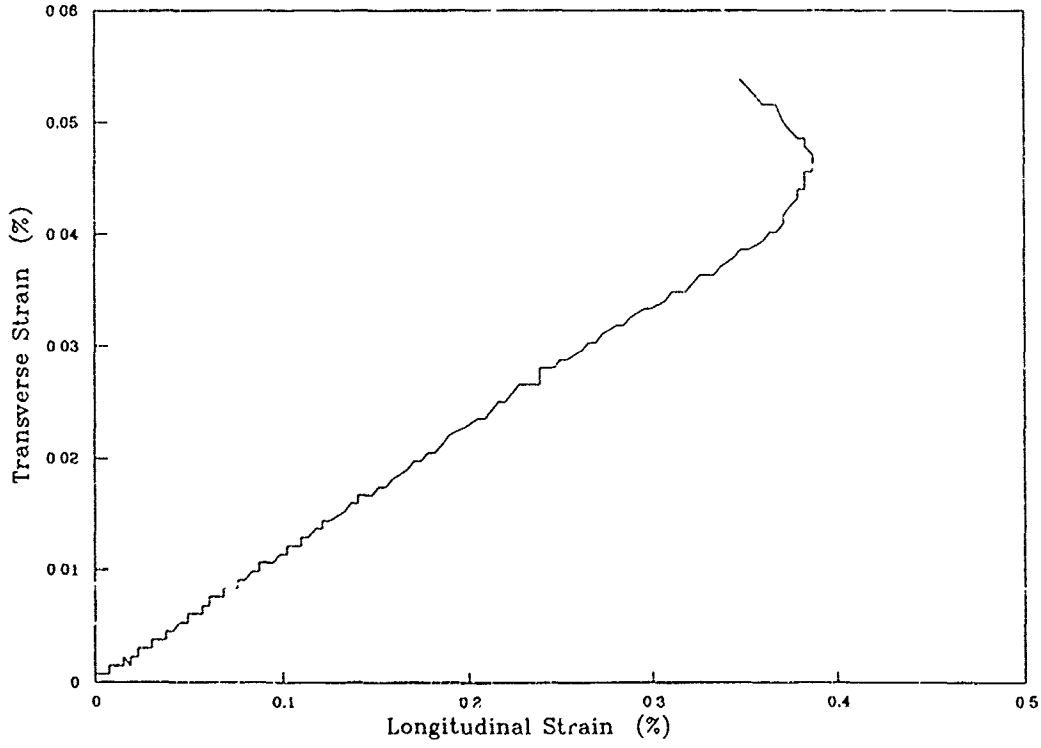

APPENDIX I

Fig. A1a RAW DATA FOR QUASI-STATIC TEST

Hybrid Carbon/Glass Specimen, Load Cell Signal (ch1)

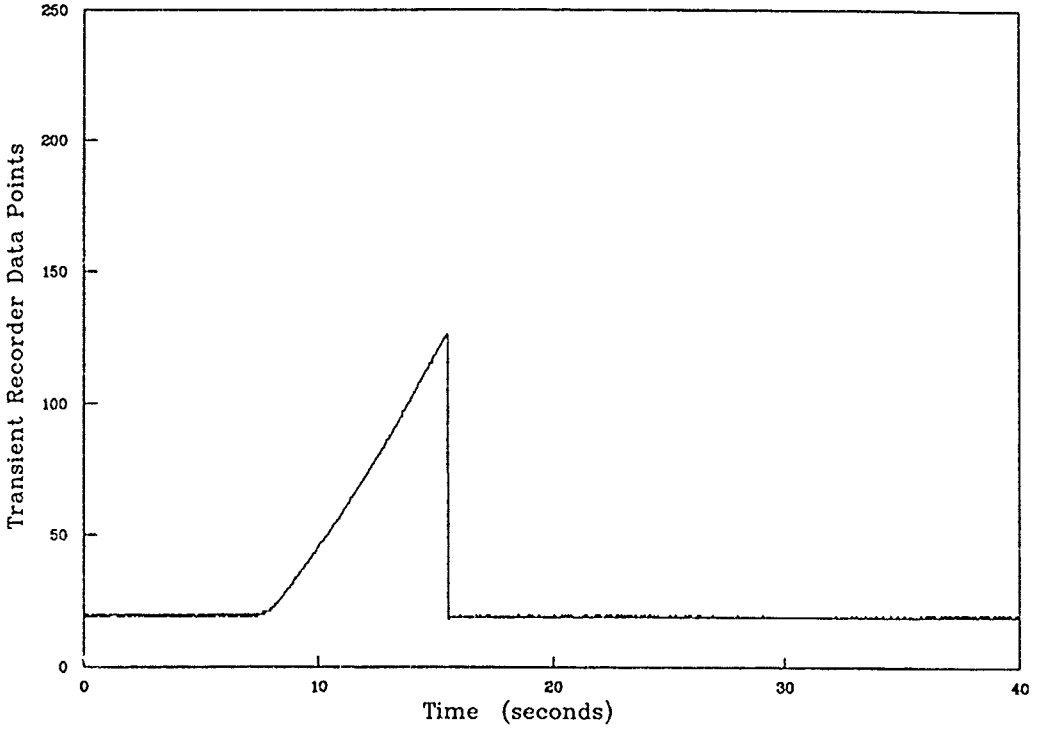

Fig. A1b RAW DATA FOR QUASI-STATIC TEST

Hybrid Carbon/Glass Specimen, Displacement Transducer Signal (ch2)

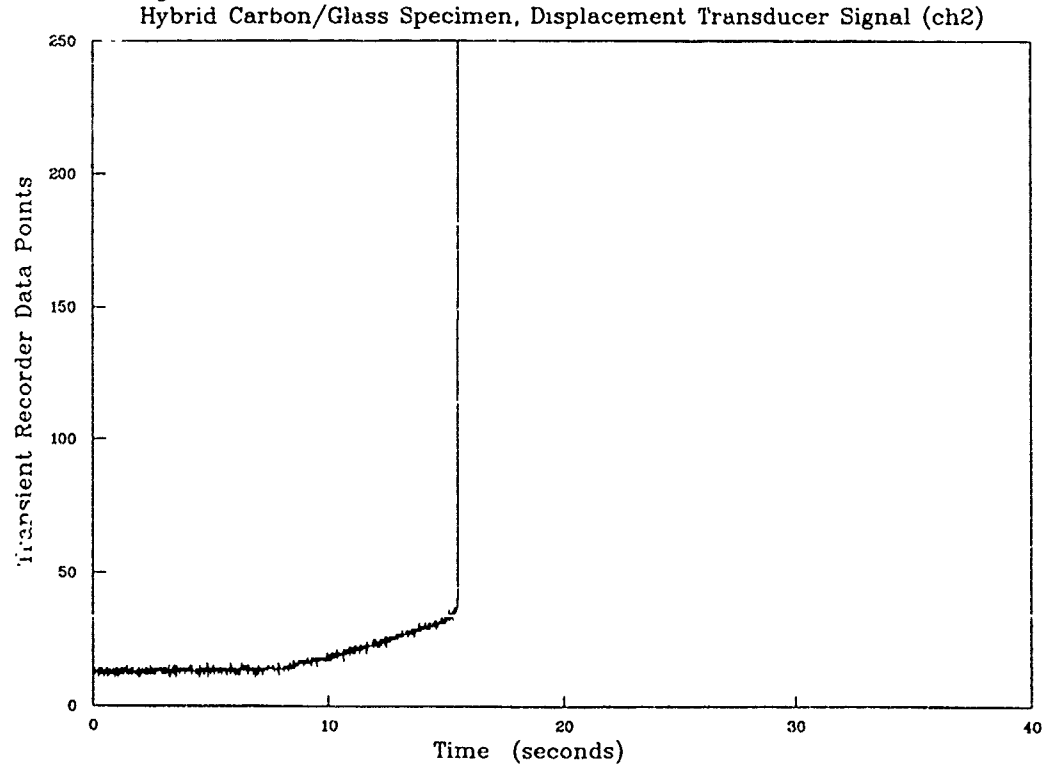

Fig. A1c RAW DATA FOR QUASI-STATIC TEST

Hybrid Carbon/Glass Specimen, Strain Gauge Signal (ch3)

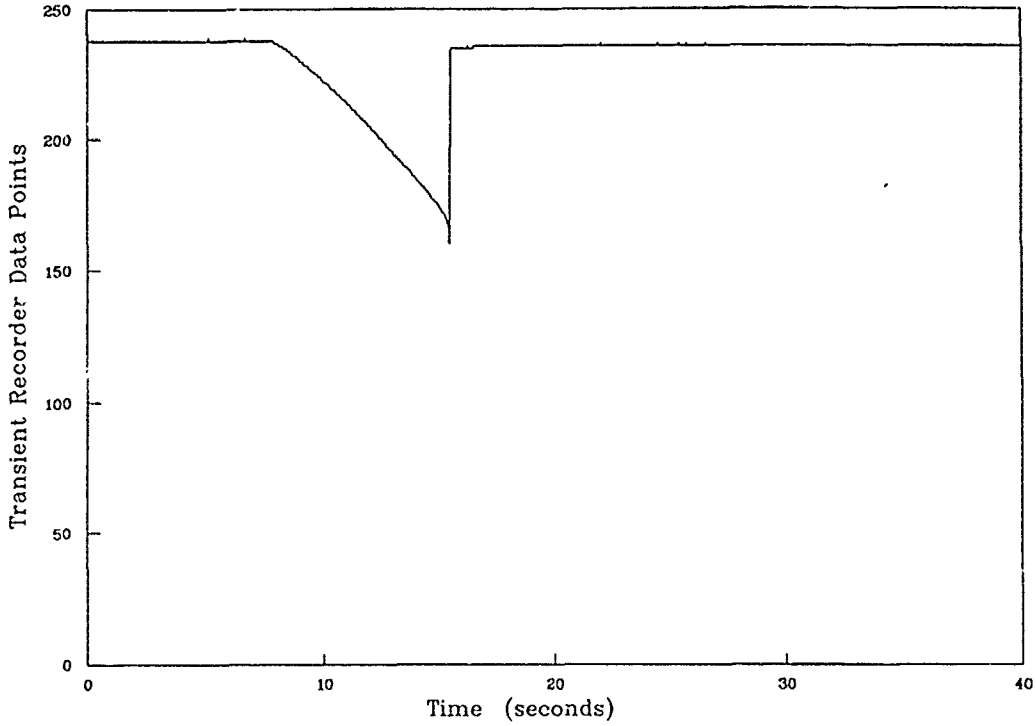

Fig. A1d RAW DATA FOR QUASI-STATIC TEST

Hybrid Carbon/Glass Specimen, Strain Gauge Signal (ch4)

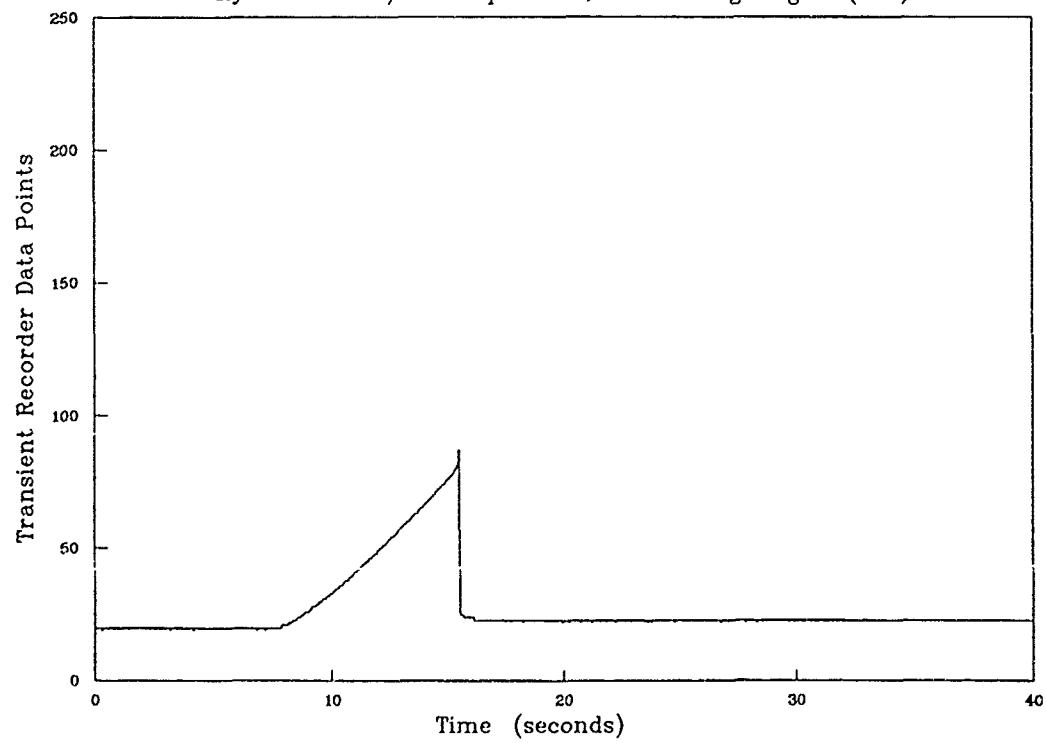

Fig. A1e RAW DATA FOR QUASI-STATIC TEST

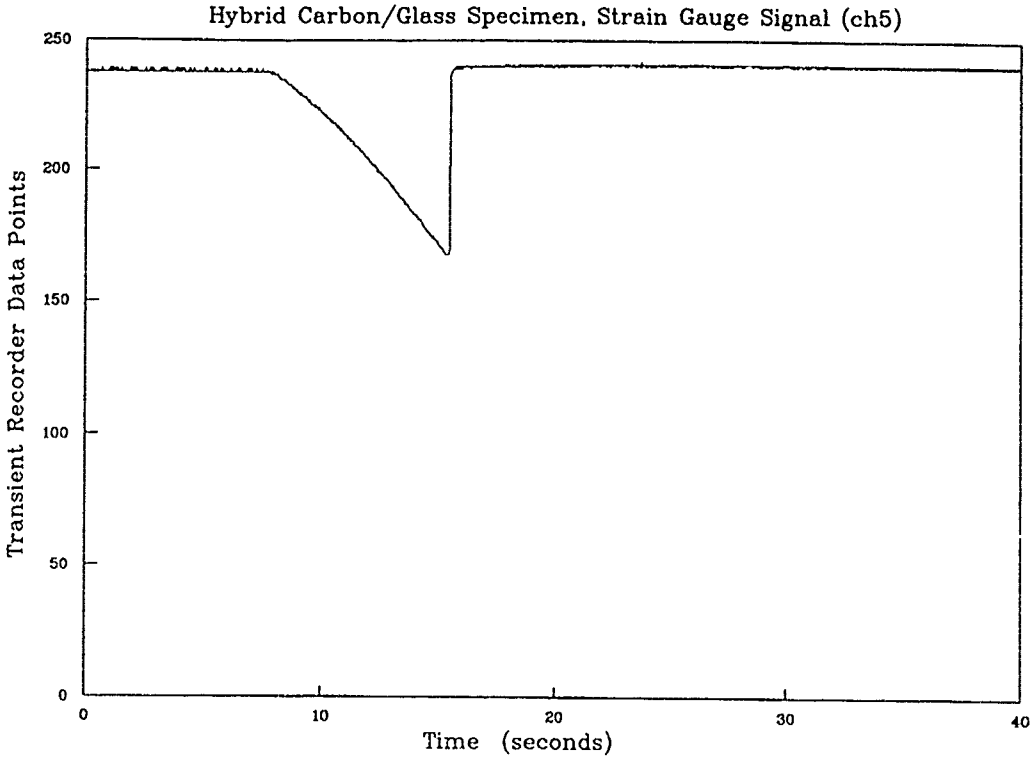

Fig. A1f RAW DATA FOR QUASI-STATIC TEST

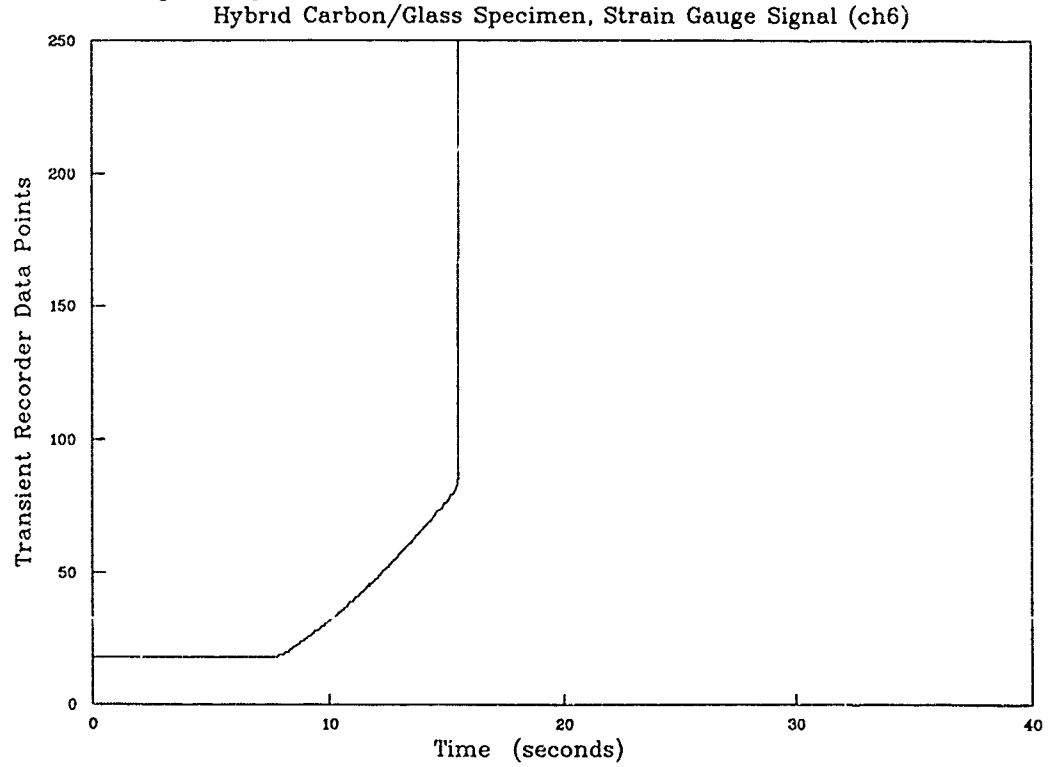

Fig. A2a RAW DATA FOR QUASI-STATIC TEST

Plain-Weave Glass Specimen, Load Cell Signal (ch1)

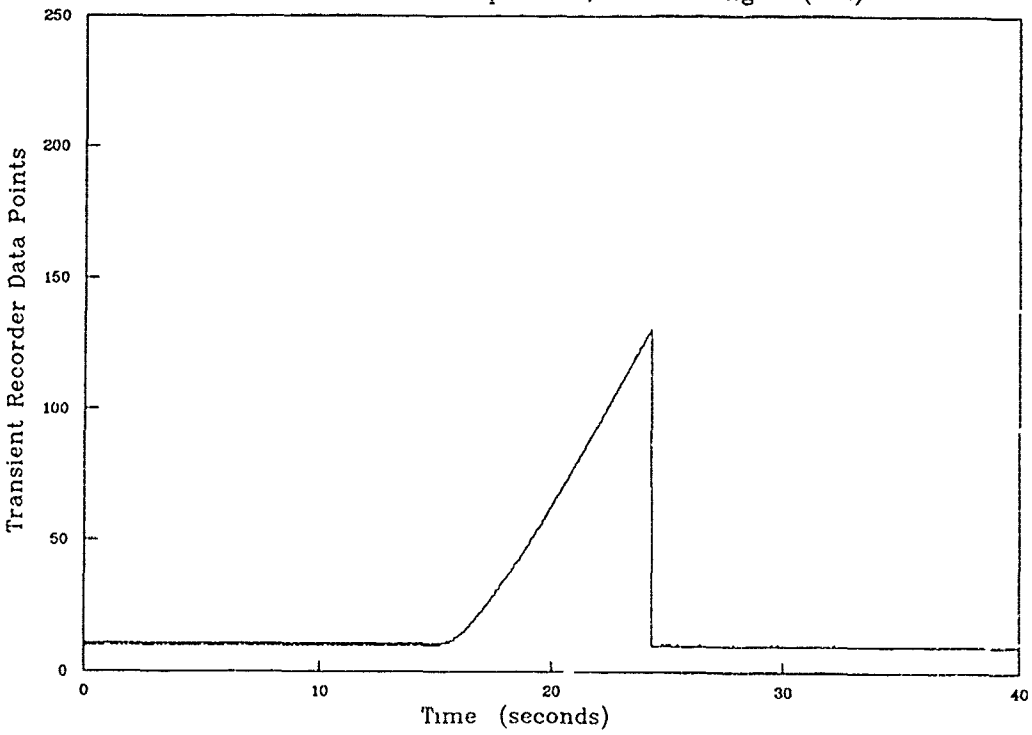

Fig. A2b RAW DATA FOR QUASI-STATIC TEST

Plain-Weave Glass Specimen, Displacement Transducer Signal (ch2)

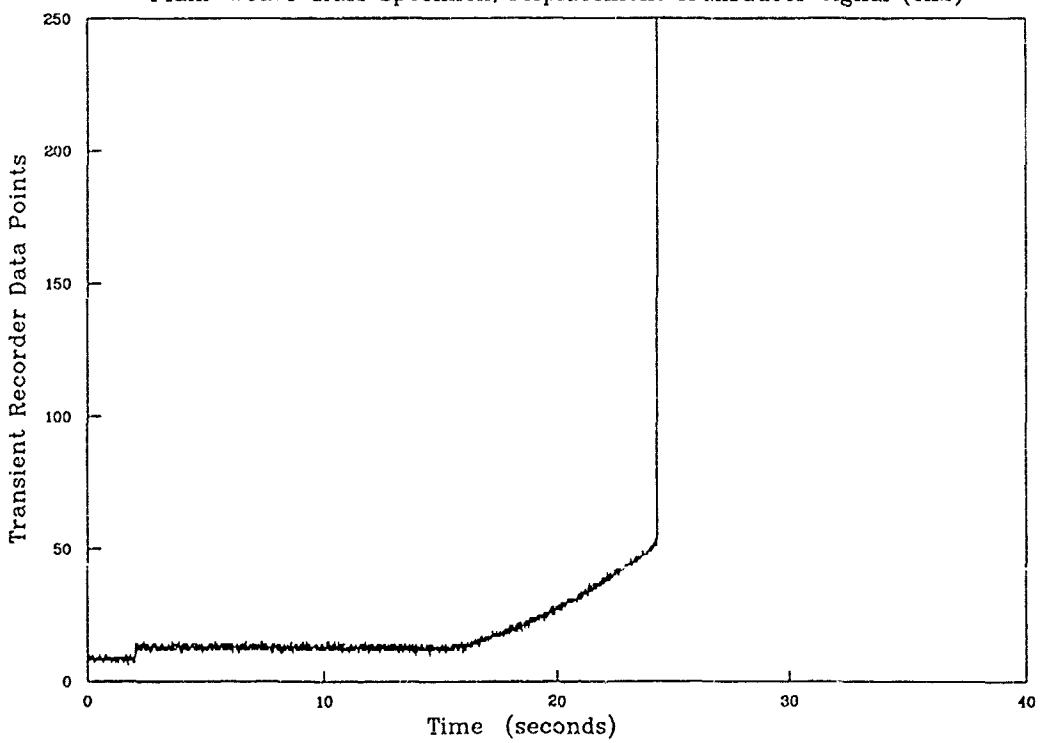

Fig. A2c RAW DATA FOR QUASI-STATIC TEST

Plain-Weave Glass Specimen, Strain Gauge Signal (ch3)

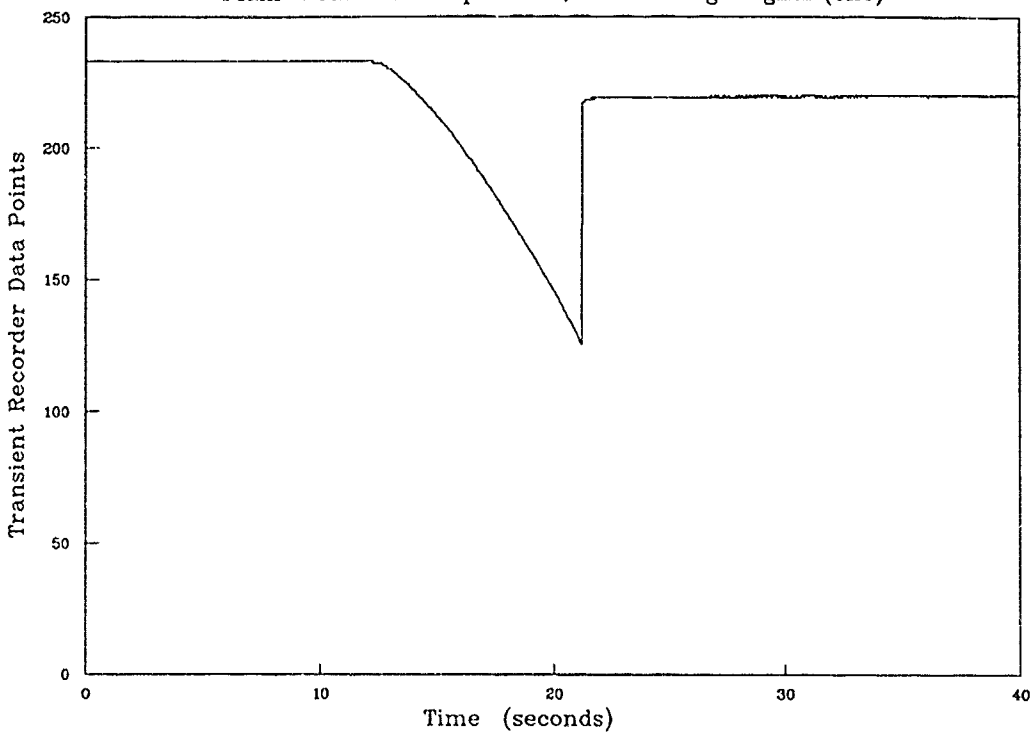

Fig. A2d RAW DATA FOR QUASI-STATIC TEST

Plain-Weave Glass Specimen, Strain Gauge Signal (ch4)

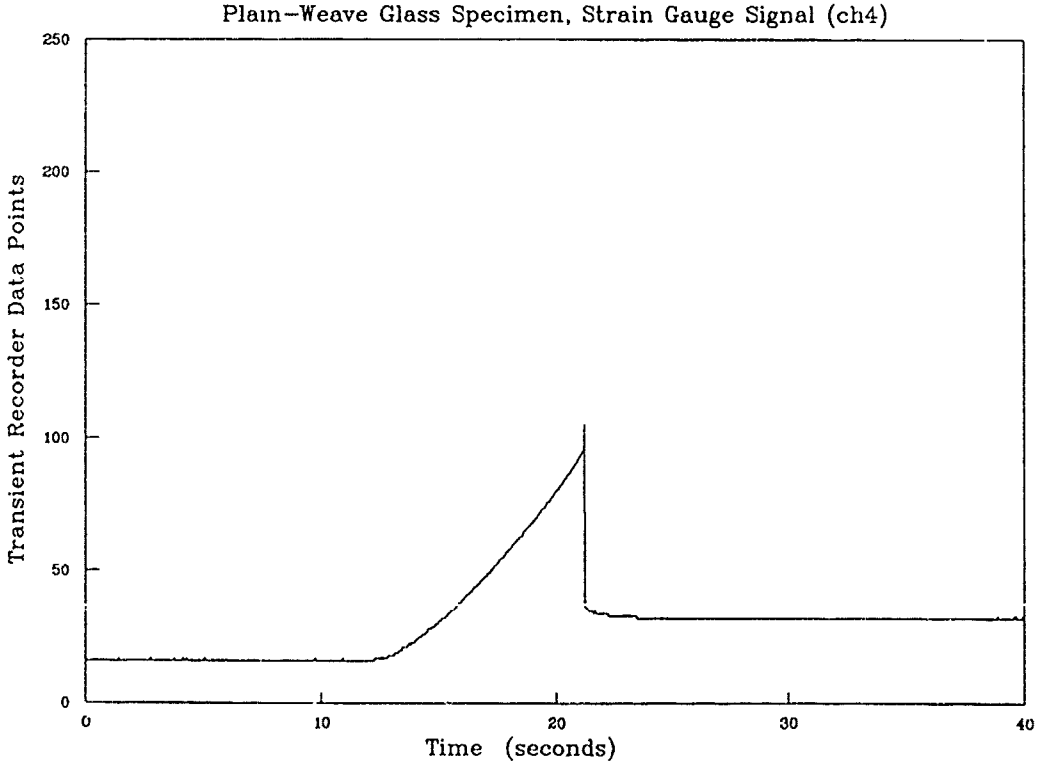

Fig. A2e RAW DATA FOR QUASI-STATIC TEST

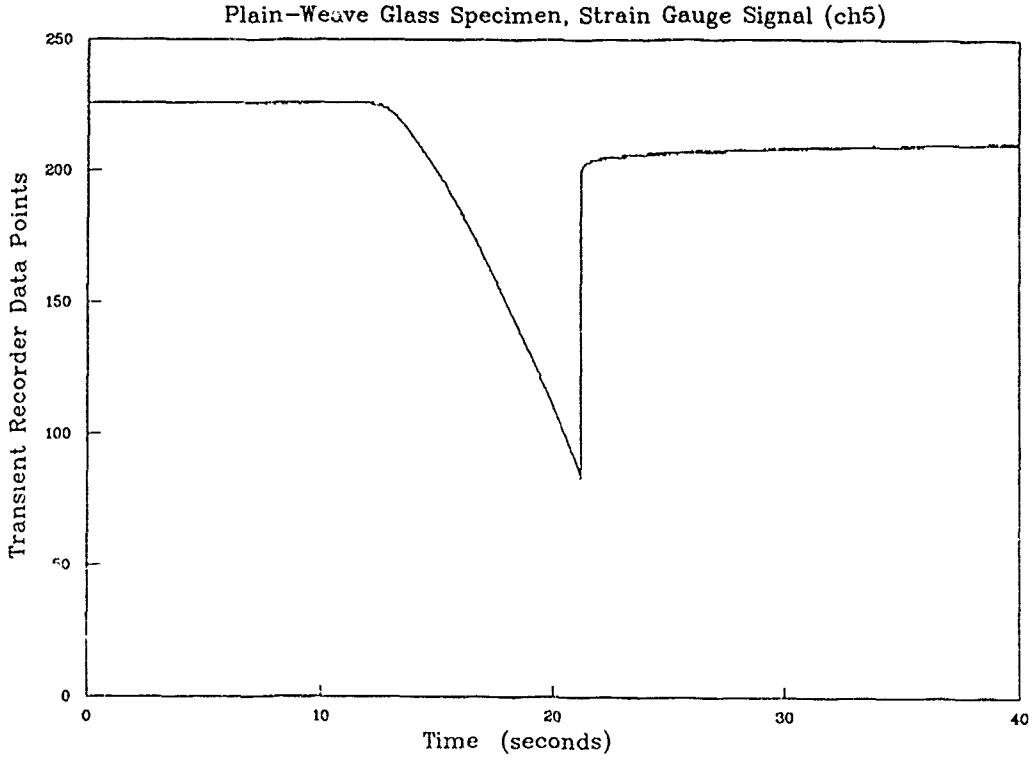

Fig. A2f RAW DATA FOR QUASI-STATIC TEST

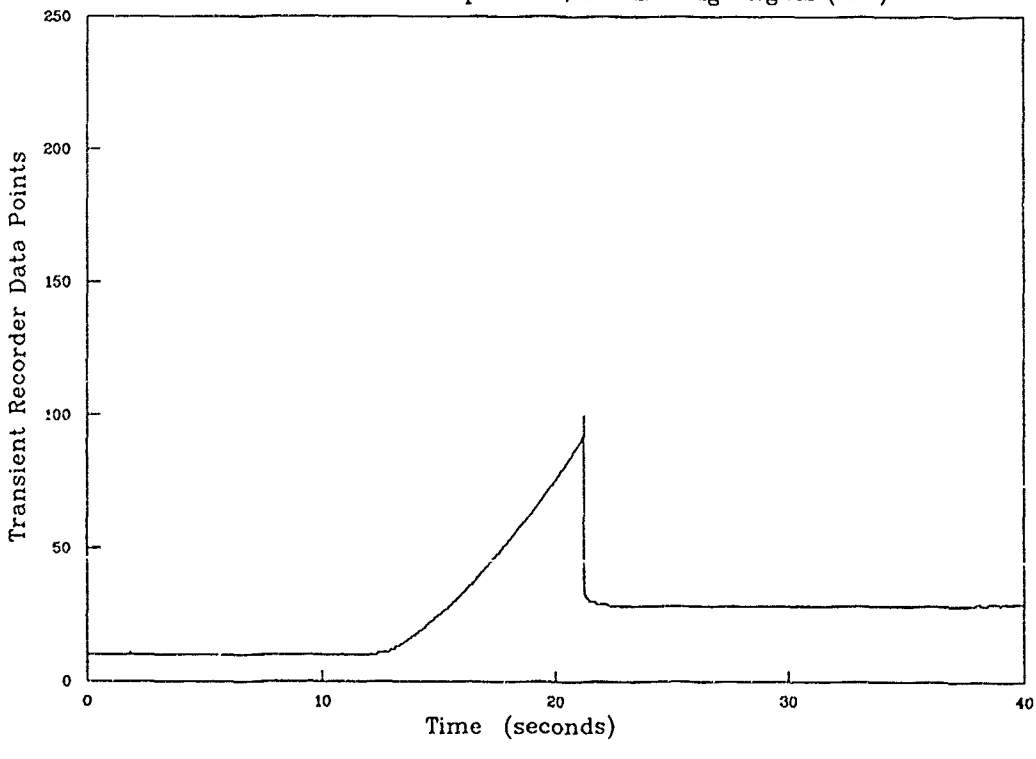

Fig. A3a RAW DATA FOR QUASI-STATIC TEST

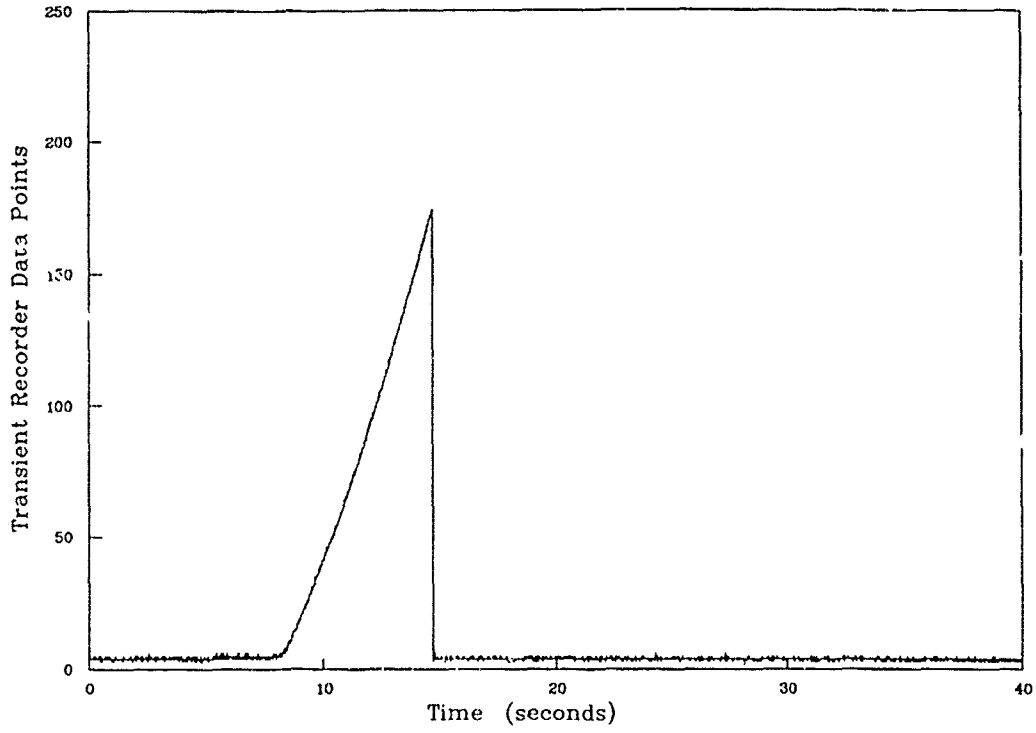

Fig. A3b RAW DATA FOR QUASI-STATIC TEST

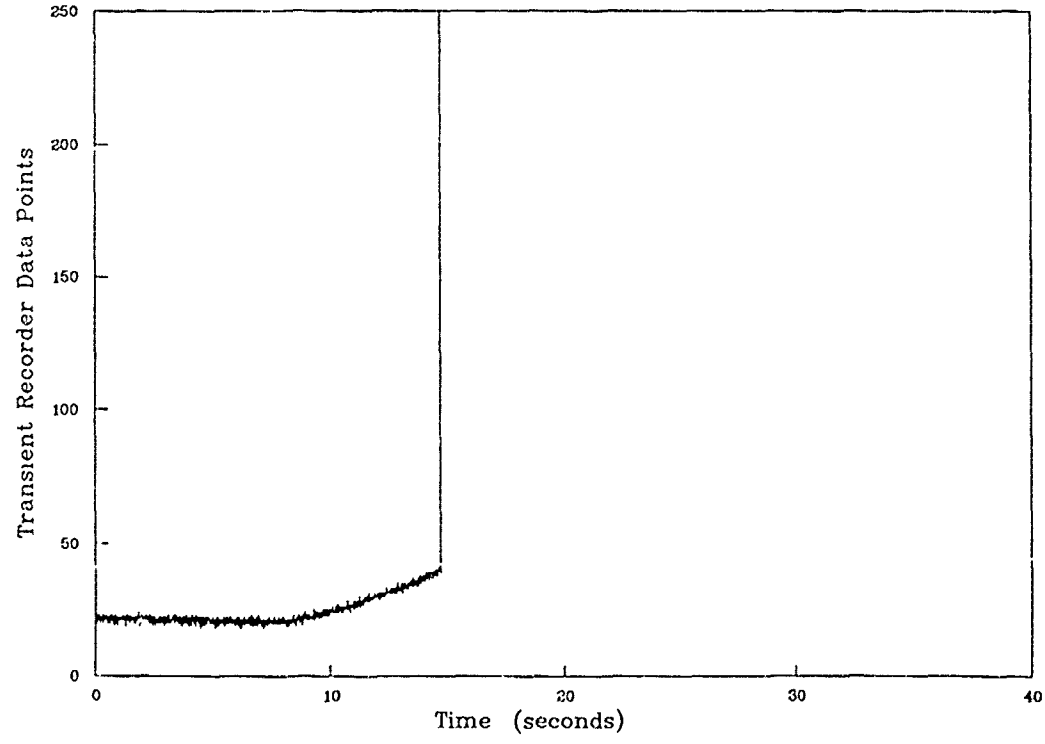

Fig. A3c RAW DATA FOR QUASI-STATIC TEST

Satin-Weave Carbon Specimen, Strain Gauge Signal (ch3)

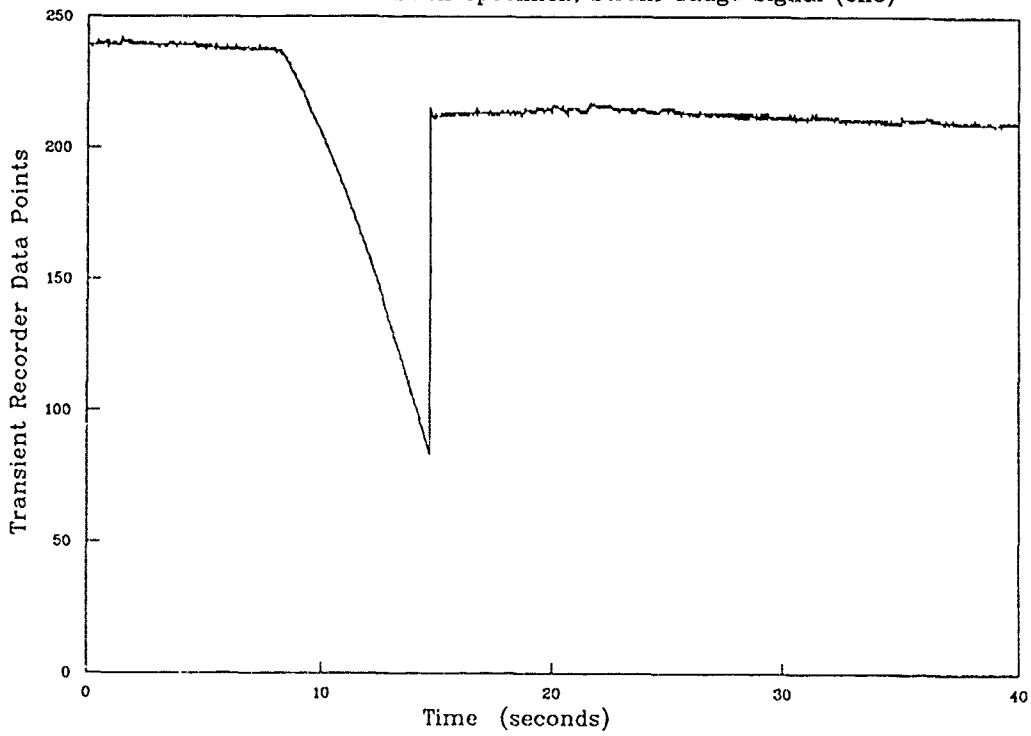

Fig. A3d RAW DATA FOR QUASI-STATIC TEST

Satin-Weave Carbon Specimen, Strain Gauge Signal (ch4)

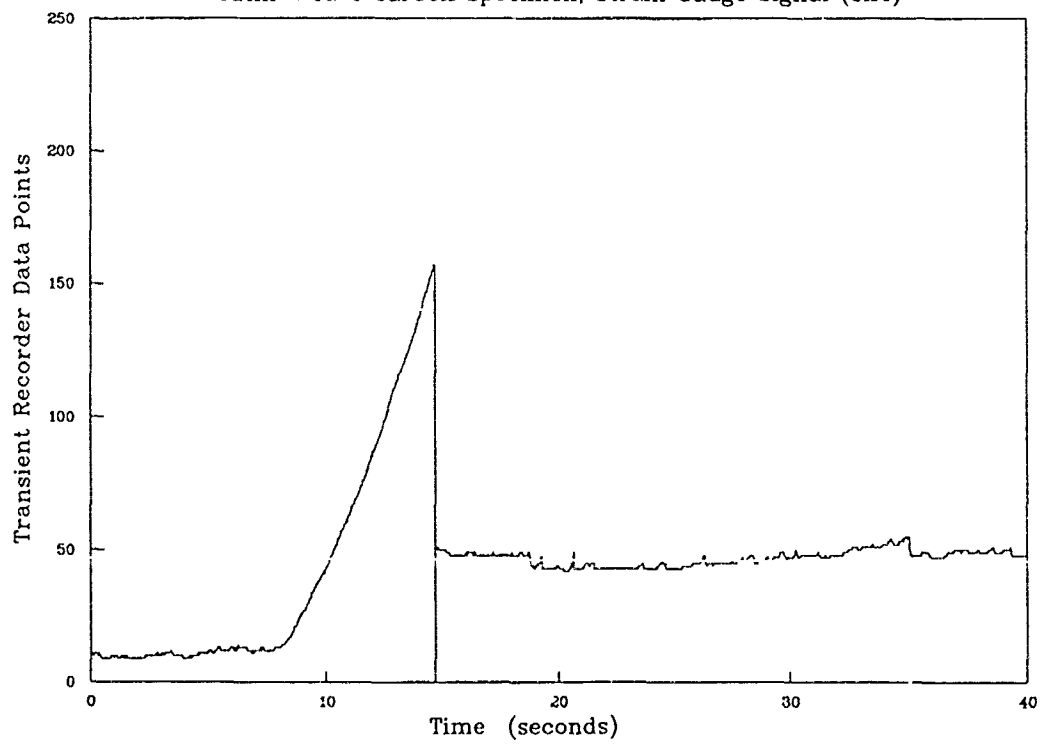

Fig. A3e RAW DATA FOR QUASI-STATIC TEST

Satin-Weave Carbon Specimen, Strain Gauge Signal (ch5)

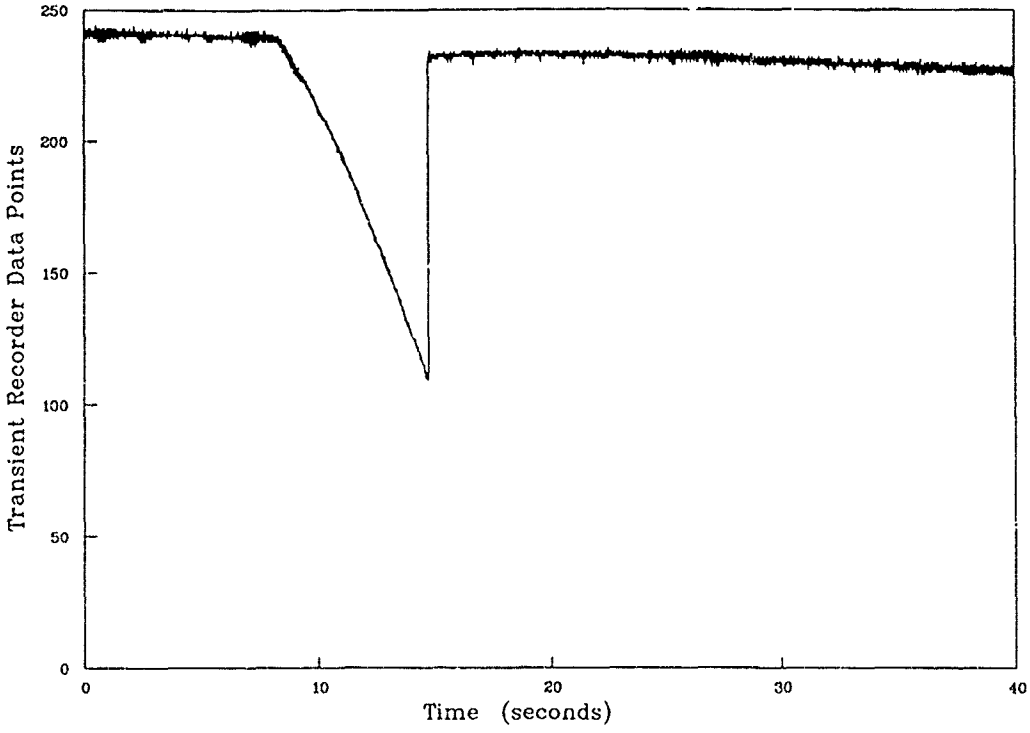

Fig. A3f RAW DATA FOR QUASI-STATIC TEST

Satin-Weave Carbon Specimen, Strain Gauge Signal (ch6)

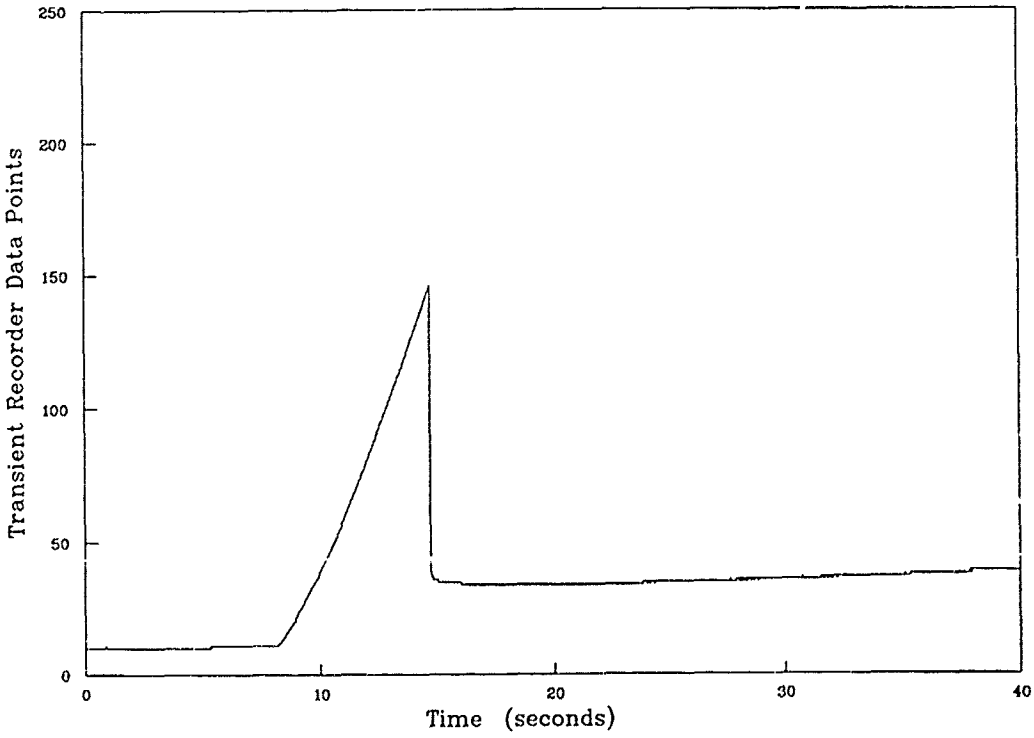

Fig. A4a STRESS v LONGITUDINAL STRAIN

Quasi-Static Test on Hybrid Carbon/Glass Specimen (ch1 v ch6)

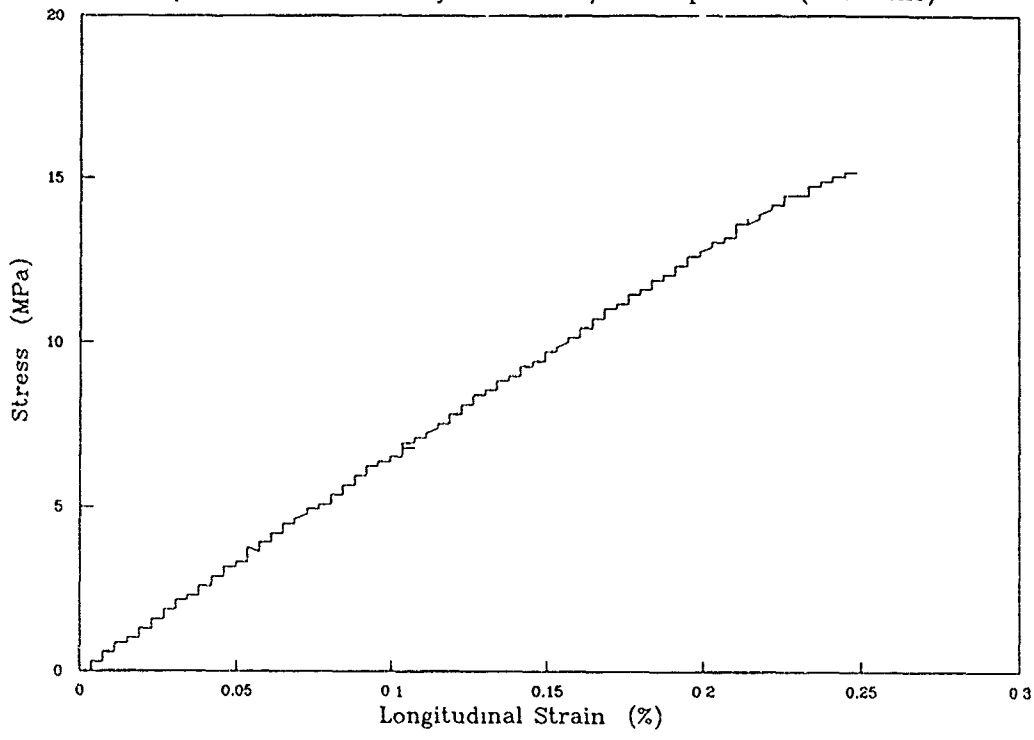

Fig. A4b STRESS v LONGITUDINAL STRAIN

Quasi-Static Test on Hybrid Carbon/Glass Specimen (ch1 v ch4)

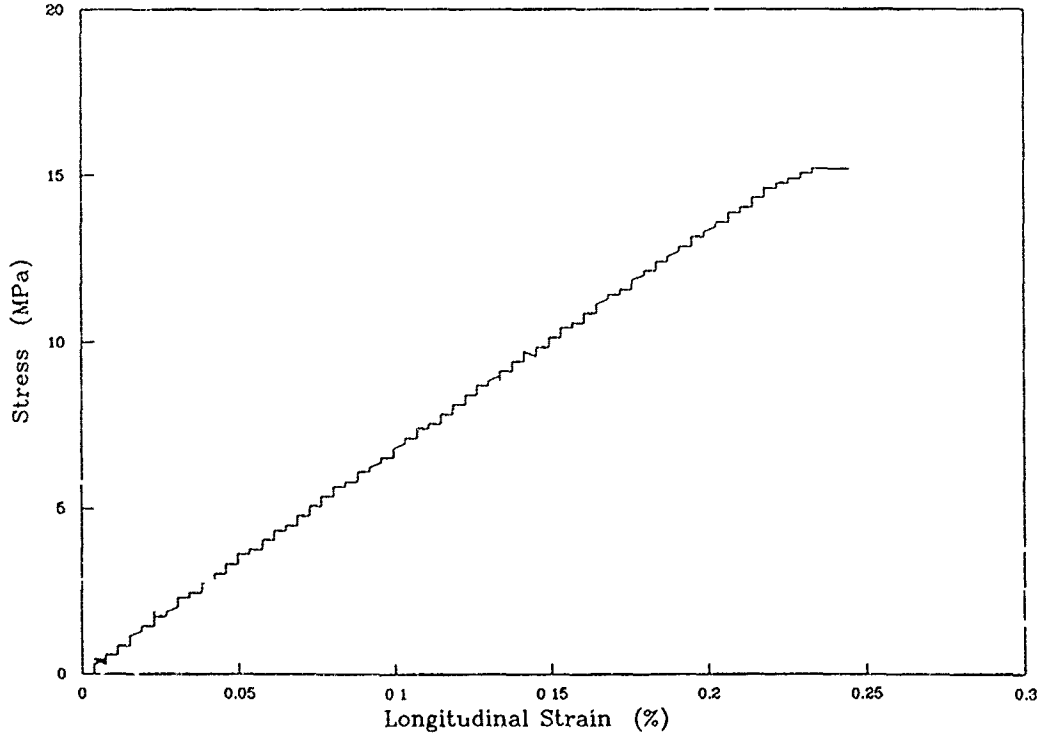

Fig. A4c TRANSVERSE STRAIN v LONGITUDINAL STRAIN

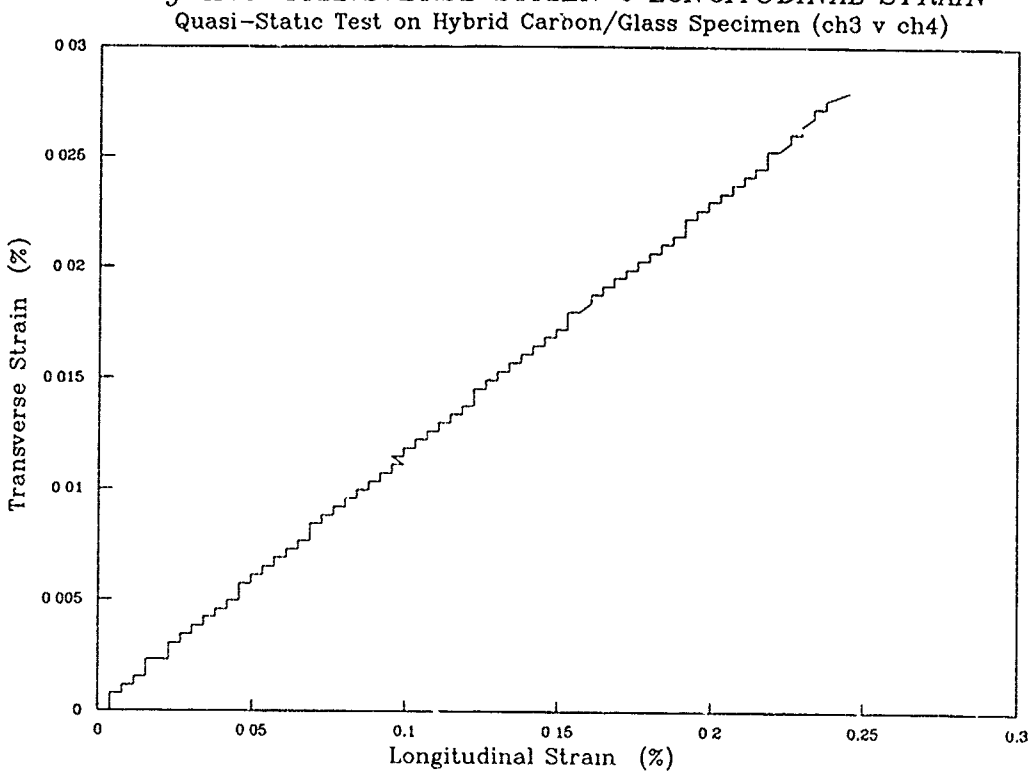

Fig. A4d TRANSVERSE STRAIN v LONGITUDINAL STRAIN

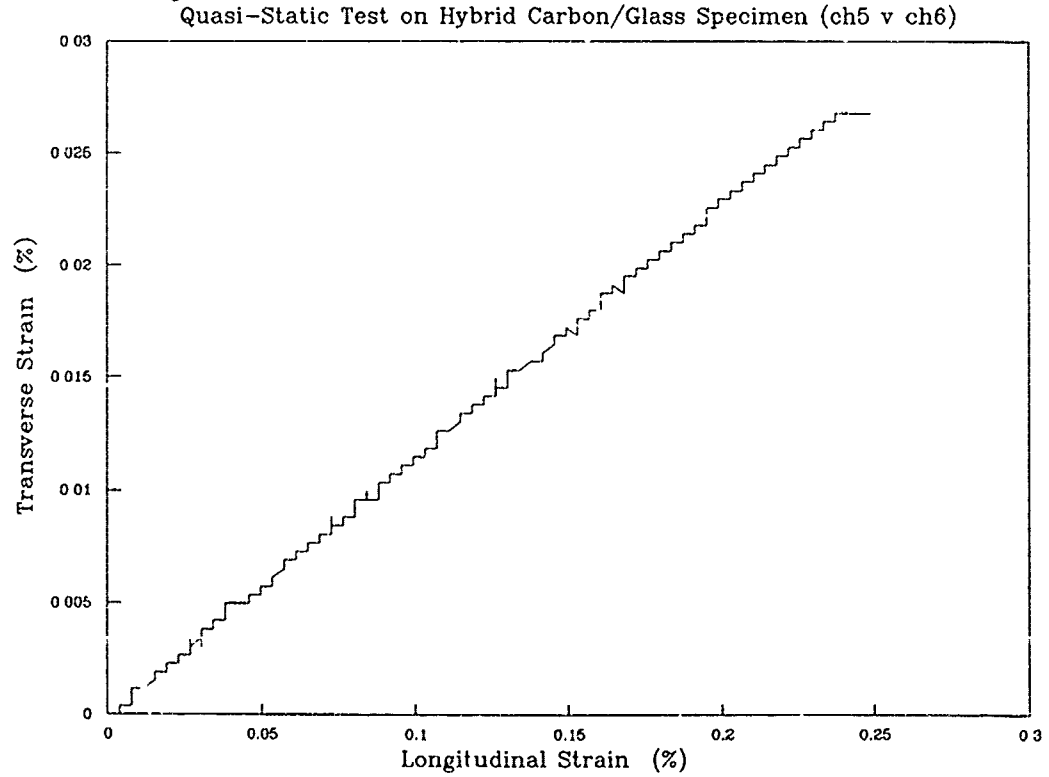

Fig. A5a STRESS v LONGITUDINAL STRAIN

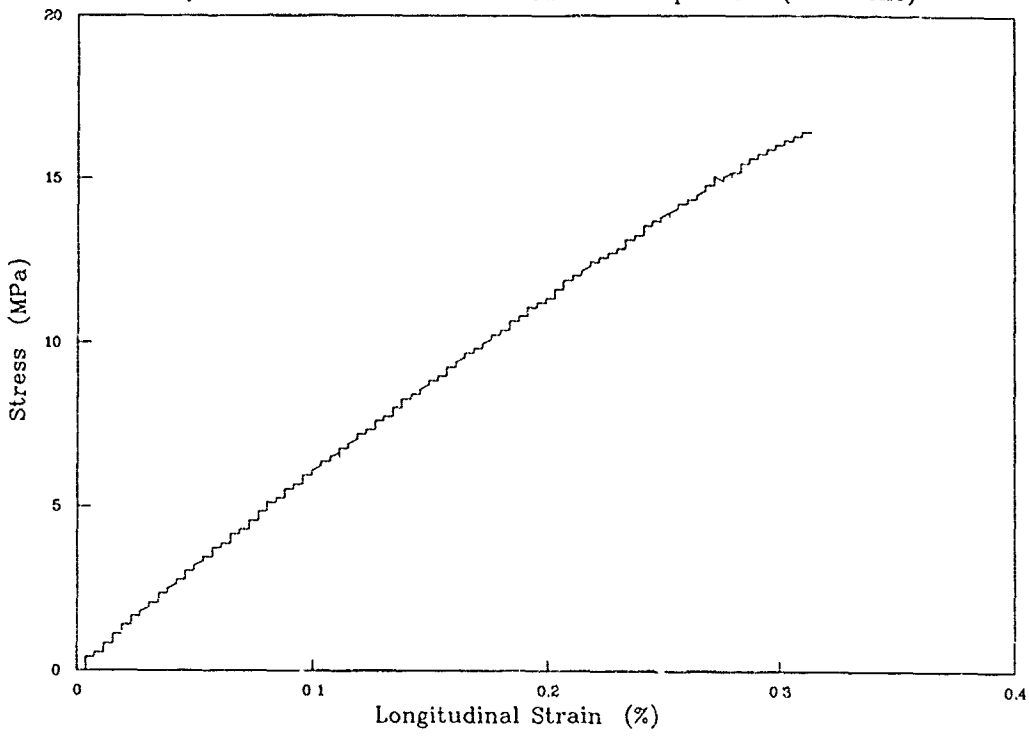

Fig. A5b STRESS v LONGITUDINAL STRAIN

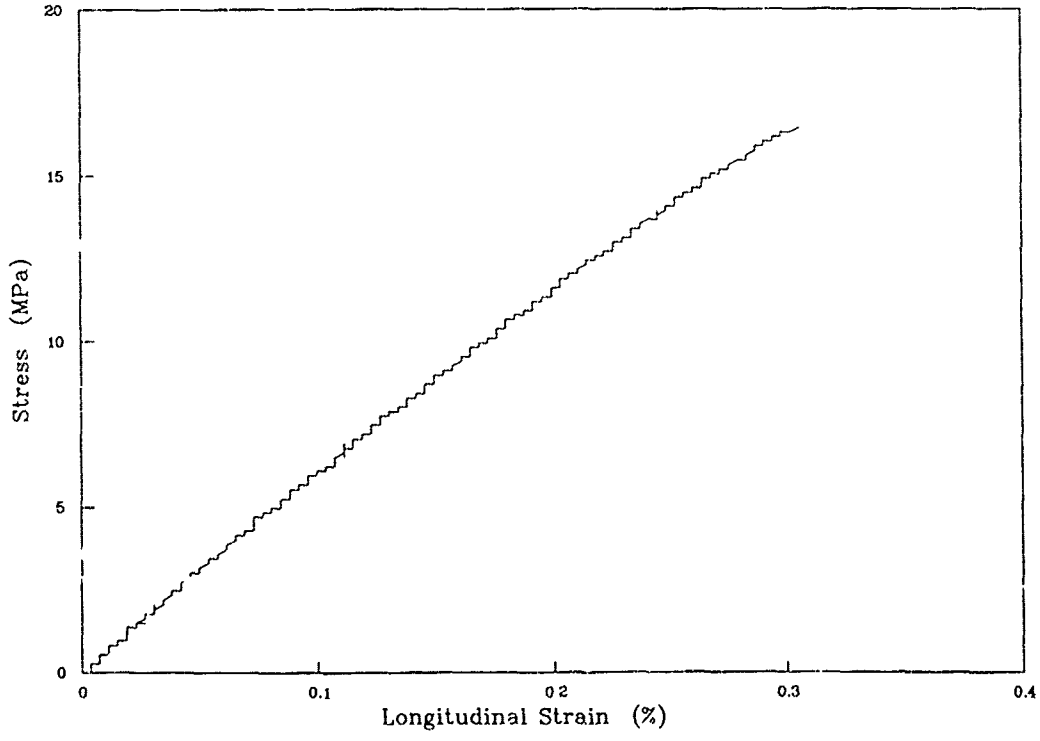

Fig. A5c TRANSVERSE STRAIN v LONGITUDINAL STRAIN

Quasi-Static Test on Plain-Weave Glass Specimen (ch3 v ch4)

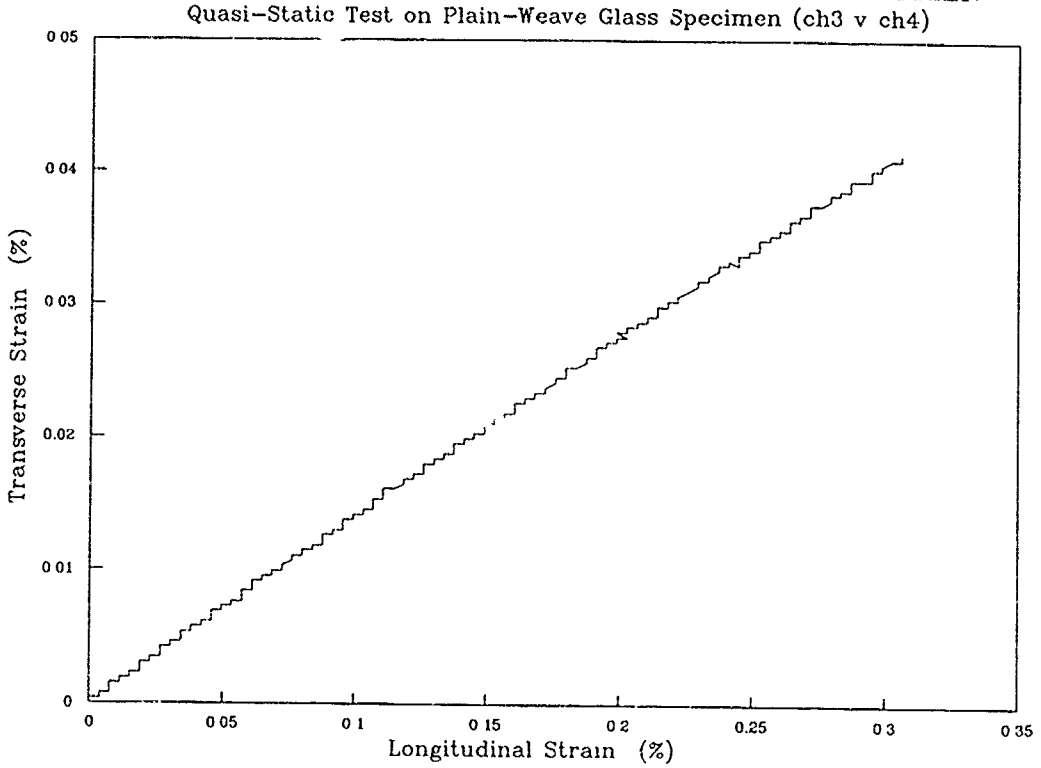

Fig. A5d TRANSVERSE STRAIN v LONGITUDINAL STRAIN

Quasi-Static Test on Plain-Weave Glass Specimen (ch5 v ch6)

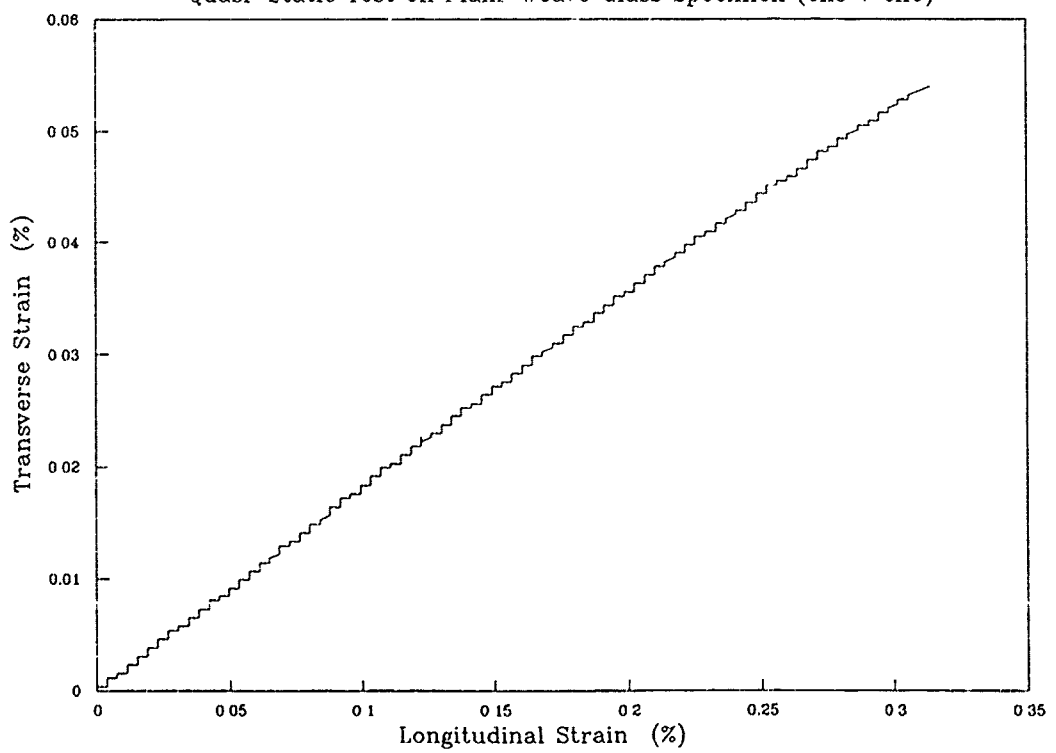

Fig. A6a STRESS v LONGITUDINAL STRAIN

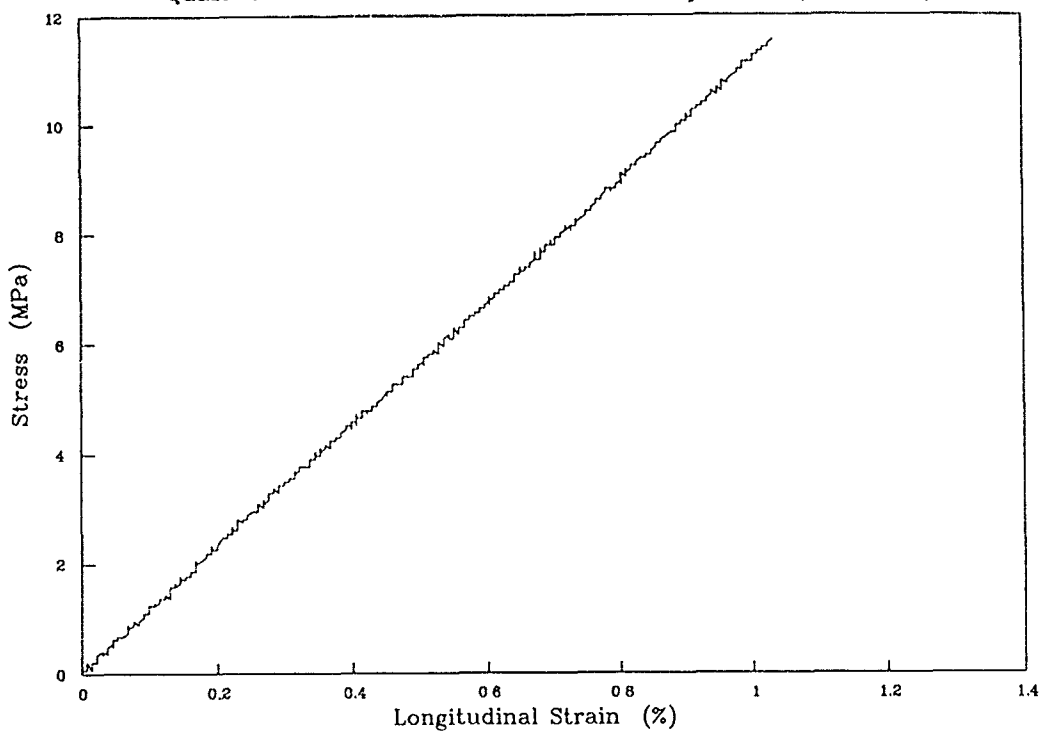

Fig. A6b STRESS v LONGITUDINAL STRAIN

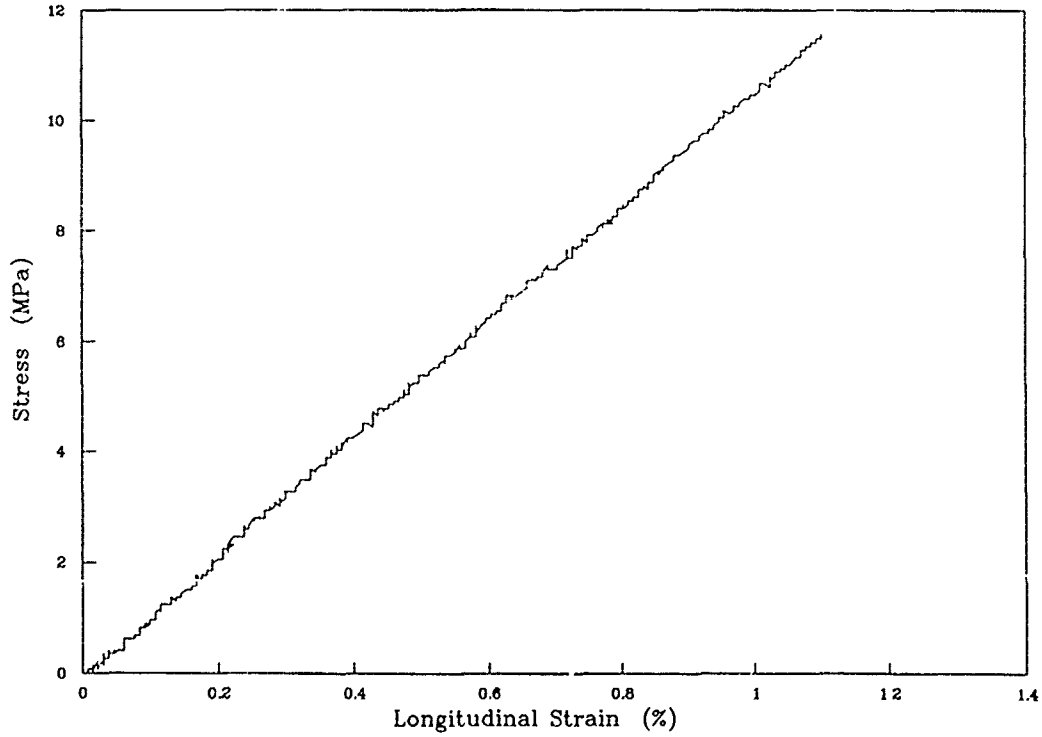

Fig. A6c TRANSVERSE STRAIN v LONGITUDINAL STRAIN

Quasi-Static Test on Satin-Weave Carbon Specimen (ch3 v ch4)

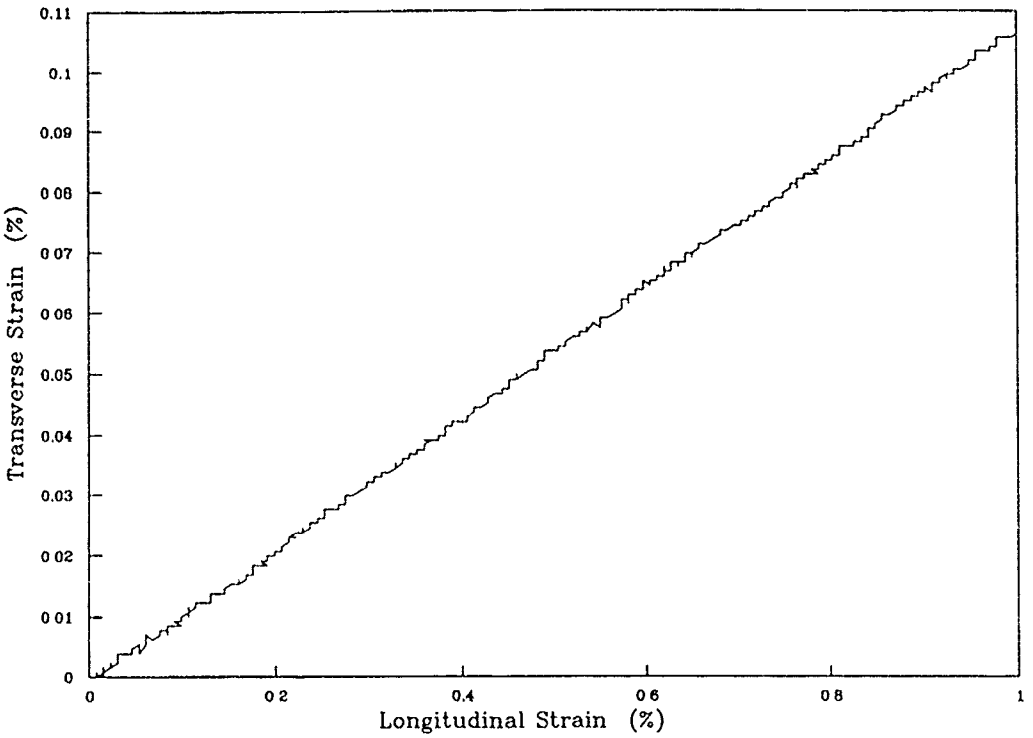

Fig. A6d TRANSVERSE STRAIN v LONGITUDINAL STRAIN

Quasi-Static Test on Satin-Weave Carbon Specimen (ch5 v ch6)

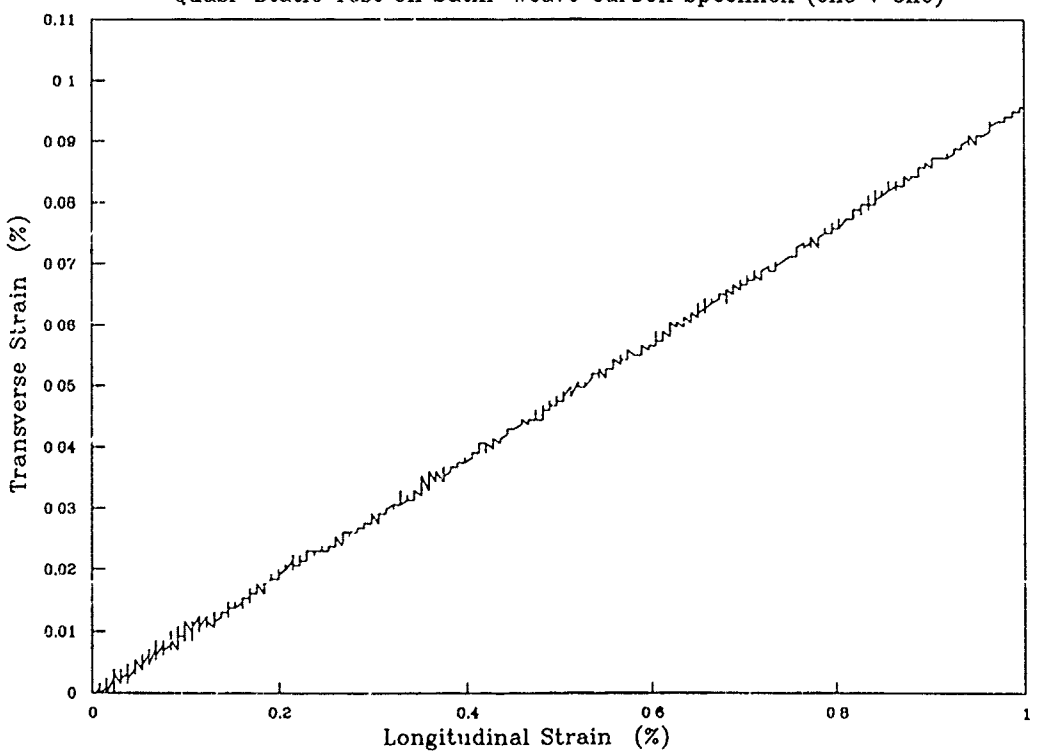

APPENDIX II

A New Type Of Shear Specimen For Measuring The Interlaminar Shear Strength Under Impact Loading

Y.L.Li J.Harding C.Ruiz

Abstract

Two new designs of shear specimen, suitable for use in the Hopkinson bar to measure the interlaminar shear strength in woven reinforced composite materials at different strain rates, are presented in this report. The finite element method was used to calculate the shear stress distribution along the shear plane. The results show a more uniform shear stress in the second design of specimen. The introduction of small notch to initiate shear failure on a pre-chosen plane results in a small stress concentration near the notch tip. However, this stress concentration is much smaller than that for the first design, a double lap shear specimen, and for other specimens previously used to measure impact shear strength.

1 Introduction

Hybrid composite materials have found wide application and there is a growing need to characterize their behaviour under both static and impact loading. Generally, a hybrid composite material contains both low elongation and high elongation fibres. The first failure is likely to be that of a low elongation fibre. The resulting stress and strain distribution after failure of a carbon ply in a hybrid carbon/glass tensile specimen has been studied[1] using the finite element method and three subsequence failure modes have been identified. One is the fracture of the nearest high elongation (glass) plies. Another is fracture of the nearest low elongation (carbon) plies. These two modes are both induced by the tensile stress concentration at the site of the first broken carbon ply. The third failure mode is delamination between failure ply and the neighbouring plies due to the large shear stress concentration on the interlaminar plane. Which mode of failure actually follows failure of the first carbon ply is determined by the ratios of the tensile strength and interlaminar shear strength to the respective applied tensile and shear stress close to the site of the first ply failure. A knowledge of the interlaminar shear strength under high rates of strain is also important when studying practical problems associated with transverse impact of composite plates there delamination is a major failure mode.

The interlaminar shear strength plays an important role, therefore, not only in failure analysis of hybrid composite materials but also in engineering design.

The measurement of interlaminar shear strength is a difficult problem under static loading and it is certainly no easier under impact loading. For static loading, the specimen should satisfy, or approximately satisfy, two conditions. One is that the distribution of the shear stress in the failure plane should be uniform. The other is that in the failure plane, the shear stress should be much larger than the other stresses, approach a state of pure shear. For impact loading, besides these two conditions, it is necessary that the specimen should be suitable for testing in a dynamic loading device such as Hopkinson bar. In theory, thin tubular specimens not only satisfy the two conditions for quasi-static loading, but also can be used in the torsional Hopkinson bar system. It is an ideal design, therefore, for comparing static and impact behaviour. However, when a composite material is to be studied, thin tubular specimens are very difficult to manufacture. This design has not, therefore, been adopted by many researchers. The search for a proper shear specimen to measure the interlaminar shear strength is not over, especially for impact loading conditions.

A larger number of testing procedures have been proposed and tried in an attempt to measure the inplane and out of plane shear properties of composite materials. These include the double lap shear test [2], the off-axis tension test [3], the $\pm 45°$ tension test [4-6], the two rail or three rail shear test [7-8], the slotted tensile test [9], the plane-twist test [10], the short beam test [11-12], the Iosipescu shear test [13-15] and the Arcan shear test [17-18]. Each of these experimental methods has disadvantages and advantages. Some of them are briefly reviewed as below.

1.1 The $\pm 45°$ shear test

The $\pm 45°$ shear test can be used to measure the inplane shear stress-strain response of a laminate. The specimen is loaded in the direction of $\pm 45°$ from the principal directions of reinforcement as shown in Fig. 1(a). If the modulus of reinforcement, E_A and E_B, are known the inplane shear modulus G_{AB} can be obtained from the modulus in the $\pm 45°$ direction using the orthotropic transformation equation:

$$G_{AB} = \left[\frac{4}{E_x} - \frac{1}{E_A} - \frac{1}{E_B} + \frac{2\nu_{AB}}{E_A}\right]^{(-1)} \tag{1}$$

where ν_{AB} is Poisson ratio. An alternative method for determining the shear modulus was proposed by Petit[5] using a single tension test on a $[\pm 45°]_s$ laminate. In the simplified form developed by Rosen[6] this gives

$$G_{AB} = \sigma_x / 2(\varepsilon_x - \varepsilon_y) \tag{2}$$

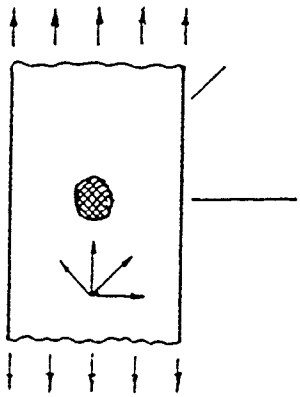

(a) ±45° shear test

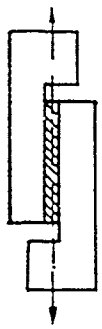

(b) Two tail shear test

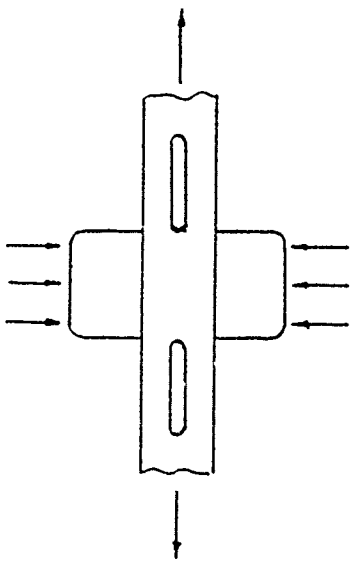

(c) Slotted tensile test

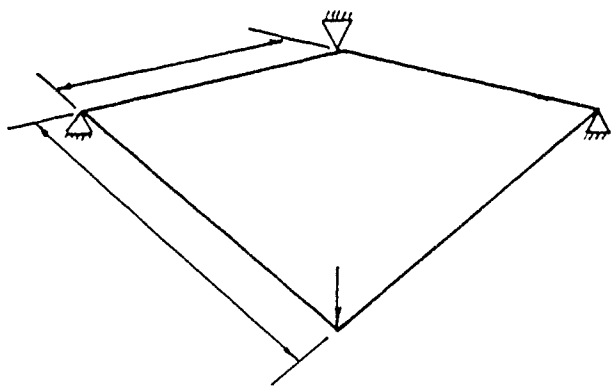

(d) Plate twist test

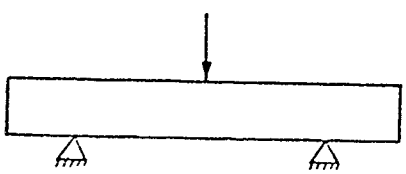

(e) Short beam test

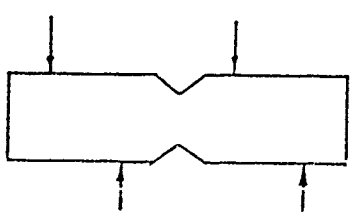

(f) Isoipescu shear test

Fig. 1

where the x-direction, the direction of loading, is at ±45° to the reinforcing directions so that the shear stress and strain are given by

$$\tau_{AB} = \sigma_x/2 \qquad \gamma_{AB} = \varepsilon_x - \varepsilon_y$$

the shear stress can also be expressed as following equation:

$$\tau_{AB} = \frac{P}{2A} \tag{3}$$

where P is the magnitude of loading in +45° or -45° off fibre direction. A is the section area of tensile coupon. The specimen can be easily used under static and impact condition. Unfortunately, the ±45° shear test only provides the inplane shear stiffness and the strength. The interlaminar shear properties cannot be measured using this specimen.

1.2 The two rail or three rail shear test

The two rail shear test first was introduced to measure the shear properties of composite material by Hennessey el al [7]. The shear stress is applied to the plate specimen by gripping the plate along one side and then applying the load along the opposite side as shown in Fig. 1(b). The shear stress in the central region of specimen is assumed to be uniform. It can be determined by the simple relationship:

$$\tau = \frac{P}{A} \tag{4}$$

where A is the section area parallel to the gripping side and P is the applied load. Whitney [19] and Garciam [20] show that the test area length-to-width aspect ratio has a major effect on the stress distribution, the magnitude of the effect varying with the laminate. Reference[19] suggests that the aspect ratio of the test section should be at least 10 in order to achieve a nearly uniform shear stress distribution. Unfortunately increasing the length can induce a strong stress concentration at the corner of the specimen so that early failure occur at this point.

The rail shear test was expected to provide the shear properties for laminates with arbitrarily orientated plies. However, as pointed out by Whitney [19] the presence of a large percentage of ±45° plies can cause stress singularities at the frame corners which distort the stress distribution throughout the test section. The rail shear test is designed for measuring the inplane shear properties . It cannot be used to measure the out of plane properties or under impact conditions.

The three rail shear test is just a symmetrical version of the two rail shear test.

1.3 Slotted tensile test

The slotted tension shear test was suggested and developed for measuring the in-plane properties of composite materials by Duggan [9]. It is based on the principle that the biaxial normal stress is equivalent to pure shear stress on the plane orientated $\pm 45°$ relative to the orthogonal axes of applied load if the magnitude of normal stresses is equal and the direction is opposite as shown in Fig. 1(c). The stress state can be simulated by loading a tension coupon in the tension along it's major axis and simultaneously compressing it along a portion of it's length in the transverse direction. The axially orientated slots in the specimen insure that the compressive force is transmitted only through the rectangular test section so that the shear stress state will be statically determinate to a good approximation. The shear stress in the test section is given by following equation:

$$\tau = \sigma \tag{5}$$

where σ is the magnitude of the tension and compression stress in the axial and the normal direction respectively. As pointed out in reference [9], the slotted shear test is both an inexpensive and material efficient test for measuring shear properties of isotropic or fibre reinforced materials. Nor are any restrictions on fibre orientation or ply-stacking order placed on the material to be tested. The problem is that special biaxial test equipment is required. This is often not readily available. Also out of plane properties cannot be obtained from the test nor can the shear properties under impact loading.

1.4 The plate twisting test

The plate twisting test is another method design to measure the inplane shear properties. It was introduced first to measure the shear properties of orthotropic materials by Hearmon el al [10] and was later improved by Tsai [21]. The principle of this method is based on the solution of the differential equation for an anisotropic plate under uniform bending and twisting moments. The specimen is a square plate fixed at three corners and loaded perpendicular to the plate at the fourth corner as shown in Fig. 1(d). In this case, the relationship between the deflection of loaded corner and the inplane shear modulus is given:

$$G_{xy} = \frac{3Pl^3}{h^3 W_L} \tag{6}$$

where P is the applied load, l and h are the length and thickness of the square plate, respectively and W_L is the deflection at the loading point. If the deflection W_L for a given load P can be measured, the shear modulus can be determined. This method can only be used to measure the inplane shear modulus of orthotropic materials. It is not available to most engineering materials and has not found wide application to composite materials.

1.5 The short beam test

The short beam shear test has become very widely used for characterizing the interlaminar shear strength of fibre reinforced composites. It involves loading a beam under either three or four point bending with the span to thickness dimensions such that an interlaminar shear failure is induced as shown in Fig. 1(e). The simplicity of the test makes it very popular as a materials screening tool and it has become a standard test method in America for measuring the interlaminar shear strength of composites. For the short beam specimen, the shear strength can be calculated from the classical relationship:

$$\tau = \frac{3P}{4bh} \tag{7}$$

where τ is the maximum interlaminar shear stress at failure, P is the maximum applied load and b and h are the width and thickness of the specimen respectively. Many studies have been done of short beam test, both experimental and analytical[11-12]. The results of stress analysis show that stress concentrations in the region of loading are very high. The strong compressive stress under the loading point can lead to a failure mode for specimen by compressive buckling or by a combination of compression and shear. The best way is to induce initial damage in the form of a vertical crack. However this makes the shear stress distribution not to be uniform so that shear stress concentrations appear in the specimen. Despite this disadvantage, the short beam specimen is still used to measure the interlaminar shear strength of composites because a better substitute has not yet been found.

1.6 Iosipescu shear test

The Iosipescu shear specimen was used in composite materials first by Walrath and Adams[13] in 1982. Since when there has been a rapidly increasing interest in the use of this test as a method for determining the shear properties of composite materials. A similar test method, the four point bending shear test has also been proposed. The specimen is strip shape with two symmetrical notches. A 110° notch angle and a notch depth of 20% of the specimen height have been suggested. The specimen is loaded anti-symmetrically as shown in Fig. 1(f). A state of nearly pure shear can be obtained in the notch region. The shear strain can be determining from strain gauges in the pure shear region. The shear stress is derived from the applied force divided by the net cross section,

$$\tau = \frac{P}{Wt} \tag{7}$$

where W is the net width between the two notches and t is the thickness of the specimen. The Iosipescu shear specimen can be used not only for measuring the shear strength but also for obtaining the shear stress - strain curve. The in-plane

and out of plane shear properties can be determined by using specimens with different lay-up sequences and fibre orientations. In other words, the interlaminar shear properties can also be measured using this test method. However although the Iosipescu shear test is a very good method for measuring the interlaminar shear properties under static condition, even though the notch is very difficult to prepare and the specimen is expensive to make, No one has yet been able to use this specimen under impact loading.

1.7 The double lap shear test

The double lap shear test has been used for measuring the interlaminar shear strength of woven hybrid composite material by the Impact Testing Group at Oxford [2]. The specimen is very easy to prepare but the principal advantage is that it is very convenient to test under impact as well as static loading. The specimen is a symmetrical design, as shown in Fig. 2, with two lap joints. The shear stress in the overlap region is assumed to be uniform and given by the simple relationship.

$$\tau = \frac{P}{2A} \tag{1}$$

where A is the overlap area of the joint and P is the applied load. A full stress analysis has been done for this specimen using the finite element method. This is descried in detail in the next section. The results show that the shear stress distribution is far from uniform, there being large shear stress concentrations at the end of the of overlap regions. The interlaminar shear strength measured using this specimen, therefore, is just a rough estimate and cannot be applied directly to the engineering design. Also, it should be noted, that this specimen is specially designed to measure the interlaminar shear strength. The inplane shear properties cannot be measured using this specimen.

The shear test methods mentioned above are those often used. Other techniques, not discussed, include the split-ring shear test, the cross-sandwich beam test and the Arcan shear test. It can be seen that which many test methods can be used to measure the in-plane shear properties of composite materials only two method, the short beam test, Iosipescu shear test and the double lap shear test, have been used to measure the interlaminar shear properties and all of those have some disadvantages. So to find a ideal method for measuring the interlaminar shear properties under static conditions is still a task for researchers.

Under impact loading, the situation is much difficult. Most of the above shear tests method cannot be used under dynamic loading conditions because the limitation imposed if wave propagation in loading device is to be adequately monitored. For the in-plane shear properties, the $\pm 45^{\circ}$ off-axis tensile test using the split Hopkinson bar loading system is a very good method for determining both shear

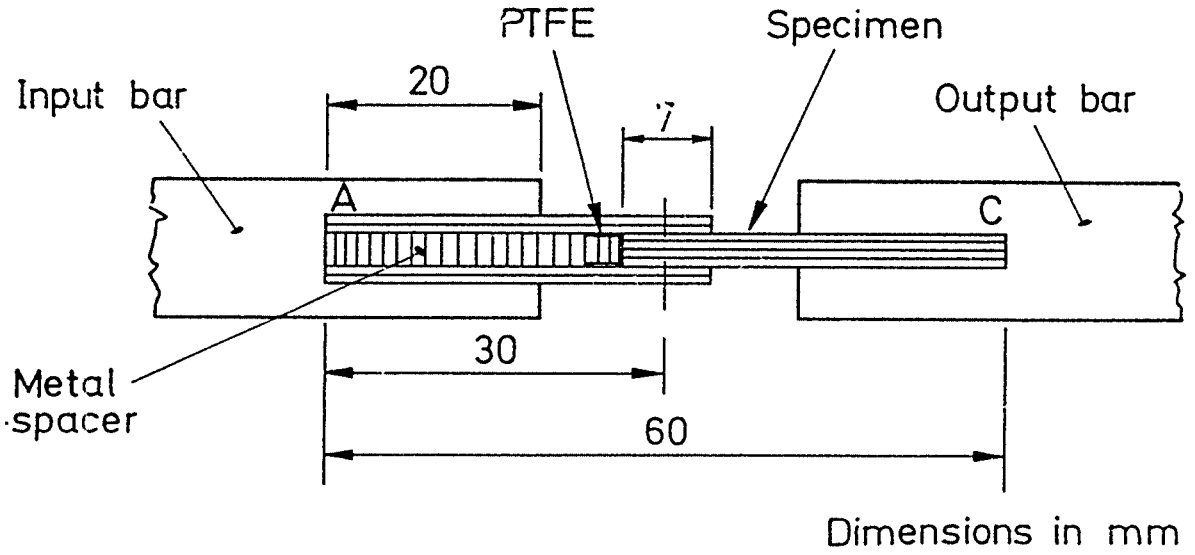

Fig. 2 Double lap shear test

strength and the stress-strain curve [4]. For the interlaminar shear properties, several version of the short beam specimen test have been completed. Sayers and Harris [22], Werner and Dharam [23], Chiem and Liu [24], again used the Hopkinson bar loading system, in attempt to measure the impact shear strength of carbon fibre composite. Conflicting results have been obtained. Thus both references[22] and [24] show that the interlaminar shear strength is dependent on the strain rate while the results in reference[23] show the interlaminar shear strength to be rate independent.

In the present report the double lap shear specimen is analysed and the shear stress distribution along the interface for different woven hybrid lay-up is calculated. Experimental results are reported which show a significant increase in the interface shear strength between the woven carbon/epoxy plies with increasing rate. In view, however, of the highly non uniform shear stress distribution in the interlaminar plane an improved version of the shear test is prepared. In the modified test the shear stress distribution along the shear plane has been determined using finite element method and both a two dimensional and a three dimensional mesh. The results show that the shear stress distribution is more uniform in the new version of shear specimen and there is agreement between the results of the two dimensional and the three dimensional analyses .

2 The Double Lap Shear test

2.1 The experimental technique

Several alternative designs of double lap interlaminar shear specimen were investigated before that shown in Fig. 2 was chosen. The specimen has a total length of 60 mm and a width of 10 mm. The shear zone length, 7 mm, was determined by the need for interlaminar shear failure to occur at a lower load than a tensile failure in other parts of the specimen. Initial tests were performed on specimens fabricated from a 5 end satin weave carbon/epoxy pre-preg manufactured by Hexcel and Genin using a type ES.36 self-adhesive epoxy resin and having a fibre weight fraction of 52% and an uncured pre-preg weight of 548 g/m^2. The fibre was woven from 3000 filament fibre tows with, respectively, 70 and 72 yarns per 10 cm in the warp and weft directions and having a dry weight of 285 g/m^2. Eight layers of pre-preg were used, with metal and PTFE spacers as shown, and a standard curing cycle was applied[2].

At quasi-static rates the specimen was fixed with epoxy adhesive into parallel-sided slots 20 mm deep in two loading bars. These were then pulled in tension in a standard Instron testing machine and the load at which the specimen failed was determined. At impact rates of loading the specimen was fixed in the same way between the input and output bars of a standard tensile split Hopkinson bar

Table 1: Effect of strain rate on the interlaminar shear strength

	Shear strength (MPa)			
Specimen No.	1	2	3	average
Quasi-static	35.3	31.0	34.0	33.4 ± 2
Impact	54.2	53.4	55.2	54.3 ± 0.9

apparatus. From strain gauges on the output bar a signal was obtained which was proportional both to the load supported by the specimen and to the velocity at the specimen/output bar input face. Similar signals from two strain gauge stations on the input bar allowed the velocity at the specimen/input bar interface and hence also the overall displacement across the ends of the specimen to be determined. From these measurements some estimate of the strain rate across the interlaminar region may be made.

2.2 Experimental results

Typical strain gauge records from such a test are shown in Figs. 3 (a), (b), and (c) for the two input bar and one output bar stations. Assuming interlaminar shear failure occured at the peak load for the record of Fig. 3 (c) and that the load was equally shared between the two interlaminar failure planes, the average stress on the interlaminar plane was 57 MPa. The failed specimen is shown in Fig. 4. Three such tests were performed and the interlaminar shear strengths so determined are compared in Table 1 with the results from three similar tests at a quasi-static rate. A marked increase in the interlaminar shear strength with increasing strain rate is apparent.

2.3 Finite element analysis of double lap specimen

The finite element mesh used in a two dimensional stress analysis of the double lap specimen is shown in Fig. 5. There are 120 isoparametrical elements, each with eight nodes. Since the specimen is symmetrical about the center line only half is modelled. As the original motive behind this work was an interest in the impact response of hybrid composites the finite element analysis has performed for four different ply lay-ups, an all carbon, an all glass and two hybrid lay-ups, one with four inner plies reinforced with carbon and the outer two each of glass and the other with the four inner layers of glass and outer two each of carbon. These are illustrated in Fig. 6 (a), (b), (c) and (d) respectively. Only the first of these corresponds to the experimental arrangement described above. The applied loading, 245 KN, is the same in four analyses, giving a average shear stress on the interlaminar plane of 35 MPa, about the level at which the all carbon lay-up failed in the quasi-static tests.

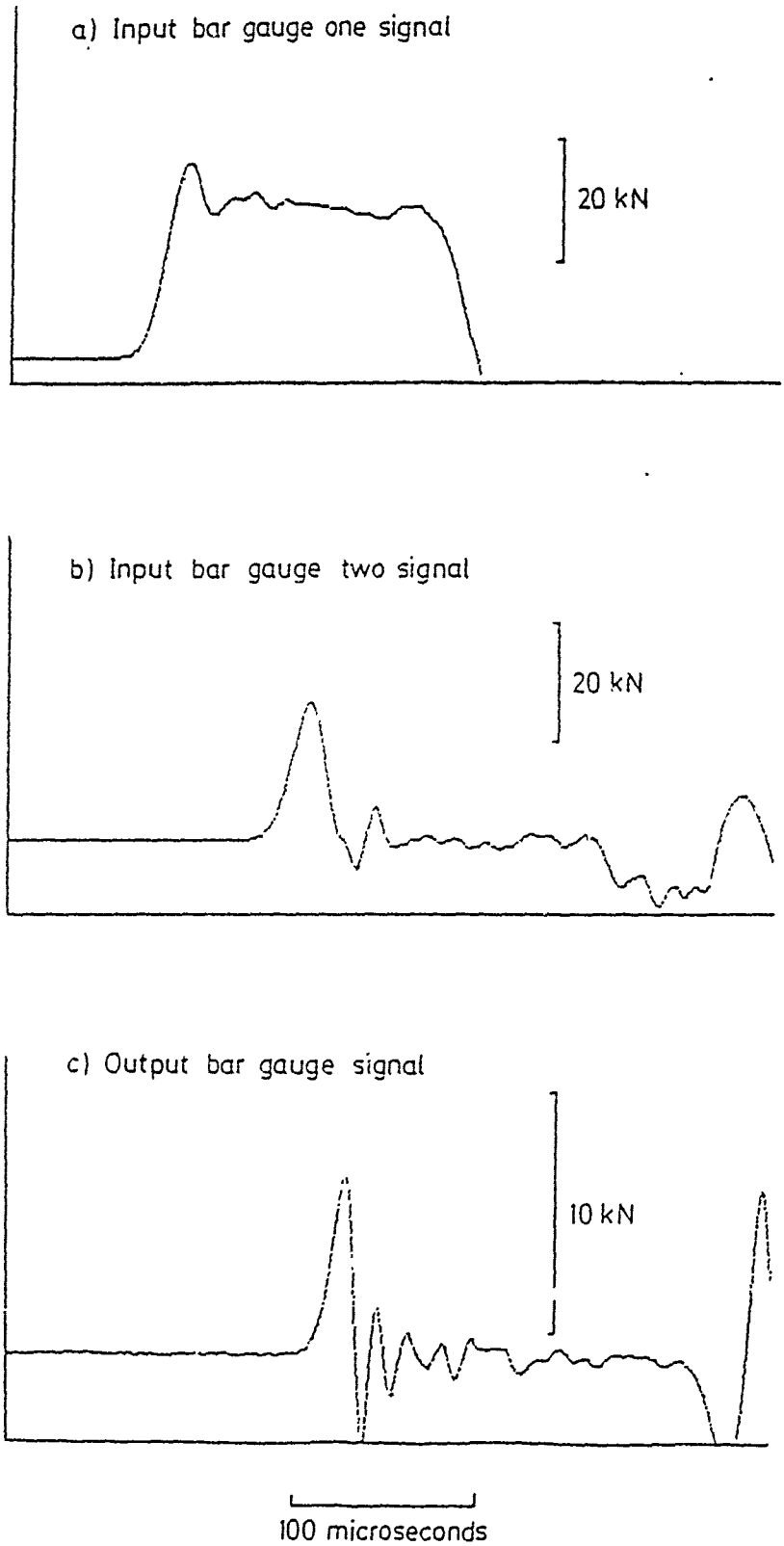

Fig. 3 Typical strain gauge records for impact test on double lap shear specimen

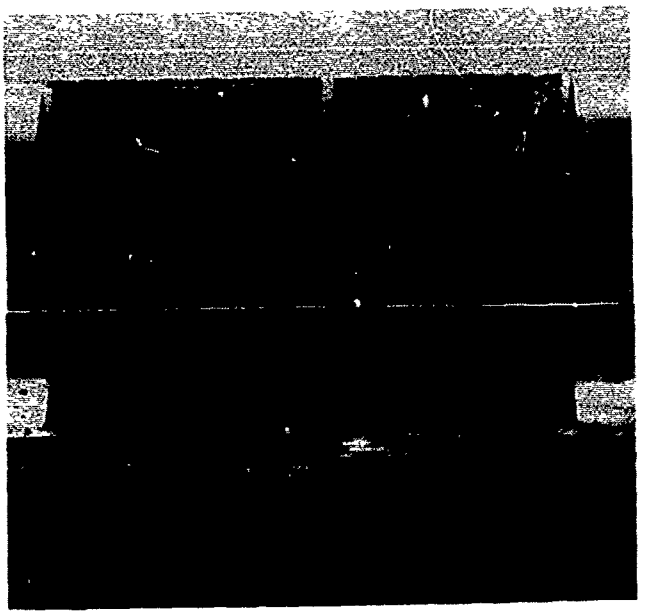

Fig. 4 Failed Specimen

Fig. 5 Finite Element Mesh for Double-Lap Shear Specimen

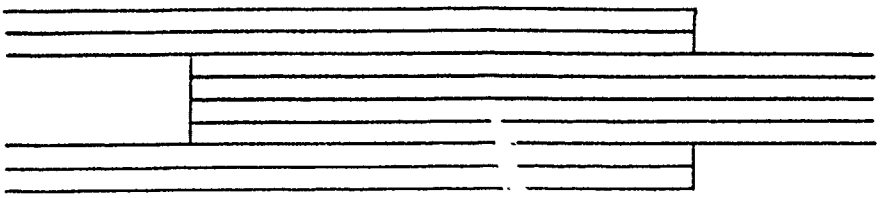

(a) all carbon

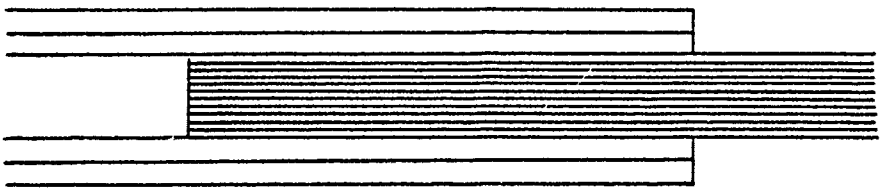

(b) carbon/glass interface; carbon outer plies

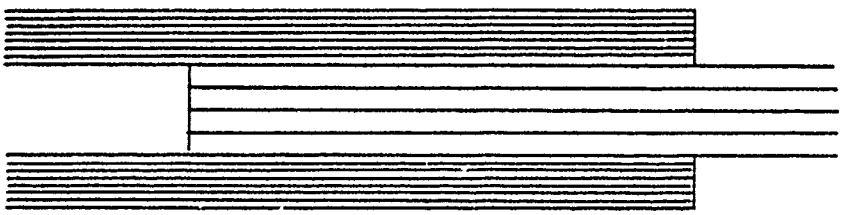

(c) carbon/glass interface; glass outer plies

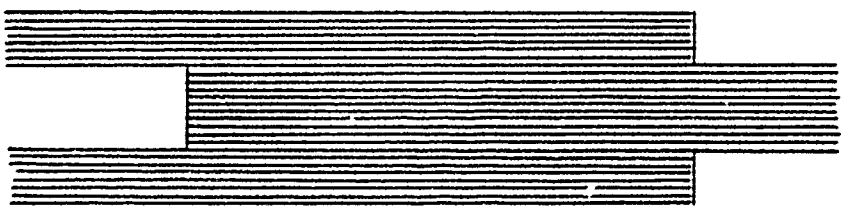

(d) all glass

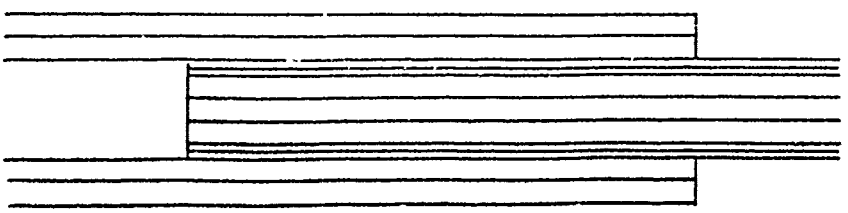

(e) carbon/glass interface; optimum lay-up

Fig. 6 Stacking sequences for double lap shear specimen

The elastic properties assumed for the carbon and glass reinforced plies were the same as those used in the earlier report[1]. The results of the finite element analyses are shown in Figs. 7 (a),(b),(c) and (d) for the four lay-ups in Fig. 6 (a), (b), (c) and (d), respectively. The variation in the shear stress on the interlaminar plane over the 7 mm shear zone length and for a further 3.5 mm to either side is shown in each case. For the all carbon and all glass lay-ups the same general trend is observed with very marked, and nearly equal, shear stress concentrations at either end of the shear zone and a minimum shear stress at the mid-point of the shear zone. The ratio of maximum to minimum shear stress is less for the all carbon specimen, about 5.5 : 1, than for the all glass specimen, where it rises to about 9 : 1. The effect of using lay-ups with different reinforcing fibres on either side of the interface is to increase one of these stress concentrations while reducing the other. Thus, when the four inner plies are glass reinforced the maximum shear stress rises to about 140 MPa at the input end and falls to about 50 MPa at the output end. With a minimum shear stress of about 20 MPa the ratio of maximum to minimum shear stress becomes 14 : 1. The reverse effect is obtained when the four inner plies are carbon reinforced, the corresponding shear stress values being, respectively, 46 MPa, 147 MPa and 10 MPa, giving a maximum to minimum ratio again of about 14 : 1.

From these results it is clear that even in the best case, i.e. the all carbon lay-up, the shear stress variation is very large so that experimental measurements made with this design of specimen can only give an average value of interlaminar shear strength at the given rate of loading. If these large stress concentrations lead to an early initiation of failure this average value may be a underestimate of the true interlaminar shear strength under a uniform shear loading. It should be noted, However, that the shear stress distribution on the interlaminar plane close to a ply tensile failure[1] shown a very similar variation to that found here so that, in practice, the present results may be more directly relevant to that particular problem. In the all glass lay-up, Fig. 7 (d), the lower elastic moduli lead to greater bending deflections and a bigger variation of shear stress on the interlaminar plane. Introducing different reinforcing fibres either side of interlaminar plane, Figs. 7 (b) and (c), make the problem significantly worse. These results suggest that, if this type of specimen is to be used to determine the effect of loading rate on the interlaminar shear strength at the interface between a carbon reinforced and a glass reinforced ply, the optimum lay-up would have all plies carbon reinforced except for the two plies on the inner surface of each shear zone, see Fig. 6(e). Since this general design of specimen is reasonably easy to both fabricate and test and may be expected to give results indicating the general trends in the effect of loading rate on the interlaminar shear strength it has value in investigating overall effects. For a more precise determination of interlaminar shear strengths, however, an improved specimen design is required. This is the subject of the next section.

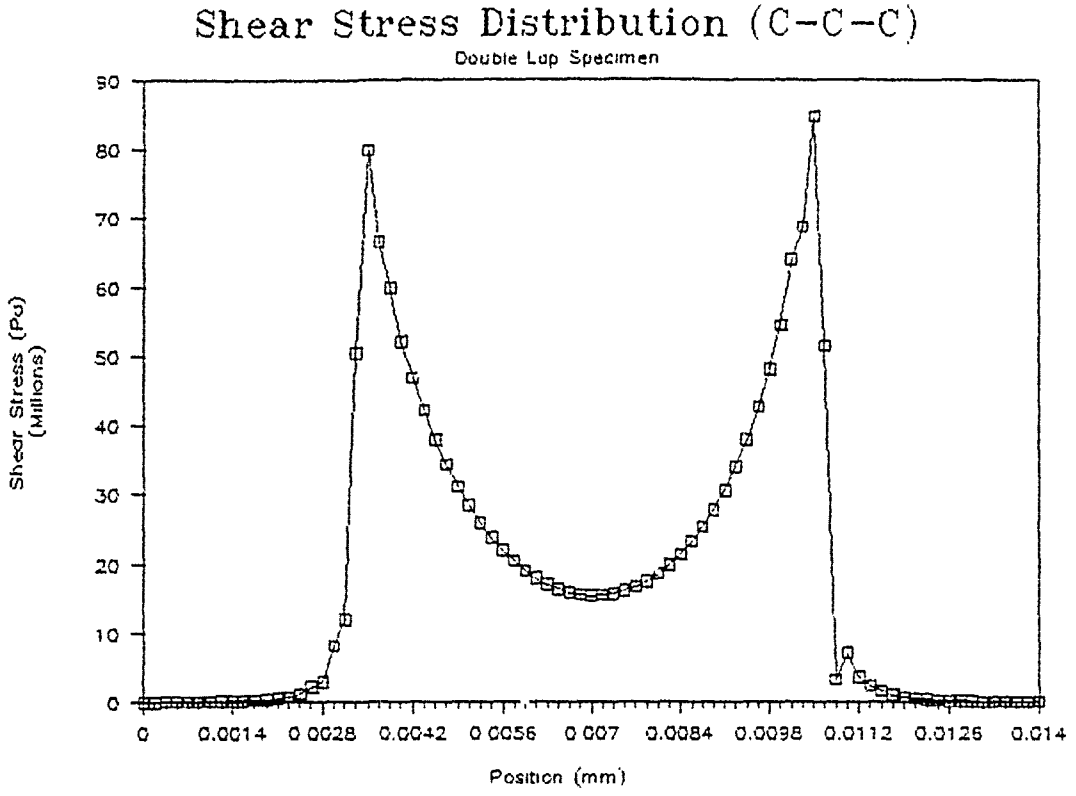

(a)

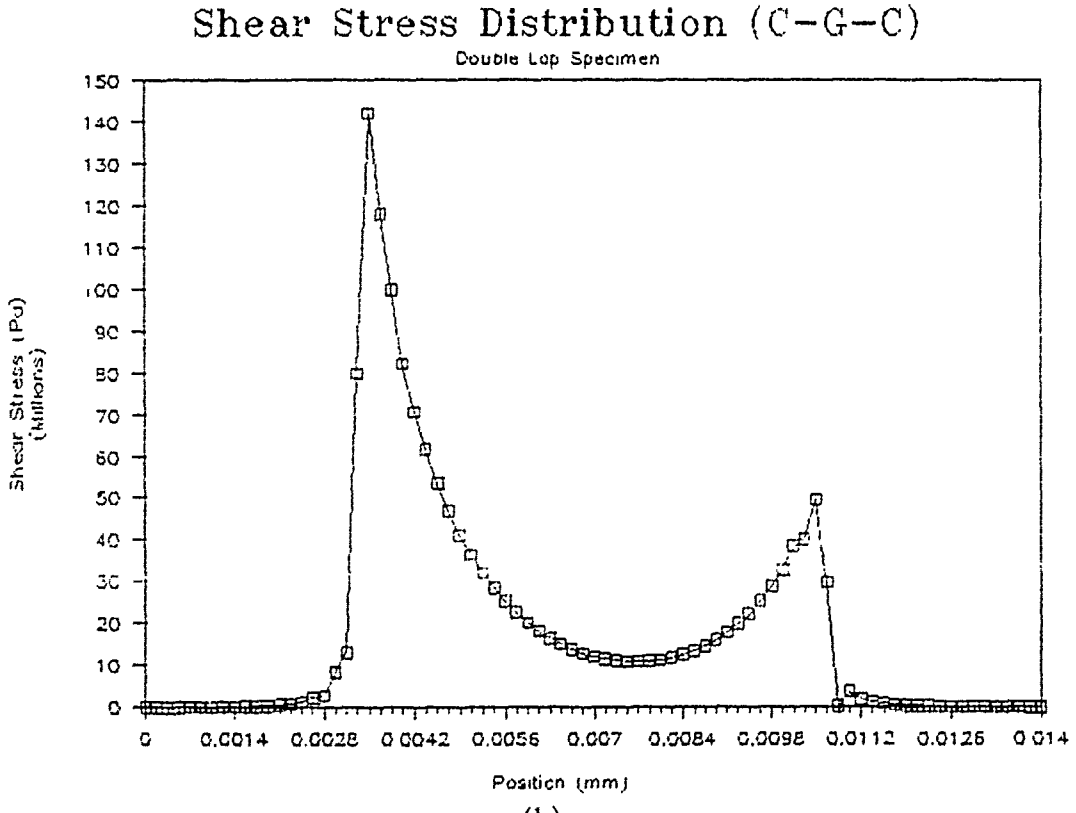

(b)

Fig. 7 Shear stress distribution on failure plane for stacking sequences Fig. 6 (a)- (d)

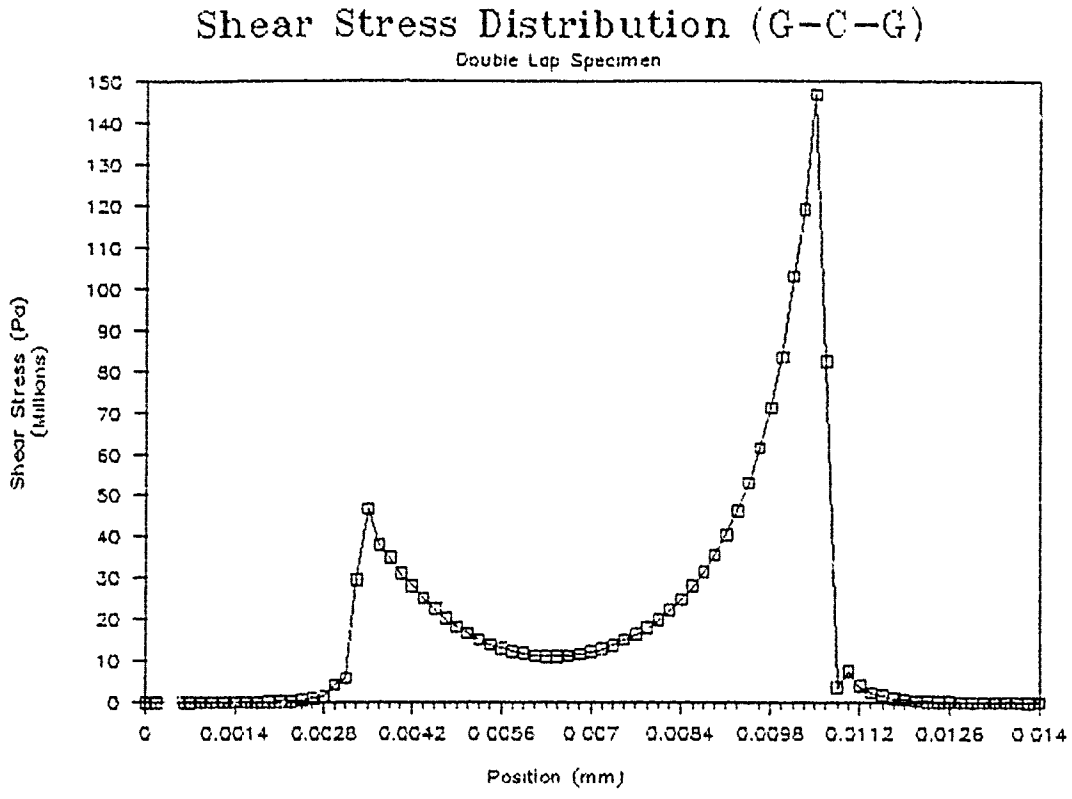

(c)

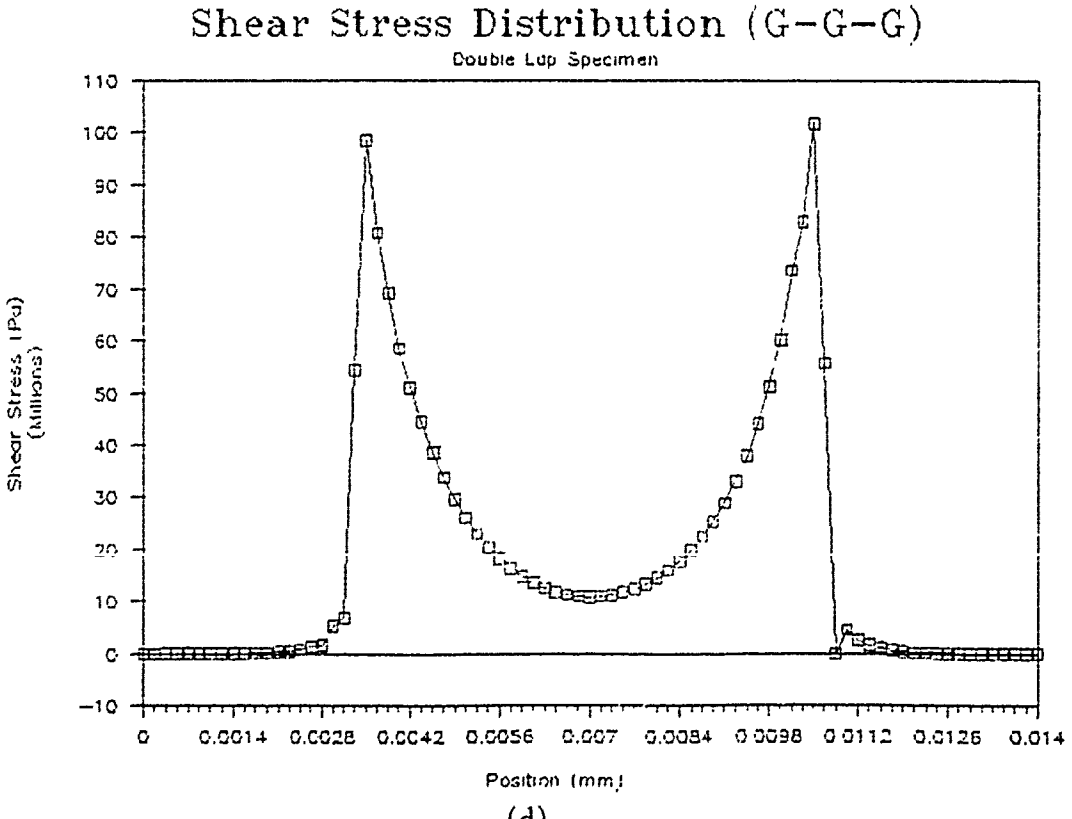

(d)

Fig. 7 Shear stress distribution on failure plane for stacking sequences Fig. 6 (a)- (d)

3 Improved Interlaminar Shear Specimen

3.1 Specimen design and test method

The results of the finite element analyses of the different lay-ups in the double lap shear specimen suggest that the greater the bending stiffness of the material either side of the shear interface the smaller the variation in shear stress on the interface plane. This bending stiffness can be increased by replacing parts of the composite specimen with metallic back-up pieces. A possible way of doing this is illustrated in Fig. 8. Two thin composite laminates, forming a double specimen, are fixed with epoxy adhesive between a parallel-sided slot in the large diameter input bar and a thin flat plate integral with the smaller diameter output bar. The input and output bar may form part of a split Hopkinson bar system, for testing in either tension or compression, so that specimen arrangement is suitable for use under impact loading. A major drawback is that there is no longer a well-defined interlaminar failure plane and there may well be a tendency for failure to occur at the loading-bar/specimen interface. To meet these two problems it is proposed that when fabricating the specimens thin strips of PTFE should be inserted at each end of the interlaminar plane on which it was desired that the specimens should fail, i.e. a carbon-carbon, glass- glass, or carbon-glass interface as required. After curing the laminate and cutting the test specimens to size, $10mm \times 7mm \times 1.5mm$, the PTFE is removed to leave two "notches" and a reduced cross-section to carry the shear loading

Before constructing this modified testing system several finite element analyses were carried out to determine whether the shear stress on the expected failure plane was sufficiently uniform and significantly higher than those on other planes in the specimen. The results of these analyses are described below.

3.2 Two-dimensional finite element analysis of modified shear test

The large bar effectively acts as a stiff grip and the magnitude of its bending stiffness is very important in reducing the shear stress variation on the failure plane. To allow a two-dimensional analysis, therefore, the large bar assumed to have a rectangular cross-section of total depth 12 mm which gave the same bending stiffness as that for the part circular cross-section, diameter 19 mm, which it actually has at section AA, see Fig. 8.

With this assumption and the finite element mesh shown in Fig. 9 five different specimen lay-ups were studied, an all-call specimen with and without notches introduced by means of PTFE strips, an all-glass lay-up with such notches, and two hybrid lay-ups, also with notches, one with the carbon plies fixed to the

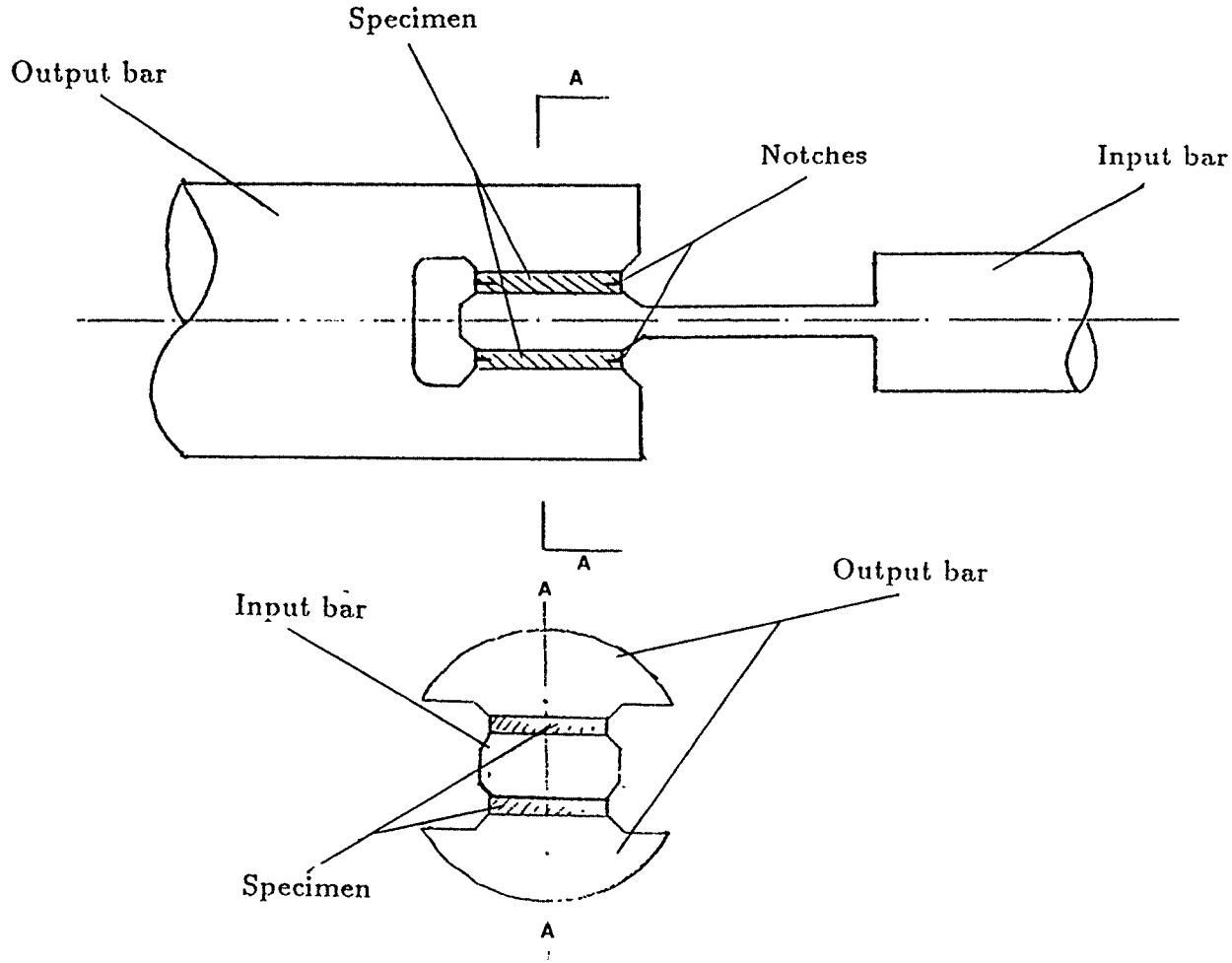

Fig. 8 Modified Version of Shear Test

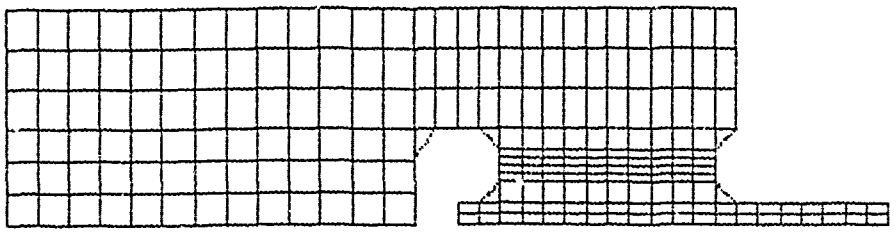

Fig. 9 Two dimensional finite element mesh for modified shear test

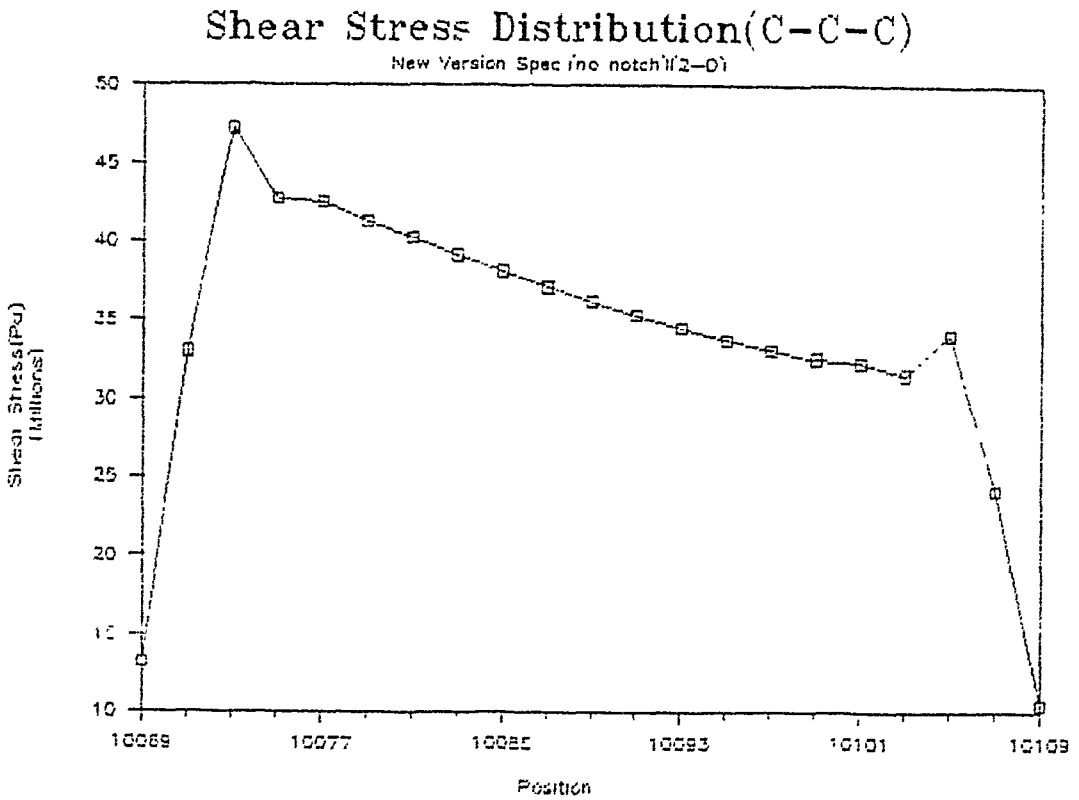

Fig. 10 Shear stress distribution on central plane of modified shear specimen (all carbon lay-up; without notch)

input bar and the other with the carbon plies fixed to the output bar. Interface elements are used to model the notch region. These allow the surface to slide laterally but prevent that two surfaces overlap in normal direction. The results of these analyses, showing the variation in the shear stress over the 10 mm length of central interlaminar shear plane are given in Fig. 10 and Figs. 11 (a) to (d) respectively.

Comparing the two analyses for the all-carbon lay-up it is apparent both that the shear stress distribution is much more uniform here than in the previous double lap design and also that the presence of the notches, which are of nominal length 1 mm and so reduce the shear zone length to 8 mm, has only a small effect on the stress distribution. The ratio of the maximum to the minimum shear stress on the interface increasing slightly, from 1.4 : 1 without notches to 1.7 : 1 with notches. In both cases this is much better than the ratio of 5.5 : 1 for the all carbon lay-up in the double lap shear specimen. Comparing the analyses for the four notched specimens, Figs. 11 (a), (b), (c) and (c), it can be seen that the ratio of maximum to minimum shear stress on the failure plane is almost constant, i.e. it does not depend on the particular hybrid lay-up. This is an important advantage of this design of specimen. There is, however, an apparent negative shear stress at each end of the failure plane in the region of the notches whenever they are prevent.

3.3 Three-dimensional finite element analysis of modified shear test

In the two-dimensional analysis the input bar at section A-A was taken to have a rectangular cross-section of the same bending stiffness as that for the actual circular cross-section. In order to check the validity of this assumption and also to permit an estimate of the shear stress variation in the width direction a three-dimensional finite element analysis has been performed. Both 20-node and 15-node element were used and the mesh, shown in Fig. 12, includes parts of input and output bars. The same load is applied as in the previous two-dimensional analysis and the same five specimen conditions were studied.

Results for the variation of shear stress on the interlaminar plane in the loading direction along either the centre-line or the edge of the specimen are shown in Figs. 13 and Fig. 14 (a), (b), (c) and (d). In each case the shear stress is higher, by about 30%, at the edge of the specimen than at the center. This may be due to an increased effective bending stiffness of input bar near the edges of specimen due to the overshoot of the bar either side of the specimen. This could be checked by analyzing for a redesigned input bar with this region having a rectangular cross-section. If this were to give a better stress distribution it would be relatively easy to modify the existing input bar along those lines.

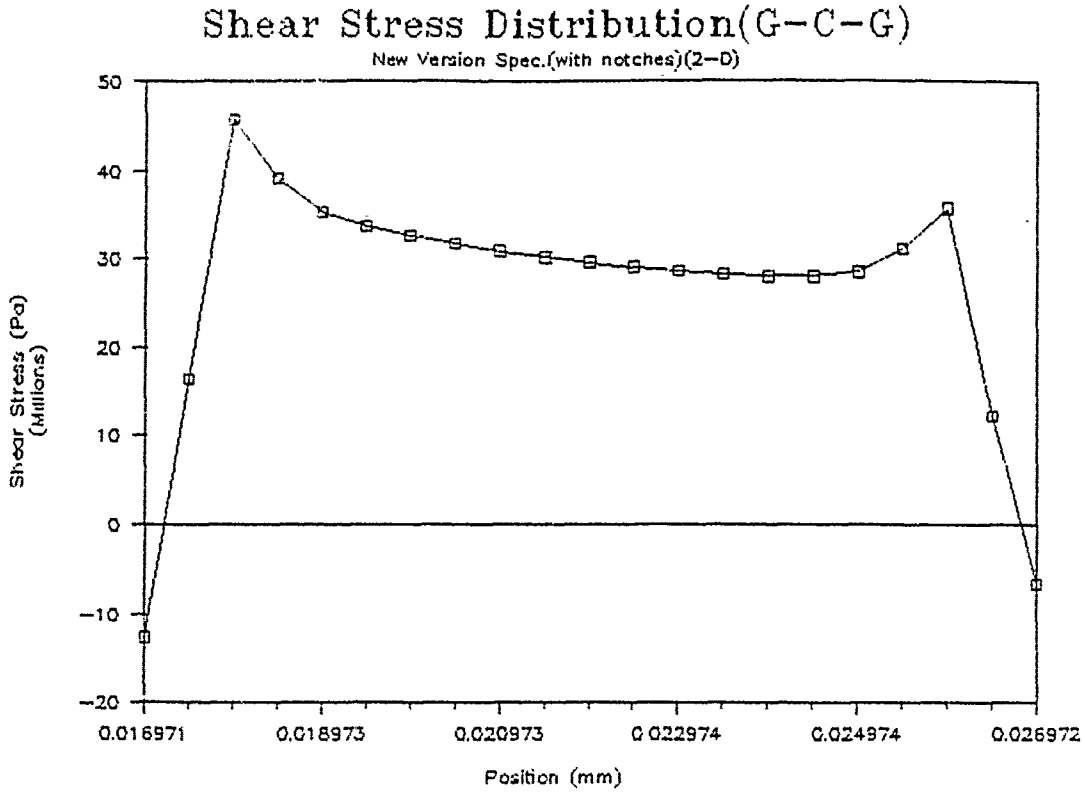

(c) carbon/glass interface; glass outer plies

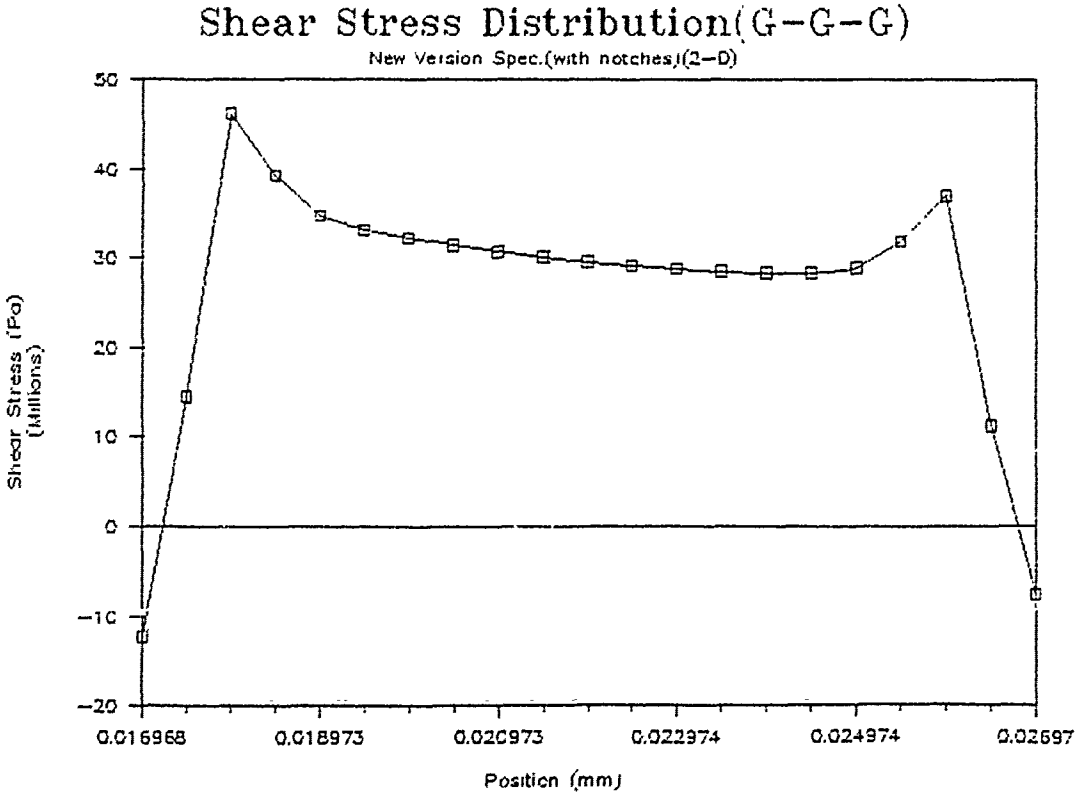

(d) all glass lay-up

Fig. 11 Shear stress distribution on central plane of modified shear specimen (with notches)

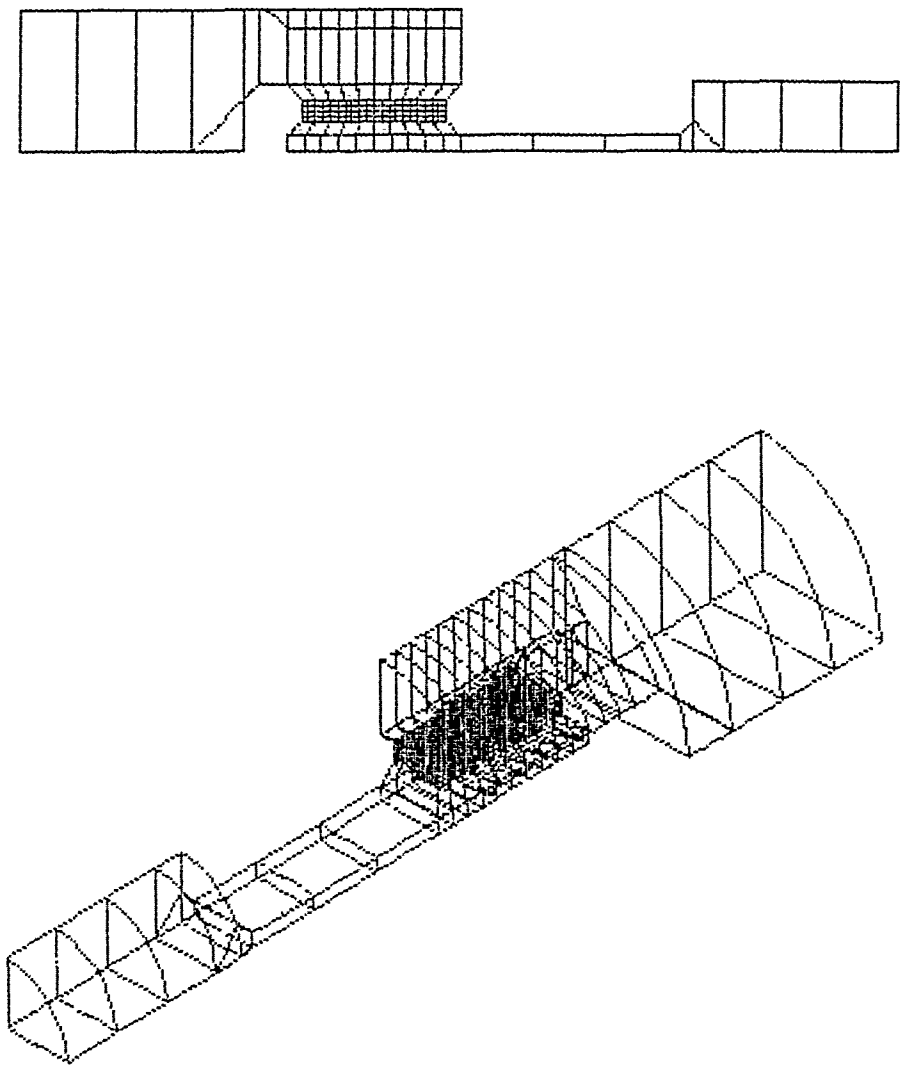

Fig. 12 Three dimensional finite element mesh for modified shear test

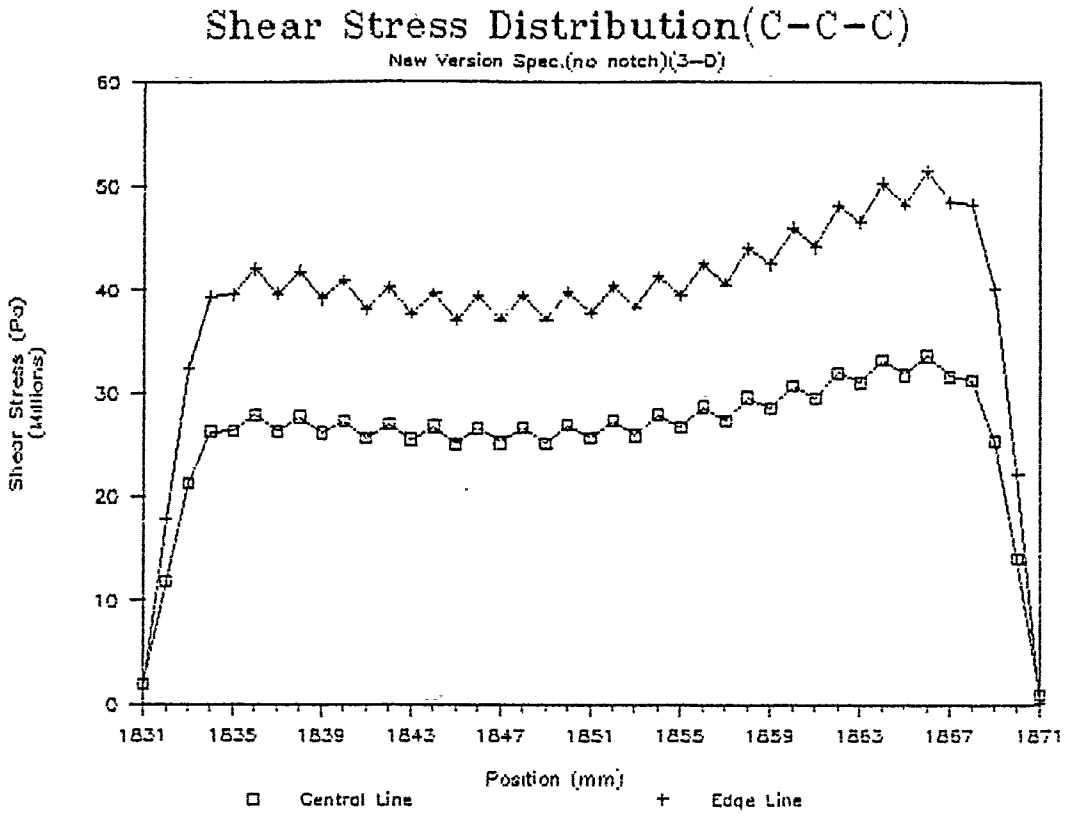

Fig. 13 Shear stress distribution on central plane of modified shear specimen (all carbon lay-up; without notch)

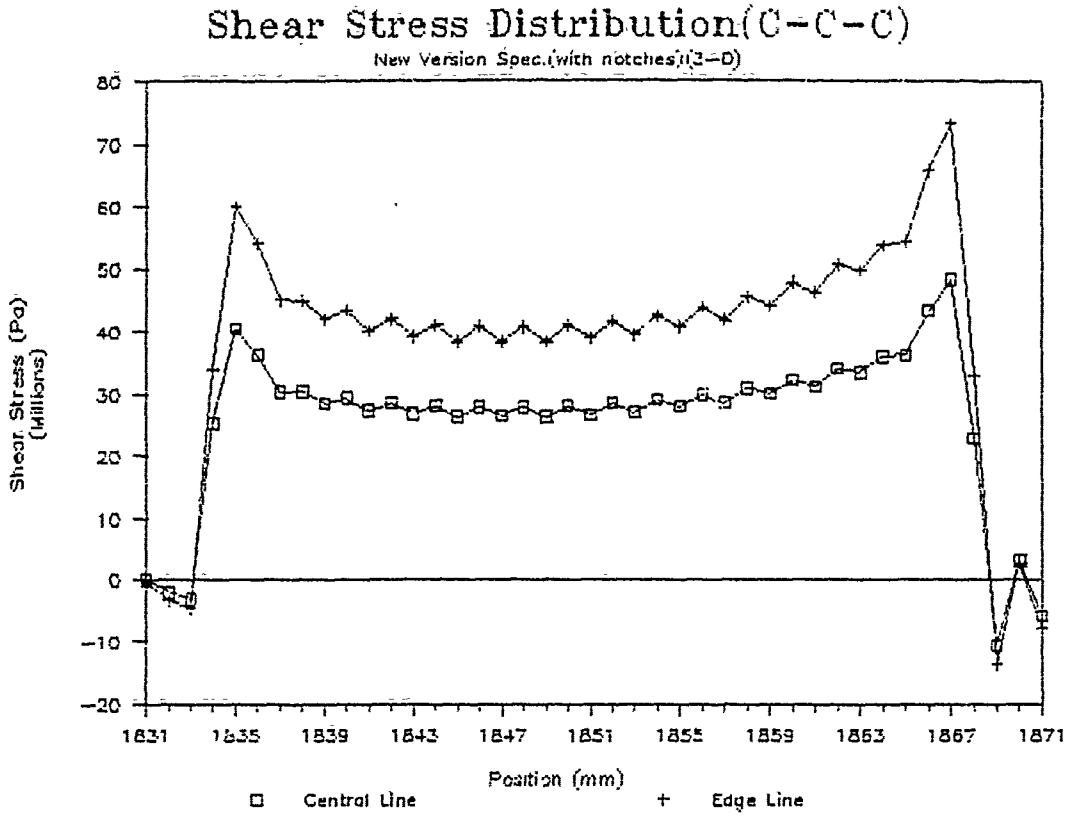

(a) all carbon lay-up

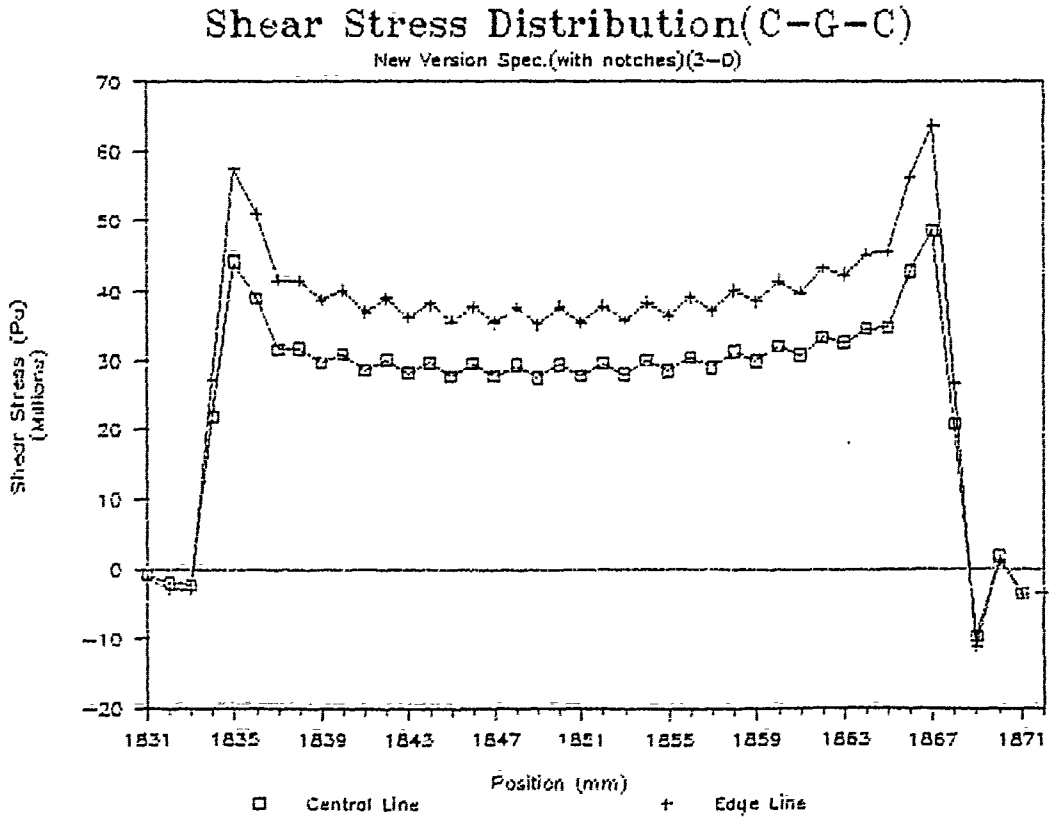

(b) carbon/glass interface; carbon outer plies

Fig. 14 Shear stress distribution on central plane of modified shear specimen (with notches)

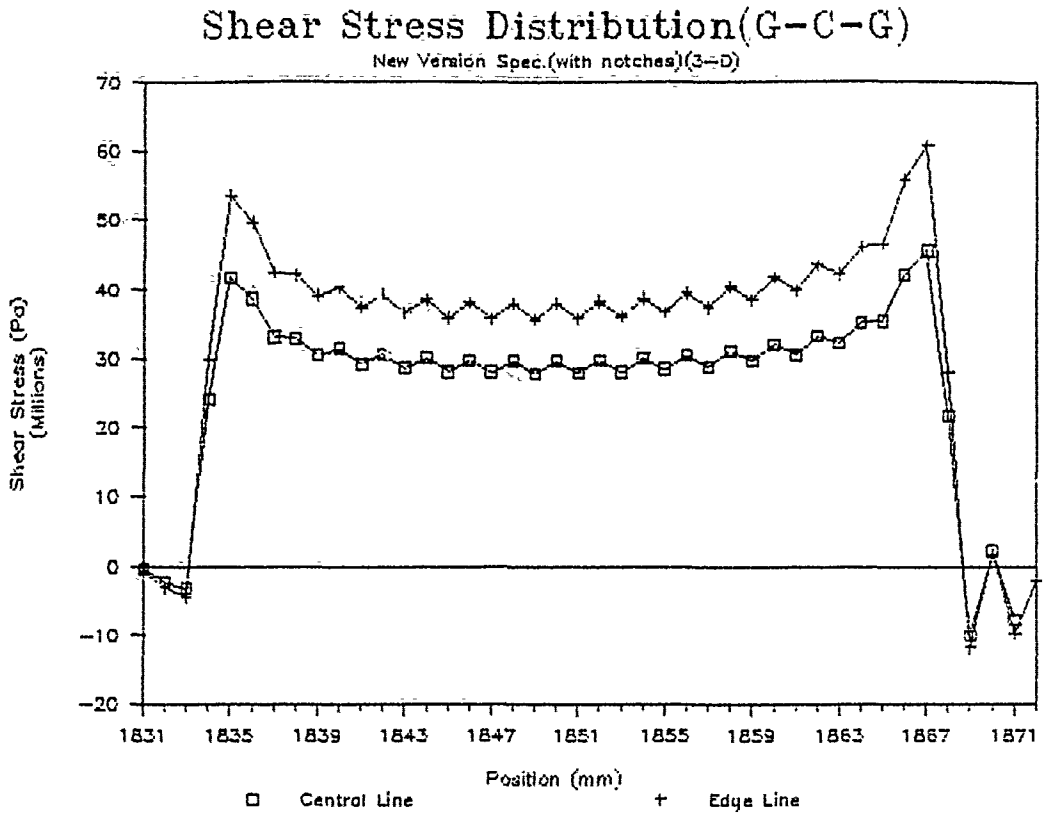

(c) carbon/glass interface; glass outer plies

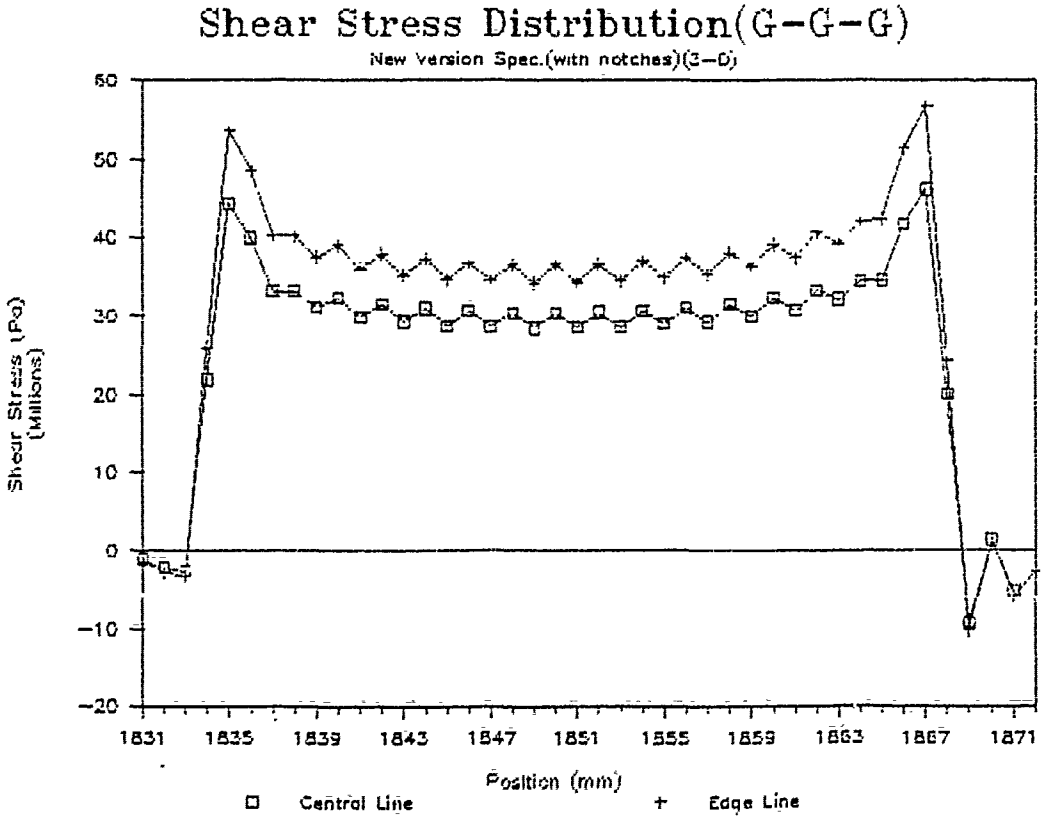

(d) all glass lay-up

Fig. 14 Shear stress distribution on central plane of modified shear specimen (with notches)

Without notches the all carbon lay-up shows a almost constant shear stress distribution. Introduction of notches leads to a marked shear stress concentration at each end of the shear region in all four lay-ups but over most of the intervening region the shear stress is again almost constant. As with the two-dimensional analysis the ratio of maximum to minimum shear stress along the center-line, 1.8 : 1 for all carbon and 1.6 : 1 for the all glass, is almost independent of the hybrid lay-up. This is also true of the shear stress variation along the outer edge of the specimen where the corresponding ratio ranges 1.9 : 1 for the all carbon lay-up to 1.7 : 1 for all glass lay-up.

4 Summary

So far experimental results have only been obtained for an all carbon lay-up using the double lap shear specimen. An all glass lay-up has been prepared and double lap shear tests on this material are about to be performed. In view of the much better shear stress distribution on the failure plane for the modified shear test, loading bars to this design have been constructed and strain gauges fixed.

REFERENCES

[1] Y.L.Li, C.Ruiz and J.Harding "Failure Analysis of Woven Hybrid Composite by Using Finite Element Method," *to appear*

[2] J.Harding,Y.L.Li, and M.E.C.Taylor "Characterisation of Impact Strength of Woven Carbon Fibre/Epoxy Laminate," *to appear*

[3] C.C.Chamis and J.H.Sinclair "10° Off-Axis Tensile Test for Intralaminar Shear Characterization of Fibre Composite," *NASA Tech. Note, No. NASA TN D-8215 (April 1976)*

[4] J.Harding,K.Saka and M.E.C.Taylor "Behaviour of Fibre-reinforced Composite Under Dynamic Tension," *Third Progress Report, O.U.E.L., No.1654/86*

[5] P.H.Petit "A Simplified Method of Determining the Inplane Shear Stress-Stain Response of Unidirectional composite," *Composite Materials: Testing and Design ASTM STP 460, ASTM 83-93 (1969)*

[6] B.W.Rosen "A Simple Procedure for Experimental Determination of the Longitudinal Shear Modulus of Unidirectional composite," *J. Composite Materials, (6) 552-554 (oct. 1972)*

[7] J.M.Hennessey, J.M.Whitney and M.B.Riley "Experimental Methods for Determining Shear Modulus of Fibre Reinforced Composite ," *AFML-TR-65-42 (Sept. 1965)*

[8] D.F.Sims "In-Plane Shear Stress-Strain Response of Unidirectional Composite Materials," *J.Composite Materials (7) 124-148 (Jan. 1973)*

[9] M.F.Duggan " An Experimental Evaluation 0f the Slotted-tension Shear Test for Composite Materials," *Experimental M 20(7) 233-239 (JAN. 1980)*

[10] R.F.S Hearmon and E.H.Adams "The Bending and Twisting of Anisotropic Plate,," *British Journal Appl. Physics, vol.3,150-156 (1952)*

[11] C.A.Berg, J.Titosh and M.Israeli "Analysis of Short Beam Bending of Fibre Reinforced Composite,," *Composite Materials: Testing and Design(2nd conf.) ASTM STP 497, ASTM 206-218(1972)*

[12] J.M.Whitney and C.E.Browning "On Shear-Beam Shear Test for Composite Materials," *Experimental Mechanics, 25(3) 294-300(Sept. 1985)*

[13] D.E.Walrath and D.E.Adams "The Iosipescu Shear Test as Applied to Composite Materials," *Experimental Mechanics, 23(1): 105-110(MARCH 1983)*

[14] D.F.Adams and D.E.Walrath "Further Development of The Iosipescu Shear Test Method," *Experimental Mechanics, 27(2), 113-119(MARCH 1987)*

[15] D.F.Adams and D.E.Walrath "Current Status of the Iosipescu Shear Test Method," *J. Composite Materials, (21) 494-507 (June 1987)*

[16] J.L.Sullivan,B.G.Kan and Van Oene "Shear Properties and a stress analysis Obtained From Vingle-ester Iosipescu Specimen," *Experimental Mechanics, 3(24) 223-(March,1984)*

[17] M.Arcan "The Iosipescu Shear Test as Applied to Composite Materials," *Experimental Mechanics, 3(24) 66-67(MARCH 1984)*

[18] A.Voloshin and M.Arcan " Failure of Unidirectional Fibre-Reinforced Materials-New Methodology and Results," *Experimental Mechanics, 20(8) 280-284(Aug. 1980)*

[19] J.M.Whitney, D.L.Stansbargar and H.B.Howell "Analysis of Rail Shear Test–Application and Limitation," *J.Composite Materials, 5 (Jan. 1971) 24-*

[20] R.Garciam,T.A.Weisshaar and R.R.McWithey "An Experimental and Analysis Investigation of the Rail Shear-test Method as Applied to Composite Materials," *Experimental Mechanics, 20(8) 273-279(Aug. 1980)*

[21] S.W.Tsai "Experimental Determination of the Elastic Behaviour of the Orthotropic Plate," *J.Engrg. for Industry, 315-318 (Aug.1965)*

[22] K.H.Sayers and B.Harris "Interlaminar Shear Strength of a Carbon Fibre Reinforced Composite Materials under Impact Condition," it J. Composite Materials, 7 (1973), 129-133

[23] C.Y.Chiem and Z.G.Liu "High Strain-rate Behaviour of Carbon Fibre Composite," *Mechanical Behaviour of Composites and Laminates, Edited by W.A.Green and M.Micunovic, Elsevier Applied Science*

[24] "The Dynamic Response of Graphite Fibre-Epoxy Laminate at High Shear Strain rate," *J. Composite Materials 20,(July 1986), 365-374*

[25] T.Parry and J.Harding "The Failure of Glass-Reinforced Composites under Dynamic Torsional Loading," *O.U.E.L. Report. No. 1365/81*

APPENDIX III

The Interlaminar Shear Strength of Woven Carbon, Woven Glass and Woven Carbon/Glass Hybrid Laminates Under Static and Impact Loading

Y.L.Li, J.Harding and M. E. C. Taylor
Department of Engineering Science
University of oxford

Abstract

In this report, double-lap shear specimens are prepared from woven carbon and woven glass plies and the shear strength determined on the interlaminar plane between 1) two carbon plies, 2) two glass plies and 3) one carbon and one glass ply specimens were prepared from dry woven mats hand lay-up in an epoxy resin matrix. All carbon specimens were also prepared from a satin weave carbon /epoxy pre-preg. Tests are performed under static loading using an Instron Testing Machine and under impact loading using a tensile split Hopkinson bar. The results show that the interlaminar shear stress is highest for the specimens prepared from the carbon/epoxy pre-preg under both static loading and impact loading. For the specimens prepared from dry woven mats and epoxy resin under static loading the interlaminar shear strength is highest for the hybrid hand lay-up and is lowest for the all glass hand lay-up. For the all carbon hand lay-up the interlaminar shear strength is slightly less than that of the hybrid specimen. The results also show that interlaminar shear strength is remarkably strain rate dependent. The interlaminar shear strength increases by about 72.6% under impact loading for the all glass material, 70.4% for the all carbon material and 55.6% for the hybrid material. Under impact loading the interlaminar shear strength is highest for the all carbon hand lay-up and is lowest for the all glass hand lay-up. For the hybrid specimen it is slightly less than for the all carbon hand lay-up.

1 Introduction

In many cases composite materials are used in the form of laminates. This is especially true for the woven composite materials. In such materials delamination is one of the main failure modes. The critical value of the interlaminar shear strength for failure, therefore, is a very important parameter for engineering design and the analytical study of the failure process [1]. The experimental measurement of the interlaminar shear strength is very difficult. The main reason is that the thickness of composite laminates is very small compared with the other dimensions. It is extremely difficult, therefore, to obtain a pure shear state along the thickness direction so that the failure is dominated by shear. There are only a few reports [2,3] concerned with the interlaminar shear strength measurement up to now, particularly under dynamic loading[4,5].

The first type of specimen used to measure the interlaminar shear strength under static and impact loading in Oxford was a thin-walled tubular specimen. This was tested in a torsional split Hopkinson bar apparatus[6]. More recently a double lap design of shear specimen has been developed[7]. The advantages of this specimen design are that the specimen can be loaded easily in the split Hopkinson tension bar device, the specimen failure is dominated by the interlaminar shear stress and failure occurs on a predetermined plane. It is possible, therefore, to measure the interlaminar shear strength between a carbon ply and a glass ply in the hybrid specimen. In reference[8] the interlaminar shear stress distribution along the shear failure plane for three different double-lap specimens are calculated using the finite element method. The results show that the shear stress distribution is far from uniform. There are shear stress concentrations at each end of the failure plane. This is a general problem in the design of shear specimens. So the experimental results measured using this specimen design give only an approximate estimate of the interlaminar shear strength. However, this specimen may be used to compare the interlaminar shear strength at different strain rates and for different types of interface.

In this report, the interlaminar shear strengths between two carbon plies, two glass plies and a carbon ply and a glass ply are experimentally measured under static loading and impact loading using the double lap shear specimen.

2 Experimental techniques

2.1 Materials and specimens

The double lap shear specimen design is shown in Fig. 1 . The shear stress distribution along failure plane can be found in reference[8]. The materials of

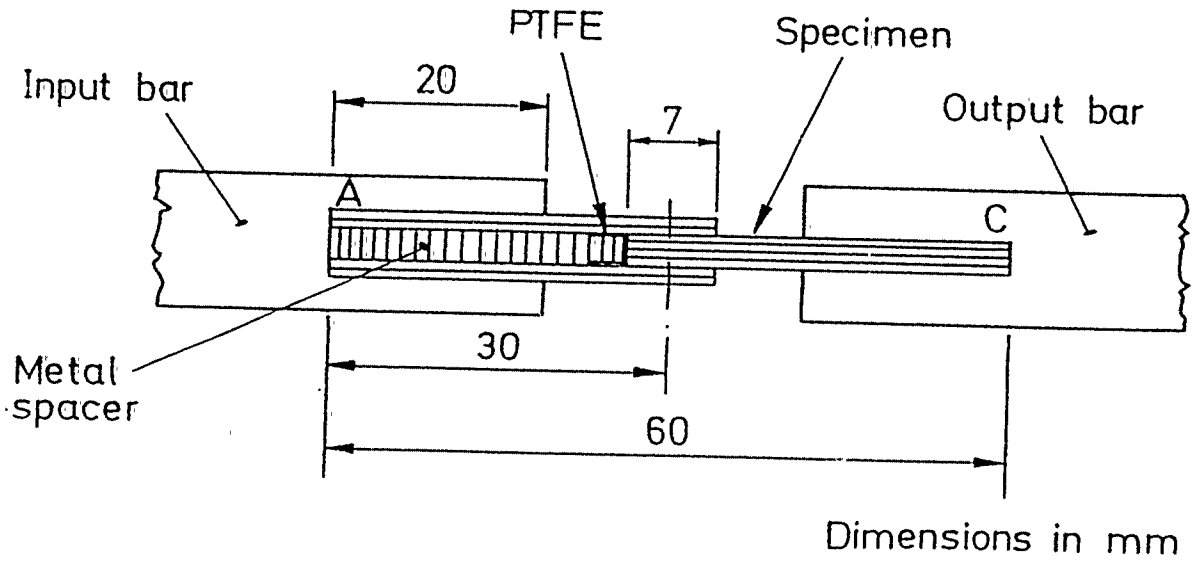

Fig. 1 Double Lap Shear Specimen

specimen are pre-preg of all carbon and hand lay-up of all carbon, all glass and carbon/glass hybrid.

2.1.1 Pre-preg of all carbon

For the initial tests, the specimens were made from a woven carbon/epoxy pre-preg available in the laboratory. This employed a 5-end satin weave fabric, woven from 3000 filament fibre tows with, respectively, 70 and 72 yarns per 10 cm in the warp and weft directions, and having a dry weight of 285g/m^2. The pre-preg was manufactured by Hexcel and Genin using a type ES. 36 self-adhesive epoxy resin to give a fibre weight fraction of 52% and an uncured pre-preg weight of 548g/m^2. Eight layers of pre-preg were laid up, using metal spacers covered with PTFE as shown in Fig. 2, and then covered by peel ply, pin-prink film, breather fabric and Nylon bagging film as shown in Fig. 3. This was then placed inside an autoclave at an air pressure of 90 psi on top of the Nylon bagging film and evacuated to 20 inches of mercury underneath the Nylon bagging film. The autoclave was placed inside a small oven. The temperature was raised over a period of an hour to 125°C, held for 2 hours and then allowed to cool to room temperature. Specimens of 10 mm width were cut from the resulting laminates using a diamond saw.

2.1.2 Hand lay-up

When specimens are prepared from dry fabrics the use of a vaccum and a high pressure is particularly important if the void content of the final materials is to be minimized. However under high pressure some resin loss occurs making the final fibre volume fraction higher than intended. In order to reduce resin loss a small autoclave of 160 x 90 x 10 mm inside dimension was used. The arrangement inside the small autoclave, as shown in Fig. 4, is similar to that for the pre-preg material. Three metal plates covered by PTFE were used to make sure that the laminate is of double lap shape in section and the overlap length is about 7 mm. The material in the small autoclave, as for the pre-preg lay-up, was covered by peel ply, pin-prink film, breather fabric and Nylon bagging film but only evacuated to 25 inches of mercury underneath the Nylon bagging film to limit resin loss.

The matrix uses the Ciba-Geigy XD 927 epoxy resin system, with 100 parts by weight of resin to 36 parts by weight of hardener and a cure schedule in which the temperature raised over a period of an hour to 100^{O}C, held for 16 hours and then allow to cool to room temperature at the rate of 8^{O}C/hour.

All dry fabrics were of plain weave construction. The carbon fibre fabric was woven from Toray 3000 filament fibre tows, type T300 - 3000A, and had a weight of 189g/m^2 and an approximate thickness of 0.28 mm. The fibres were supplied with a surface treatment suitable for use with epoxy resin. The fabric has a relatively

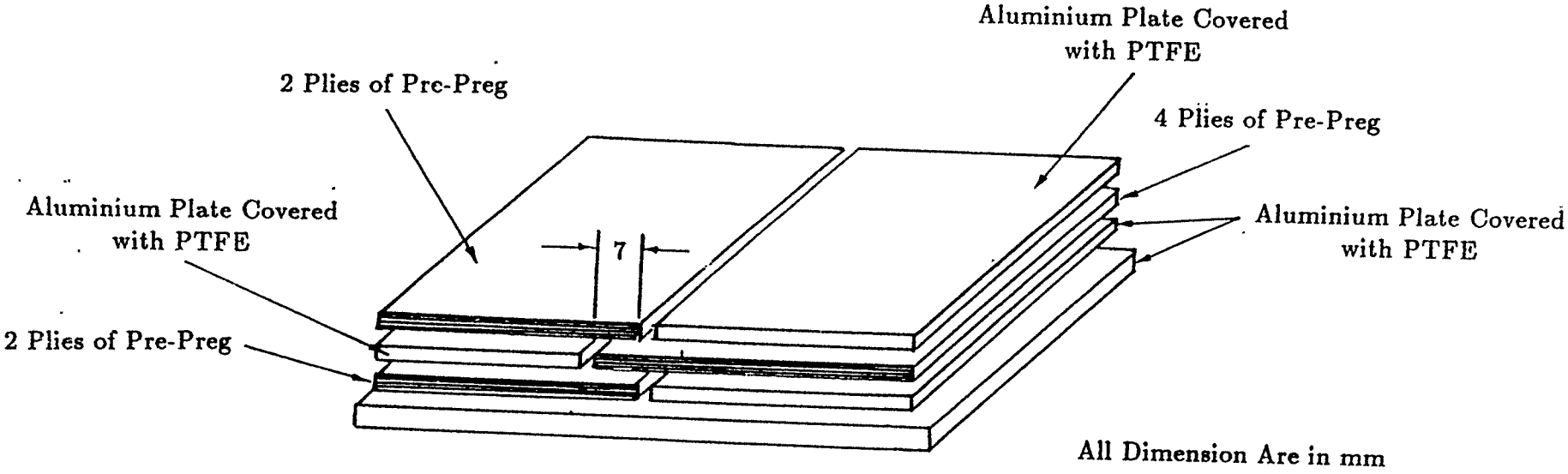

Fig. 2 Preparation of All Carbon Pre-preg Specimen

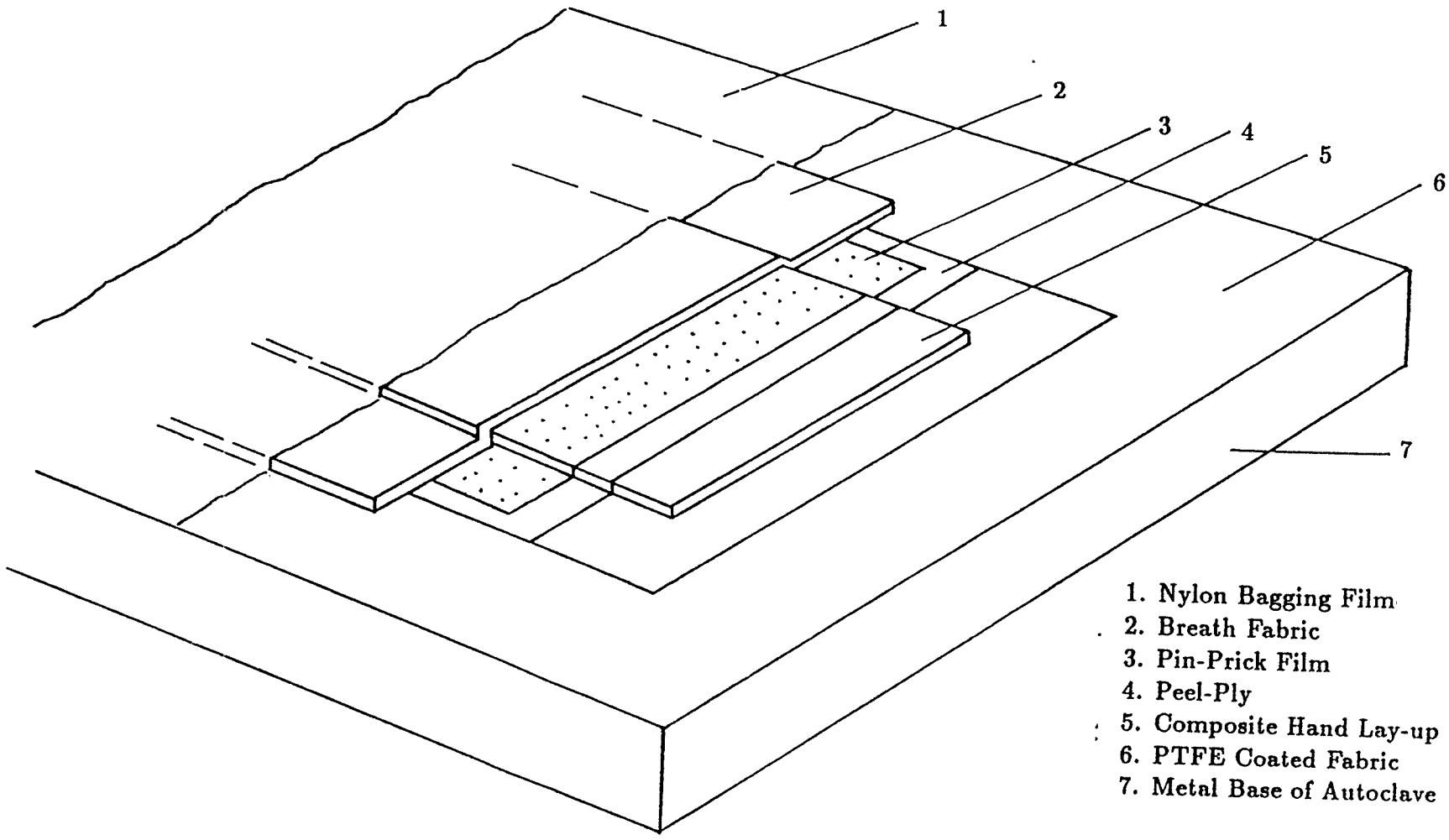

Fig. 3 Arrangement of Autoclave

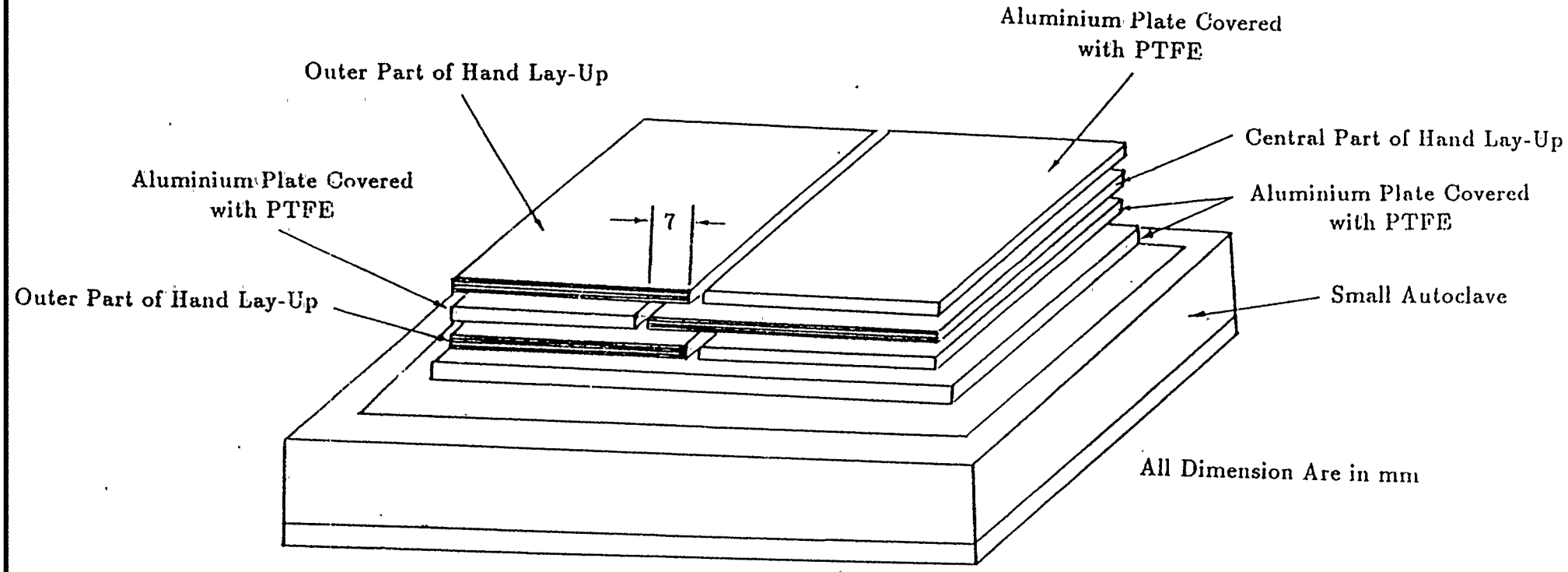

Fig. 4 Preparation of Wet Hand Lay-up Specimen

coarse weave geometry, with only 47 ends and picks per 10 cm. The glass fabric was woven from continues E - glass fabrics, designation 11 x 2EC5, and has a weight of $96g/m^2$ and approximate thickness of 0.10 mm. With 252 ends and 173 picks per 10 cm, the weave was much finer than for the carbon fabrics. The fibre finish type 205, was suitable for both epoxy and polyester resin.

For the all carbon shear specimen two different stacking sequences were used as shown in Fig. 5 (a) and (b). One is composed of a total of eight layers and the fibre weight fraction is 39.0%. These specimen was found to fail along the pre-chosen failure plane under static loading but to fail in tension in the central part under the dynamic loading. For this reason the second lay-up was prepared with 5 plies in the central region (fibre weight fraction 45.7%). All these specimen failed in shear under impact loading although some still also failed simultaneously in tension.

Finite element analysis[8] indicate that for the hybrid specimen shear stress variation on the failure plane are minimized if the stacking sequence show in Fig. 5(c) is used. With this lay-up shear failures were obtained under static loading but tensile failures were sometimes obtained under impact loading. Here again, therefore, an improved lay-up, see Fig. 5(d), was used which gave shear failure under dynamic loading. In this case simultaneous tensile failures were sometimes obtained , this time in one of the outer ligaments.

The lay-up for the all glass specimens is shown in Fig. 5(e) with 11 plies in the central part. Two different laminates were prepared, the first having received a modified curing schedule, remaining for 13 hours at ambient temperature before the temperature was raised to 100°. Specimens from both laminate failed by shear at both loading rate. Table 1 list the various types of specimen and the strain rates at which they were tested.

2.2 Equipment

2.2.1 Loading system

For quasi-static tests in the Instron Test Machine the specimen is glued between two small slotted bars one of which has a strain gauge load cell with a static calibration of $428\mu V/kN$. The integrated output from a pair of linear variable differential transformer is used to determine the displacement across the specimen.

The impact tests are performed used a split tensile Hopkinson bar loading by means of a gas-gun shown schematically in Fig. 6 and in the photograph of Fig. 7 and Fig. 8. In this arrangement, the projectile is cylindrical in form and

(a) All Carbon Pre-Preg and Hand Lay-Up (1) (8 plies)

(b) All Carbon hand Lay-Up (2)(11 Plies)

(c) Hybrid hand Lay-Up (1)(11 Plies)

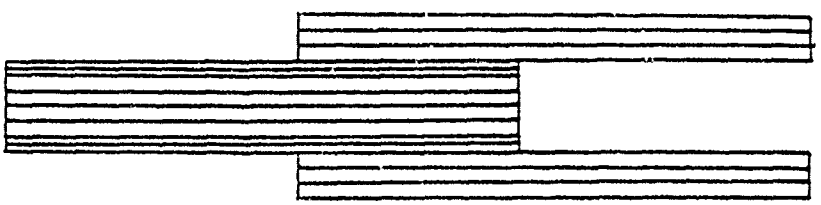

(d) Hybrid hand Lay-Up (2)(14 Plies)

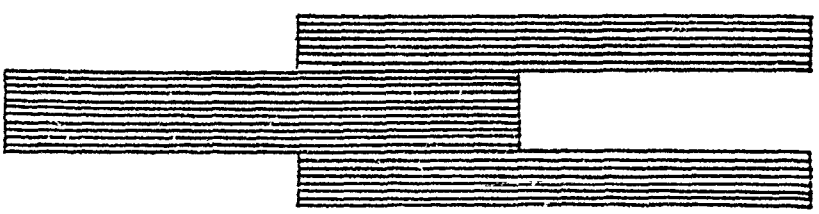

(e) All Glass hand Lay-Up (25 Plies)

Fig. 5 Stacking Sequence of the Specimens

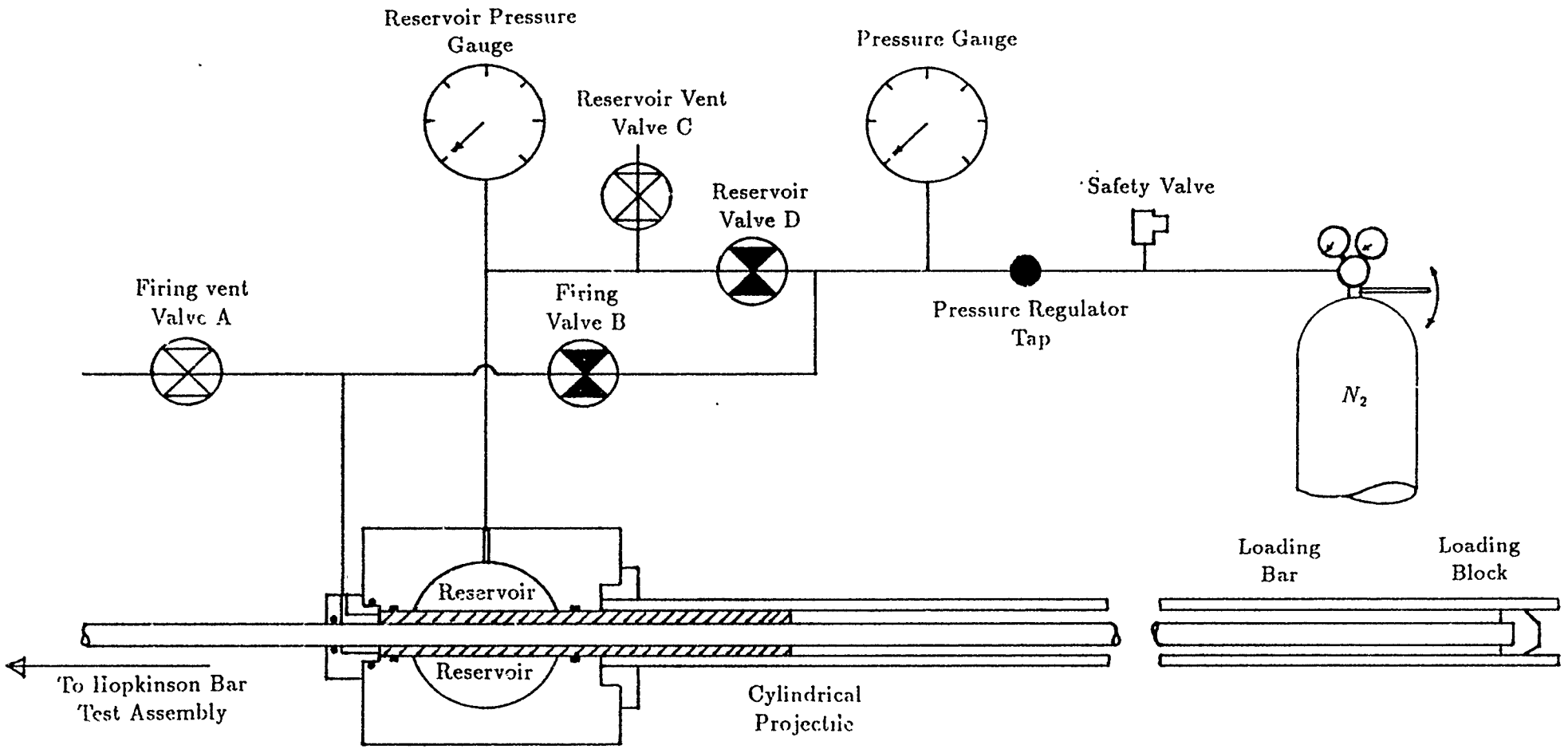

Fig. 6 Schematic Diagram of Tensile Gus-Gun

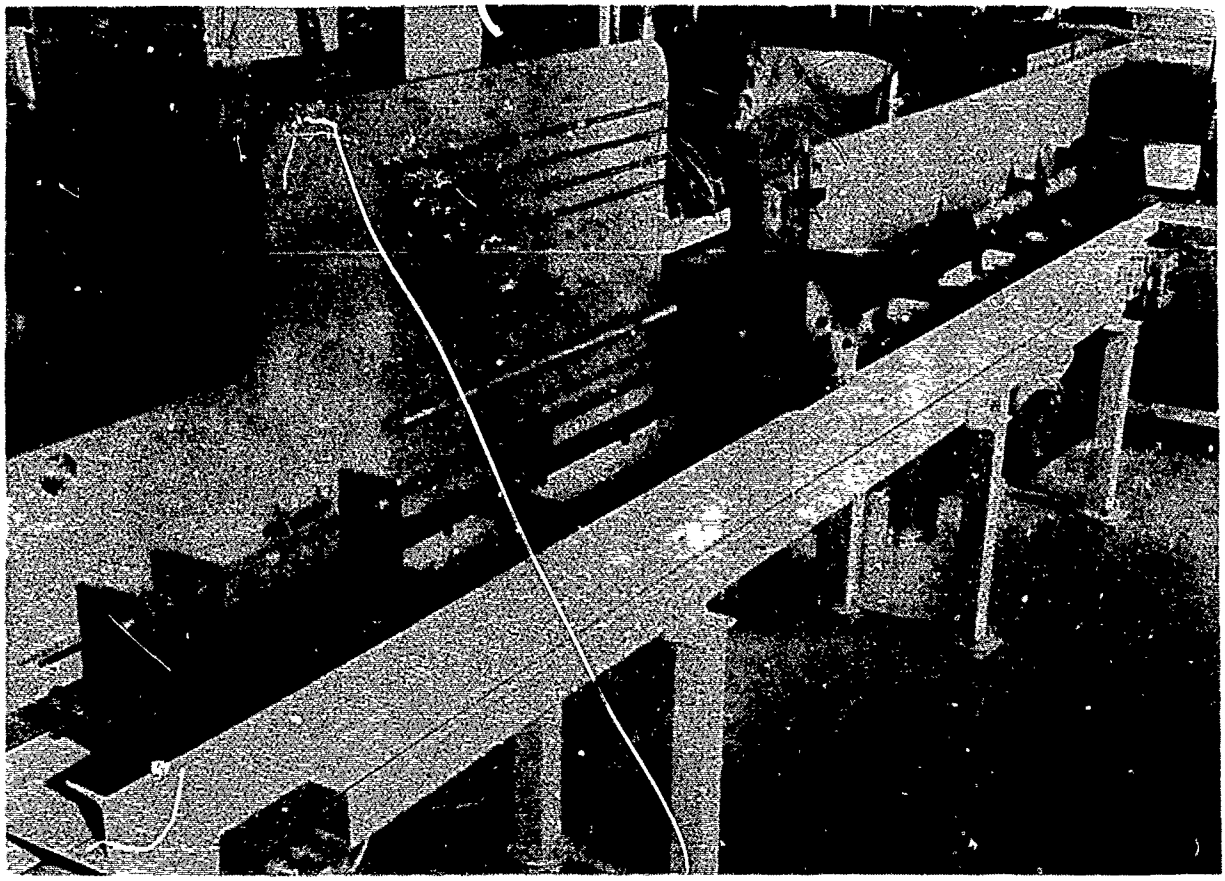

Fig. 7 General View of Tensile Gas-gun

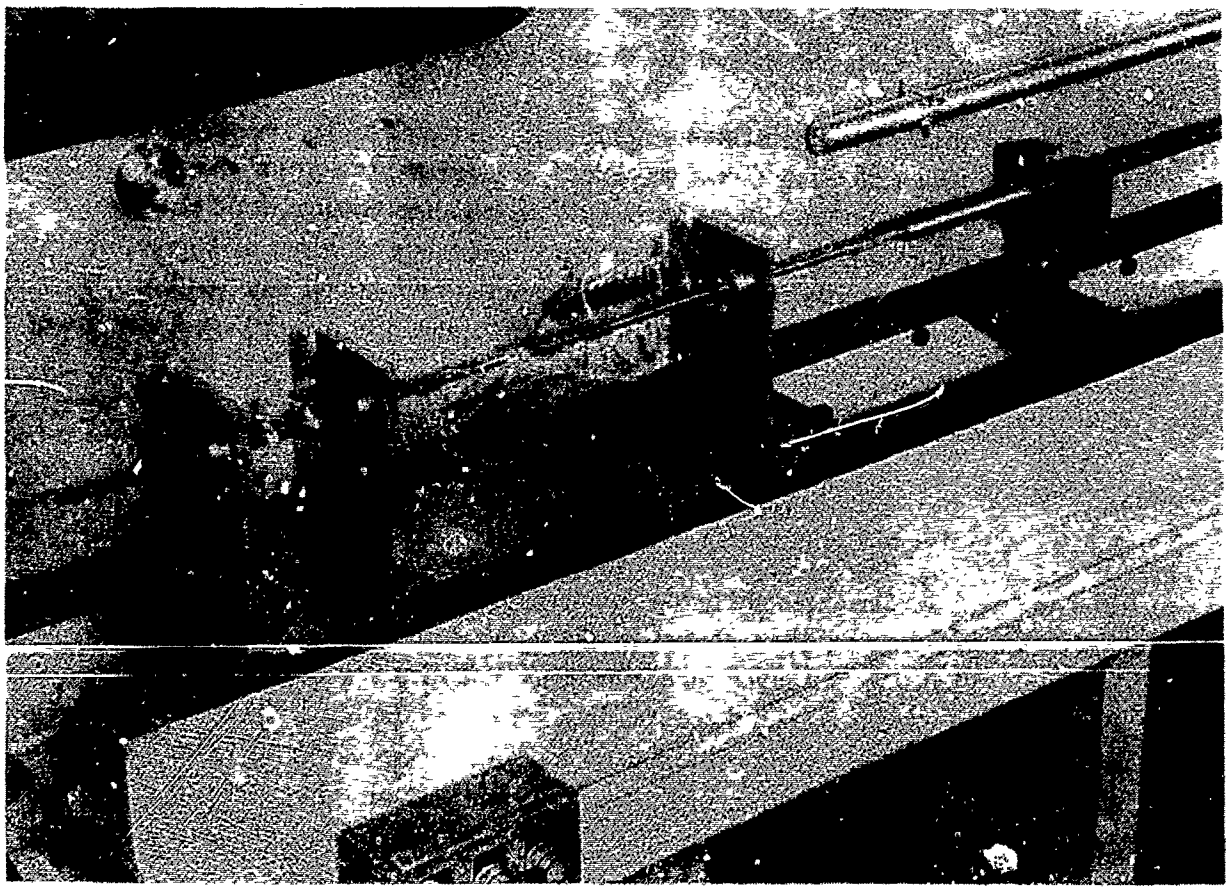

Fig. 8 Hopkinson Bar Test Assembly for Tensile Gas-gun

Table 1: Test having been done

interlaminar zone	carbon/ carbon		carbon/ glass		glass/ glass	
resin percentage	39.0	45.7	49.1	42.0	52.5	56.7
number of layer	8	11	7 + 4*	10+4	11	11
central layers	4	5	3+4	4+4	5	5
test situation	static	static dynamic	static	static dynamic	static dynamic	static dynamic

7 + 4*: seven layers of carbon reinforced ply and four layers of glass reinforced ply.

slides freely on the loading bar which extends through the back of the gun to the split Hopkinson bar test assembly. When the projectile impacts the loading block, which is attached to the right-hand end of the loading bar, a tensile wave is set up which travels back along the loading bar to the test assembly. This consists of the input bar, the specimen and the output bar.

There are two gauge stations on the input bar which can record the incident stress wave and reflecting stress wave and one gauge station on the output bar which records the output stress wave. At each gauge station, four electrical resistance strain gauges were attached at 90^O intervals and wired in opposite pairs to maximise the sensitivity of strain measurement and cancel any bending strain. The gauges were connected to a purpose built bridge circuit box with a stabilized bridge voltage of 5 volts. A static calibration gives 643.24 $\mu V/kN$ for gauge station I, 609.65 $\mu V/kN$ for gauge station II and 642.12 $\mu V/kN$ for output bar gauge station.

2.2.2 Electronic recording equipment

The signals from the three gauge stations are amplified using a FYLDE 351UA(UNI-AMP) amplifier, and then stored in Data lab type 912 two channel transient recorder. They are displayed on the screens of TRIO CS-1212 (20 MHz) oscilloscopes. Afterwards, the experimental data are stored on floppy discs in an IBM-PC computer and a hard copy obtained on an Epson printer. A block diagram and the recording system is given in Fig. 9 and typical strain gauge signals are shown in Fig. 10.

In the quasi-static tests, a load-time trace is obtained from a strain gauge load

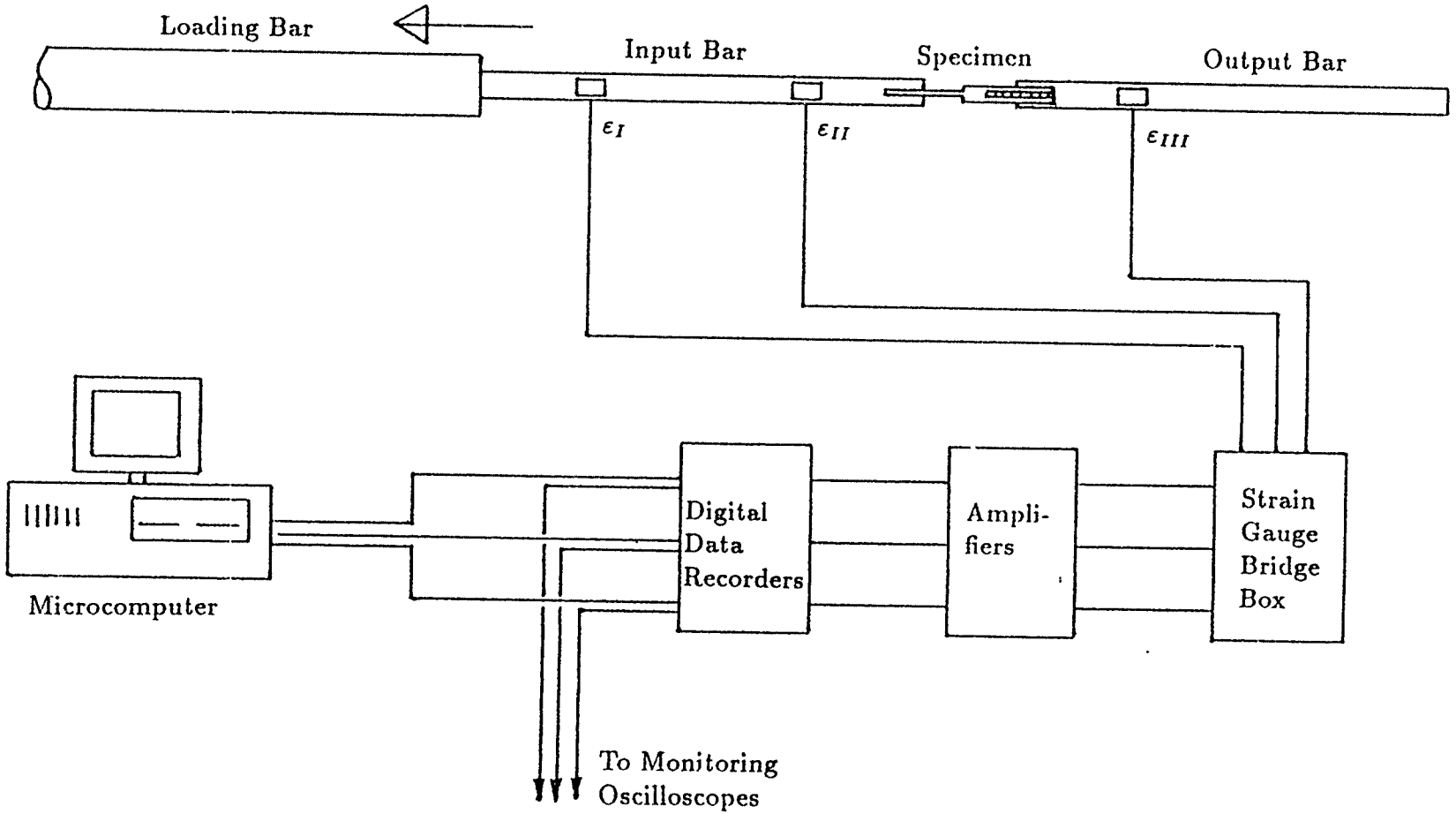

Fig. 9 Schematic Diagram of Electronic Apparatus Used for Impact Test

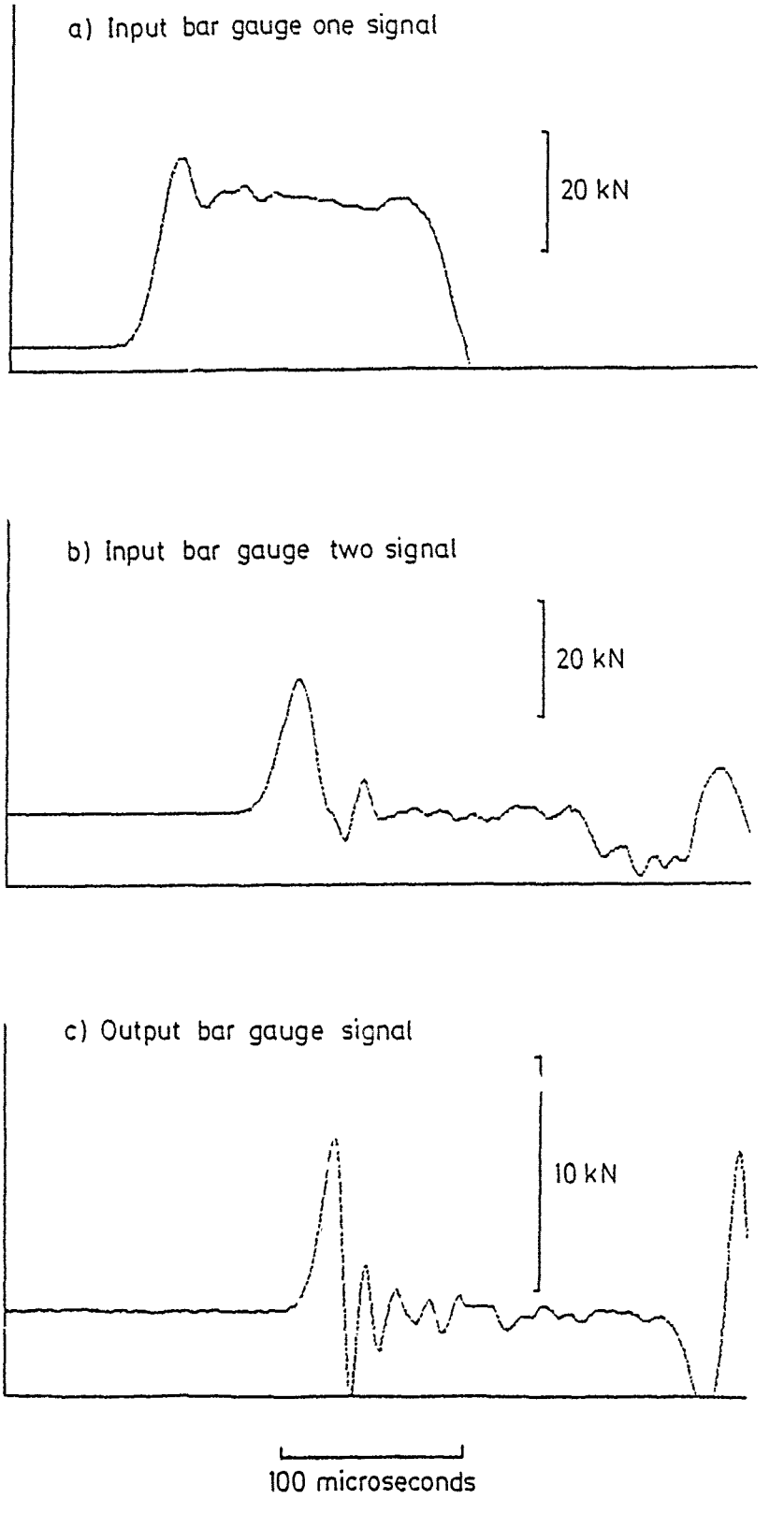

Fig. 10 Strain Gauge Signals for Impact test on All-Carbon Pre-Preg Specimen

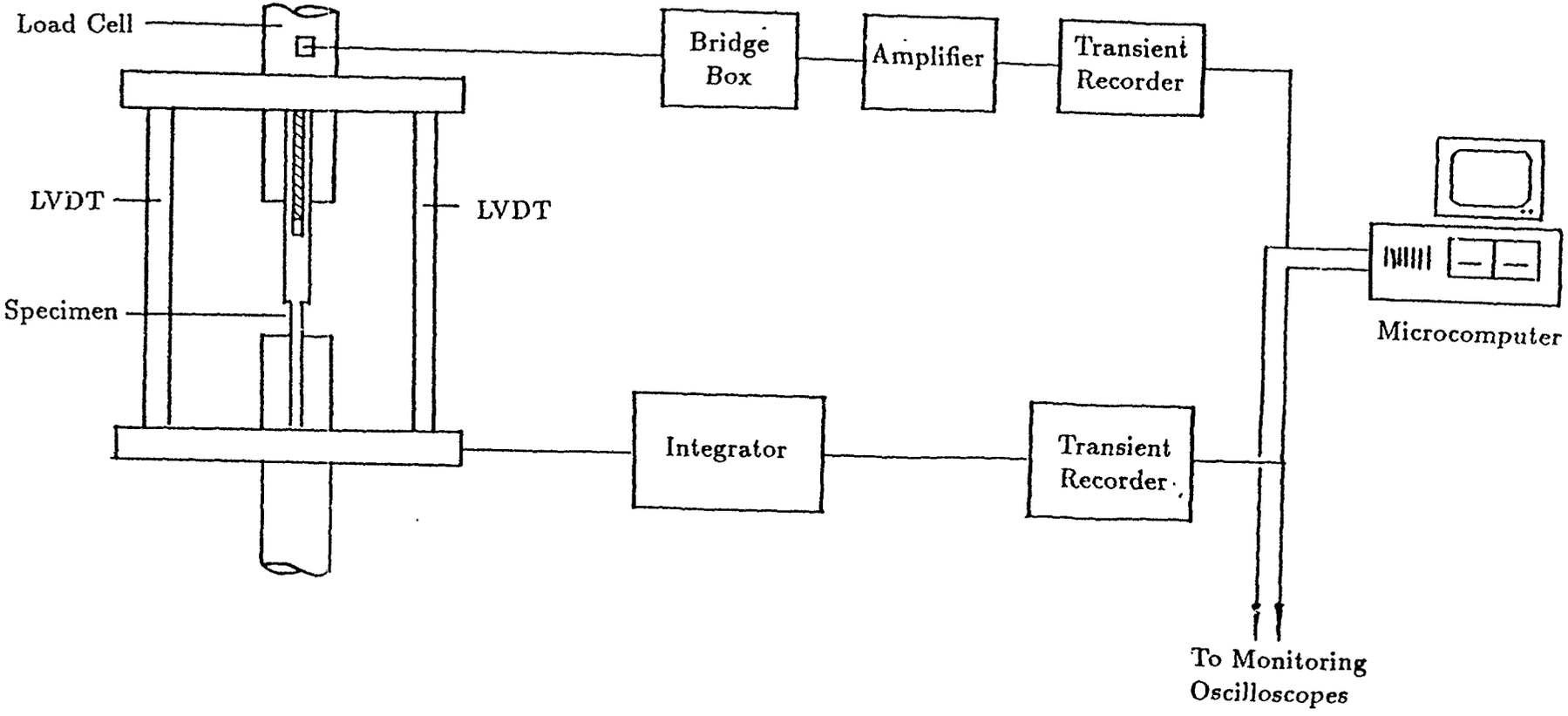

Fig. 11 Schematic Diagram of Electronic Apparatus Used for Quasi-static Test

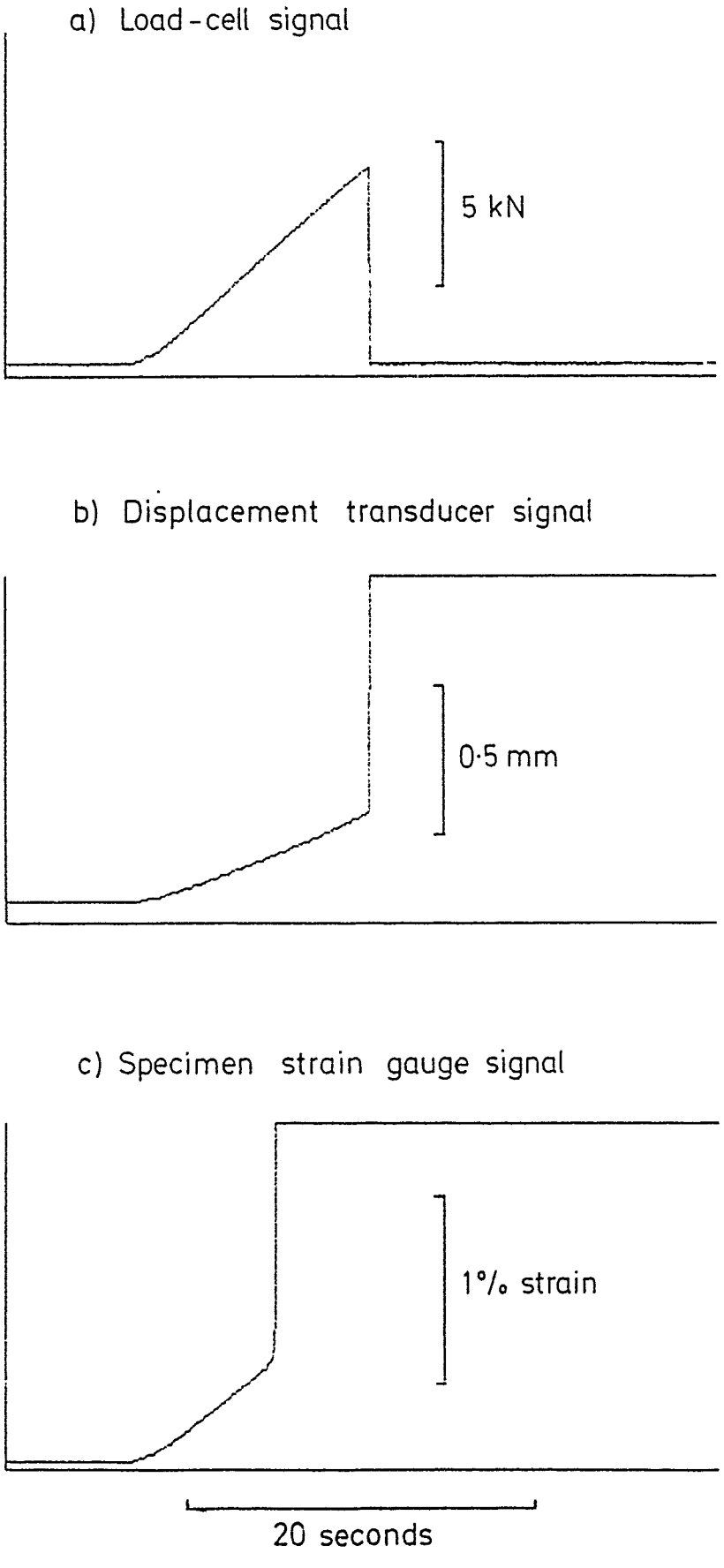

Fig. 12 Raw Data for Quasi-Static test on All-Carbon Pre-Preg Specimen

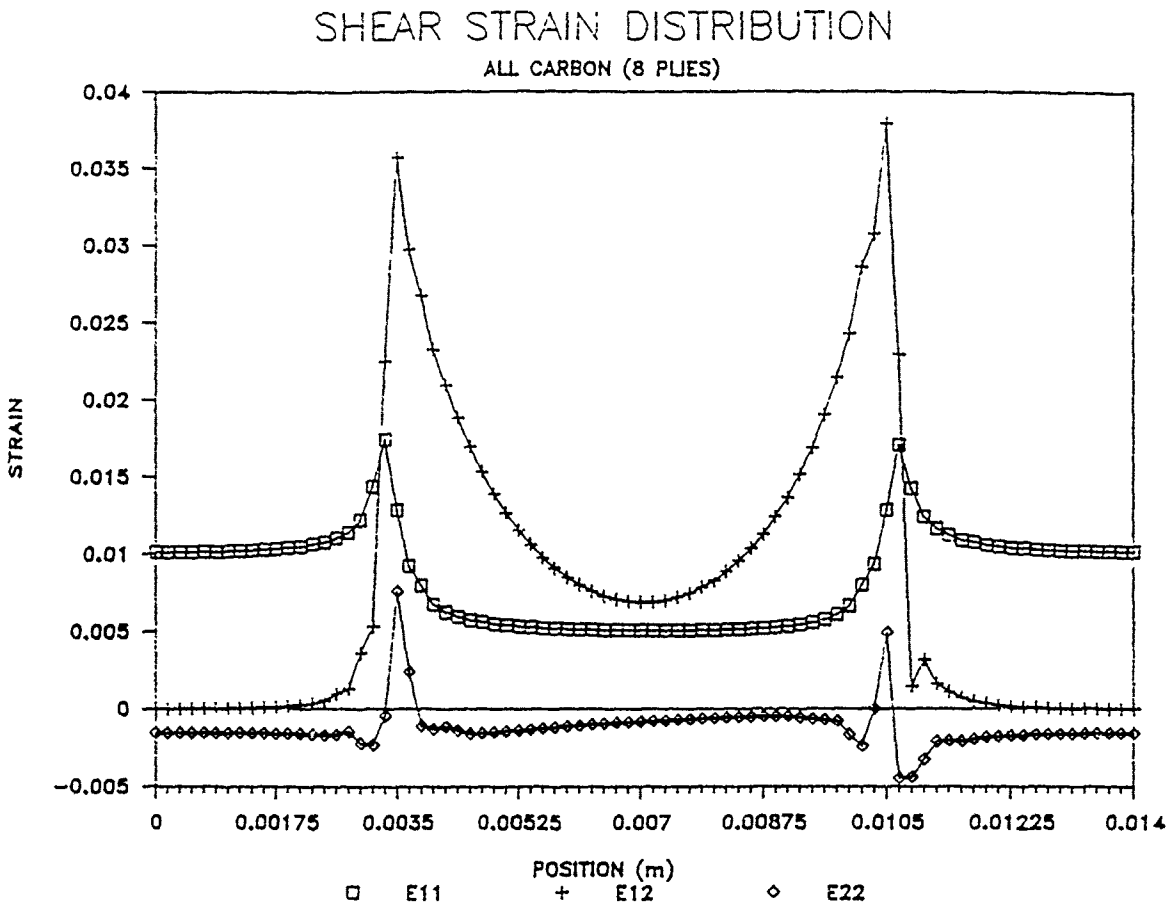

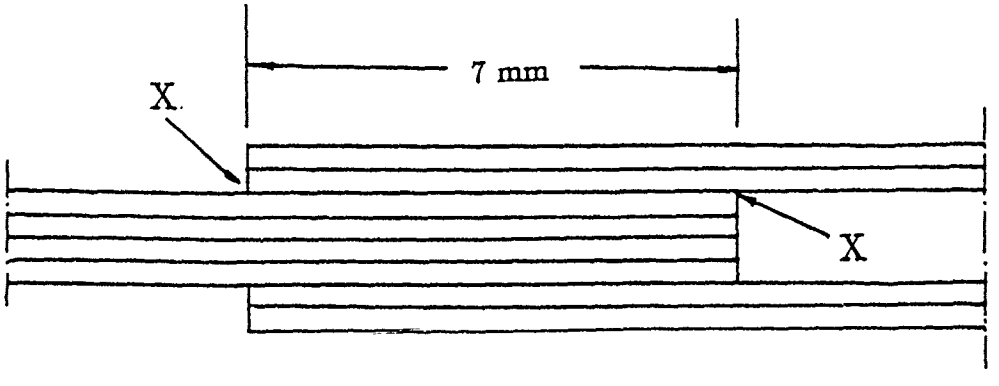

Fig. 13 Shear Strain Distribution Along Shear Plane for All Carbon Specimen (8 Plies)

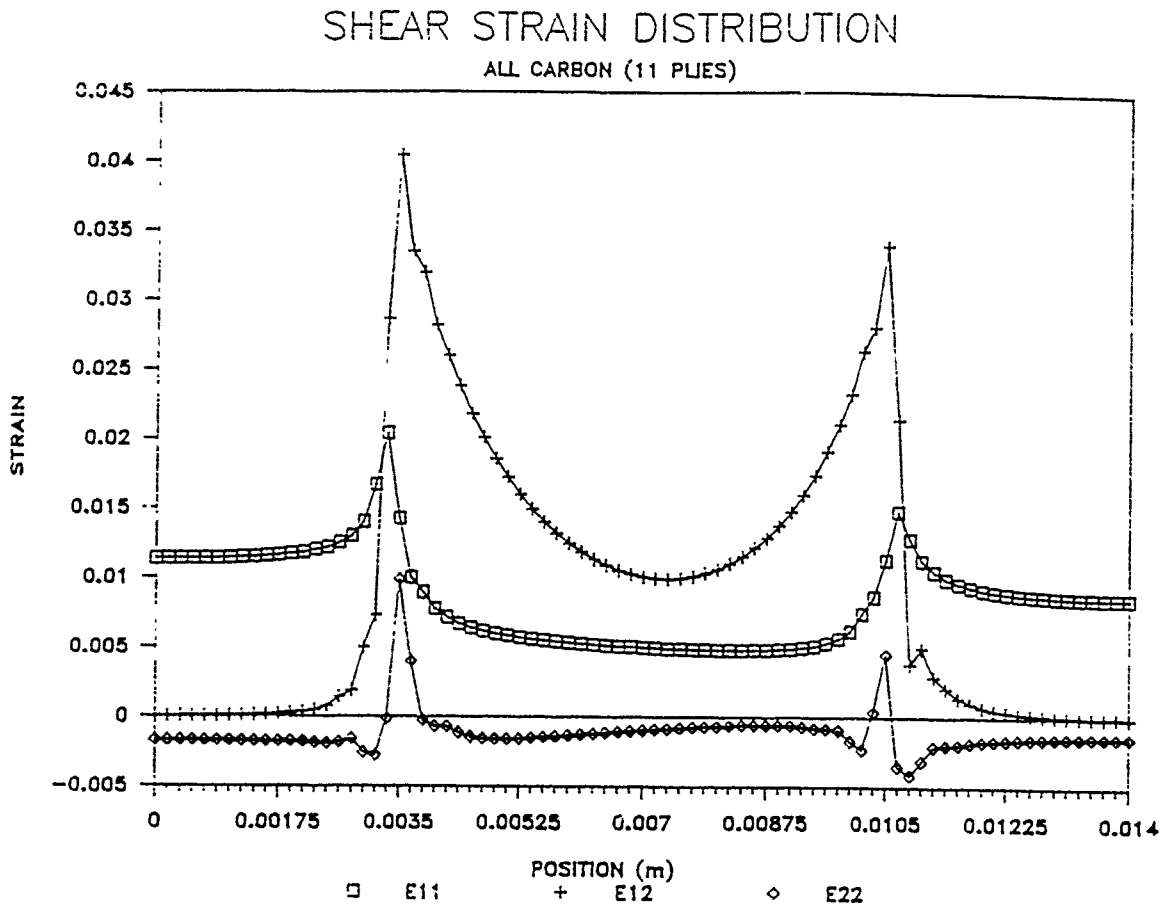

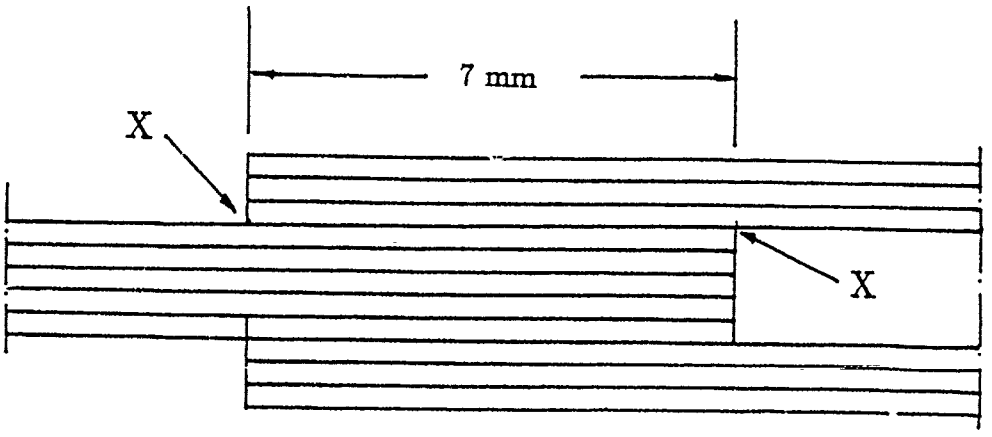

Fig. 14 Shear Strain Distribution Along Shear Plane for All Carbon Specimen (11 Plies)

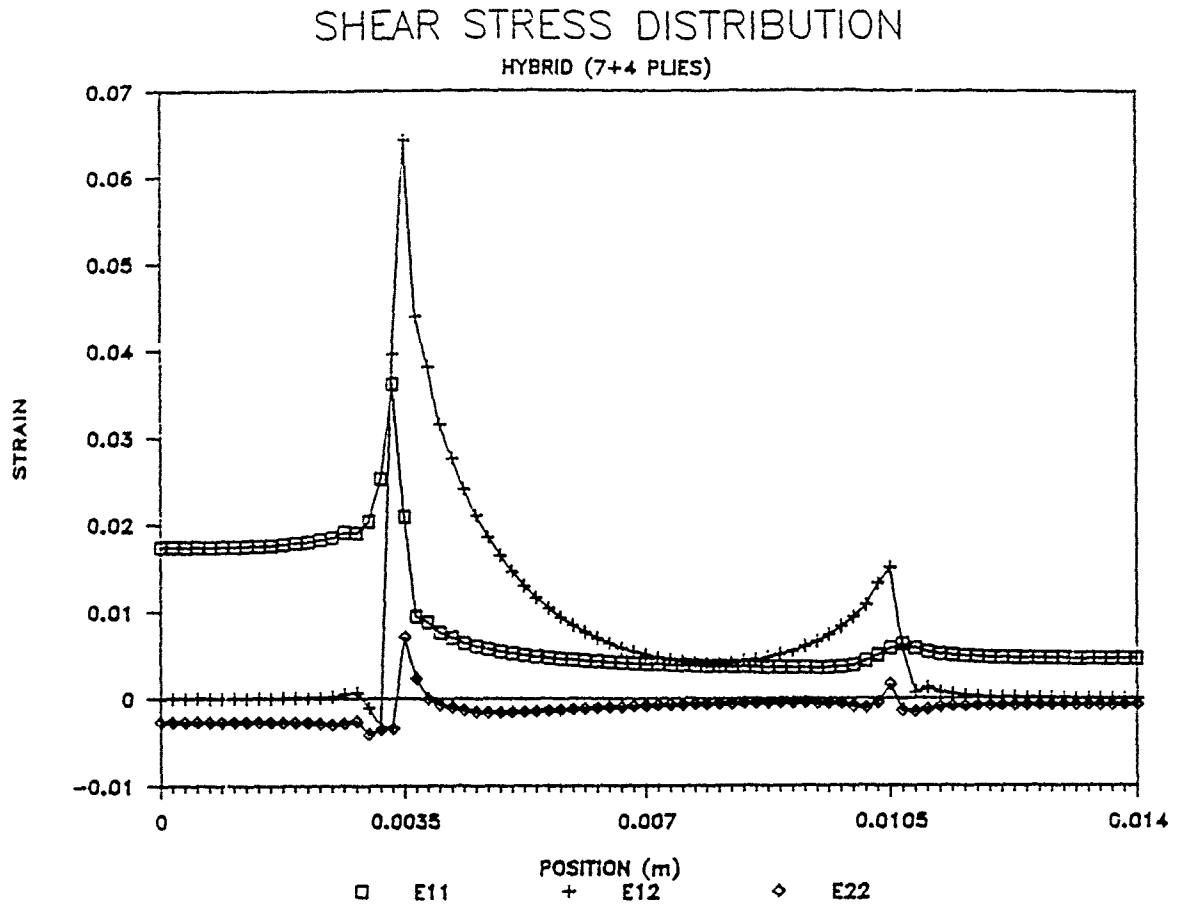

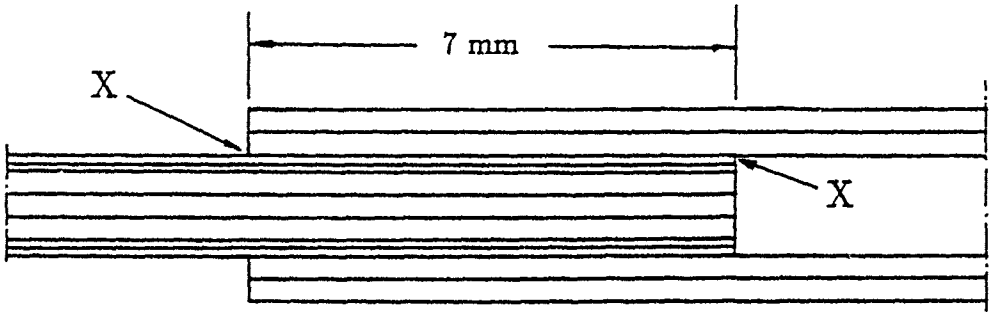

Fig. 15 Shear Strain Distribution Along Shear Plane for Hybrid Specimen (11 Plies)

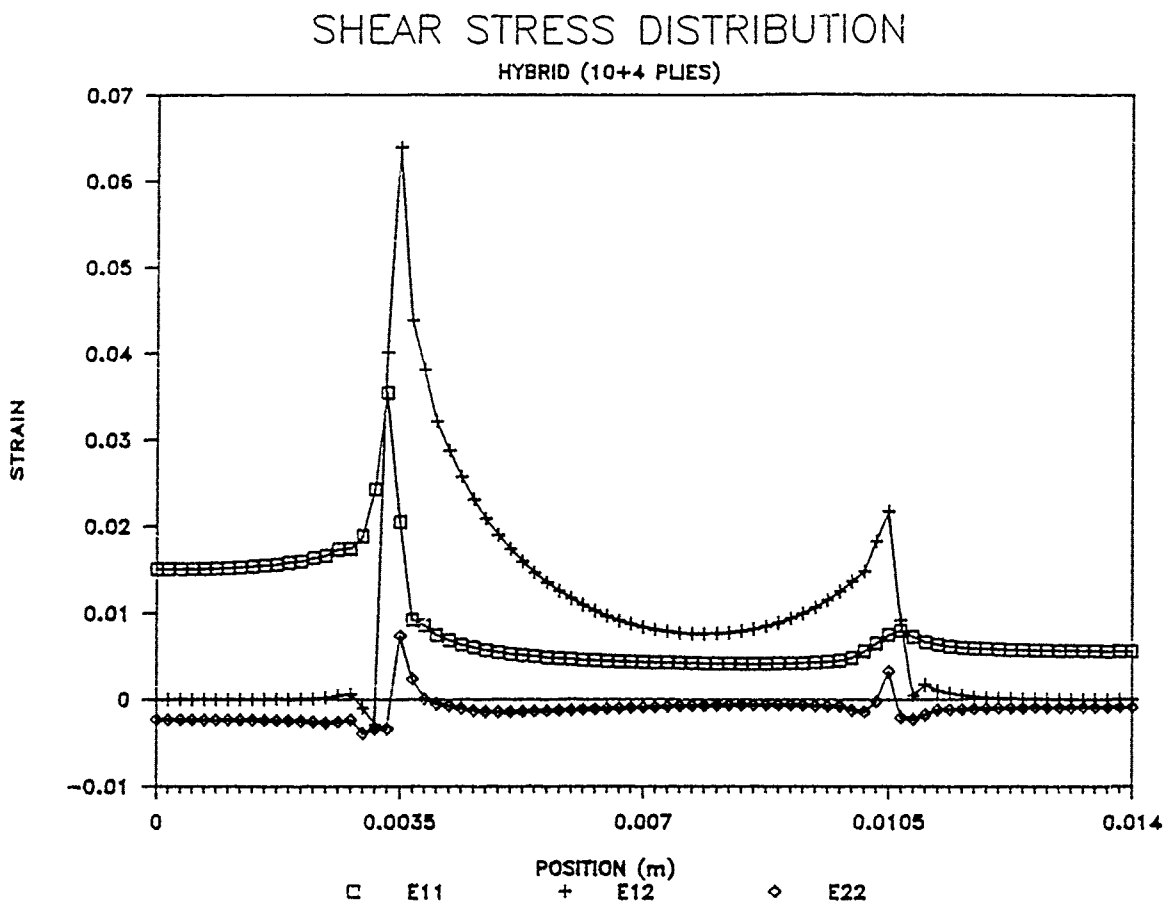

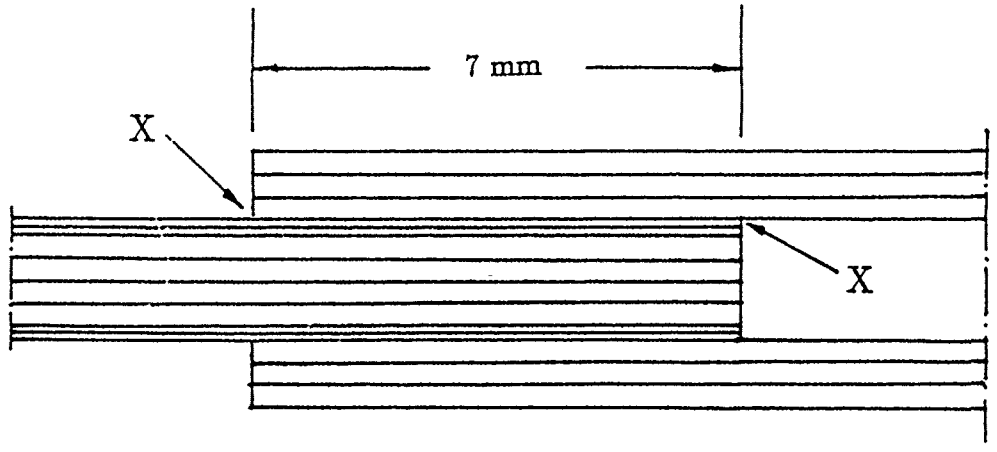

Fig. 16 Shear Strain Distribution Along Shear Plane for Hybrid Specimen (14 Plies)

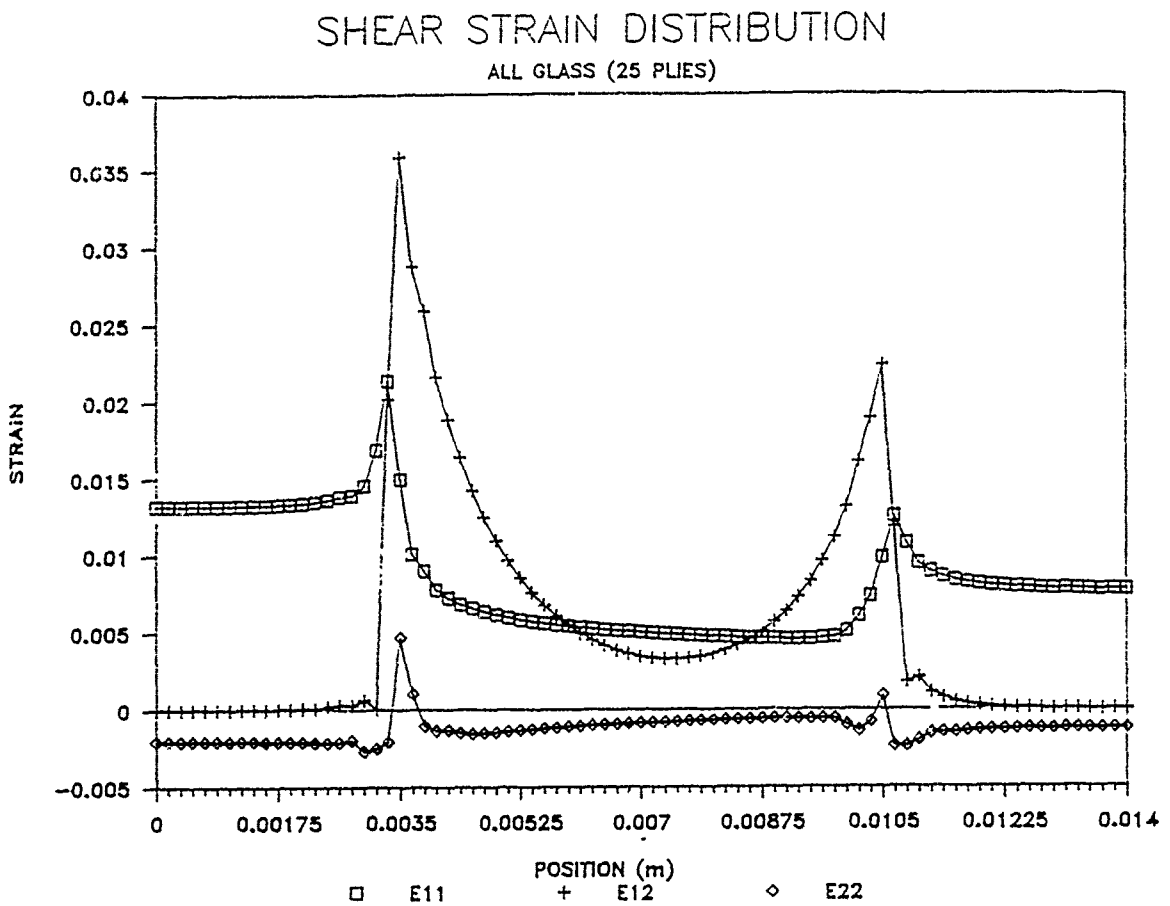

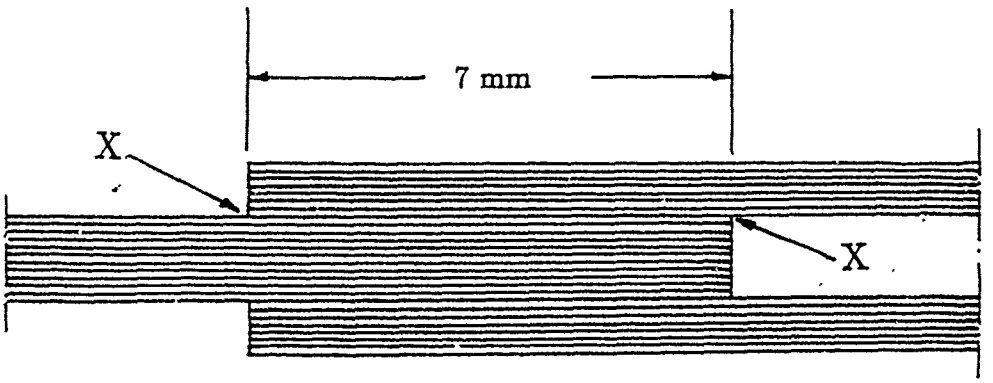

Fig. 17 Shear Strain Distribution Along Shear Plane for All Glass Specimen (25 Plies)

cell while the displacement across the ends of the specimen is measured using a pair of linear variable differential transformer(LVDT's) is parallel with the specimen. A block diagram of the recording system is shown in Fig. 11 and the typical signals obtained are shown in Fig. 12.

2.3 Analysis of test data

2.3.1 The principle of analysis

The quasi-static case

For the quasi-static test, the specimen shear loading can be calculated from the load cell signal and the calibration factor. The average shear strength at failure is given by dividing the maximum load by the total area of the shear plane, assuming the load to be shared equally between the two interlaminar planes. The displacement across the ends of the specimen gives a measure of the average tensile strain No experimental measurement of the shear strain on the interlaminar plane was attempted but from finite element analyses of the five specimens shown in Figs. 13 to Fig. 17, in which a 1% tensile strain is applied across the ends of the specimen, the average interlaminar shear strain is seen to be roughly equal to the average tensile strain in the specimen in each case. Consequently an estimate of the average interlaminar shear strain may be obtained from the measured average tensile strain.

The dynamic case

Generally speaking, if the incident wavelength is much larger than the diameter of the input bar, the one dimensional stress wave theory is valid and may be used in the Hopkinson bar analysis. This was the case in the present tests. Supposing that ε_i, ε_r and ε_t are the incident, reflected and transmitted strain waves respectively, the displacement, velocity and stress at the input and output ends of the specimen are given by:

$$V_1 = C_1(\varepsilon_i + \varepsilon_r) \tag{1}$$

$$V_2 = C_2\varepsilon_t \tag{2}$$

$$U_1 = \int_{t_1}^{t} V_1 dt = C_1 \int_{t_1}^{t} (\varepsilon_i - \varepsilon_r) dt \tag{3}$$

$$U_2 = \int_{t_2}^{t} V_2 dt = C_2 \int_{t_2}^{t} \varepsilon_t dt \tag{4}$$

$$\sigma_1 = \rho_1 {C_1}^2 (\varepsilon_i + \varepsilon_r) \tag{5}$$

$$\sigma_2 = \rho_2 {C_2}^2 \varepsilon_t \tag{6}$$

where subscripts 1 and 2 represent the input and output ends of the specimen and ρ_1, C_1 and ρ_2, C_2 represent the density and elastic wave speed in the input and output bars respectively. For test in compression or tension, the average strain, strain rate and stress in the specimen can be obtained from:

$$\dot{\varepsilon}_{SA} = \frac{V_1 - V_2}{L_S} \tag{7}$$

$$\varepsilon_{SA} = \frac{U_1 - U_2}{L_S} \tag{8}$$

$$\sigma_{SA} = \frac{1}{2}(\sigma + E_2 \varepsilon_t) \tag{9}$$

where L_S is the gauge length of specimen, σ is the stress obtained from the incident and reflected stress waves and E_2 is the modulus of the output bar. This is the standard Hopkinson bar analysis. Fig. 18 shows the specimen assembly and the Lagrange(x,t) diagram for the tensile Hopkinson bar system.

In previous work[9] on the tensile testing of unidirectionally-reinforced CFRP, the strain-time signals from the three gauge stations, ε_I, ε_{II} and ε_{III}, when subjected to the standard Hopkinson bar analysis, give the results shown in Fig. 19. Note that in Fig. 19, $\varepsilon_i = \varepsilon_I$, $\varepsilon_r = \varepsilon_I - \varepsilon_{II}$ at $t > T_1$ and $\varepsilon_t = \varepsilon_{III}$. Good agreement was obtained between the stress levels σ_1 and $E_2\varepsilon_{III}$, determined at the input and output ends of the specimen. In this calculation, some modification of the stress wave speed in the grip regions of the loading bars, AA-CC and BB-DD in Fig. 18, was made to allow for the presence of the composite but the change in impedance in these regions compared with that in the loading bars alone was so small, for this particular test material, that wave reflections at section AA and BB were insignificant. The almost identical profile for the strain - time signals for gauge stations I and II at time up to T_1, see Fig. 19, confirmed that this procedure was justified.

However, in tests of woven glass reinforced specimen[10], the modulus of the specimen in significantly lower and, in some cases, the thickness of the specimen in the grip region considerably larger. In this case a more significant change in the impedance across the sections at AA and BB might be expected, affecting the validity of the standard Hopkinson bar analysis. A reflection from section AA would be expected to show up as a divergence between the signals from gauge stations I and II at even earlier time, i.e. at T_1' rather than T_1 see Fig. 20. Although, in practice, this small difference might be difficult to detect because T_1' and T_1 lie on the steeply rising part of curve.

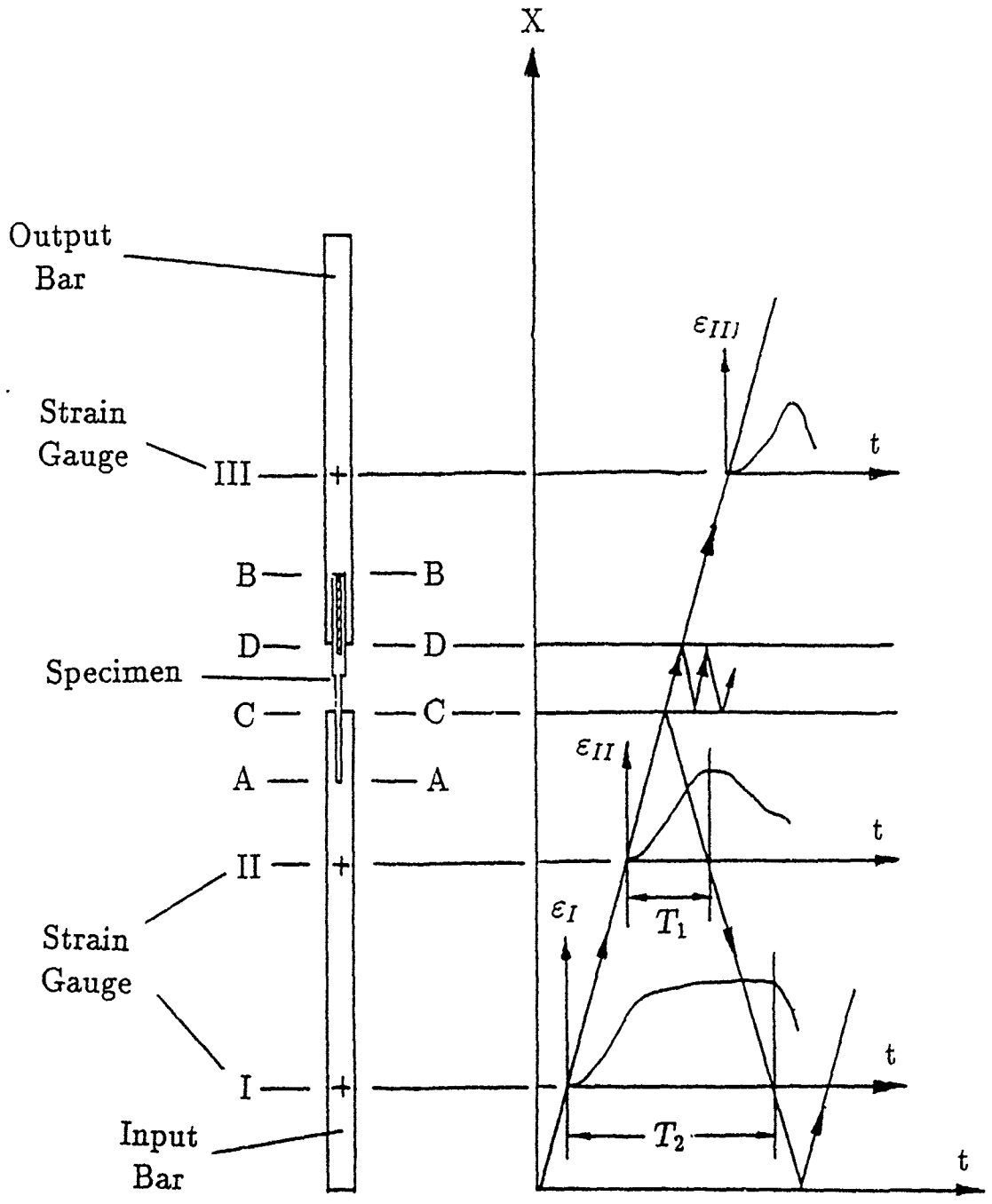

Fig. 18 Test Arrangement and Associated Langrange (x,t) Diagram

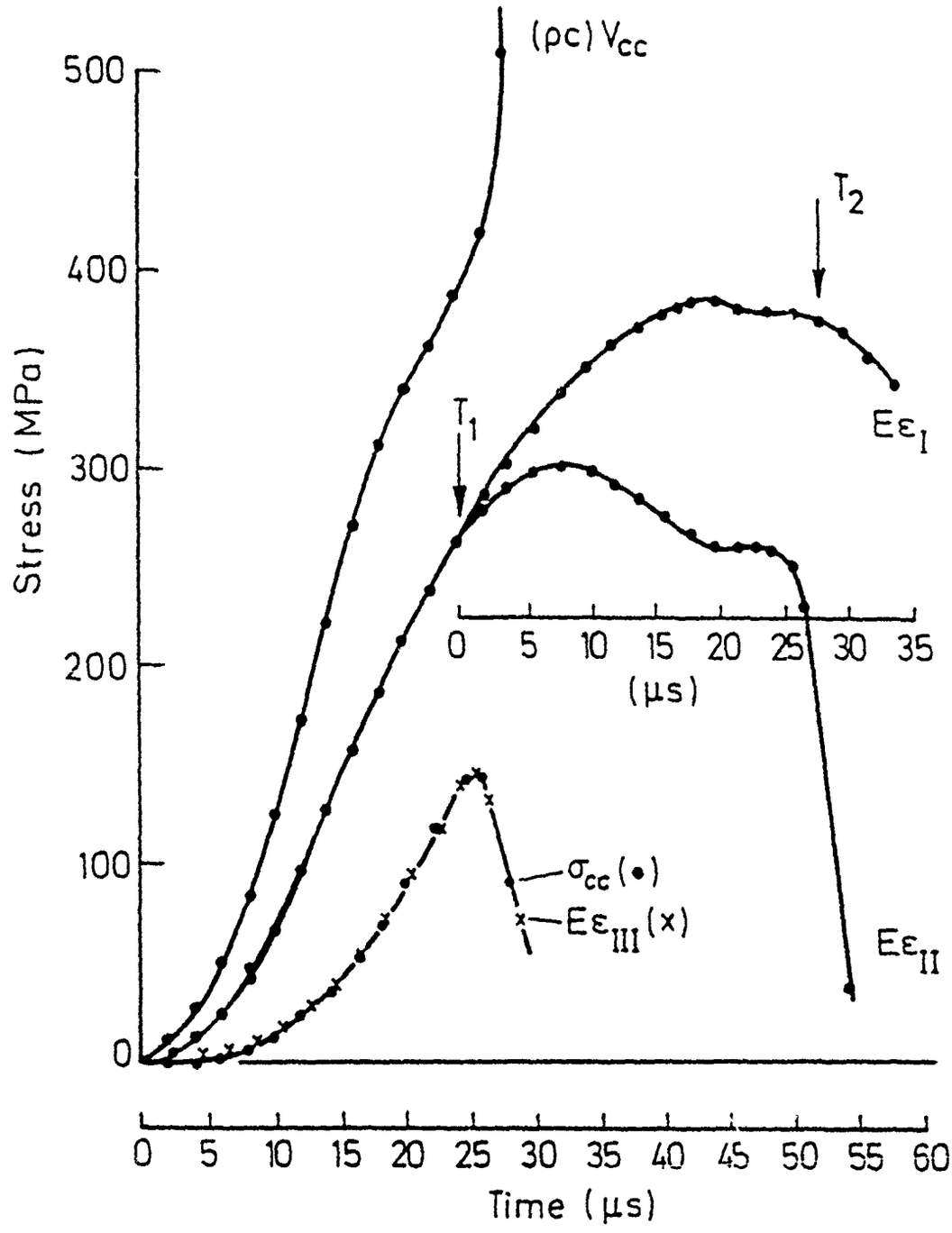

Fig. 19 Hopkinson Bar Analysis for Unidirectionally-Reinforced CFRP Specimen (from ref. [9])

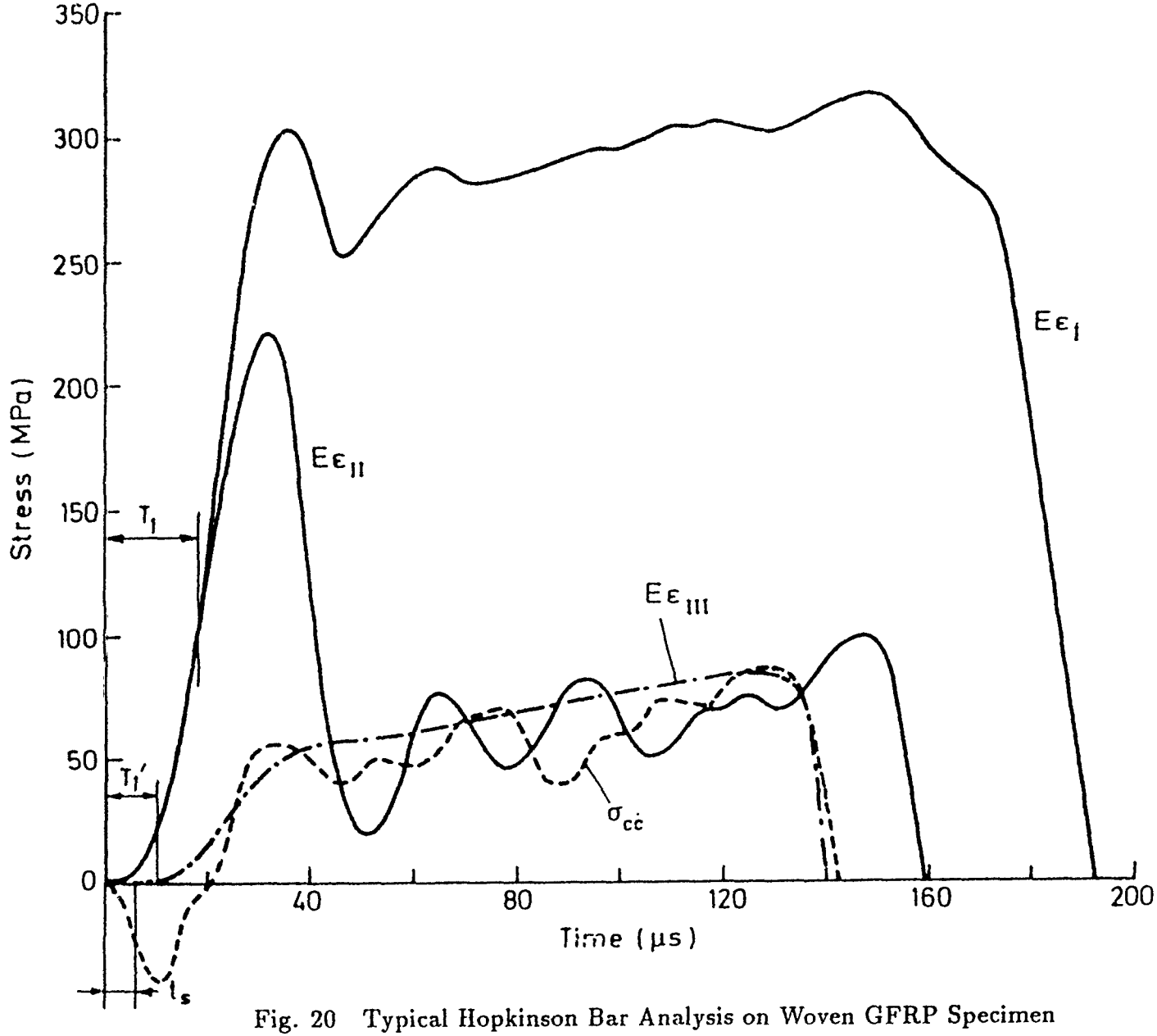

Fig. 20 Typical Hopkinson Bar Analysis on Woven GFRP Specimen (from ref. [10])

If it is assumed that these reflections remain small enough to be ignored, the stress variation at the input end of the specimen, σ_{cc}, is calculated from ϵ_I and ϵ_{II} in the standard way and is shown as the dotted curve in Fig. 20. It is compared with the stress at the output end of the specimen, $E_2\epsilon_{III}$, shown chain - dotted in Fig. 20 where t_s is the estimated transit time for a stress wave to cross the specimen.

Although, in its general form, the stress variation at the input is similar to that at the output end of the specimen, the almost exact agreement found in the unidirectional material test[10] is not reproduced. In practice, therefore, the specimen stress is always determined from the transmitted wave, equation (6), due to the very limited accuracy with which the input stress level, σ_{cc}, may be determined, derived as it is from a small difference between a large incident and a large reflected stress wave.

In the reference [10], the effort of stress wave reflections at sections AA and BB on the Hopkinson bar analysis for woven reinforced material has been studied. The resulting stress-strain curve shows a slight decrease in dynamic modulus when the stress is based on the output bar gauge. The modulus remain unaltered when the stress used is the average of that on each face of the specimen, see Fig. 21. In practice the modulus is always checked independently in the tension set up, using strain gauge attached directly in the specimen.

In the present work, using the standard Hopkinson bar wave analysis, the displacement across the specimen during the test was determined and, with the assumptions given above, interlaminar shear stress-strain curves derived using the computer analysis described in the next section, typical results for which are given in Fig. 22.

2.3.2 Computer analysis of experimental data

The various strain signals are stored in the dual- channel transient recorders and transferred directly in digital form to the microcomputer and then processed using a specially written program. The operator chooses the time zero for the gauge I trace from which the computer calculates, in terms of the densities and Young's moduli of the loading bars and the specimen, the corresponding time zero's for the gauge II and III traces and the time T_1, defined in Fig. 18, for the reflected wave first to reach the gauge station II. The signals from gauge stations I and II are then computed as stress-time traces, after subtracting the calculated time delay between them. The resulting curves may be compared on the chart recorder, a typical example being given in Fig. 22(a) for the test on carbon pre-preg specimen. The two computed time curves should be coincident at times $< T_1$ and should only begin to diverge when the time exceeds T_1. If necessary the operator can choose

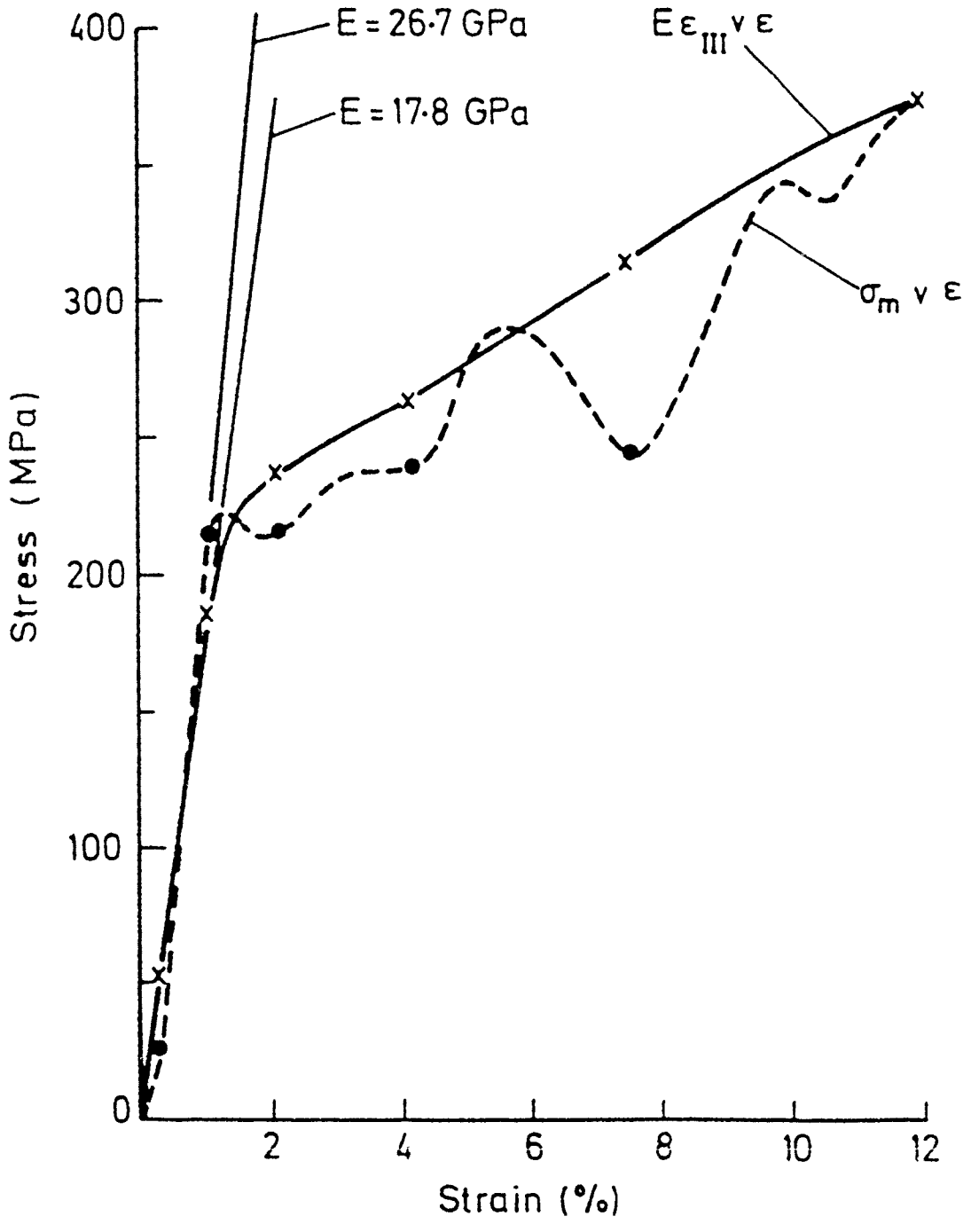

Fig. 21 Stress-Strain Curves Based on Fig. 20 Analysis Ignoring Wave Reflection in Specimen Grip Region (from ref. [10])

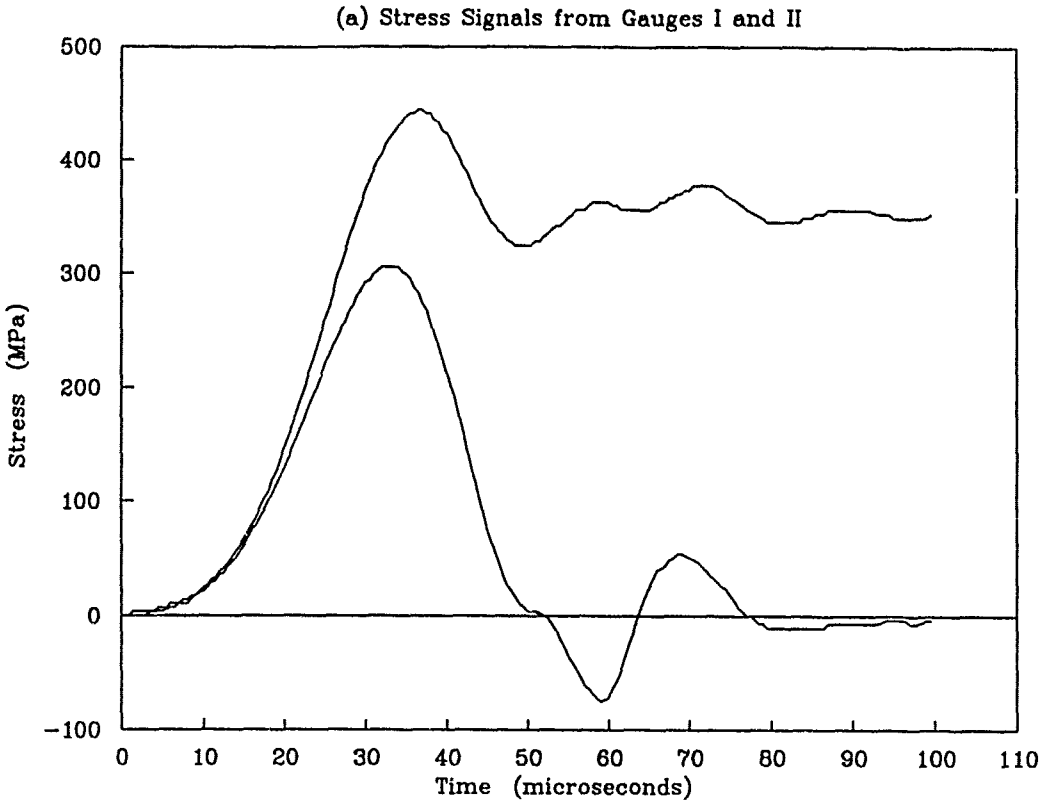

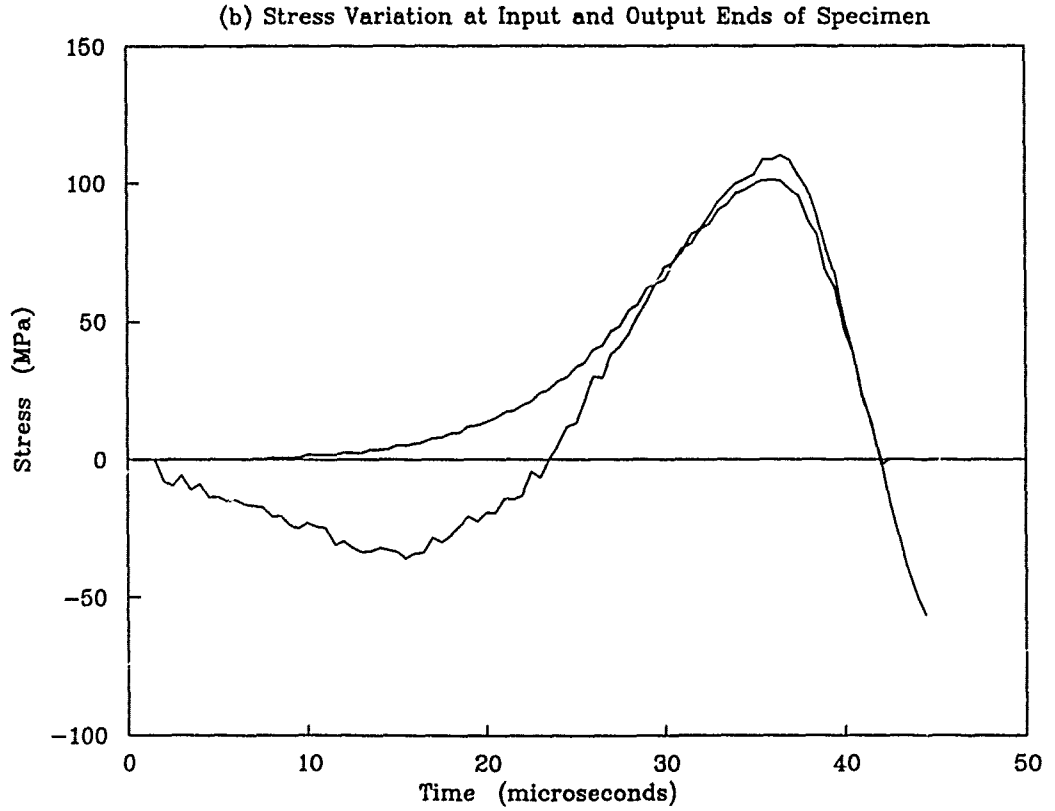

Fig. 22 Hopkinson Bar Analysis for All-Carbon Pre-Preg Specimen

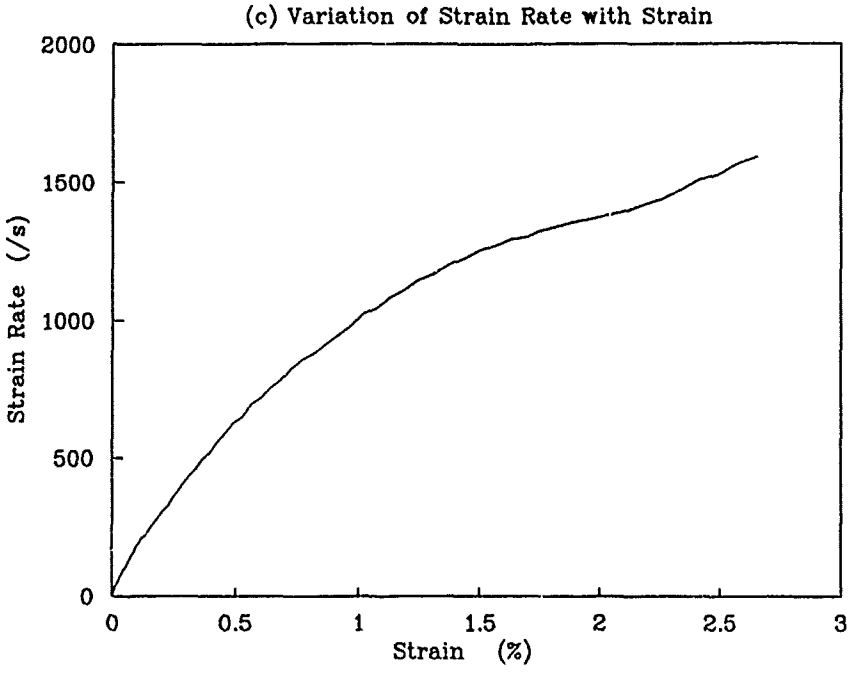

Fig. 22 Hopkinson Bar Analysis for All-Carbon Pre-Preg Specimen

to override the computed time between gauge stations I and II in order to improve the initial coincidence of the two curves. This has not been done in Fig. 22(a). From the two curves of Fig. 22(a) the computer then calculates the stress and particle velocity at the input end of the specimen, and compares the resulting stress curve with that for output end of the specimen. This is calculated from the signal derived from the gauge at station III, again after subtracting the computer calculated time delay to the start of the trace. The two curves shown in Fig. 22(b) are obtained. A close agreement between the two stress-time curves is apparent, confirming that stress equilibrium across the specimen has been achieved during the course of the test. Again the operator can choose to override the computed time delay to the start of trace III if this will improve the agreement between the computed curves of Fig. 22(b). Since gauge stations II and III are equi-distant from the specimen it would be expected that the two stress-time curves would show the rapid unloading due to fracture at about the same time so a logical basis on which to make any adjustment to the time delay between stations II and III would be to ensure that the unloading lines coincide. No such adjustment was necessary in the test of Fig. 22(b).

The computed stress-strain curve and strain rate-strain curve for this test are shown in Figs. 22 (d) and (c). It is clear that, although the average shear strain rate increases continuously throughout the test, it lies between 800 and 1200/s over the most significant region, i.e. where damage is developing and fracture is propagating. To allow comparison between different tests an average strain rate may be defined as the fracture strain divided by the time to fracture, where the fracture point is taken to coincide with the maximum stress. In the test of Fig. 22 this gives an average strain rate of 640/s. This definition, therefore, is likely to give a value for the average strain rate somewhat less than the controlling strain rate during fracture of the composite.

The effect of an adjustment to the computer calculated time delay between the gauge signals of stations I and II has been demonstrated in reference[11]. The results show that reducing the time delay between the gauge I and gauge II signals has a significant effect both on the tensile modulus and on the fracture strain. In performing the computer analysis of the experimental data, the time delay between gauge signals I and II is adjusted, if necessary, to give initial coincidence of the two curves at $t < T_1$ and, in the tension test, the resulting stress-strain curve is expected to show an initial linear-elastic region. An adjustment to the computed time delay between gauge signals from stations II and III results in only a slight change of the modulus and the fracture strain. In general, however, adjustments are not required to the delay between the gauge II and gauge III signals.

Table 2: Interlaminar shear strength of all carbon pre-preg specimens under quasi-static loading (fibre weight fraction 50%)

Specimen No.	1	2	3	average
Shear strength	35.3	31.0	34.0	33.4

Table 3: Interlaminar shear strength of all carbon hand lay-up specimens under quasi-static loading (fibre weight fraction 39.0%)

Specimen No.	1	2	3	average
Shear strength	25.34	25.34	27.97	26.22

3 Results

3.1 Quasi-static tests

Several quasi-static tests have been performed on each of seven types of specimen. For the all carbon pre-preg material, three such tests were successful, the average shear stress at failure in each test being listed in Table. 2. Two sets of hand lay-up all carbon specimens have been tested, having fibre weight fractions of 39.2% and 45.0% respectively. The results are listed in Tables. 3 and 4 respectively and two view of the failure specimen for the fibre weight fraction of 45.0% shown in Fig. 23. The average shear stress-strain curves for specimens whose fibre weight fraction is 45.0% are shown in Fig. 24. Tests were also performed on hand lay-up hybrid and hand lay-up all glass specimen. For the former two different stacking sequences were tested, with fibre weight fraction of 42% and 49%. For the latter the first set had undergone a faulty cure cycle, see section 2.1.2, and hand a fibre weight fraction of 52.0%. A second set was prepared which was given the current cure cycle. This set had a fibre weight fraction of 56.7%. The results of all four sets of tests are listed in the Tables 5, 6, 7, and 8. The average shear stress-strain curves for the hybrid specimens with a fibre weight fraction of 49.1% are shown

Table 4: Interlaminar shear strength of all carbon hand lay-up specimens under quasi-static loading (fibre weight fraction 45.0%)

Specimen No.	1	2	3	4	average
Shear strength	27.04	24.88	28.29	25.46	26.42

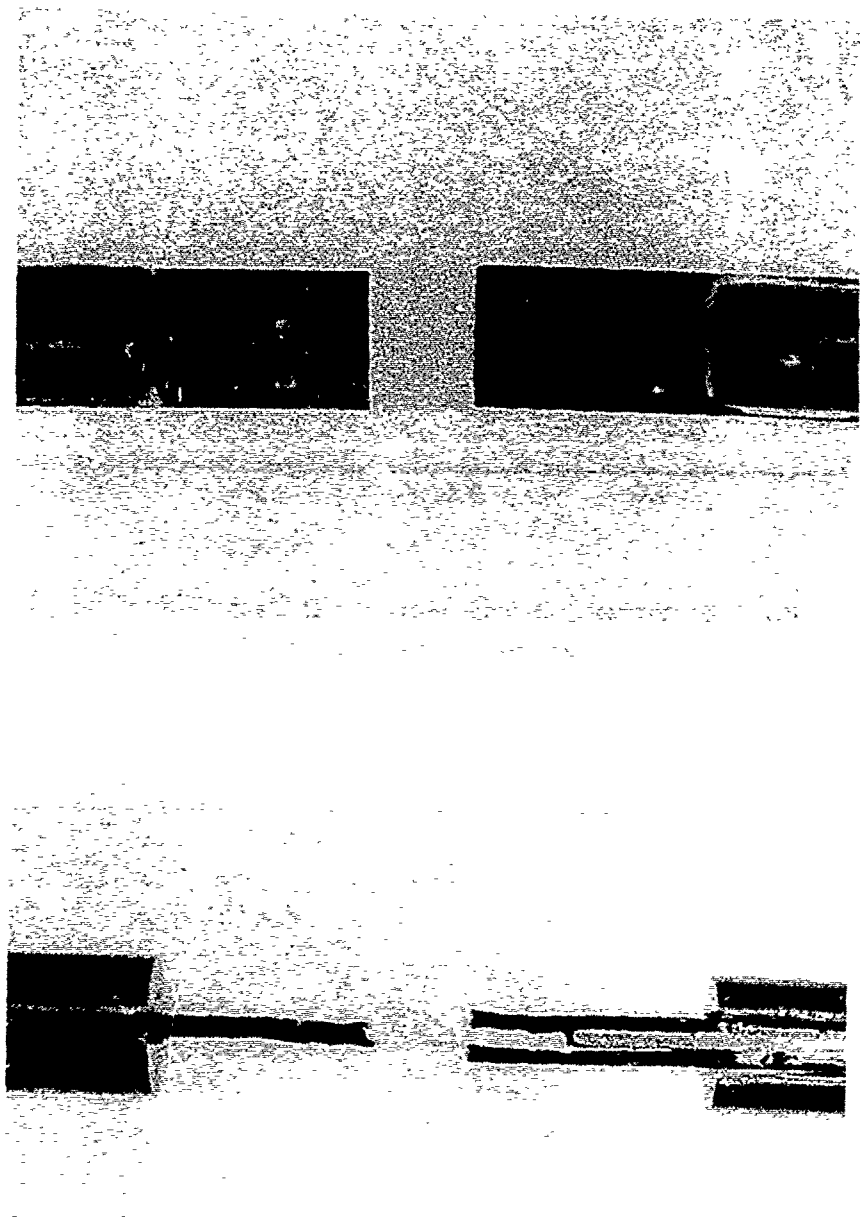

Fig. 23 Failed Specimen, All-Carbon Hand Lay-Up

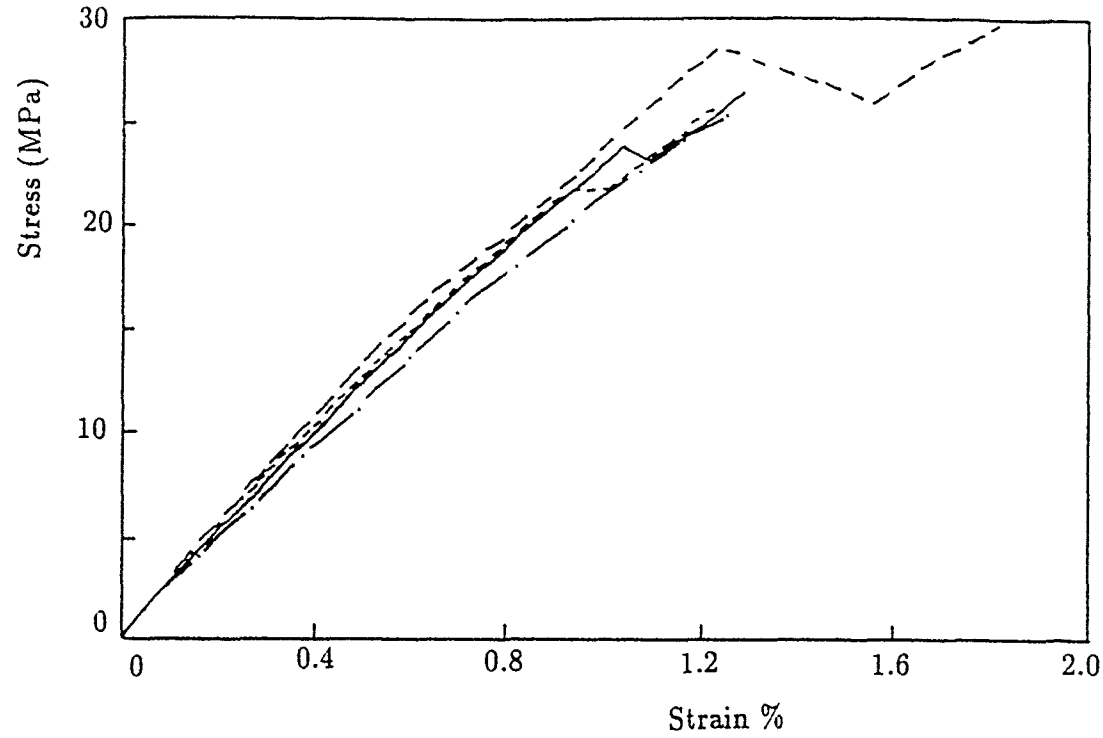

Fig. 24 Stress-Strain Curves for All Carbon Hand Lay-Up under Quasi-Static Loading

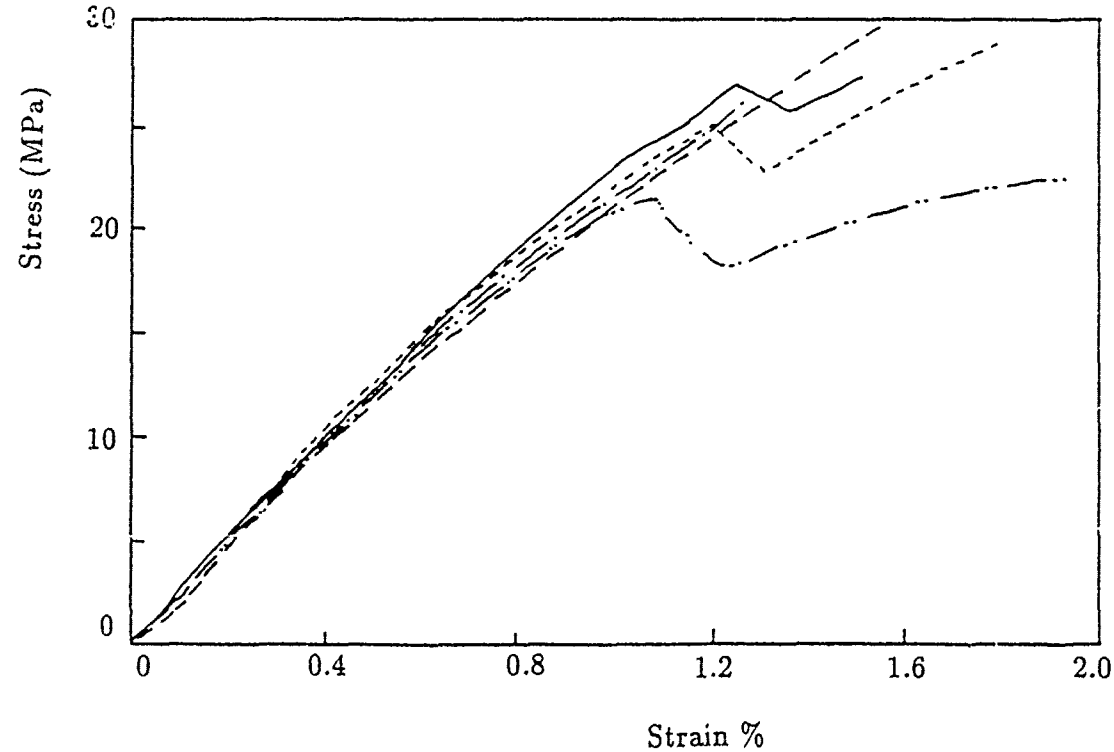

Fig. 25 Stress-Strain Curves for Hybrid Hand Lay-Up under Quasi-Static Loading

Table 5: Interlaminar shear strength of hybrid hand lay-up specimens under quasi-static loading (fibre weight fraction 42.0%)

Specimen No.	1	2	3	4	5	average
Shear strength	28.28	22.49	30.29	26.76	25.40	26.57

Table 6: Interlaminar shear strength of hybrid hand lay-up specimens under quasi-static loading (fibre weight fraction 49.1%)

Specimen No.	1	2	3	4	5	6	average
Shear strength	29.78	29.05	27.80	23.88	25.00	27.10	27.10

in Fig. 25. Two view of the failed specimens are shown in Figs. 26 and 27 for a hybrid and all glass specimen respectively. From the results it can be seen that the fibre weight fraction has a slight effect on the interlaminar shear strength. For the all carbon hand lay-up, the shear strength increase from 26.22 MPa at a fibre weight fraction of 39.0% to 26.42 MPa at a fibre weight fraction of 45.0%, an increase of less than 1%. A similar behaviour is shown by the hybrid carbon hand lay-up specimen where the interlaminar shear stress increases from 26.57 MPa at a fibre weight fraction of 42% to 27.10 MPa at a fibre weight fraction of 49.1%, an increase of about 2.0%. For the all glass hand lay-up, however, the opposite behaviour is observed, the interlaminar shear strength decreasing slightly from 20.76 MPa at a fibre weight fraction of 52.5% to 20.24 MPa at a fibre weight fraction of 56.7%, a reduction just over 1%. Here, however, the comparison may be affected by the different curing cycle. If these effect are ignored, the average quasi-static interlaminar shear strength is found to be 26.84 MPa for the hybrid lay-up, 26.32 MPa for the all carbon hand lay-up and 20.5 MPa for all glass hand lay-up.

Under quasi-static loading all the specimens fail along the expected shear plane. Macrographs of the fracture surfaces for the all carbon pre-preg and the hand lay-

Table 7: Interlaminar shear strength of all glass hand lay-up specimens under quasi-static loading (fibre weight fraction 52.5%)

Specimen No.	1	2	3	average
Shear strength	21.37	20.32	20.58	20.76

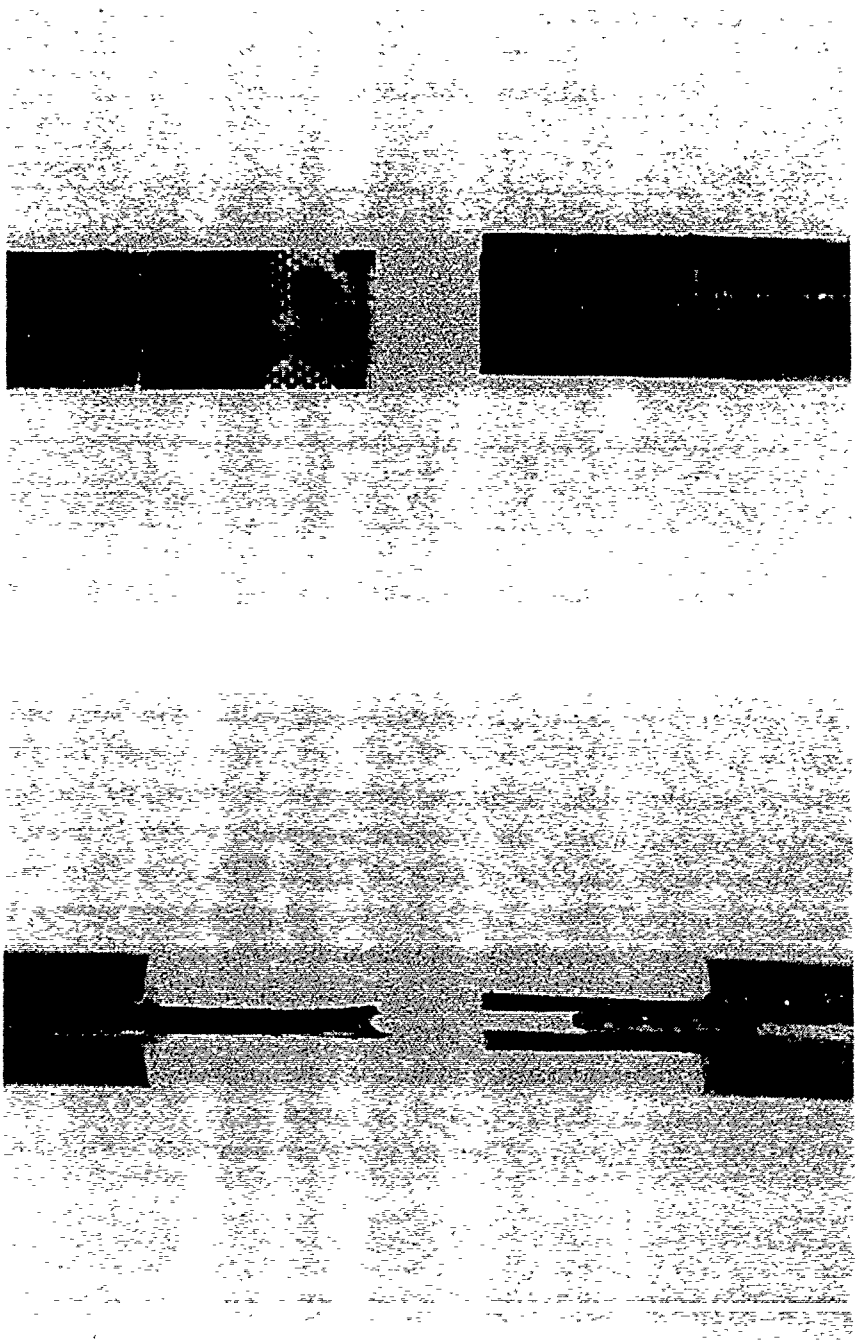

Fig. 26 Failed Specimen, Hybrid Hand Lay-Up

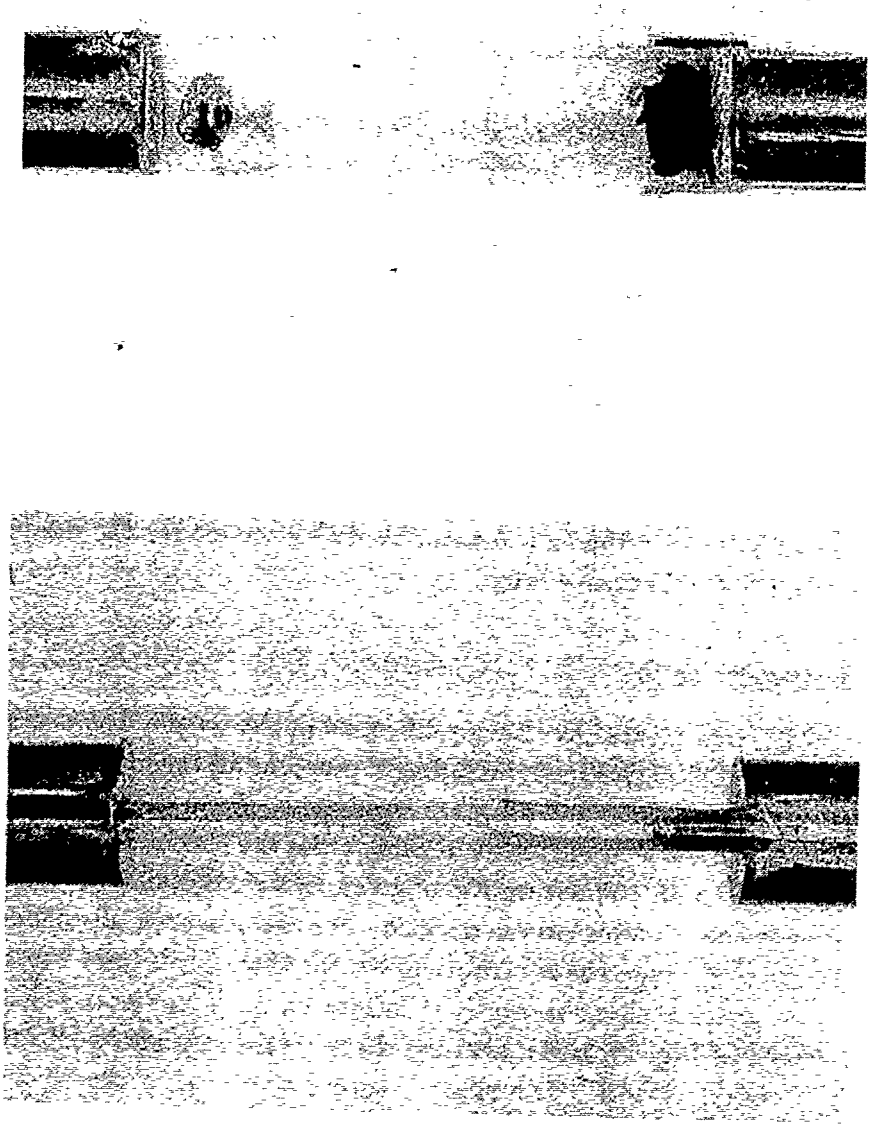

Fig. 27 Failed Specimen, All-Glass Hand Lay-Up

Table 8: Interlaminar shear strength of all glass hand lay-up specimens under quasi-static loading (fibre weight fraction 56.7%)

Specimen No.	1	2	3	4	5	average
Shear strength	19.10	16.70	20.96	23.11	21.34	20.24

Table 9: Interlaminar shear strength of all carbon pre-preg specimens under impact loading (fibre weight fraction 50%)

Specimen No.	1	2	3	average
Shear strength	54.2	53.4	55.2	54.3

up all carbon, hybrid and all glass specimens after testing are shown in Figs. 23, 26 and 27 at a magnification of ~2x. All the photographs show that at least one of the fracture surfaces is composed of two regions, one region is resin rich and the other fibre rich. In fact this is a reasonable failure mode for the double lap shear specimen as will be discussed later.

3.2 Impact test

Tests at a high strain rate have been performed in the tensile Hopkinson bar device on each of five types of specimen including a pre-preg all carbon specimen and hand lay-up all carbon , hybrid and all glass specimens. Using the standard Hopkinson bar wave analysis the average tensile strain across the specimen during the test was determined and, with the assumptions given before, dynamic interlaminar shear stress-average shear strain curves derived. For the pre-preg all carbon specimen, the shear stress-average shear strain curves for three such tests are compared in Fig. 28. The average shear strength at failure for each specimen is listed in Table 9. Also shown in Fig. 28 is the average shear strain rate applied to the specimen during the course of test. The shear fracture occurs at a the shear strain rate between 1200 and 1500 1/s. Similar responses are obtained for the hand lay-up all carbon specimens as shown in Fig. 29. The average shear strength at failure for each specimen is listed in Table 10. For the hand lay-up hybrid specimen, shear fracture occurs at an average shear strain rate of about 1200 1/s, as shown in Fig. 30. The average shear strength at failure is listed in Table 11. For the hand lay-up all glass specimens failure occurs at the highest shear strain, about 4%, in a region of decreasing strain rate following a peak strain rate at about 2% shear strain. This is true for both fibre weight fractions, see Figs. 31 and 32. The corresponding interlaminar shear strengths at failure are listed in Table 12

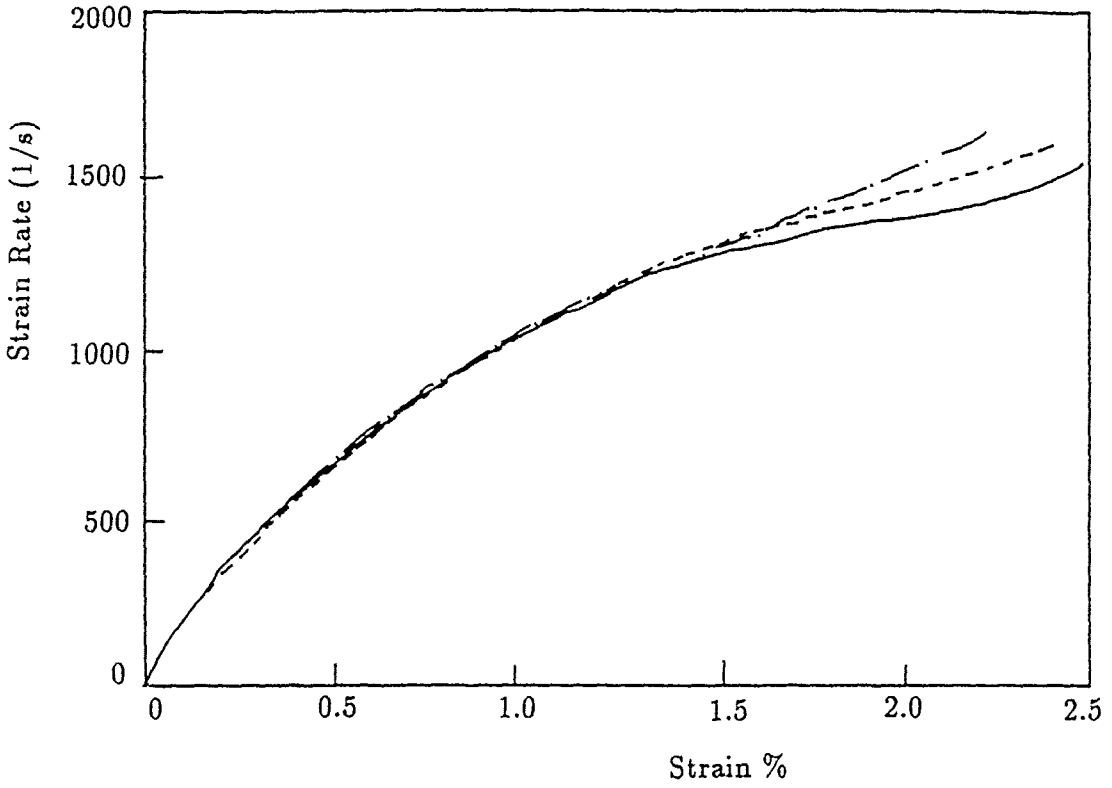

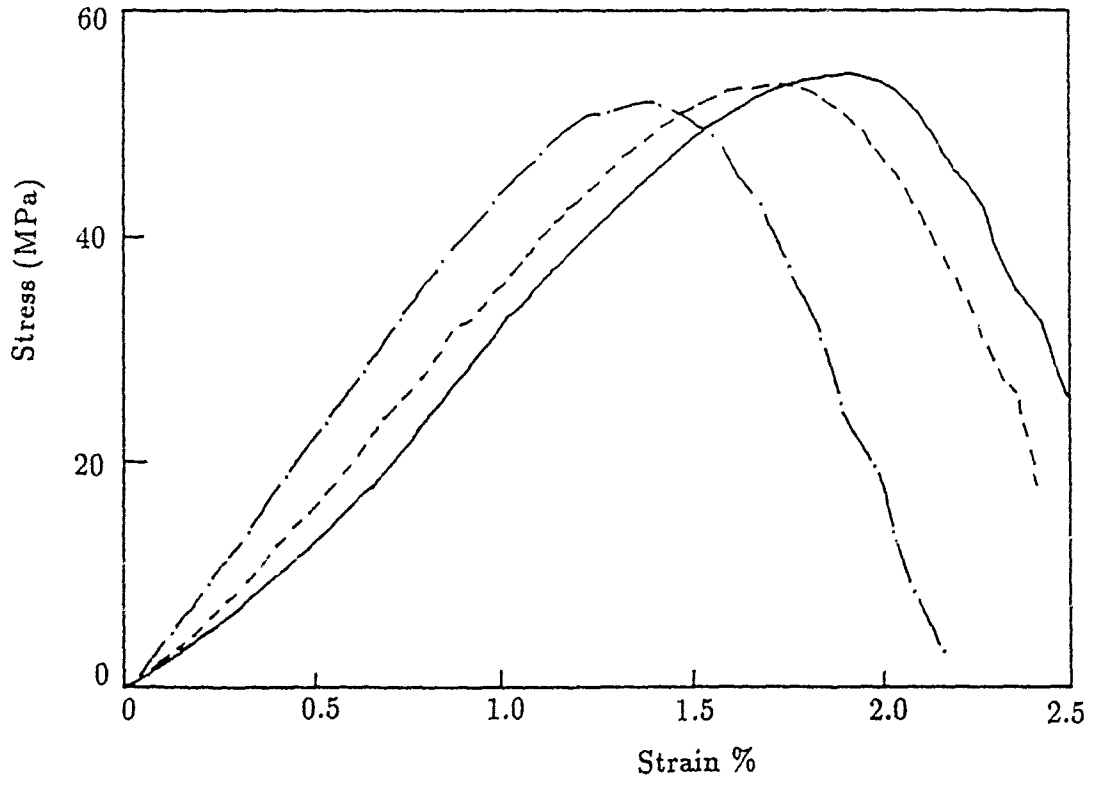

Fig. 28 Stress-Strain Curves for All Carbon Pre-preg under Impact Loading

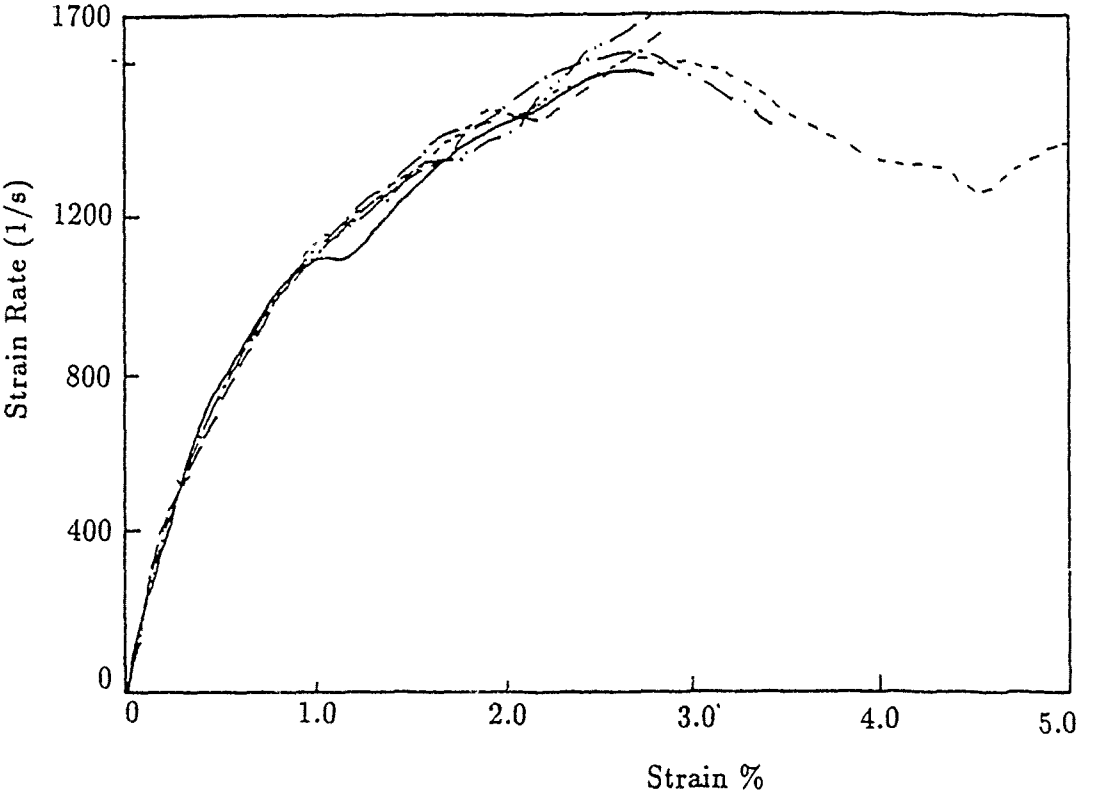

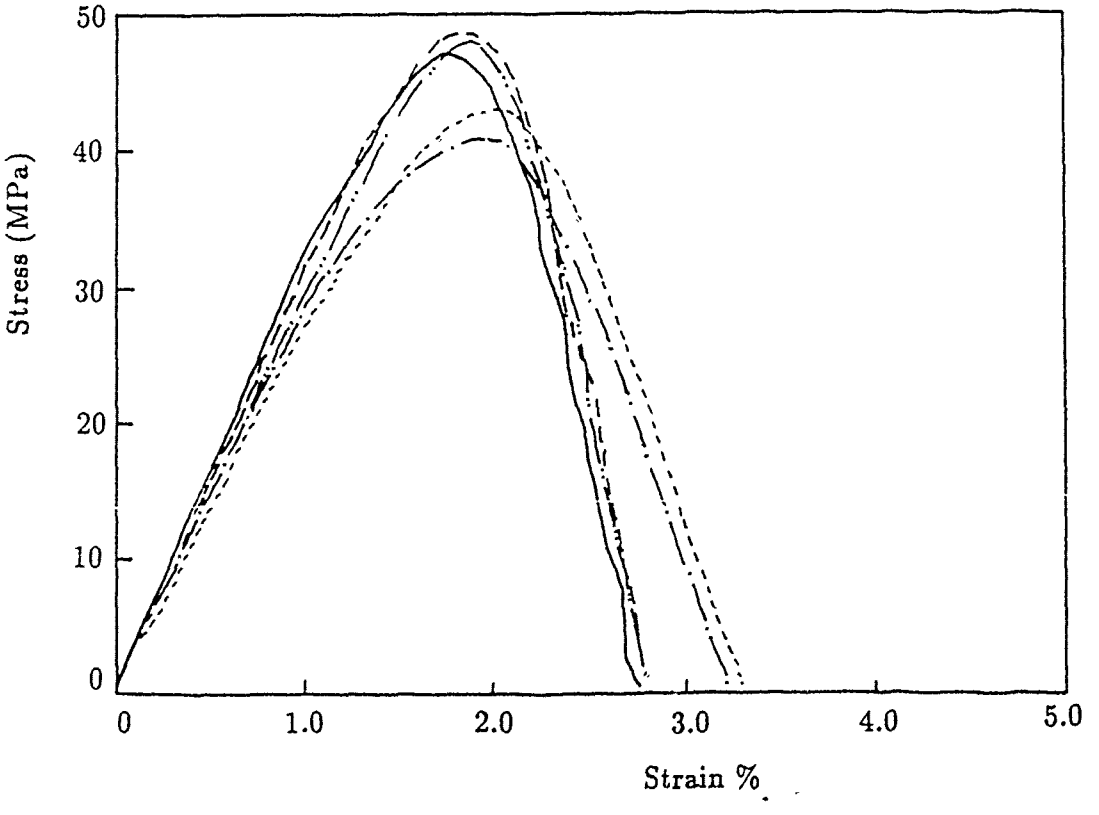

Fig. 29 Stress-Strain Curves for All Carbon Hand Lay-Up under Impact Loading

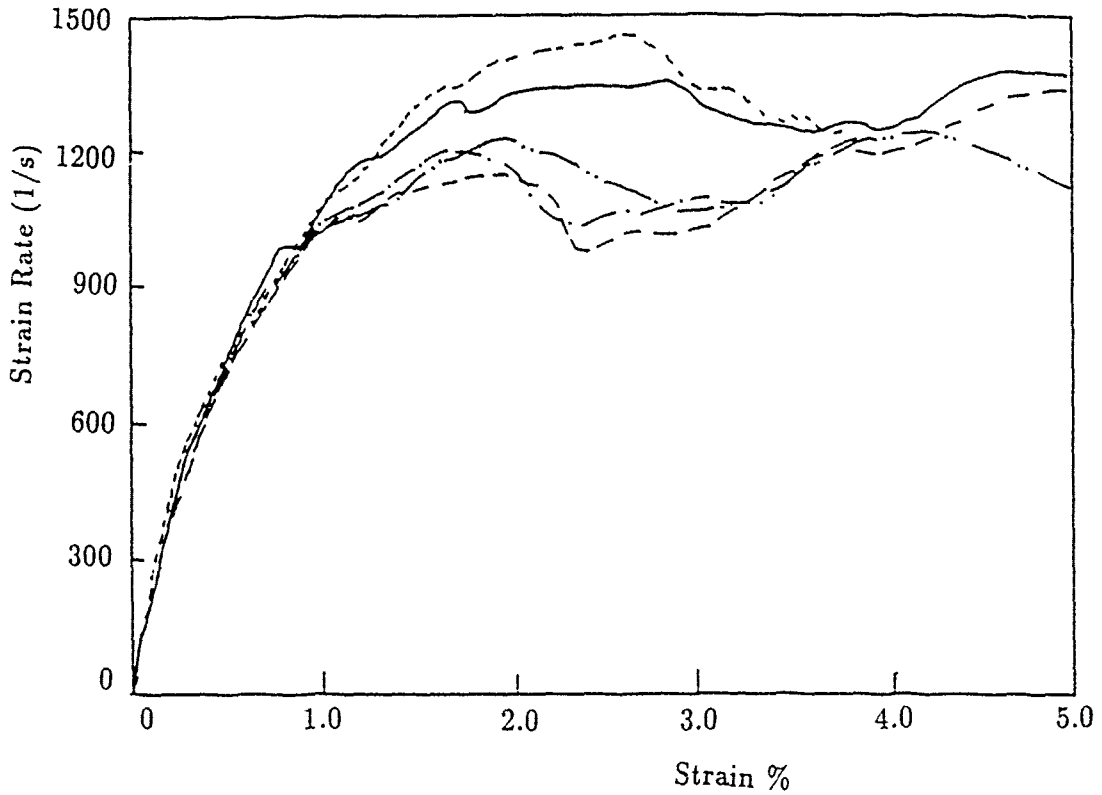

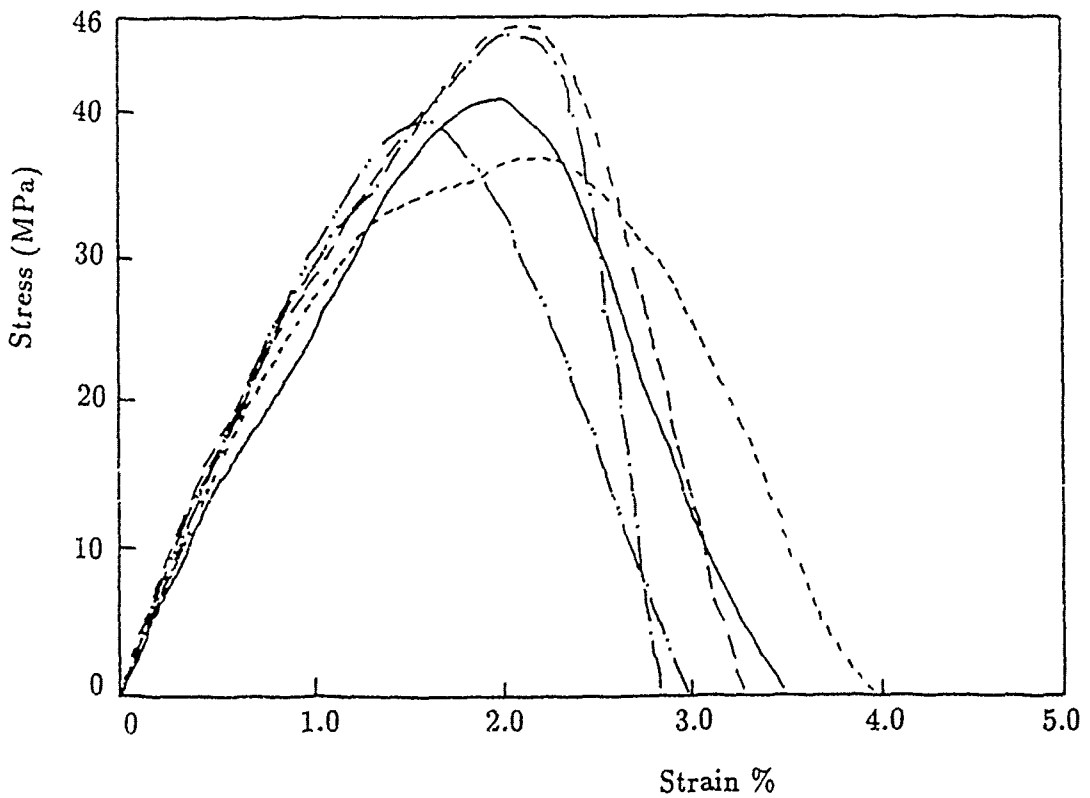

Fig. 30 Stress-Strain Curves for All Hybrid Hand Lay-up under Impact Loading

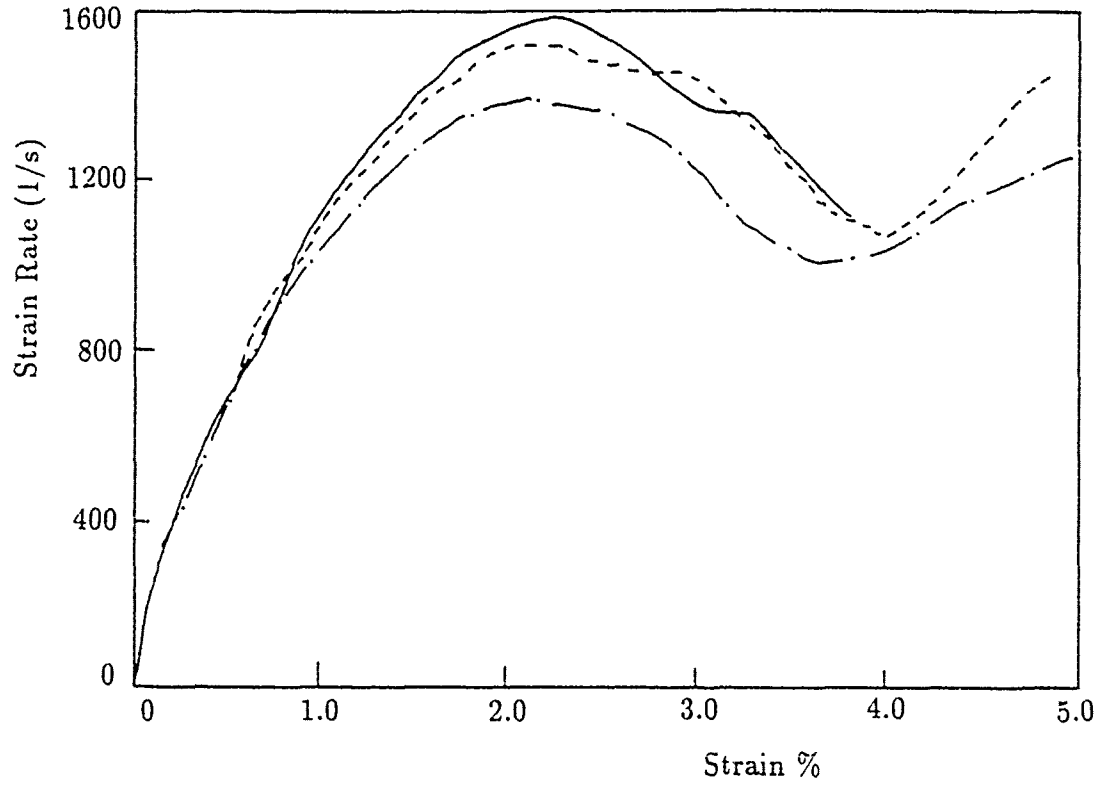

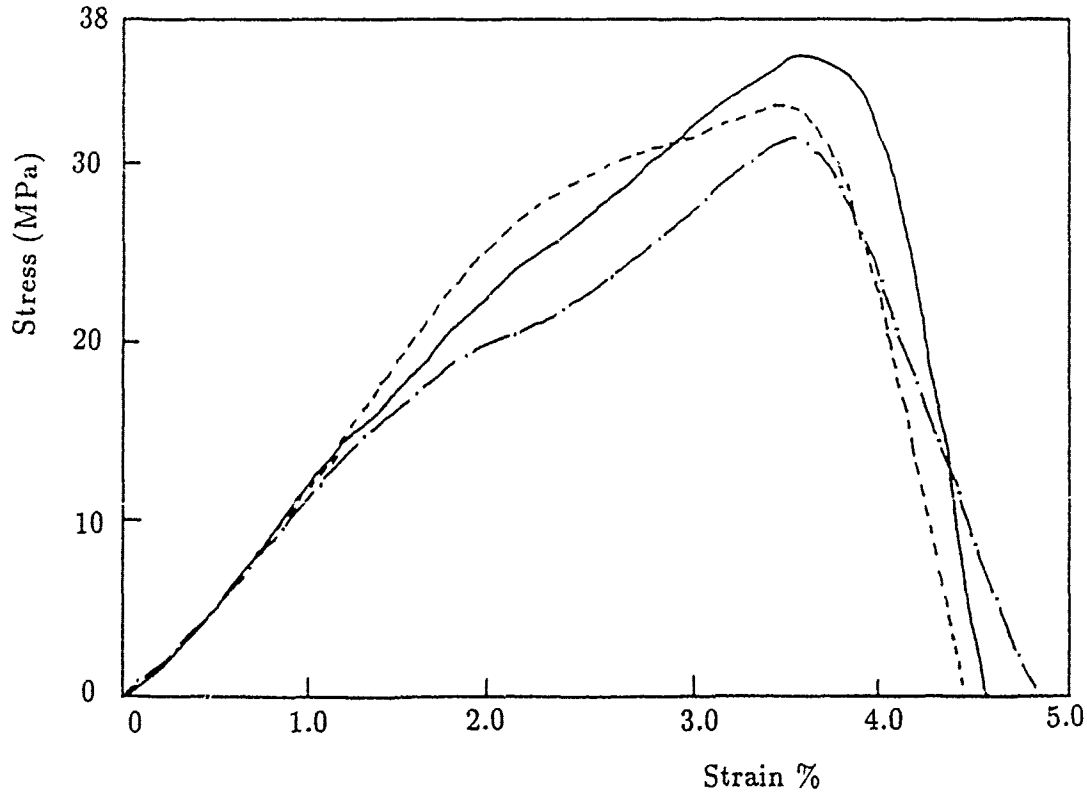

Fig. 31 Stress-Strain Curves for All Glass Hand Lay-up (1) under Impact Loading

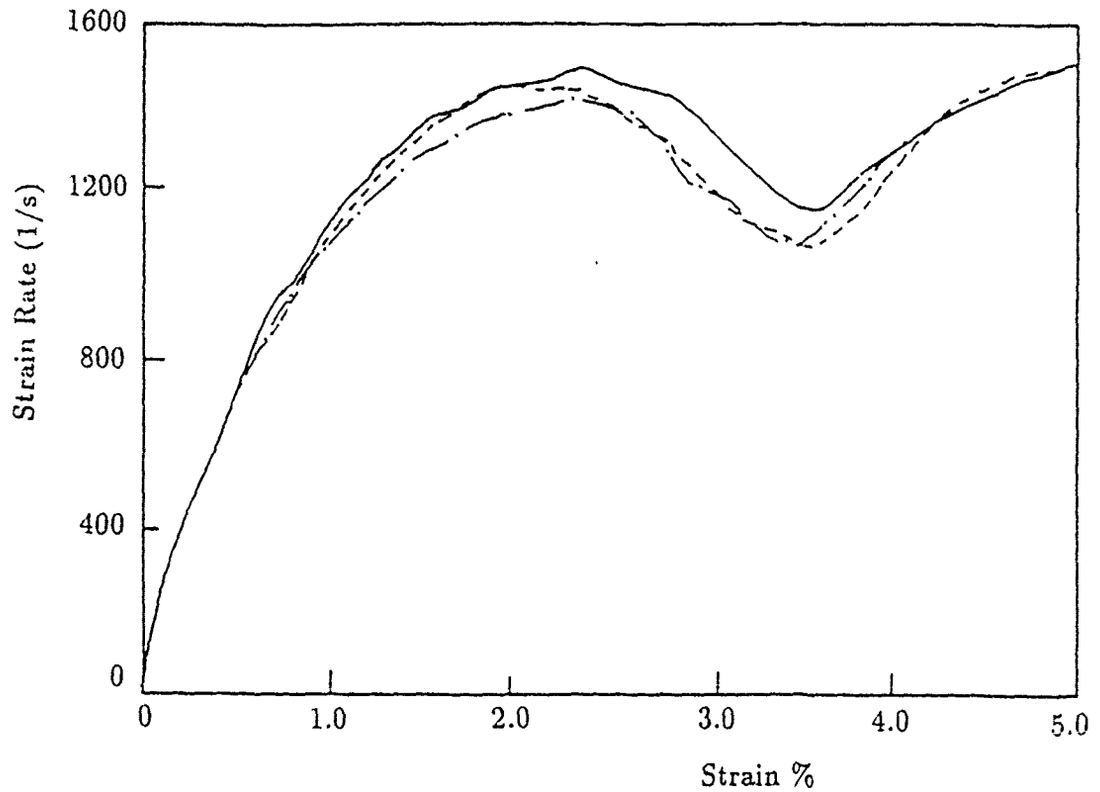

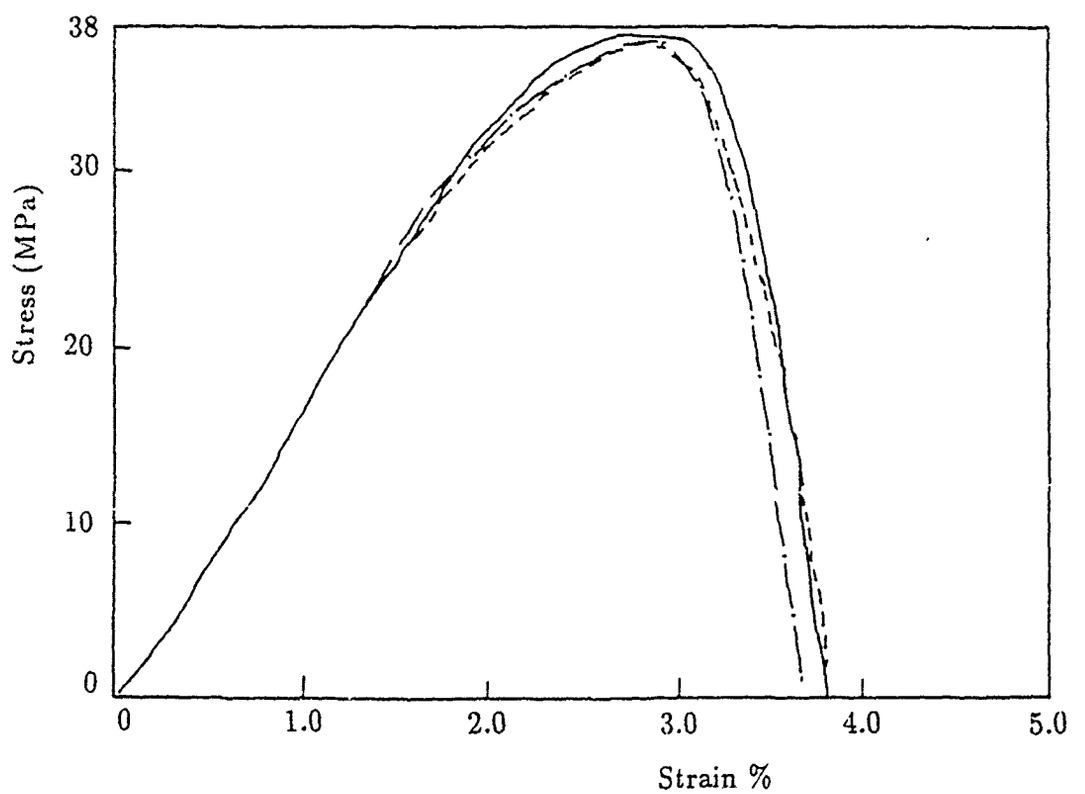

Fig. 32 Stress-Strain Curves for All Glass Hand Lay-up (2) under Impact Loading

Table 10: Interlaminar shear strength of all carbon hand lay-up specimens under impact loading
(fibre weight fraction 45.7%)

Specimen No.	1	2	3	4	5	6	average
Shear strength	49.05	48.03	42.89	40.60	47.11	42.35	45.01

Table 11: Interlaminar shear strength of hybrid hand lay-up specimens under impact loading
(fibre weight fraction 42.0%)

Specimen No.	1	2	3	4	5	average
Shear strength	40.02	45.79	36.43	39.20	45.16	41.36

for the fibre weight fraction of 52.5% and Table 13 for the fibre weight fraction 56.7%. Here an increase in fibre weight fraction is associated with an increase in interlaminar shear strengths, from 33.36 MPa for the fibre weight fraction of 52.5% to 37.39 MPa for the fibre weight fraction of 56.7%. This contrasts with the decrease, by about 0.76% found under the quasi-static loading.

As in the quasi-static tests the fracture surfaces of impacted specimens show two clearly different regions, one resin rich and the other fibre rich. This will be discussed in more detail later. In all tests the all glass specimens failed along the interlaminar shear plane, as shown in Fig. 33(a). Three of the all carbon specimens and four of the hybrid specimens also failed along the two shear plane as intended. The other three all carbon specimens failed additionally in tension, two as in Fig. 33(b) and one in Fig. 33(c). One of the hybrid specimens failed in the two shear plane and also in tension in one of the leg as shown in Fig 33 (d).

Table 12: Interlaminar shear strength of all glass hand lay-up specimens under impact loading
(fibre weight fraction 52.5%)

Specimen No.	1	2	3	average
Shear strength	31.65	32.88	35.55	33.36

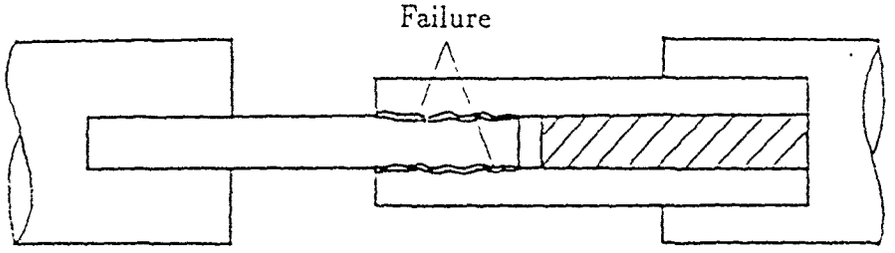

(a) Shear Failure

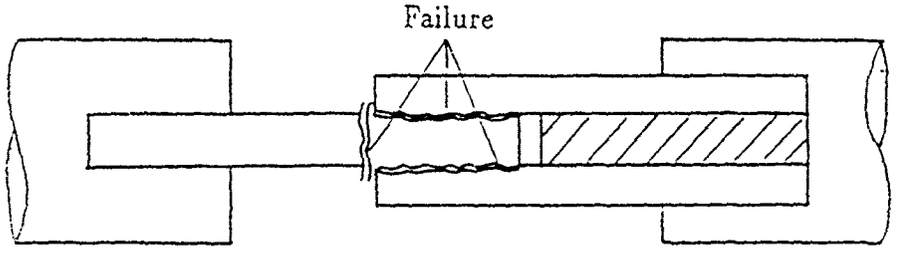

(b) Shear Failure and Tensile Failure in Central Part

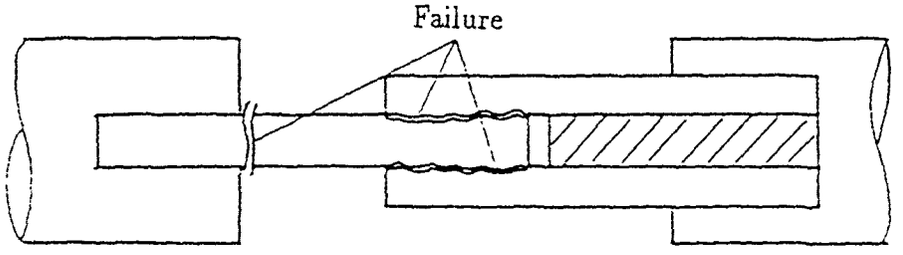

(c) Shear Failure and Tensile Failure in Central Part

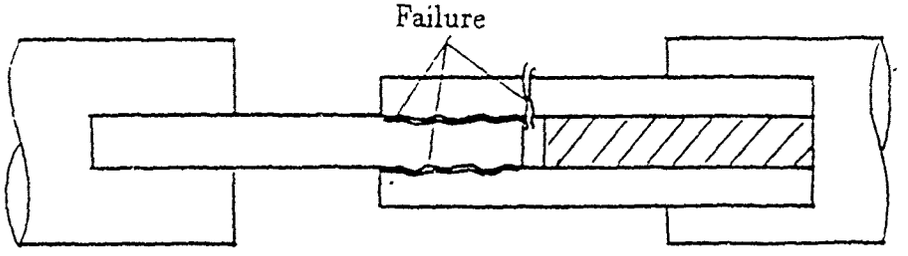

(d) Shear Failure and Tensile Failure in One of the Legs

Fig. 33 Failure Mode of Specimen

Table 13: Interlaminar shear strength of all glass hand lay-up specimens under impact loading (fibre weight fraction 56.7%)

Specimen No.	1	2	3	average
Shear strength	37.25	37.50	37.43	37.39

3.3 Fracture appearance of double lap shear specimens

3.3.1 The failure mode predicted

The double lap shear specimen is actually composed of two single lap joints. In the overlap region between the central part and the outer parts, there is some resin like adhesive in the single joint. Assuming that the central part is connected with the outer parts by a layer of resin, as shown in Fig. 34, interlaminar shear stress concentration would be expected at points A and D which cracks might, therefore, be expected to originate. As these cracks propagate to points A' and D' the shear stress get even higher. Thus the cracks propagate in a catastrophic manner to points A" and D" where finally they join across the thickness of the resin. This leads to a predicted fracture appearance as shown in Fig. 35, having two regions as expected, see Figs. 23, 26 and 27.

3.3.2 The observation of the fracture surface

Further evidence for this failure mode was obtained when the failure surface of several specimens was examined in the scanning electron microscope. The fracture surfaces was coated with a thin film of gold and the central part of the failed specimens observed at magnifications of $\sim$ 100x to $\sim$1000x. Points to be examined in the electron microscope were chosen in region 1, region 2 and at the interface, the jump region. these are labelled A_i, C_i and B_i, respectively, in Fig. 35. Because the central part was choose for examination, region 1 was expected to be the fibre rich region,in which the fracture occurred between the central fibres and the resin, and region 2 to be the resin rich region in which the fracture occurred between the resin and the outer fibres.

Fig. 36 shows the photographs taken from the fracture surface of an all glass specimen. The magnifications of photographs A_1 and C_1 are $\sim$500x, B_1 is $\sim$100x and A_2, B_2 and C_2 are $\sim$1000x. From the photographs C_1 and C_2 it can be seen that resin covers the surface in region 2. There are a lot of grooves on the surface from which fibres have pulled out. Around each groove a shear failure band inclined at about 45^O to the groove can be seen. It is clear that the surface of region 2 occupied by the resin as expected. In contrast many bare fibres are visible on the surface of region 1, see photographs A_1 and A_2 in Fig. 36. In the resin

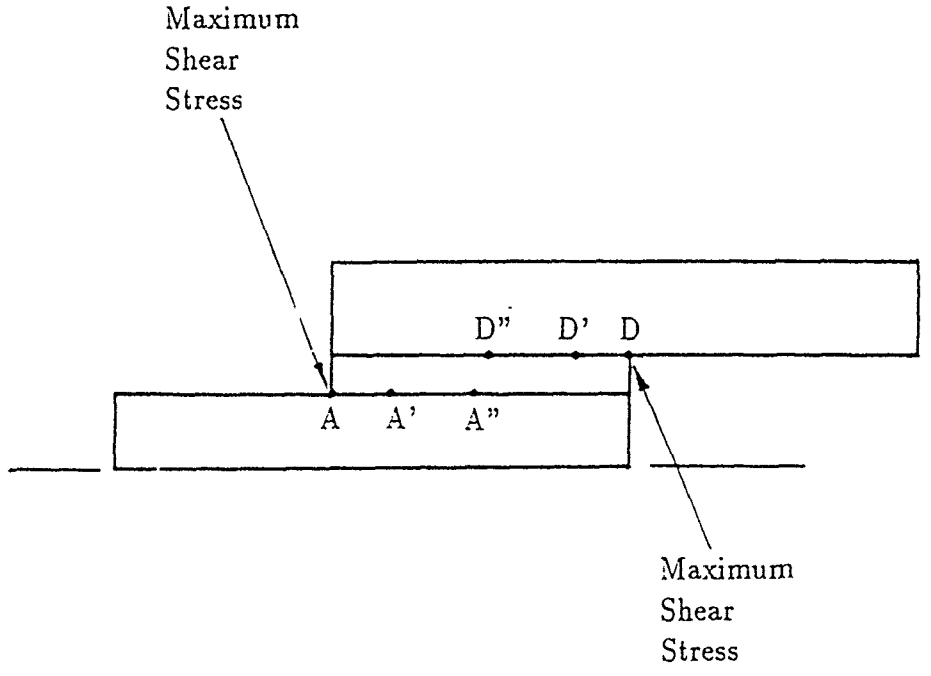

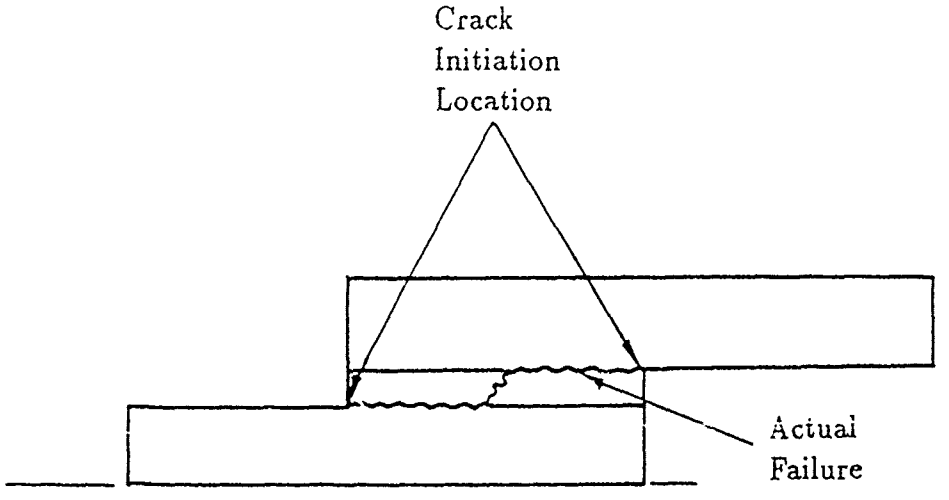

Fig. 34 Failure Mode Predicted

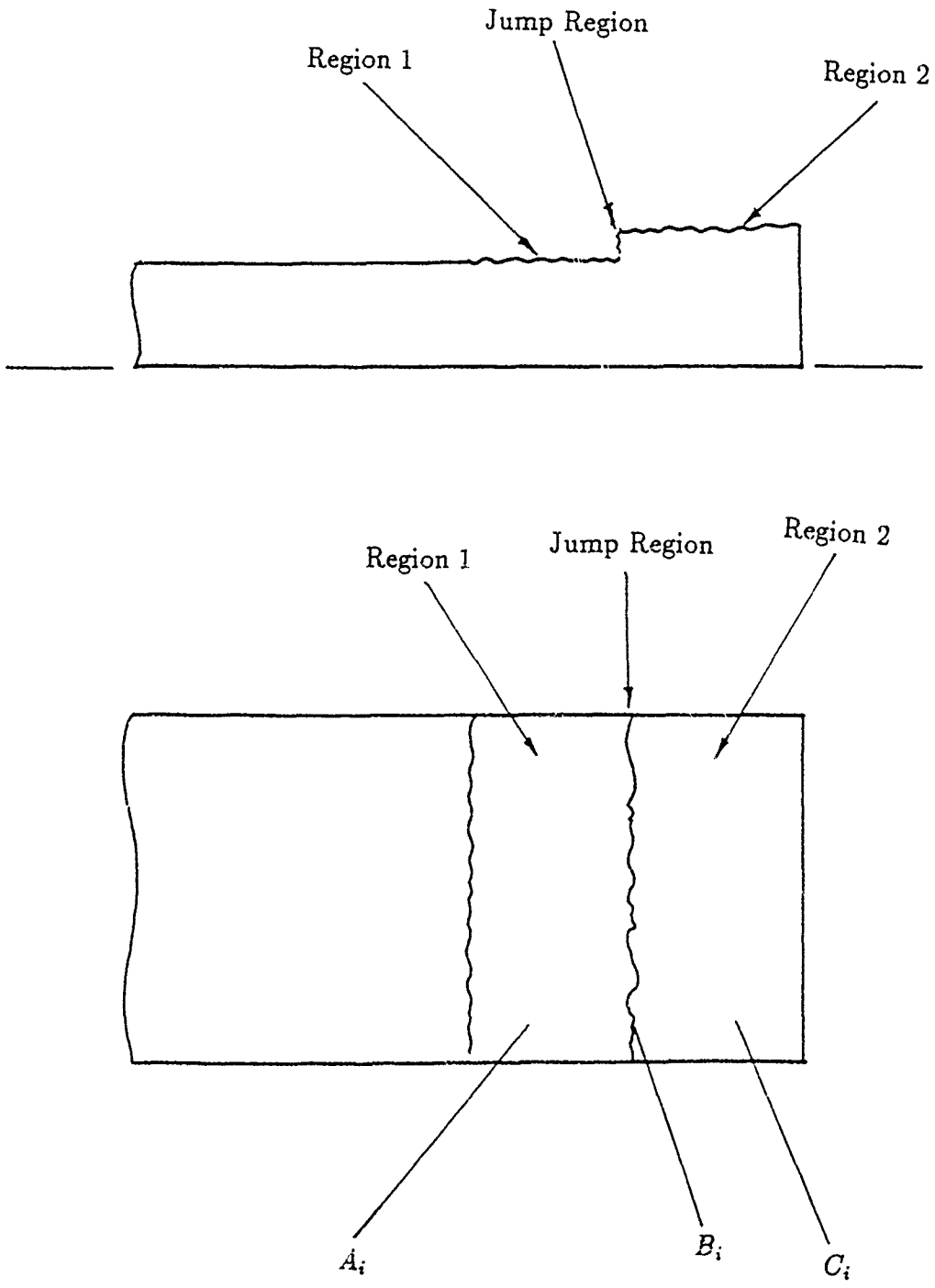

Fig. 35 Fracture Surface Observed and Arrangement of SEM Photographs

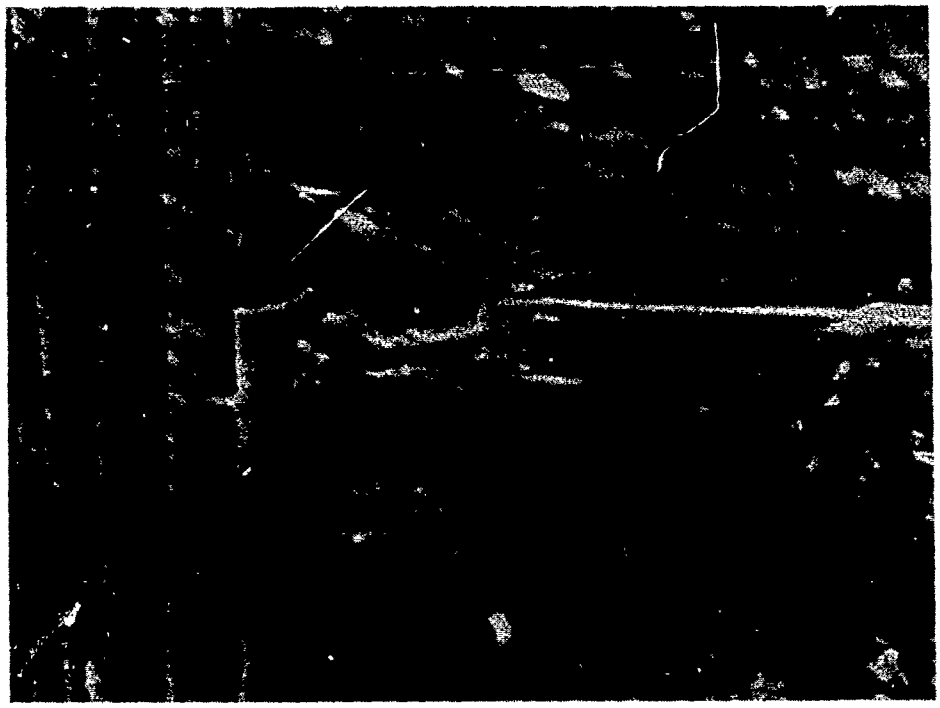

(a) Picture C_1 for Region 2 (~500x)

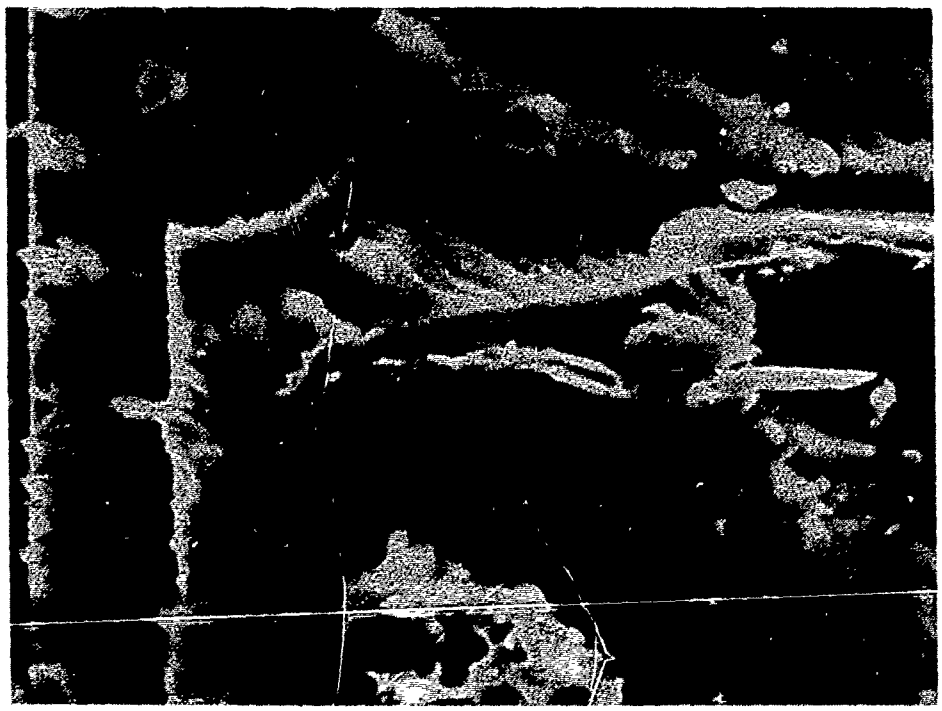

(b) Picture C_2 for Region 2 (~1000x)

Fig. 36 Scanning Electron Micrographs of Fracture Surface (All-glass hand lay-up under quasi-static loading)

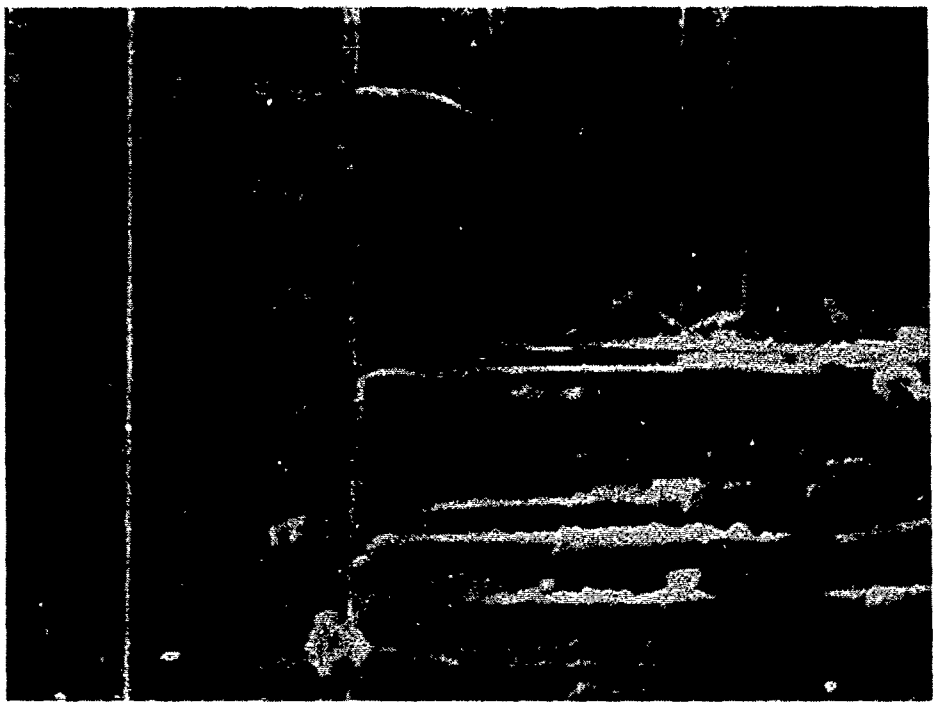

(c) Picture A_1 for Region 1 (~500x)

(d) Picture A_2 for Region 1 (~1000x)

Fig. 36 Scanning Electron Micrographs of Fracture Surface (All-glass hand lay-up under quasi-static loading)

(e) Picture B_1 for Jump Region (~500x)

(f) Picture B_2 for Jump Region (~1000x)

Fig. 36 Scanning Electron Micrographs of Fracture Surface (All-glass hand lay-up under quasi-static loading)

region between the fibre shear failure bands at 45° can again be seen. From the pictures B_1 an B_2 for the jump region show a clearly marked boundary between two regions, as shown before in the photographs of Figs. 23, 26 and 27. This boundary steps from region 1, occupied by the fibres, to the region 2, occupied be the resin. It is clear that the failure mode on the interlaminar shear plane is as described in section 4.3.1.

Similar fracture appearances can be seen in the all carbon hand lay-up specimen, shown in Fig. 37 and in the hybrid hand lay-up specimen shown in Fig. 38 in which the photographs of region 2 and jump region only be shown. Unfortunately, the photograph in the region 1 has not been taken. Fig. 39 show the photographs which were taken from three different region of the all glass specimen failing under the impact loading. All the failure surface is as the same as the all glass specimen failing under quasi-static loading. It is quite clear that the fracture surfaces have the same appearance in the quasi-static and impact loading. These again prove the prediction done in section 4.3.1.

4 Discussion

In the present work, the wet hand lay-up techniqe was successfully used to make double lap shear specimens. In this procedure the double lap geometry the section must be maintained during the curing process, especially the symmetry of the specimen and the length of the overlap region. This can be achieved by fixing the three pieces of metal plate to a base plate. The resin weight fraction is difficult to control during the curing process because resin is likely to leak out under pressure. This can make the resin weight fraction too low and the void fracture too high in the specimen. To solve this problem care and experience is needed. The micrograph of tested specimens show that it is possible to make adequate specimens using the wet hand lay-up techniqe.

All the specimens tested under quasi-static loading failed by interlaminar shear on the pre-chosen plane as required. This is an advantage of this specimen design in comparison with other specimen designs. It is very important for specimen in which the interlaminar shear strength is required on a pre-chosen plane between a carbon and a glass ply. Under impact loading, all specimens failed on the pre-chosen plane, but some of the specimens also failed in tension in either the central part or one of the legs at the same load as caused shear failure. This implies that the interlaminar shear strength increases more with strain rate than the tensile strength. Since the tensile strength of glass reinforced composites increases most markedly with strain rate it is not surprising that the problem here did not arise. In the all carbon hand lay-up three out of six specimens failed only on the shear plane at an average stress of 44 MPa. The other three failed also in tension. In

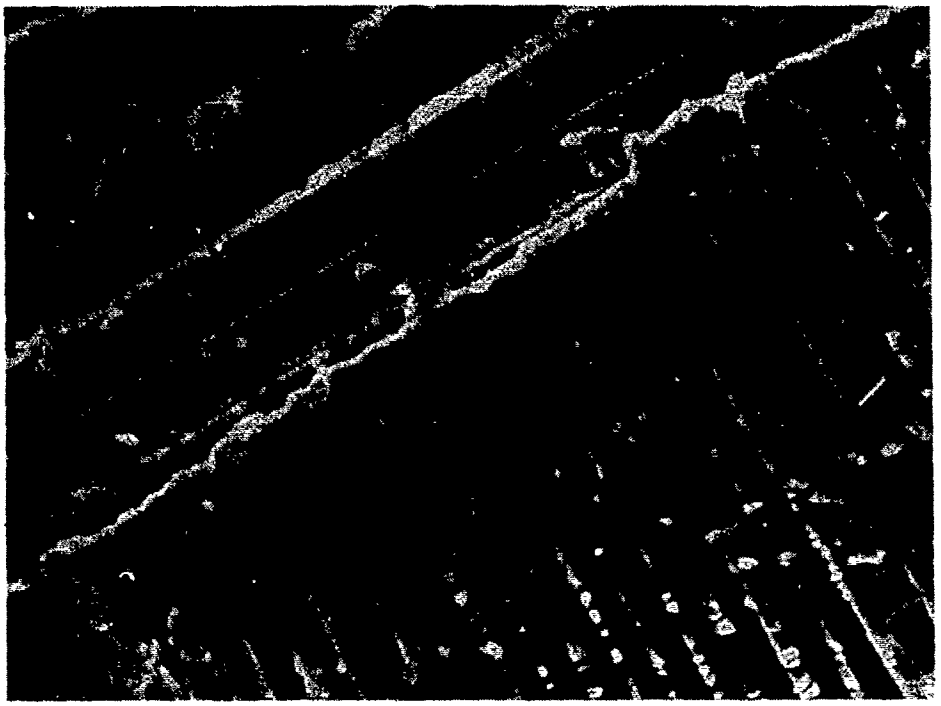

(a) Picture C_1 for Region 2 (~500x)

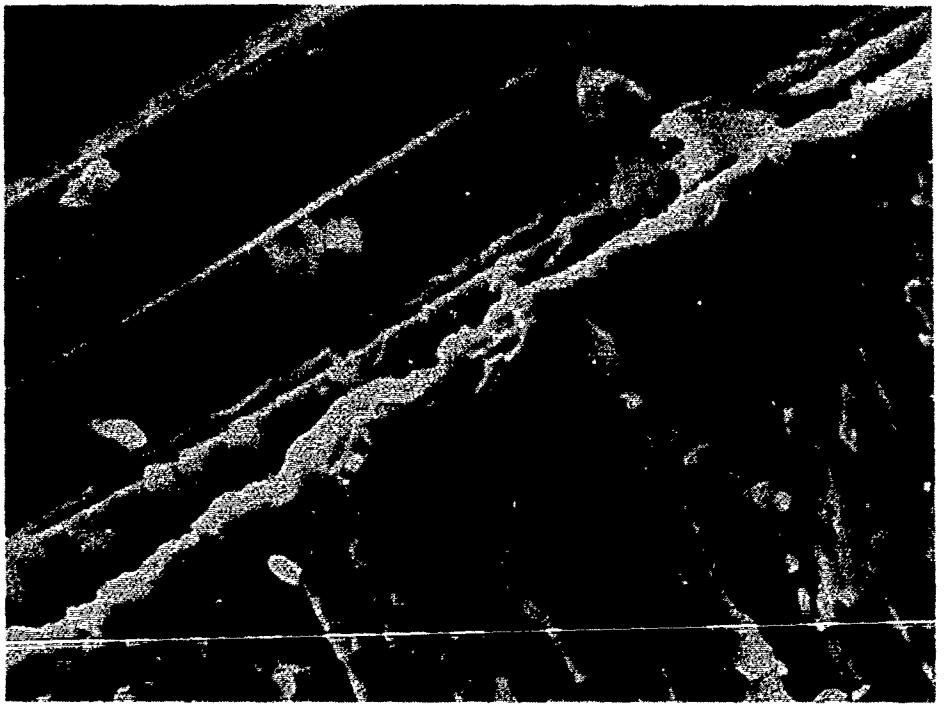

(b) Picture C_2 for Region 2 (~1000x)

Fig. 37 Scanning Electron Micrographs of Fracture Surface (All-carbon hand lay-up under quasi-static loading)

(c) Picture A_1 for Region 1 (~500x)

(d) Picture A_2 for Region 1 (~1000x)

Fig. 37 Scanning Electron Micrographs of Fracture Surface (All-carbon hand lay-up under quasi-static loading)

(e) Picture B_1 for Jump Region (~500x)

(f) Picture B_2 for Jump Region (~1000x)

Fig. 37 Scanning Electron Micrographs of Fracture Surface (All-carbon hand lay-up under quasi-static loading)

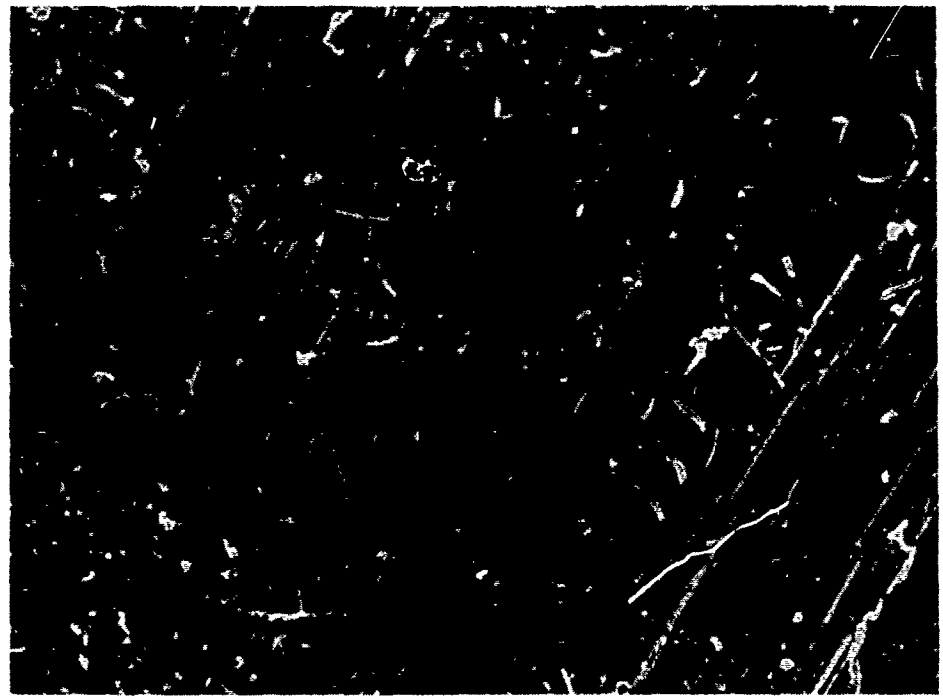

(a) Picture C_1 for Region 2 (~500x)

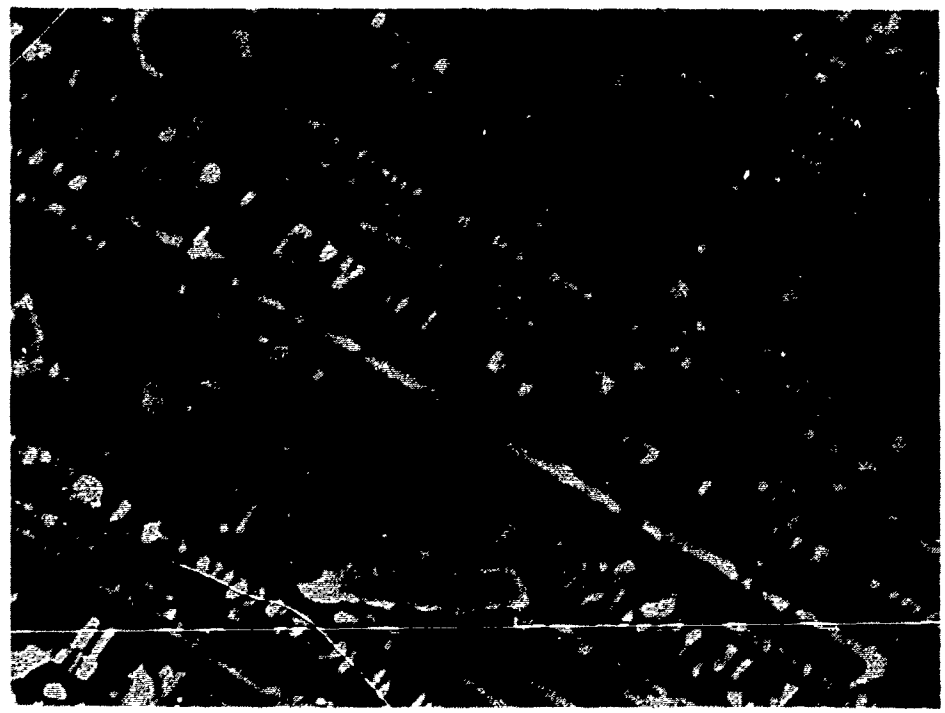

(b) Picture C_2 for Region 2 (~1000x)

Fig. 38 Scanning Electron Micrographs of Fracture Surface (Hybrid hand lay-up under quasi-static loading)

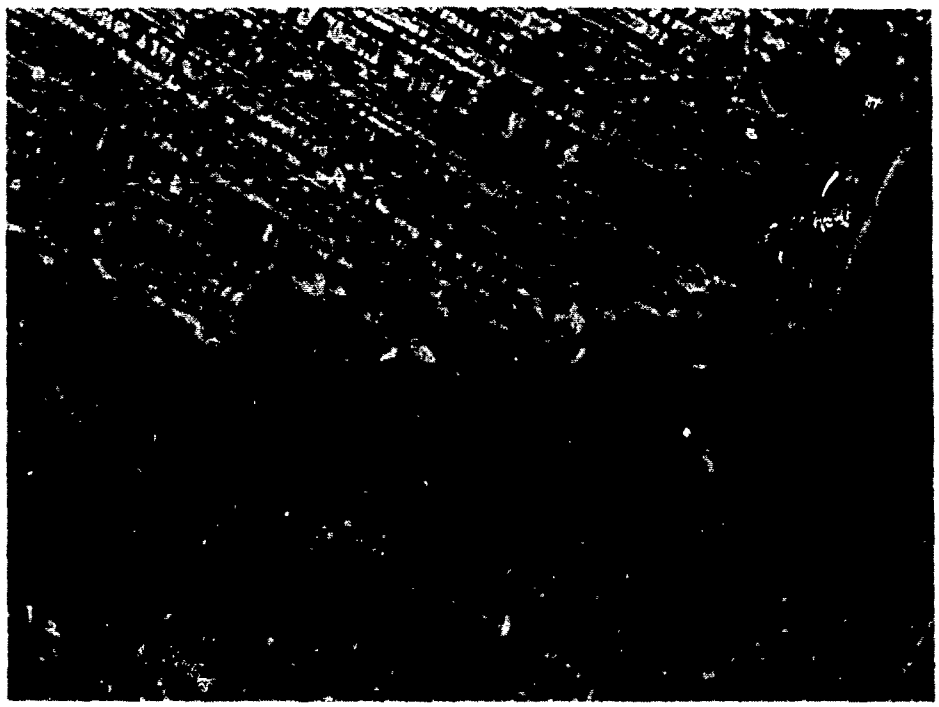

(c) Picture B_1 for Jump Region (~500x)

(d) Picture B_2 for Jump Region (~1000x)

Fig. 38 Scanning Electron Micrographs of Fracture Surface (Hybrid hand lay-up under quasi-static loading)

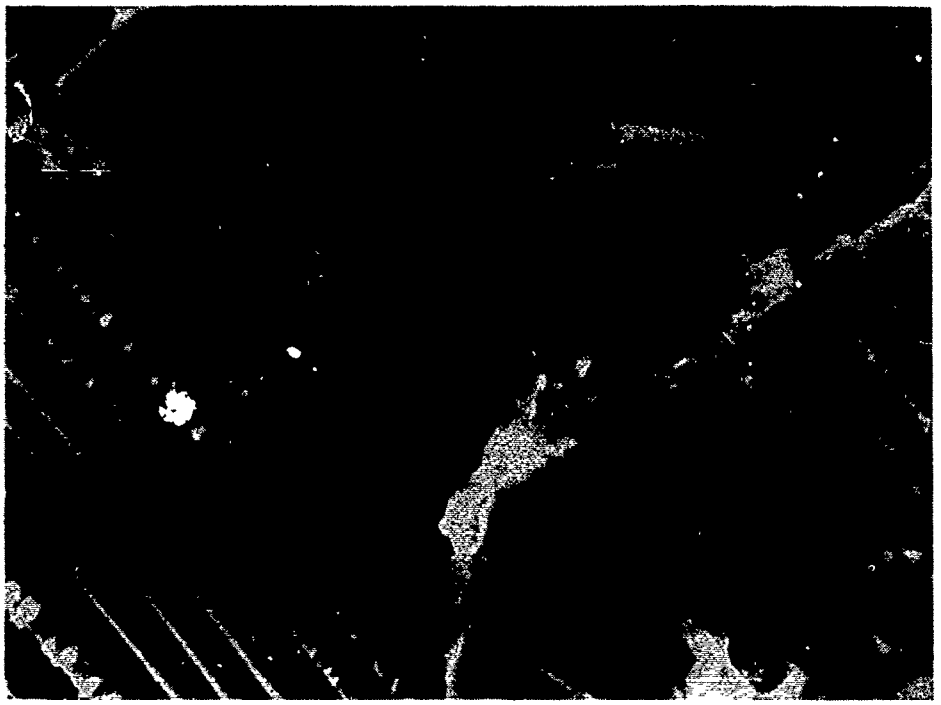

(a) Picture A_1 for Region 1 (~500x)

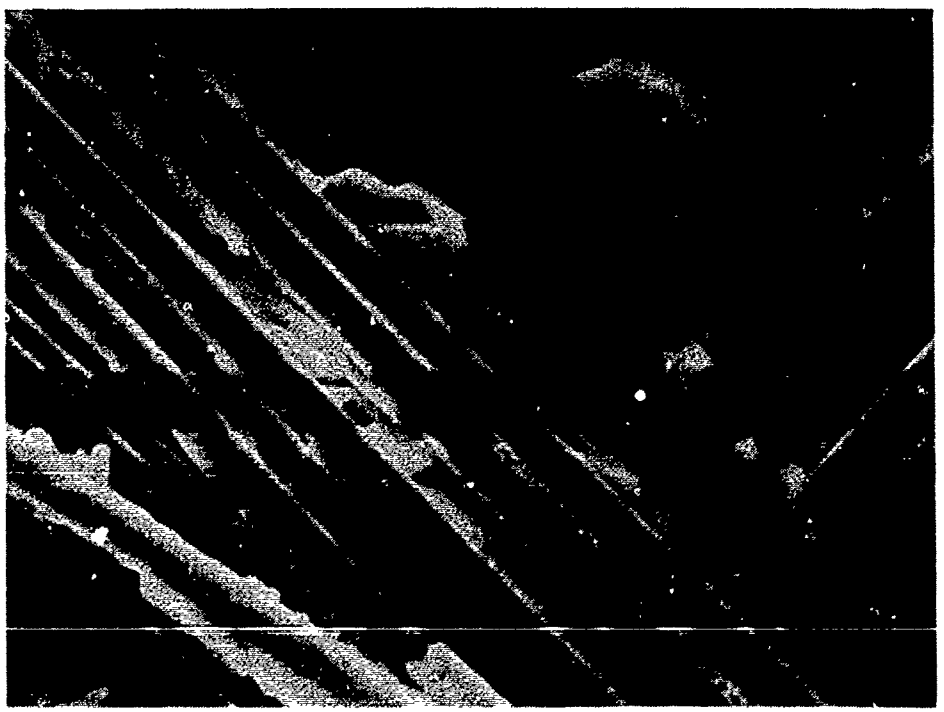

(b) Picture A_2 for Region 1 (~1000x)

Fig. 39 Scanning Electron Micrographs of Fracture Surface (All-glass hand lay-up under impact loading)

(c) Picture C_1 Taken from Region 1 (~x1000)

Fig. 39 Scanning Electron Micrograph of Fracture Surface of All Glass Hand Lay-up under Impact Loading

Table 14: The comparison of interlaminar shear strength under quasi-static and impact loading

	all carbon pre-preg	all carbon hand lay-up	hybrid hand lay-up	all glass hand lay-up
quasi-static	33.4	26.32	26.84	20.50
impact	54.3	45.01	41.36	35.38
increase%	62.6	70.4	55.6	72.6

these tests the average shear strength is 46.01 MPa, higher than that obtained when failure was by shear alone. This suggests that our specimen design is just in the borderline, favoring tensile and shear failure equally at impact strain rates and tensile failures can be avoided by increasing the thickness of central part or outer parts.

The experimental results show that the interlaminar shear strength of all the materials which have been tested is significantly strain rate dependent. The comparison of results under quasi-static and impact loading is given in Table 14. The shear strength increases by about 62.6% between the quasi-static and impact loading rates for the pre-preg all carbon material, by about 70.4% for the wet hand lay-up all carbon material and by about 55.6% for the hybrid hand lay-up material, the small increase. For the all glass hand lay-up material, the strain rate effect is different for the two fibre weight fractions. The interlaminar shear strength increases by about 60.7% for the fibre weight fraction of 52.5% and about 84.7% for the fibre weight fraction of 56.7%, the largest increase. It should be recalled that the difference in the shear strength between these two materials is only about 0.76% under quasi-static loading. So the strain rate effect on the interlaminar shear strength for the all glass hand lay-up seems to be connected to the fibre weight fraction of the material, the higher the fibre weight fraction, the higher the shear strength increase. This still needs more experimental work to be proved.

Considering only the hand lay-up specimens and ignoring effect of fibre weight fraction, never more than about 2% of the interlaminar shear strength under quasi-static loading, the average interlaminar shear strength is lowest for the all-glass interface, at about 20.5 MPa, and about equal for the all-carbon and carbon-glass interface, at about 26.5 MPa. Under impact loading the all-glass interface remains the weakest, with a shear strength of between 33.4 and 37.4 MPa, depending on fibre weight fraction, giving a mean value of about 35.4 MPa. Now, However, the all-carbon interface is clearly the strongest, with a shear strength of about 45 MPa and the hybrid interface lies between these limits with a shear strength of about 41.4 MPa.

A simple explanation for this change in the relative interlaminar shear strength with strain rate is not immediately apparent. It should be noted that, in addition to the complication arising from the effect of fibre weight fraction on the shear strength in the all-glass lay-up there is also a much coarser weave than the glass mat. This was necessary in order to allow direct comparison with the composite specimens previously tested in quasi- static and impact tension [9,12] to which the numerical modelling techniques described elsewhere[1] have been applied and for which the critical interlaminar shear strengths determined here were required. Clearly further experimental work with a careful control of the various parameters involved is required before more fundamental conclusions can be reached.

5 Conclusion

- The wet hand lay-up techniqe is successful in making double lap shear specimen. More experience is needed for efficient control of the weight fraction of fibres and resin.
- The double lap shear specimen design is suitable for comparing the interlaminar shear strength between the different materials and for investigating the stain rate effect on the interlaminar shear strength but the absolute values obtained should be treated with cautions.
- Under quasi-static loading, the interlaminar shear strength is about same for the all carbon and the hybrid hand lay-up and is lowest for the all glass hand lay-up. It is the highest for the all carbon pre-preg.
- Under impact loading, the interlaminar shear strength remains lowest for the glass hand lay-up but is now higher for the all carbon hand lay-up than for the hybrid specimens. It is highest of all for the all carbon pre-preg.
- The interlaminar shear strength is markedly strain rate dependent, increasing by about 72.6% for the all glass hand lay-up, 70.4% for the all carbon hand lay-up, 62.6% for the all carbon pre-preg and 55.6% for the hybrid hand lay-up.

6 Acknowledgments

This research was sponsored by the Air Force office of Scientific Research, Air Force Systems Command, USAF, under Grant No. AFOSR-87-0129.

REFERENCES

[1] Y.L.Li, C.Ruiz and J.Harding "Failure Analysis of Woven Hybrid Composite by Using Finite Element Method," *O.U.E.L., No. 1791/89*

[2] D.post, F.L.Dai, Y.Gau and P.Ifju "Interlaminar Shear Moduli of Cross-Ply Laminates: An Experimental Analysis," *J. Composite Materials, Vol. 23 pp 264-279 (March 1989)*

[3] D.E.Walrath and D.E.Adams "The Iosipescu Shear Test as Applied to Composite Materials," *Experimental Mechanics, 23(1): pp105-110(MARCH 1983)*

[4] C.Y.Chiem and Z.G.Liu "High Strain-rate Behaviour of Carbon Fibre Composite," *Mechanical Behaviour of Composites and Laminates, Edited by W.A.Green and M.Micunovic, Elsevier Applied Science*

[5] S.M.Werner and K.H.Dharan "The Dynamic Response of Graphite Fibre-Epoxy Laminate at High Shear Strain rate," *J. Composite Materials 20,(July 1986), 365-374*

[6] T.Parry and J.Harding "The Failure of Glass-Reinforced Composites under Dynamic Torsional Loading," *O.U.E.L. Report. No. 1365/81*

[7] J.Harding, L.Y.Li, K.Saka and M.E.C.Taylor "Characterisation of the Impact Strength of Woven Carbon/Epoxy Laminates," *Proc. 4th. Oxford conf. on ' Mechanical Properties of Materials a High Rates of Strain', March 1989 (Institute of Physics) Edited by J.Harding, pp.403-410*

[8] Y.L.Li, J.Harding and C.Ruiz "A New Type of Shear Specimen for Measuring the Interlaminar Shear Strength under Impact Loading," *to appear*

[9] J.Harding and L.M.Welsh "Impact Testing of Fibre-Reinforced Composite Materials,," *In Progress in Science and Engineering of Composite, T.Hayashi, K.Kawata and S.Unekawa eds., ICCM-IV Tokyo (1982) pp845-852*

[10] K.Saka and J.Harding "Behaviour of Fibre-reinforced Composite Under Dynamic Tension," *O.U.E.L., No.1543/84*

[11] K.Saka and J.Harding "Behaviour of Fibre-reinforced Composite Under Dynamic Tension," *Second Progress Report, O.U.E.L., No.1654/86*

[12] J.Harding, K.Saka and M.E.C.Taylor "Effect of Strain Rate on the Tnsile Failure of Woven-Reinforced Carbon/Glass Hybrid Composites," *Proc. IMPACT 87, (DGM Informationsgesellschafft mbH, Oberursel), 2, (1987), pp.579-586*

APPENDIX IV

ANALYSIS OF FAILURE IN WOVEN CARBON/EPOXY LAMINATES UNDER QUASI-STATIC AND IMPACT LOADING

by

J. Harding and Y. L. Li

Report No. OUEL 1846/90

University of Oxford
Department of Engineering Science
Parks Road
OXFORD
OX1 3PJ

Tel. (0865) 273000

ANALYSIS OF FAILURE IN WOVEN CARBON/EPOXY LAMINATES UNDER QUASI-STATIC AND IMPACT LOADING

J. Harding and Y. L. Li
Department of Engineering Science
University of Oxford
Parks Road
OXFORD
OX1 3PJ

ABSTRACT

A finite element method is used to determine the tensile stress concentration factors and the interlaminar shear stresses close to a failed ply in a woven carbon reinforced epoxy laminate under tensile loading. Ply failure is modelled by a reduction in stiffness in the loading direction. Different reductions in stiffness, representing either matrix break-up or fibre tow fracture are studied and the redistributed stress system, for the case where delamination follows initial ply failure, is also determined. The results of the theoretical analyses are discussed in the light of experimental data from tensile tests on a similar laminate at both a quasi-static and an impact rate of loading and the failure process at each rate of strain is described.

INTRODUCTION

A recent attempt[1] to use laminate theory and a Tsai-Wu type failure criterion to predict the failure strength of woven carbon/glass hybrid laminates at both quasi-static and impact rates of loading achieved only limited success. In part this was because the laminate theory approach ignores out-of-plane stresses, which will vary with the stacking sequence, but also because it was assumed that the carbon reinforced plies, in which failure always initiated, all failed at the same critical level of applied stress. For this purpose "failure" of the carbon reinforced plies was taken to correspond to a reduction in stiffness in the direction of loading so that they carried a smaller proportion of the increased load which was subsequently required before the glass-reinforced plies also "failed" and overall catastrophic fracture of the laminate ensued. A possible mechanism for this reduction in stiffness without loss of load carrying capacity might be the break up of the resin matrix, making it easier for the axially-aligned woven fibre tows to straighten under the applied load although eventually, of course, an <u>increased</u> stiffness should result once all the fibre tows have become aligned with the loading direction.

In order to estimate the critical stress at which the carbon reinforced plies might "fail" the maximum tensile stress was determined in tests on non-hybrid woven carbon reinforced laminates at both a quasi-static and an impact rate of strain. However, since this was the stress at which overall failure was obtained in these non-hybrid laminates, it will be a measure of the fracture strength of the carbon tows and is likely, therefore, to be an overestimate of the stress to give a "failure" determined by the break up of the resin. This was confirmed by the observation that in the experimentally determined stress-strain curves for the hybrid laminates the departure from a linear elastic response was always at a stress level below that predicted for first ply failure in the theoretical analysis.

A further complication arises since, in practice, experimental results show that the critical fracture stress, both for single carbon fibres and for carbon fibre tows, follows a statistical distribution[2] so that not all fibres will fracture simultaneously. Although this statistical variation is expected to be much less significant both for a woven rather than a unidirectional reinforcement and for the resin break-up process rather than for fibre fracture, the assumption of a single critical load at which all the carbon-reinforced plies will "fail" is likely to be a gross over simplification. In reality the failure process in any given woven-reinforced ply almost certainly involves both a break-up of the resin matrix and the fracture of individual fibres or fibre tows followed by some combination of fibre pull-out and delamination. Since a laminate theory approach cannot be expected to take account of all these various processes the limited success achieved in the previous attempt at predicting hybrid tensile strength is not surprising.

However it is possible, using the finite element method, to make at least some qualitative progress towards distinguishing between those processes which depend on the magnitude of the tensile stress, e.g. fibre or fibre tow fracture, and those which depend on the magnitude of the shear stress, e.g. delamination and fibre pull-out. The present report describes an attempt to do this for a non-hybrid plain weave carbon-reinforced laminate. Initiation of failure is modelled by a local reduction in the tensile stiffness for a given ply. Different reductions in stiffness are used, a smaller reduction to represent failure by the break-up of the resin matrix, a larger reduction to represent fracture of the given carbon reinforced ply. In each case the tensile and shear stress distributions close to the failed region are estimated. The

relative values of tensile stress concentration, in the adjacent plies, to interlaminar shear stress, at the interface between the failed ply and its nearest neighbours, will give a qualitative indication as to the next stage in the failure process. The analysis is limited to a specific lay-up of woven carbon/epoxy laminate for which experimental data are available[3,4]. The finite element method used here closely follows that described in a recent paper on the failure analysis of woven hybrid composites[5].

FINITE ELEMENT ANALYSIS TECHNIQUE

The ply lay-up in the central parallel region of the test specimen used in the earlier experimental work[3,4] is shown schematically in Fig. 1. It consists of 6 reinforcing plies each containing 5 carbon fibre tows aligned with the tensile axis, i.e. in the 01 direction. Each reinforcing ply may be divided into 15 nominally identical repeating units, or "unit cells", which are treated as if they were homogeneous and orthotropic with the elastic properties given in Table I. The in-plane elastic constants were determined experimentally in tension tests at a quasi-static rate of strain[4]. Poisson's ratio, ν_{21}*, determined using the symmetry hypothesis for an orthotropic laminate, i.e. $E_1\nu_{21} = E_2\nu_{12}$, is also listed. The finite element analysis also requires a knowledge of the elastic properties in the through-thickness direction, direction 03. In the absence of any experimental data on the elastic properties in this direction an estimated value for E_3 of 6.0GPa, based on the rule of mixtures and a fibre volume fraction of 50%, was assumed and the corresponding Poisson's ratio, ν_{13}, was taken to be 0.15. More recent experimental work has given elastic properties in the through-thickness direction as listed in Table II. It is not thought likely that the small differences observed between the two sets of values will have a significant effect on the conclusions of the finite element analysis.

TABLE I
Elastic Constants for Carbon Reinforced Plies

	E_1 (GPa)	E_2 (GPa)	ν_{12}	ν_{21}	ν_{21}*
Carbon-reinforced ply	45.3	43.3	0.14	0.09	0.13

TABLE II
Elastic Constants for Carbon Reinforced Plies in Through-Thickness Direction

	E_3 (GPa)	ν_{13}	ν_{31}*	ν_{23}	ν_{32}*
Carbon-reinforced ply	6.7	0.11	0.02	0.11	0.02

The analysis assumes a state of plane strain. A mesh consisting of 180 elements, each 0.2mm long, see Fig. 2, was used, there being 10 such elements along the length of each unit cell. Initial tensile failure is assumed to occur in one of the elements adjacent to the central cross-section of the specimen and is modelled by a reduction in the longitudinal modulus, E_1, by a factor of 0.1, 0.01 or 0.001. This is followed either by a further tensile failure in a neighbouring ply, controlled by the local tensile stress concentration, or by a delamination between the failed ply and its immediate neighbours, controlled by the local shear stresses. Which of these mechanisms operates will depend on the redistributed stress system in the vicinity of first failure.

A difficulty arises when attempts are made to model the delamination process. If delamination is modelled simply as a crack between two frictionless surfaces the shear stress concentration at the singularity is not significantly reduced by the delamination process but merely moves with the delamination crack tip, i.e. the delamination extends catastrophically through to the ends of the specimen. While such behaviour is sometimes observed in specimens with unidirectional reinforcement, it does not describe the response seen in the present woven-reinforced materials. Here, therefore, an arbitrarily chosen friction coefficient of 0.5 is assumed on the crack surfaces between which slip is allowed to occur. The delamination process is then modelled using the ABAQUS interface element, for which, since there should be no relative movement until slip occurs, a modulus of 1000GPa is assumed. This also avoids interpenetration between adjoining surfaces.

Analyses were performed for delamination over 2 elements (0.2mm) on each side of the failed element (short delamination), for delamination over 5 elements (1.0mm) on each side of the failed element (corresponding to delamination over the length of a unit cell) and for delamination over 7 elements on each side of the failed element (long delamination, equivalent to half the parallel gauge length of the test specimen). In the light of experimental observations[4], first ply failure was assumed to occur when a critical strain of 1.35% was first reached in the reinforcing plies. This corresponds to the condition for tensile fracture rather than matrix break-up. Since, however, only tensile stress concentration factors around the failed ply are determined, the results are equally applicable to either situation. In contrast, for any subsequent delamination, which it was assumed took place under constant displacement at the critical strain of 1.35%, specific values of the interlaminar shear stress close to failure are determined. These are likely to be overestimates of those resulting from matrix break-up.

RESULTS

Typical finite element analyses for the tensile and shear stress distribution close to the failed ply or plies, with or without subsequent delamination, are given in Figs. 3 - 25. Each figure shows a) the tensile stress concentration factor, i.e. the increase in tensile stress over that just before failure, and b) the interlaminar shear stress determined over the 6mm parallel gauge length of the test specimen, along the interfaces between adjacent reinforcing plies, as defined in Fig. 2. The results obtained allow a study to be made of the effect of varying three different parameters, 1) the chosen reduction in ten-

sile modulus used to model tensile failure, 2) the extent of subsequent delamination and 3) the effect of one or more subsequent tensile failures in adjacent plies.

1. The effect of varying the tensile modulus

For failure in a central element of ply 4 the ABAQUS finite element package was used to determine the subsequent tensile and shear stress distribution in the 01 direction along the interfaces between the various plies. Results are presented in figs. 3, 4 and 5, respectively, for an assumed reduction in tensile modulus in the failed element of $E_1/10$, $E_1/100$ and $E_1/1000$. Stresses were determined at the Gauss points, at the top of elements in plies 1, 2 and 3, i.e. points 1T, 2T and 3T (see fig. 2) and at the bottom of elements in plies 5 and 6, i.e. points 5B and 6B. The resulting stress distributions are seen to be symmetrical about the failed element in both the loading and the through-thickness directions. The tensile stress concentration is highly localised, decaying, see fig. 3, from a maximum of ~2.1x to only about 1.1x within one element in both directions. Decreasing the tensile modulus in the failed element to $E_1/100$, see fig. 4, increases the maximum stress concentration to ~2.7x but has little effect on the width of the affected region while a further decrease in the modulus to $E_1/1000$, see fig. 5, only leads to a marginal increase in the maximum tensile stress concentration, from ~2.7x to ~2.8x.

The shear stress distribution is also symmetrical about the failed element in both the loading and the through-thickness directions. The only significant values of interlaminar shear stress are on the two interfaces immediately adjacent to the failed ply. On these planes the shear stress decays more slowly, falling to about 10% of its peak value over a distance of ~7 elements. The peak value of interlaminar shear stress increases with decreasing tensile modulus in the failed element from ~31MPa, fig. 3b, to ~49MPa, fig. 4b, and ~52 MPa, fig. 5b.

2. The effect of subsequent delamination

Assuming these local interlaminar shear stresses are high enough to cause limited delamination on the planes adjacent to the failed ply, the resulting tensile and shear stress distributions, for delamination over 2, 5 or 7 elements on either side of the failed element, are shown in figs. 6 to 14. These are, respectively, for the redistributed stress system of fig. 3 (i.e. for a reduced modulus of $E_1/10$), in figs. 6, 7 and 8, for the redistributed stress system of fig. 4 (i.e. $E_1/100$) in figs. 9, 10 and 11, and for the redistributed stress system of fig. 5 (i.e. for $E_1/1000$) in figs. 12, 13 and 14.

Delamination results in a significant reduction in the maximum tensile stress concentration. For a tensile modulus of $E_1/10$ it falls from ~2.1x, with no delamination to ~1.5x, ~1.35x and ~1.3x, respectively, with increasing delamination, see figs. 6, 7 and 8. The decay in tensile stress outside the delaminated region remains as rapid as before but within the delaminated region there is an average tensile stress concentration of the order of 1.3x, 1.15x and 1.1x, respectively. For delamination over 5 or 7 elements this region extends over the whole of one of the unit cells in fig. 1. A similar general effect of delamination on the tensile stress concentration factor is shown in figs. 9 - 11 and figs. 12 - 14, as summarised in Table III.

TABLE III
Effect of Delamination on the Tensile Stress Concentration Factor
for Initial Tensile Failure in Ply 4

Tensile Modulus in failed ply	$E_1/10$	$E_1/100$	$E_1/1000$
No delamination	2.1x	2.7x	2.8x
Delamination over 2 elements	1.5x (1.3x)	2.0x (1.6x)	2.1x (1.7x)
Delamination over 5 elements	1.35x (1.15x)	1.9x (1.4x)	2.05x (1.4x)
Delamination over 7 elements	1.3x (1.1x)	1.85x (1.3x)	2.05x (1.35x)

(Average tensile stress concentration factors over delaminated region are shown in parenthesis)

Increasing delamination has a more complex effect on the shear stresses, see Table IV. The peak value of shear stress on the adjacent interlaminar planes shows initially a small increase, from about 31 to 33MPa, following delamination over two elements, see figs. 3 and 6, but then decreases, with further delamination over 5 or 7 elements, see figs. 7 and 8, to about 22.8 or 18.8MPa, respectively. The same general trend is also shown in figs. 9, 10 and 11 (for $E_1/100$) and figs. 12, 13 and 14 (for $E_1/1000$) except that in both these cases the initial increase is larger while the subsequent decreases are smaller so that the peak interlaminar shear stress even after delamination over 7 elements remains higher that before any delamination had occurred, i.e delamination does not relieve the shear stress concentration. This implies that if the interlaminar shear stresses arising from fibre fracture were to result in delamination, the delamination crack would propagate catastrophically to the ends of the specimen gauge section. However such behaviour was never observed experimentally in the impact tests and only once in the quasi-static tests, for a specimen loaded in the warp direction, where there was evidence that delamination over the full length of the specimen had resulted from an initial tensile fracture which was arrested by the onset of delamination, final fracture subsequently propagating on a different plane[6]. It would appear, therefore, that delamination by this mechanism does not commonly occur for the woven carbon/epoxy laminate and the tensile loading conditions being studied here. There remains, of course, an effective delamination associated with the region of resin break-up.

TABLE IV
Effect of Delamination on the Peak Interlaminar Shear Stress
for Initial Tensile Failure in Ply 4
(MPa)

Tensile Modulus in failed ply	$E_1/10$	$E_1/100$	$E_1/1000$
No delamination	31.0	49.1	51.7
Delamination over 2 elements	33.0	67.1	73.8
Delamination over 5 elements	22.8	58.9	68.7
Delamination over 7 elements	18.8	54.9	67.8

3. Effect of further tensile failures

Initial tensile failure in ply 4 may lead to delamination on the adjacent interlaminar planes, as analysed in section 2 above. Alternatively it may result in an immediate tensile failure of the neighbouring plies and hence, presumably, catastrophic tensile failure of the specimen as a whole. On the basis of the tensile stress concentrations shown in figs. 4 to 6, either of the neighbouring plies, 3 or 5, appears equally likely to fail next. The tensile and shear stress distributions following failure in both plies 3 and 4 are shown in figs. 15, 16 and 17 for, respectively, $E_1/10$, $E_1/100$ and $E_1/1000$. Similar results following failure in plies 4 and 5 are shown in figs. 18, 19 and 20 and following failure in plies 3, 4 and 5 in figs. 21, 22 and 23. Although delamination is unlikely to be favoured following tensile failure in two or more plies, to complete the picture the redistributed stress systems following delamination over 7 elements after tensile failure in plies 4 and 5 are shown in figs. 24 and 25 for $E_1/10$ and $E_1/100$ respectively.

The results for the maximum tensile stress concentration, the peak interlaminar shear stress and the average tensile stress concentration over the delaminated region are compared in Table V with those obtained for failure in ply 4 alone. As would be expected both the tensile stress concentrations and the peak shear stresses are significantly higher following the tensile failure of two or more plies. However the non-symmetrical case of failure in plies 4 and 5 is only slightly worse than the symmetrical case of failure in plies 3 and 4. Failure in three plies, 3, 4 and 5, again gives significantly higher tensile stress concentrations and peak shear stresses for $E_1/100$ and $E_1/1000$, but the effect is much less marked for $E_1/10$.

DISCUSSION

Tensile stress-strain curves for the woven carbon/epoxy specimen modelled in figs. 1 and 2, under quasi-static and impact loading, are shown in fig. 26[6]. In each case a mean curve is given for loading in the warp and the weft directions. The approximate limit of linear elastic behaviour is indicated. At the quasi-static loading rate this occurs at a stress of about 250MPa and is followed by a significant region of damage accumulation before final failure at a stress of about 420MPa and a strain of 1.3%. At the dynamic rate the elastic region extends up to a stress of about 500MPa and the subsequent damage region is much less extensive, final failure occurring at a stress of about 535MPa and a strain of 1.2%. A small effect of strain rate on the tensile elastic modulus is apparent. This has been ignored in the previous finite element analyses which were all based on the quasi-static elastic constants given in Tables I and II.

It was suggested in the introduction that a possible mechanism whereby tensile failure might be initiated in woven reinforced laminates was the break-up of the resin matrix. For the woven reinforcement geometry shown in Fig. 1 the maximum extension obtained when all axially-aligned fibre tows are fully straightened over the entire 6mm parallel gauge length of the specimen is only ~0.02mm, corresponding to an anelastic strain of ~0.335%. In practice experimental evidence[3] suggests that the damage zone extends over no more than one half-wavelength of weave either side of the fracture surface, i.e. over one unit cell in Fig. 1, reducing the effective anelastic strain when averaged, as in Fig. 26, over the full gauge length, to only ~0.112%. In the event this agrees very well with the actual anelastic strain determined experiment-

TABLE V

Tensile and Shear Stress Distribution for 2 or 3 Failed Plies

Failed Plies		Tensile Modulus of Failed Plies		
		$E_1/10$	$E_1/100$	$E_1/1000$
4 only	Max Tensile Stress Concentration	2.1x	2.7x	2.8x
	Peak shear stress (MPa)	30	49	50
4 only +7Del	Max Tensile Stress Concentration	1.3x	1.9x	2.1x
	Average Tensile Stress Concentration	1.1x	1.3x	1.3x
	Peak shear stress (MPa)	19	58	69
3 + 4	Max Tensile Stress Concentration	2.5x	3.8x	4.0x
	Peak shear stress (MPa)	37	70	80
4 + 5	Max Tensile Stress Concentration	2.6x	4.1x	4.5x
	Peak shear stress (MPa)	38	75	85
3+4+5	Max Tensile Stress Concentration	2.8x	5.2x	5.8x
	Peak shear stress (MPa)	38	90	100
4 + 5 +7Del	Max Tensile Stress Concentration	1.5x	2.8x	
	Average Tensile Stress Concentration	1.2x	1.8x	
	Peak shear stress (MPa)	25	90	

ally at fracture under the impact rate of loading. It requires that resin break up occurs in all 6 reinforcing plies at a given cross-section. If we assume that this initiates in ply four in the centre of the gauge length, see fig. 27, and that resin break-up has a similar effect to delamination over the unit cell in which it occurs, then the results in Table V give an estimate of the average tensile stress concentration factor and the maximum interlaminar shear stress close to the failed ply. For a reduced tensile modulus of $E_1/10$, to model resin break-up, and for delamination over 7 elements, these are 1.1x and 19MPa respectively, although the latter is probably an overestimate as it follows from the condition that failure occurs when the overall applied strain reaches 1.35% which, as was discussed earlier, corresponds to fibre fracture rather than resin break-up.

Experimental measurements of the average interlaminar shear stress (ILSS) at failure in this laminate give values of ~26MPa under quasi-static and ~45MPa under impact loading[7]. Further local delamination, or fibre pull-out, is unlikely, therefore, in the impact tests although possible, perhaps, under quasi-static loading. Assuming that resin break-up initiates at an applied stress of ~500MPa, the limit of the linear elastic region for the impact tests in fig. 26, the local tensile stress in the adjacent plies will be raised to ~550MPa. This is unlikely to be high enough to cause tensile fracture of the

neighbouring fibres or fibre tows but could well be sufficient to promote the break up of the resin in the adjacent unit cells in plies 3 and 5, further raising the local tensile stresses, by a factor of 1.2x, and the local peak ILSS, to ~25MPa, and extending resin break-up into plies 2 and 6 and finally into ply 1.

The experimental stress levels recorded in fig. 26 are determined from the applied load and the total cross-sectional area in the specimen gauge region, nominally 17.5mm^2. If, as described above, all the carbon fibre tows remain unfractured at the point when resin break-up has occurred in all six plies, the effective stress carried by the axially-aligned carbon fibre tows will be given by the applied load divided by the cross-sectional area of these tows, approximately one third of the nominal overall cross-section, i.e. ~1600MPa for the impact stress-strain curve of fig. 26, well into the range where carbon fibres might be expected to fail in tension. The general process described above will still be valid, however, even if carbon fibres begin to fracture before this point, provided the extent of fracturing is not so great as to give complete separation of the specimen before the anelastic strain reaches ~0.11%. This is not impossible, bearing in mind the generally qualitative nature of the present discussion and the uncertainty regarding the precise values of the controlling tensile and shear stresses at which the different damage mechanisms initiate.

The principal differences between the tensile behaviour under quasi-static and impact loading are a) the much lower stress at which the anelastic damage region starts, ~250MPa, in the quasi-static tests, b) the much greater extent of this region, up to a strain of ~0.33%, and c) the lower final fracture stress, ~425MPa as compared to ~535MPa under impact loading. If the start of the anelastic region is controlled by the onset of a process of matrix break-up then the higher stress level at which this occurs in the impact tests follows from the very marked strain rate dependence of the flow and fracture stresses for epoxy resin[8,9]. More difficult to explain, however, are the extended damage region and the lower fracture stress in the quasi-static tests.

Considering, for example, the effect of strain rate on the composite fracture stress. There is experimental evidence to suggest that the tensile fracture strength of carbon fibre tows, over some six orders of magnitude, is totally insensitive to strain rate [10]. If, as suggested above, fracture of the composite in the impact tests follows resin break-up in all six reinforcing plies but with no prior fibre fracture, the actual fibre fracture strength is of the order of 1600MPa. For this also to be the fibre fracture strength in the quasi-static tests, when the stress applied to the composite specimen was only ~425MPa, it is necessary for ~20% of the axially-aligned carbon fibres to have fractured before the composite as a whole fails. However, if we model fibre fracture in terms of a reduction in the tensile modulus of $E_1/100$ (since a further reduction to $E_1/1000$ has a relatively small effect) much higher tensile stress concentration factors are developed in the neighbouring plies than for the case of resin break-up. Thus, from Table V, the peak tensile stress concentration factor in the absence of delamination is ~2.7x when one ply fractures, rising to ~4.0x when two plies fracture, high enough to give local tensile stresses of the same order as the expected fracture strength of carbon fibres. These stress concentration factors, however, are derived using a two-dimensional finite element analysis and correspond to the case of failure of the entire reinforcing ply. Fractures of individual tows or small groups of individual fibres would probably be less effective as stress raisers and catastrophic failure thereby avoided.

There is also the problem of explaining the increased anelastic region before failure at the quasi-static rate. If fibre straightening over one unit cell is the mechanism to give the anelastic strain of 0.11% in the dynamic tests then the same process over the entire gauge length of three unit cells could give the anelastic strain of 0.33% observed in the quasi-static tests. However resin break-up over the entire gauge length was not observed experimentally although it surely would have been had it taken place. Alternatively the damage region in the quasi-static tests may be the result of a combination of resin break-up and fibre straightening on the one hand and fibre fracture and pull-out on the other. A very small fibre pull-out, of the order of only 0.01mm, would be sufficient and could arise following limit-ed fibre fracture, provided catastrophic failure and rapid unloading did not precede, and thereby prevent, the pull-out process.

There are, therefore, two reasons for proposing limited fibre fracture before final failure in the quasi-static tests, namely to account for a) the different composite fracture stress levels and b) the increased region of anelastic strain. While, as suggested above, there may also be limited fibre fracture preceding final failure in the impact tests, in this case the higher tensile stresses make a subsequent early catastrophic failure more likely. Also the higher critical shear stress required for interlaminar failure or pull-out makes these processes less likely, consistent with the reduced damage strain observed under impact loading.

The results support the suggestion made earlier that the initial failure process in the given woven-reinforced ply involves break-up of the resin followed by the fracture of individual fibres or fibre tows and by limited fibre pull-out. Processes controlled by the applied shear stress, i.e fibre pull-out, play a greater part in the quasi-static tests where the shear resistance is low, leading to higher overall failure strains while fibre fracture, assuming no rate dependence of the fracture strength of carbon fibres, predominates at impact strain rates where the applied tensile stresses are higher, giving a reduced overall damage strain.

Although this discussion confirms that gross simplifications were indeed made in the previous laminate theory approach and provides instead a much more detailed description of the tensile failure process in woven carbon/epoxy laminates, it is still not easy to see how the complicated interaction between these various damage mechanisms can easily be modelled by numerical methods. We are still a long way from developing a realistic constitutive relationship for such materials which reflects the mechanical processes actually taking place during deformation. However, on the positive side, it is possible to make some assessment of the relative importance of different damage mechanisms at different rates of loading. Thus the present results would suggest that some increase in the damage which could be sustained under impact loading might be achieved if the increase in shear resistance at these rates could be minimised, possible by some appropriate surface treatment of the fibres.

CONCLUSIONS

The finite element method has been used to study the stress distribution in a woven carbon reinforced laminate following ply failure, either by break-up of the resin matrix or by fibre fracture, both with and without subsequent delamination. The results have been discussed in the light of experimental evidence obtained at both a quasi-static and an impact rate of strain.

Initial ply tensile failure may be related to break-up of the matrix at an applied stress which increases with increasing strain rate. In impact tests the subsequent anelastic deformation may be accounted for in the main by the straightening of the axially-aligned woven tows. This is followed by fibre fracture leading to immediate catastrophic failure of the laminate. At quasi-static rates of strain fibre straightening alone cannot explain the extent of the anelastic deformation. It is suggested that in this case the additional anelastic deformation derives from limited fibre fracture and some associated fibre pull-out prior to catastrophic failure of the laminate. The reduced extent of anelastic deformation under impact loading, therefore, is thought to be due, in part, to the much higher interlaminar shear strength at these rates of strain.

ACKNOWLEDGMENTS

This research was sponsored by the Air Force Office of Scientific Research, Air Force Systems Command, USAF, under Grant No. AFOSR-87-0129.

REFERENCES

1. K. Saka and J. Harding, A simple laminate theory approach to the prediction of the tensile impact strength of woven hybrid composite, Composites (in press).

2. M. G. Bader and A. M. Priest, Statistical aspects of fibre and bundle strength in hybrid composites, in Progress in Science and Engineering of Composites, T Hayashi et al., Eds., Proc. 4th. Int. Conf. on Composite Materials, ICCM IV, Tokyo, 2, 1982, 1129-1136.

3. K. Saka and J. Harding, The deformation and fracture of hybrid reinforced composites under tensile impact, in Proc. IUTAM Symposium on Macro- and Micro-Mechanics of High Velocity Deformation and Fracture, Springer-Verlag, Berlin and Heidelberg, 1987, 97-111.

4. J. Harding, K. Saka and M. E. C. Taylor, The effect of strain rate on the tensile failure of woven-reinforced carbon/glass hybrid composites, in Proc. IMPACT 87, Impact Loading and Dynamic Behaviour of Materials, DGM Informationsgesellschafft mbH, Oberursel, 2, 1987, 579-586.

5. Y. L. Li, C. Ruiz and J. Harding, Failure Analysis of Woven Hybrid Composites using a Finite Element Method, Composites Science and Technology (in press).

6. J. Harding, K. Saka and M. E. C. Taylor, Behaviour of Fibre-Reinforced Composites under Dynamic Tension (Third Progress Report), Oxford University Engineering Laboratory Report No. OUEL 1654/86, 1986.

7. J. Harding, Y. L. Li and M. E. C. Taylor, The Effect of Strain Rate on the Interlaminar Shear Strength of Woven-Reinforced Laminates, to appear in Proc. ECCM-4, Stuttgart, September 1990

8. U. S. Lindholm, Some Experiments with the Split Hopkinson Pressure Bar, J. Mech. Phys. Solids, 12, 1964,317-335.

9. L. M. Welsh and J. Harding, Dynamic Tensile Response of Unidirectionally-Reinforced Carbon/Epoxy and Glass/Epoxy Composites, in Proc. 5th. Int. Conf. on Composite Materials, ICCM V, TMS-AIME, 1985, 1517-1531.

10. J. Harding and L. M. Welsh, A Tensile Testing Technique for Fibre-Reinforced Composites at Impact Rates of Strain, J. Mater. Sci., 18, 1983, 1810-1826.

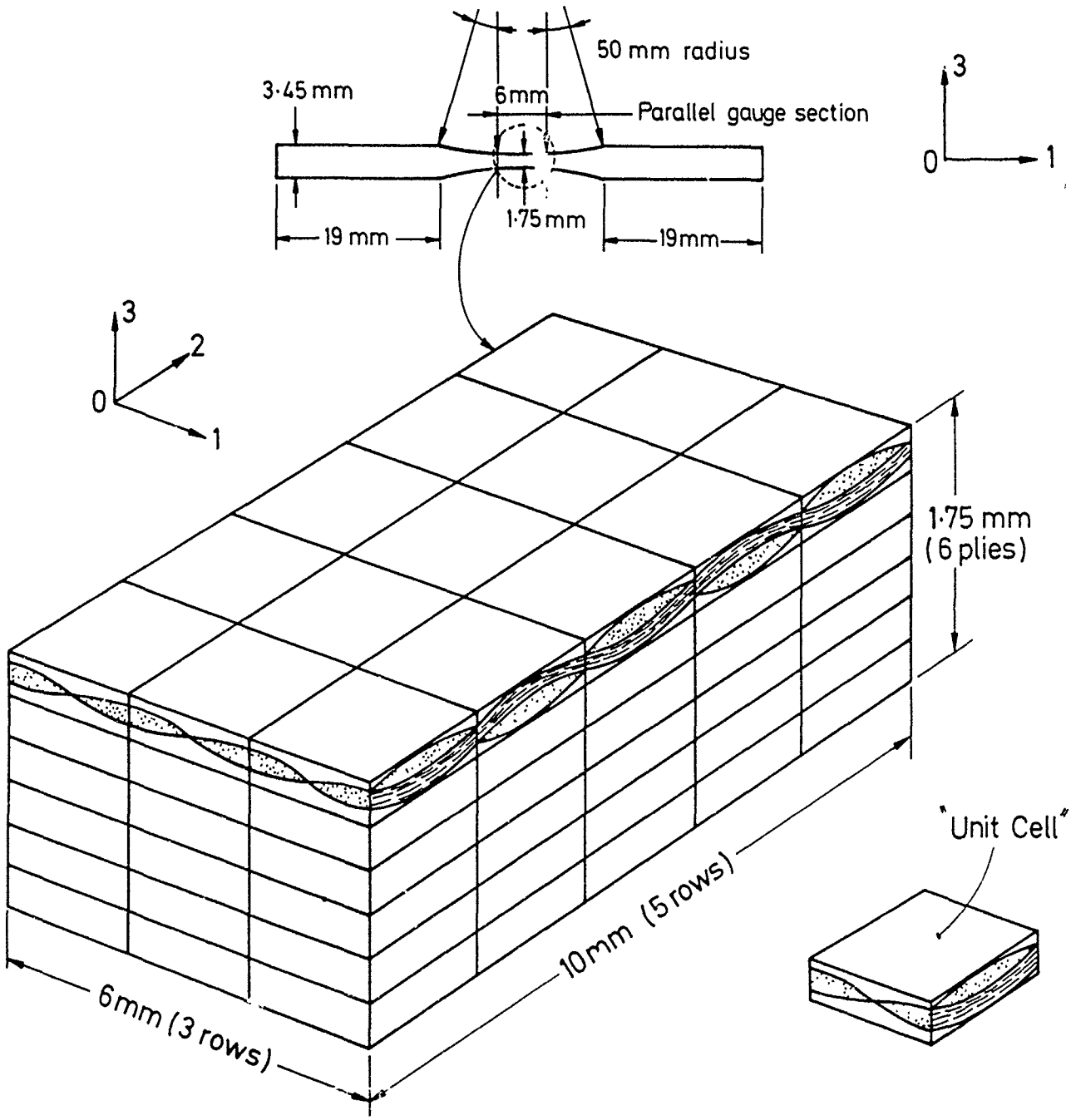

Fig. 1
Idealised Model of Ply Lay-Up in Central Parallel
Region of Composite Tensile Test Specimen

Fig. 2 Finite Element Mesh and Ply Numbering

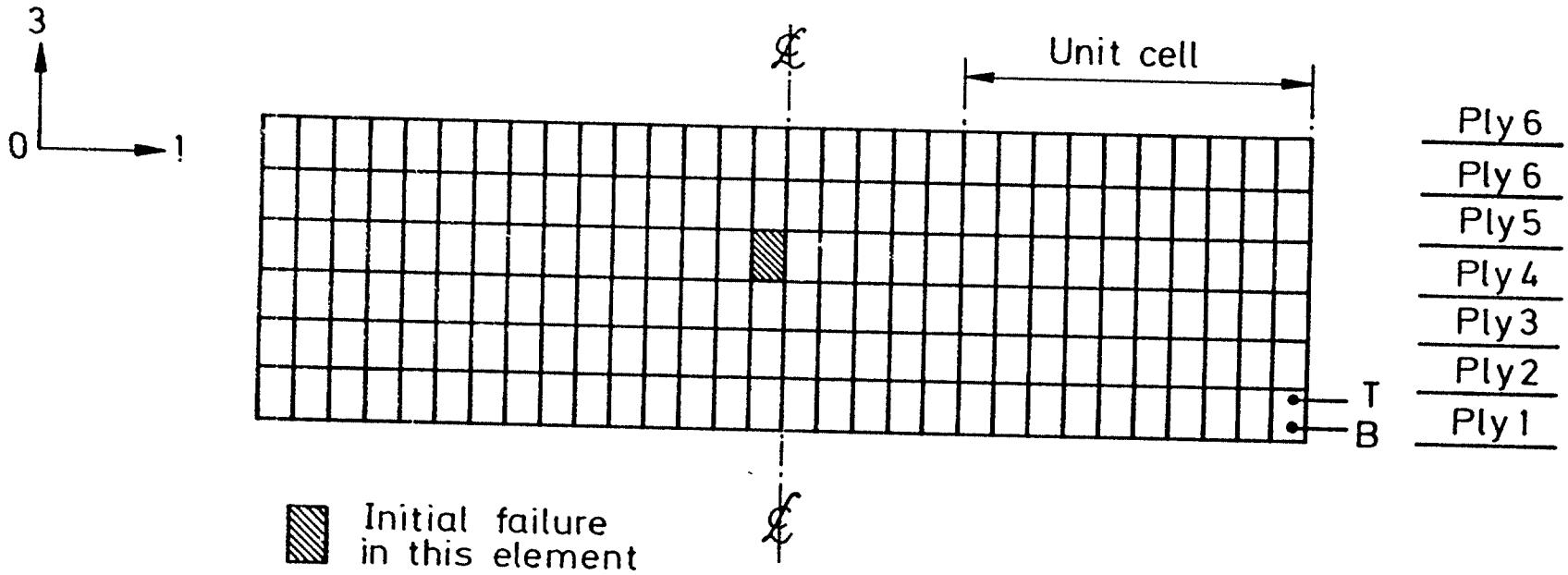

Fig. 3
Tensile and Shear Stress Distribution for Failure
in Ply 4 (modulus reduction: x0.1)

a) Tensile stress concentration factor

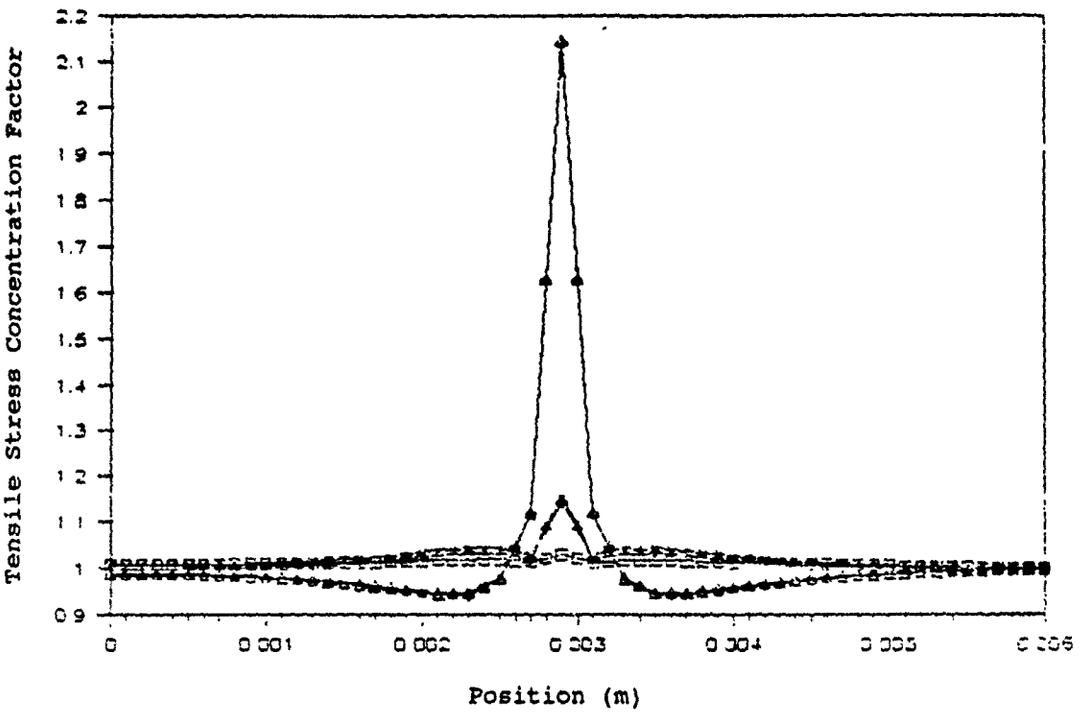

b) Interlaminar shear stress (MPa)

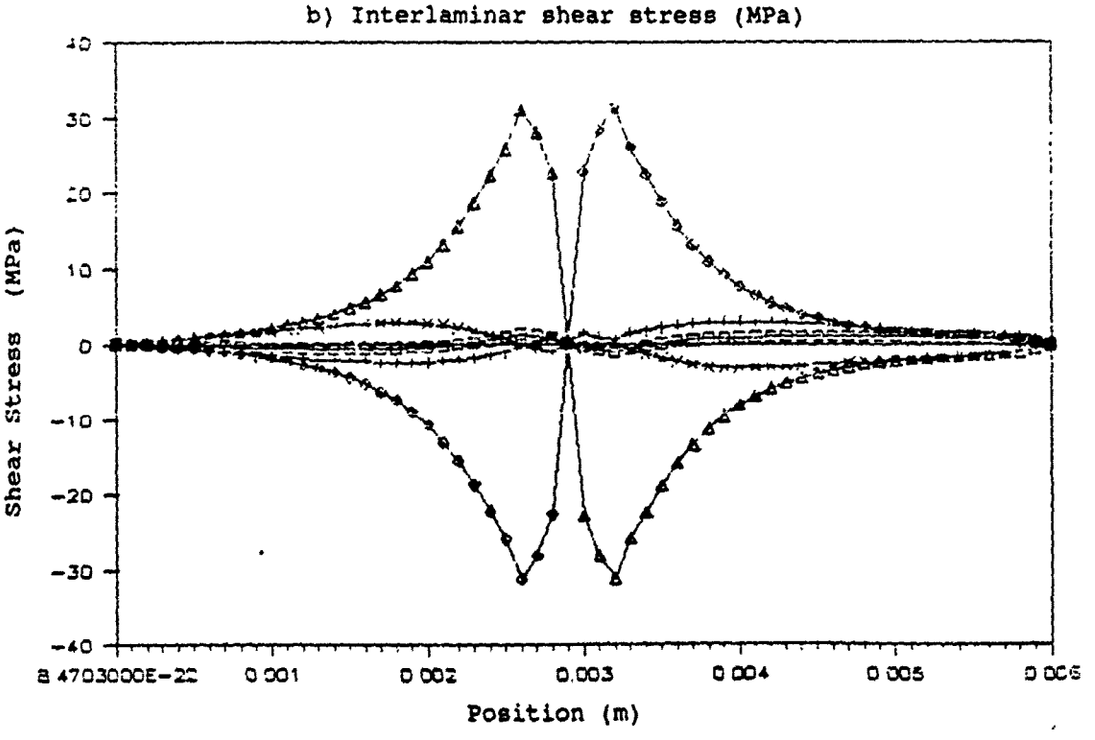

Fig. 4
Tensile and Shear Stress Distribution for Failure
in Ply 4 (modulus reduction: x0.01)

a) Tensile stress concentration factor

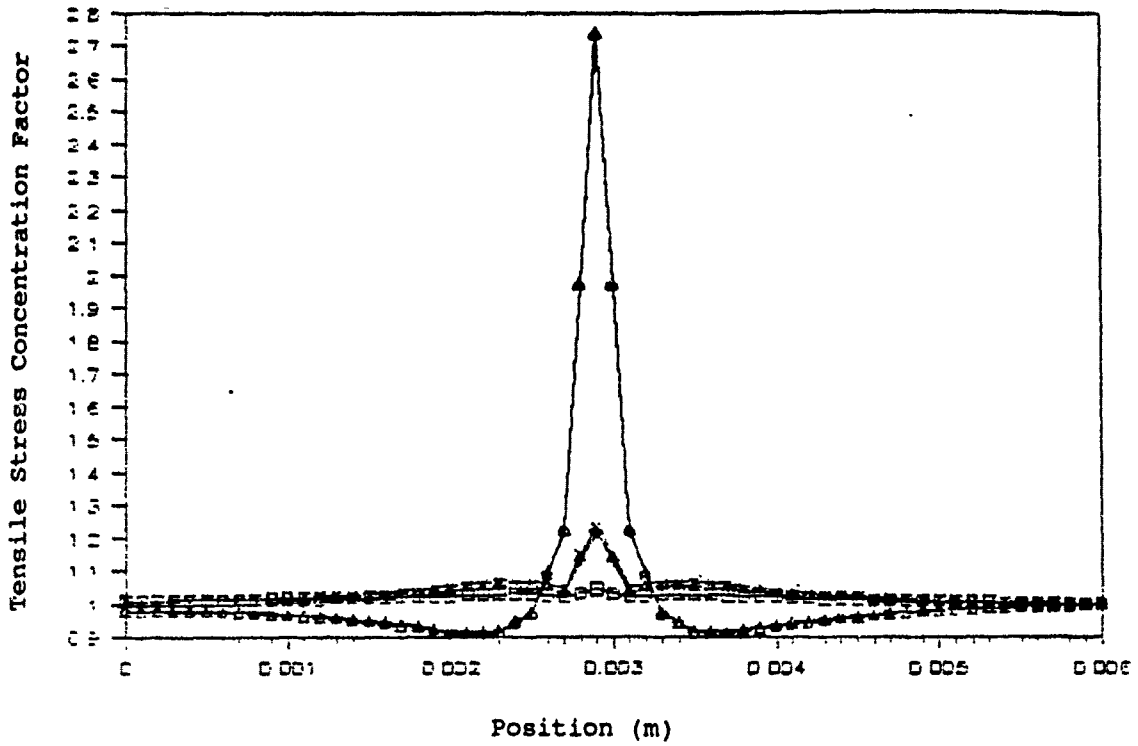

b) Interlaminar shear stress (MPa)

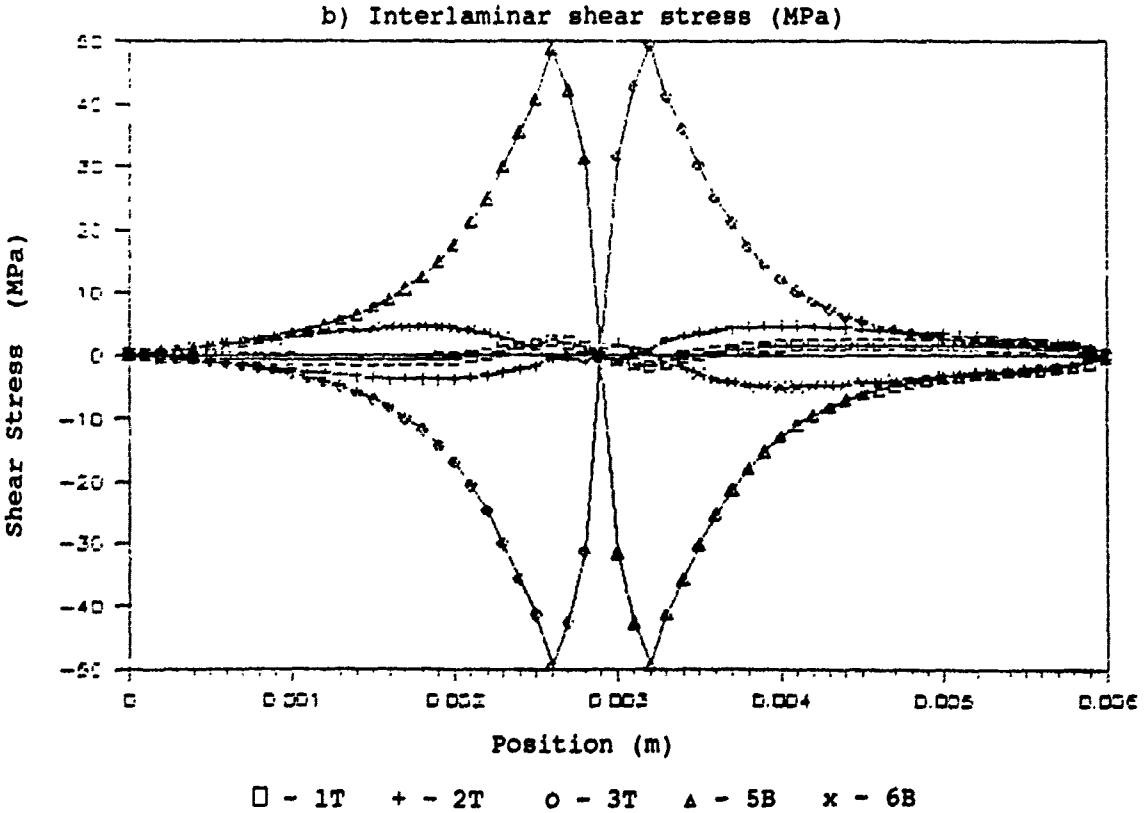

Fig. 5
Tensile and Shear Stress Distribution for Failure in Ply 4 (modulus reduction: x0.001)

a) Tensile stress concentration factor

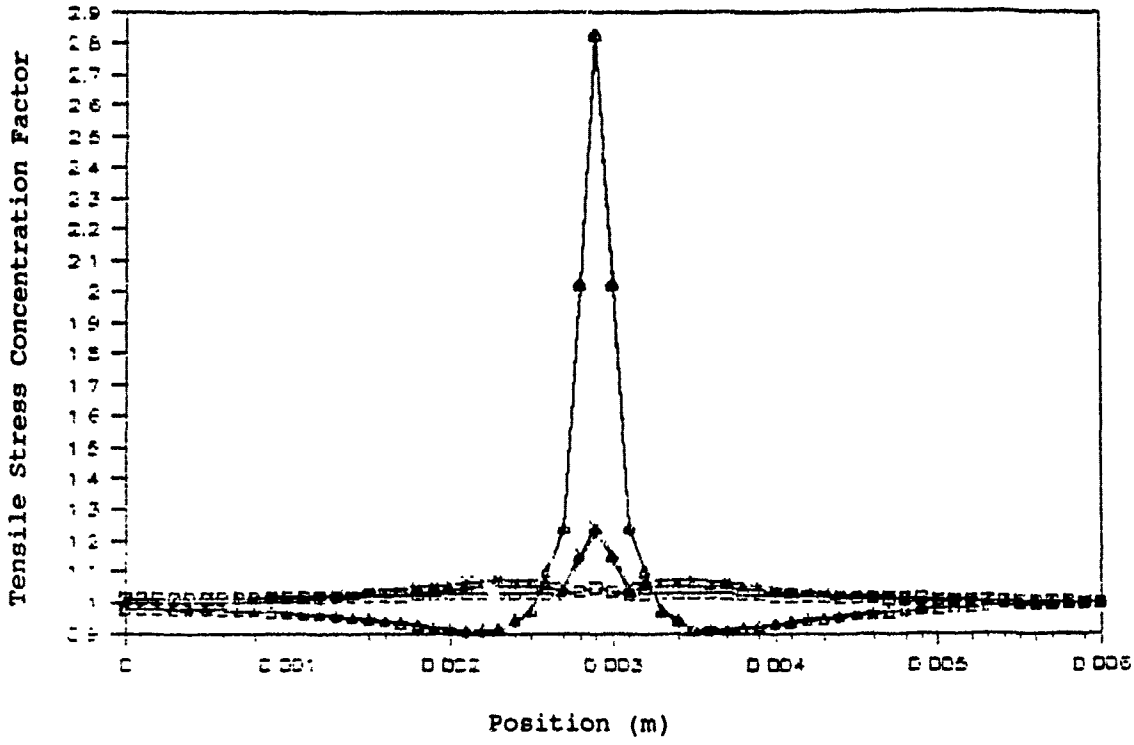

□ - 1T + - 2T o - 3T ▵ - 5B x - 6B

b) Interlaminar shear stress (MPa)

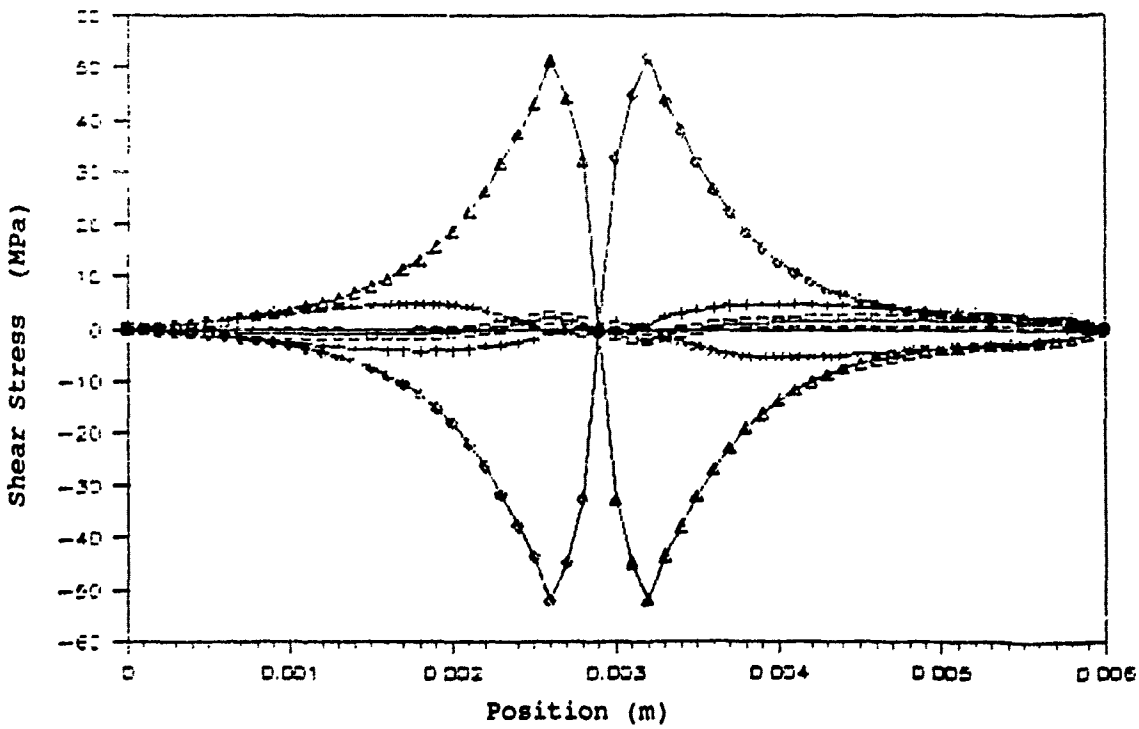

□ - 1T + - 2T o - 3T ▵ - 5B x - 6B

Fig. 6
Tensile and Shear Stress Distribution for Failure in Ply 4
and Delamination over 2 Elements (modulus reduction: x0.1)

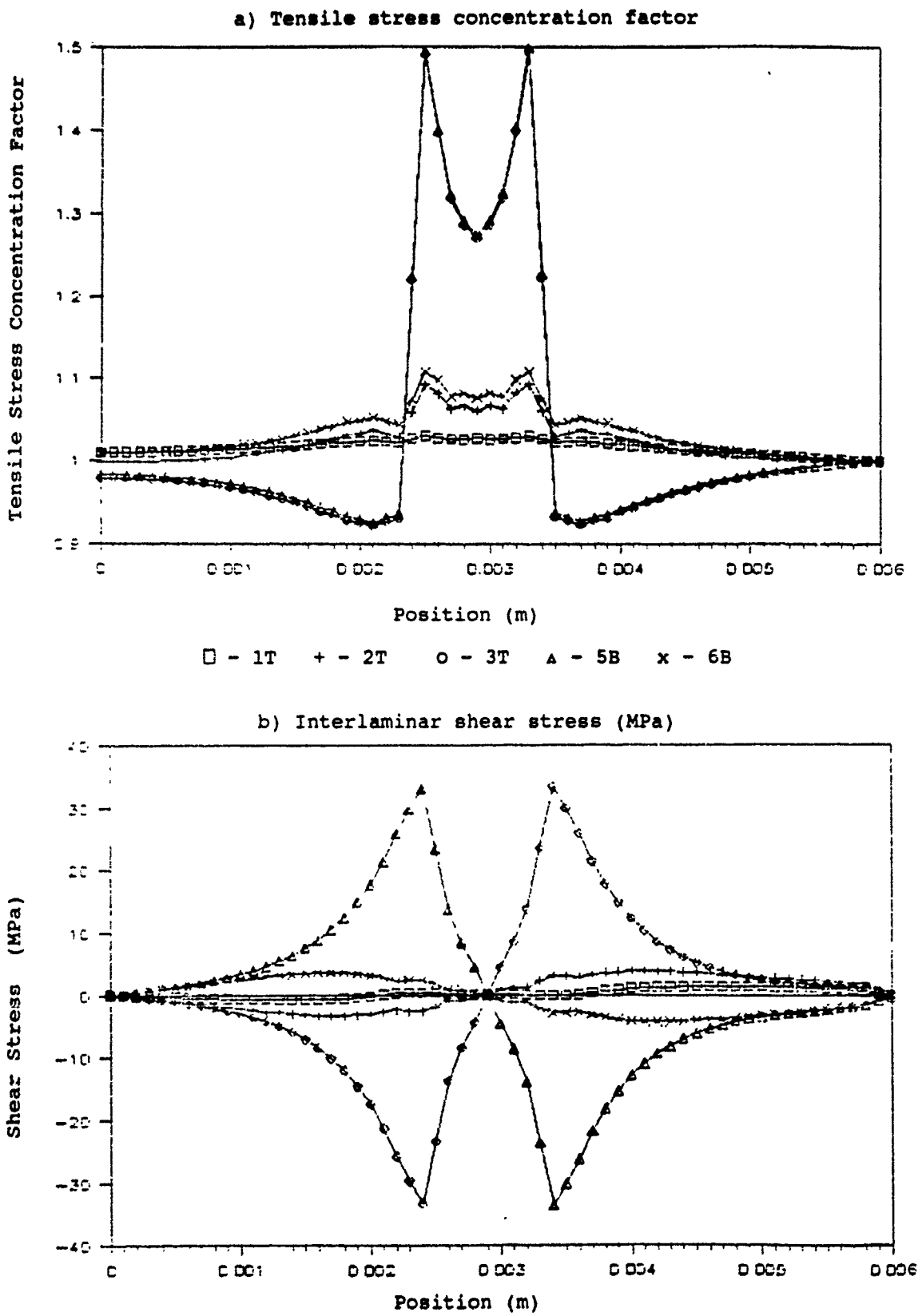

Fig. 7
Tensile and Shear Stress Distribution for Failure in Ply 4
and Delamination over 5 Elements (modulus reduction: x0.1)

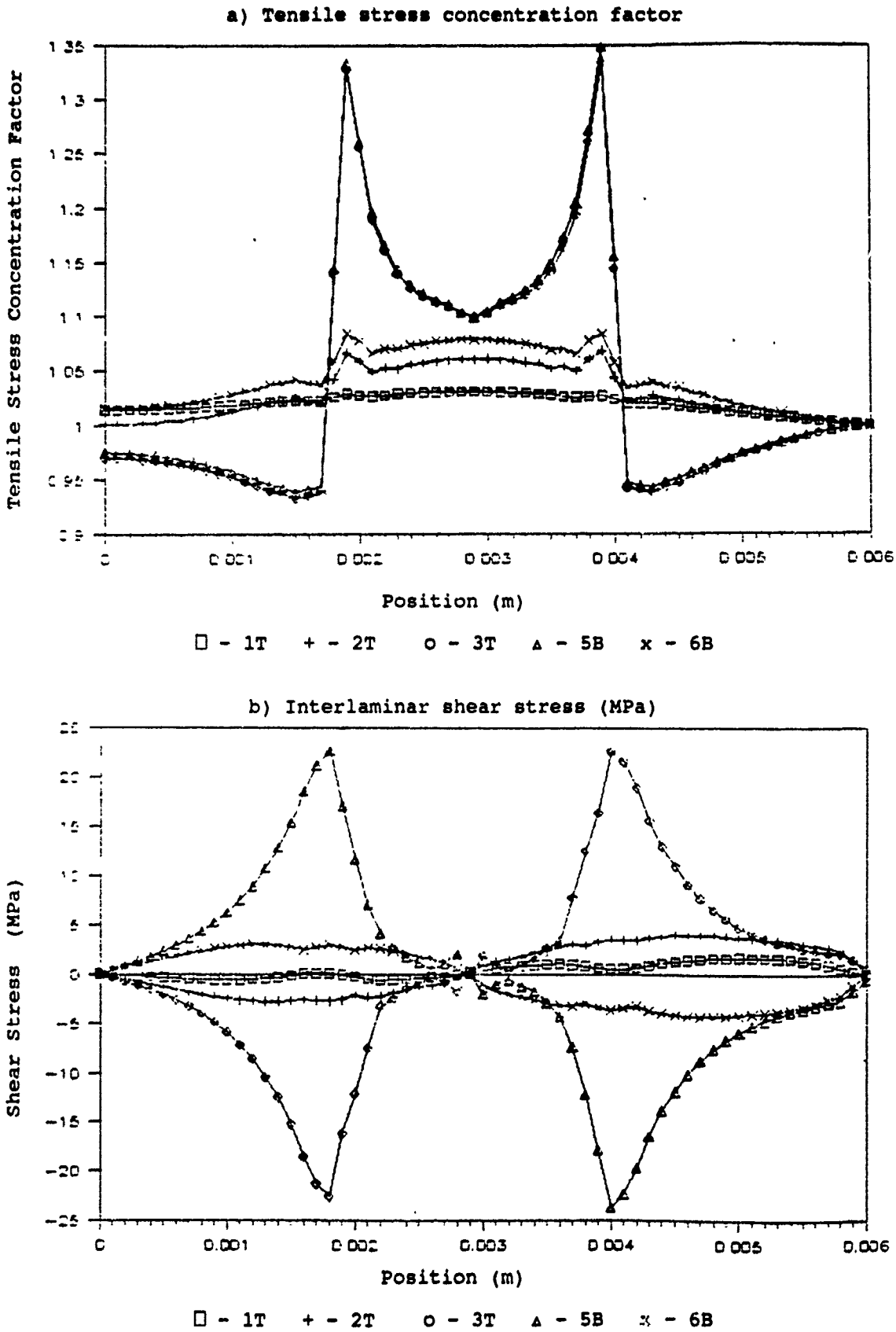

Fig. 8
Tensile and Shear Stress Distribution for Failure in Ply 4
and Delamination over 7 Elements (modulus reduction: x0.1)

a) Tensile stress concentration factor

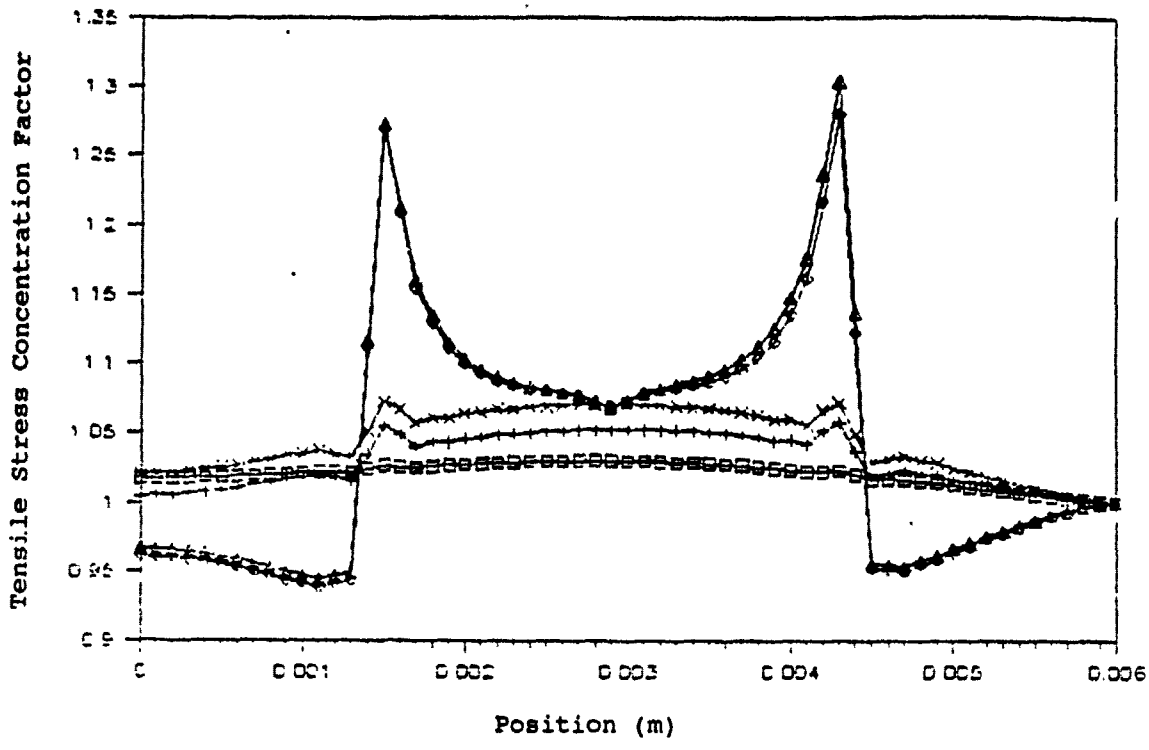

□ - 1T + - 2T o - 3T Δ - 5B x - 6B

b) Interlaminar shear stress (MPa)

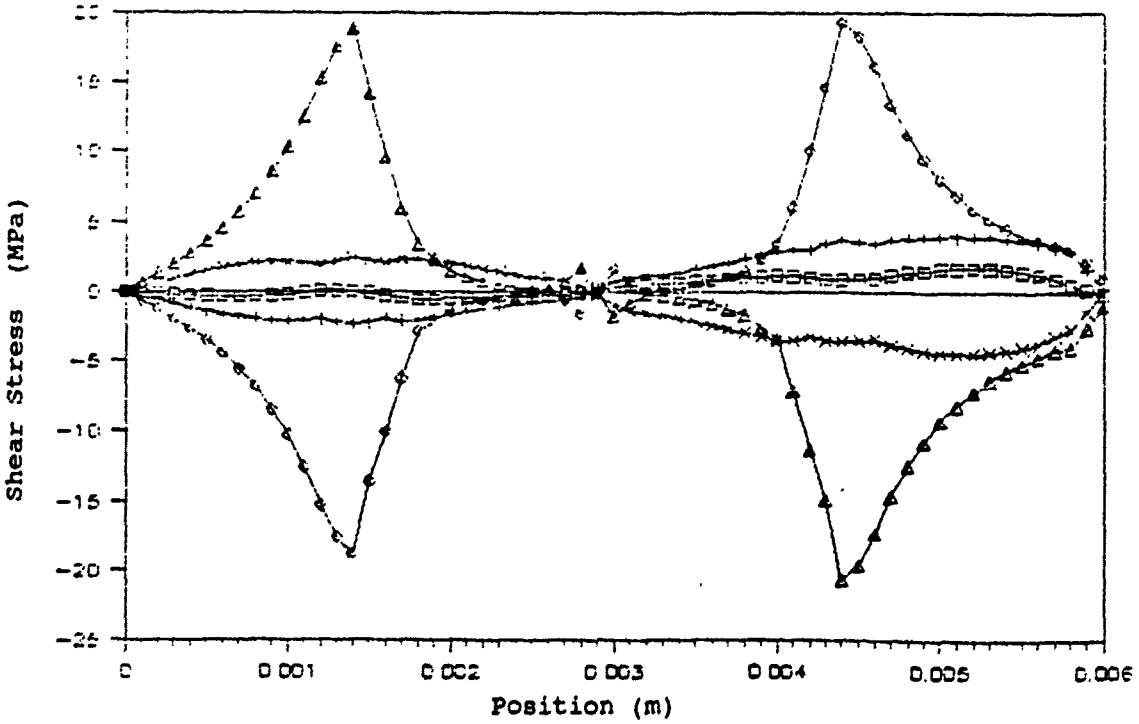

□ - 1T + - 2T o - 3T Δ - 5B x - 6B

Fig. 9
Tensile and Shear Stress Distribution for Failure in Ply 4
and Delamination over 2 Elements (modulus reduction: x0.01)

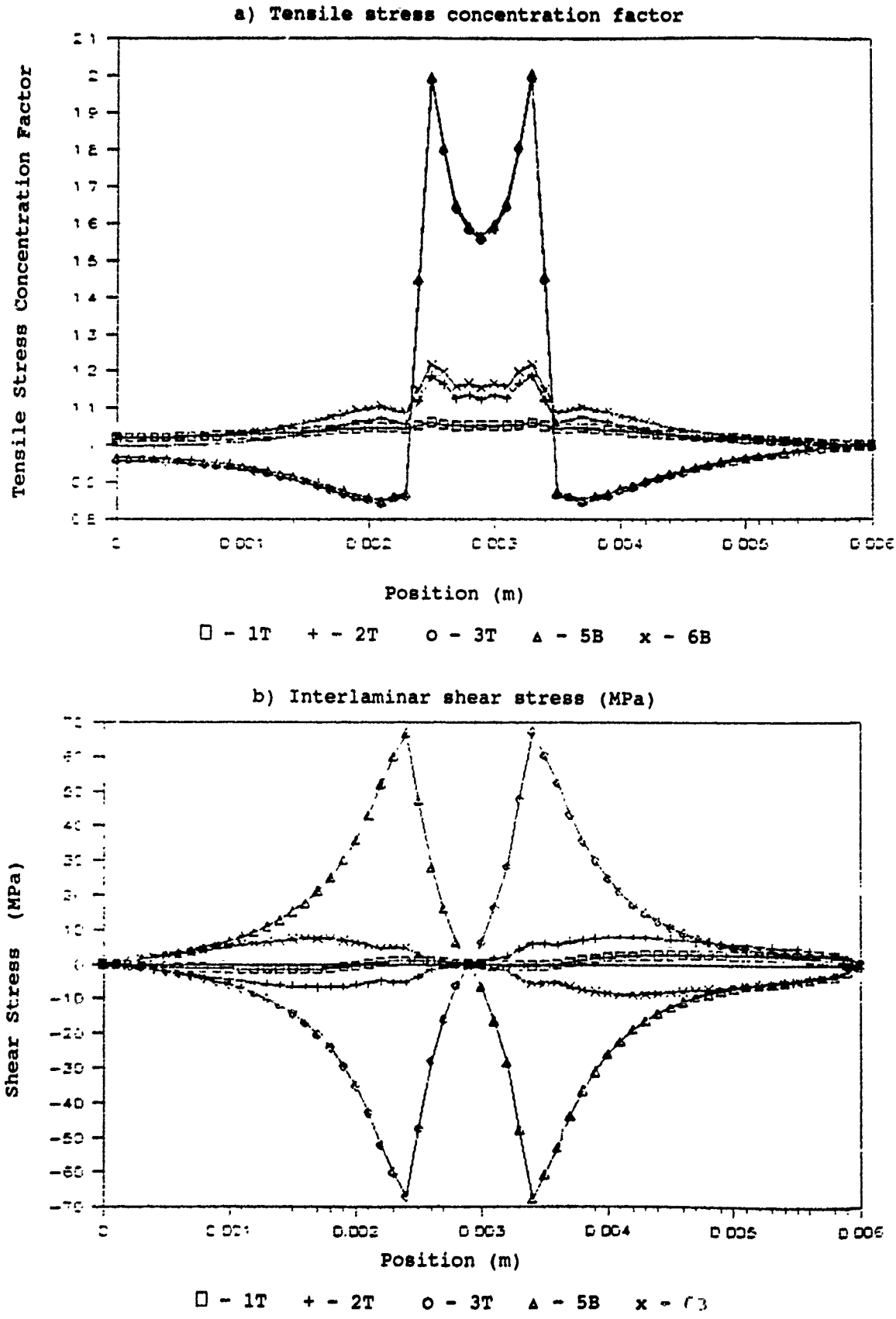

Fig. 10
Tensile and Shear Stress Distribution for Failure in Ply 4
and Delamination over 5 Elements (modulus reduction: x0.01)

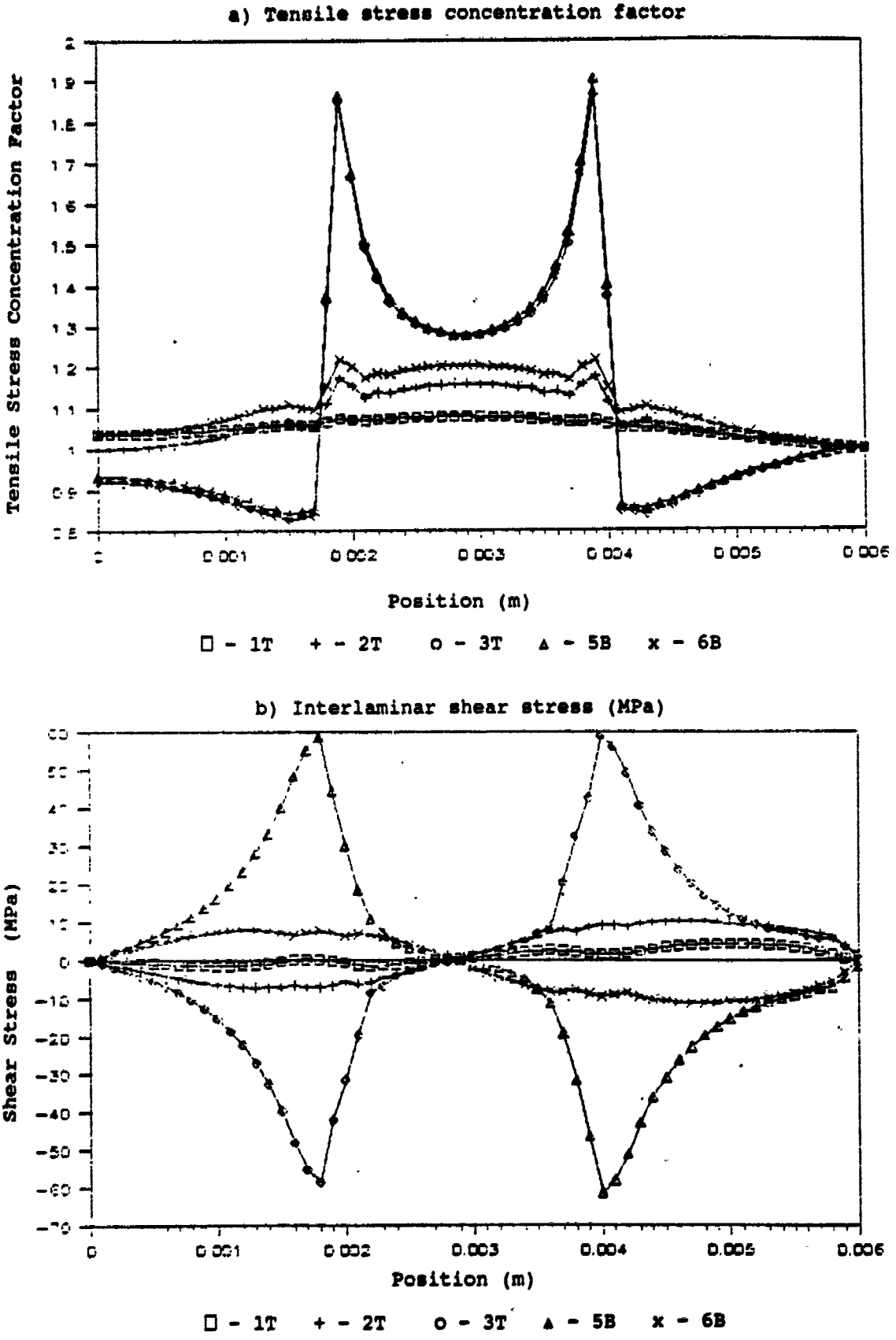

Fig. 11
Tensile and Shear Stress Distribution for Failure in Ply 4
and Delamination over 7 Elements (modulus reduction: x0.01)

a) Tensile stress concentration factor

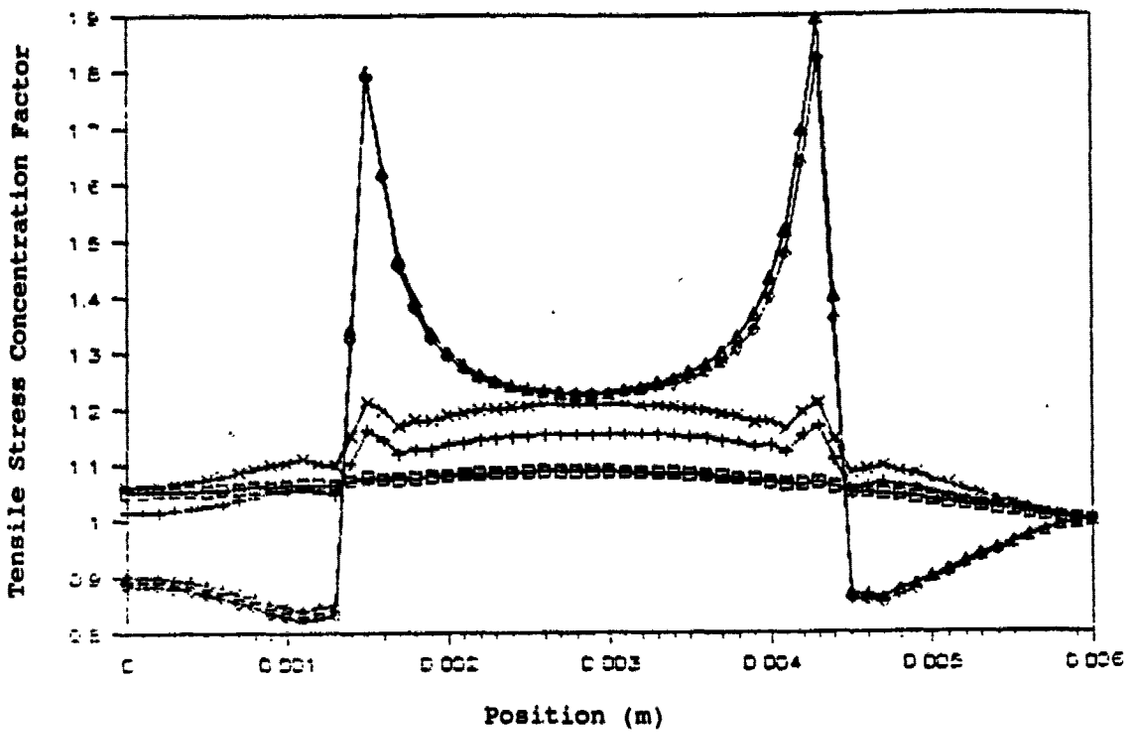

b) Interlaminar shear stress (MPa)

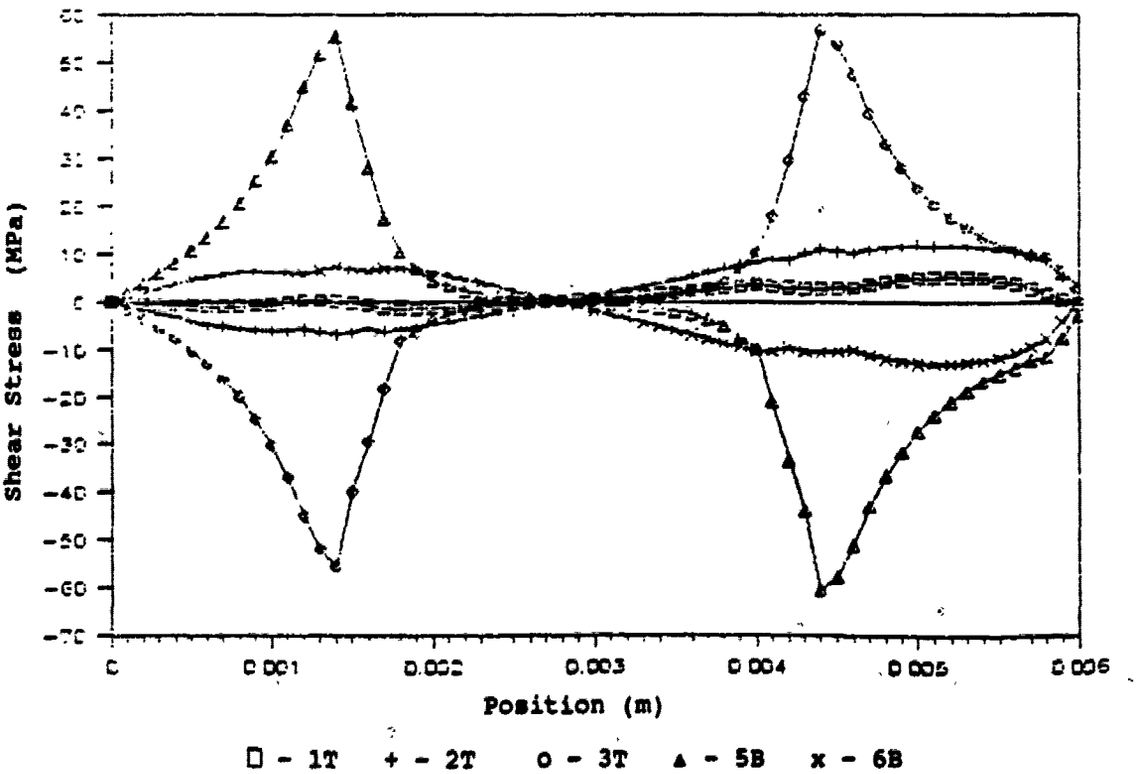

Fig. 12
Tensile and Shear Stress Distribution for Failure in Ply 4
and Delamination over 2 Elements (modulus reduction: x0.001)

a) Tensile stress concentration factor

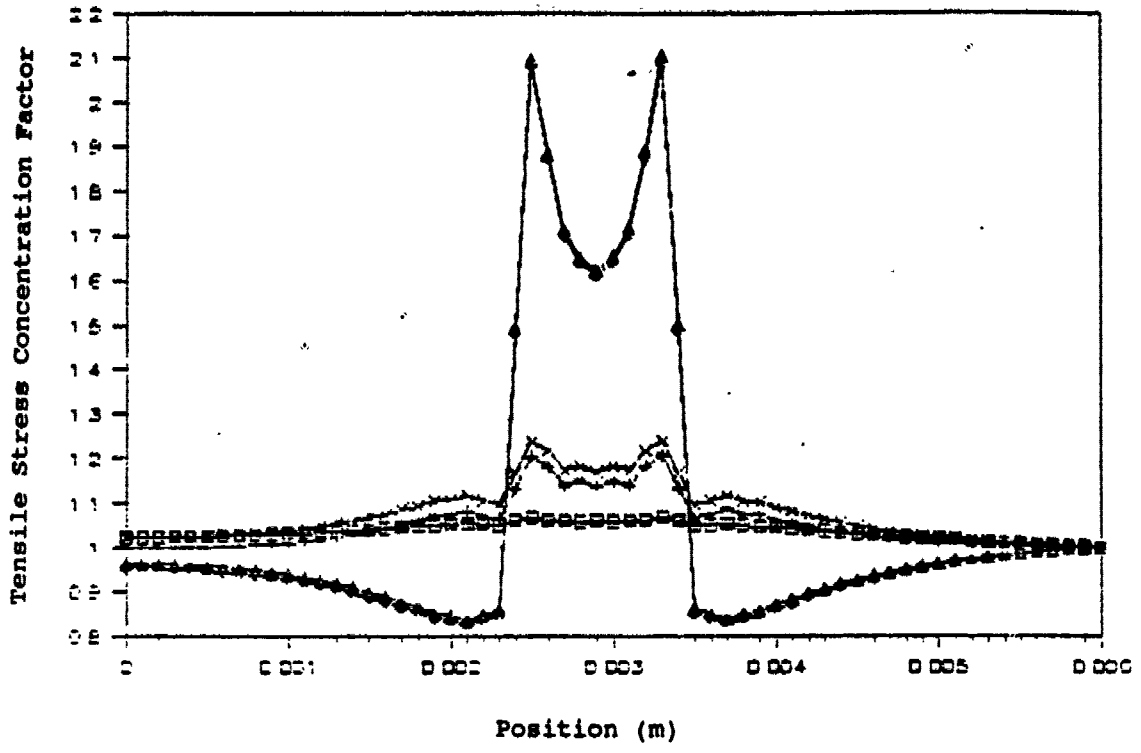

b) Interlaminar shear stress (MPa)

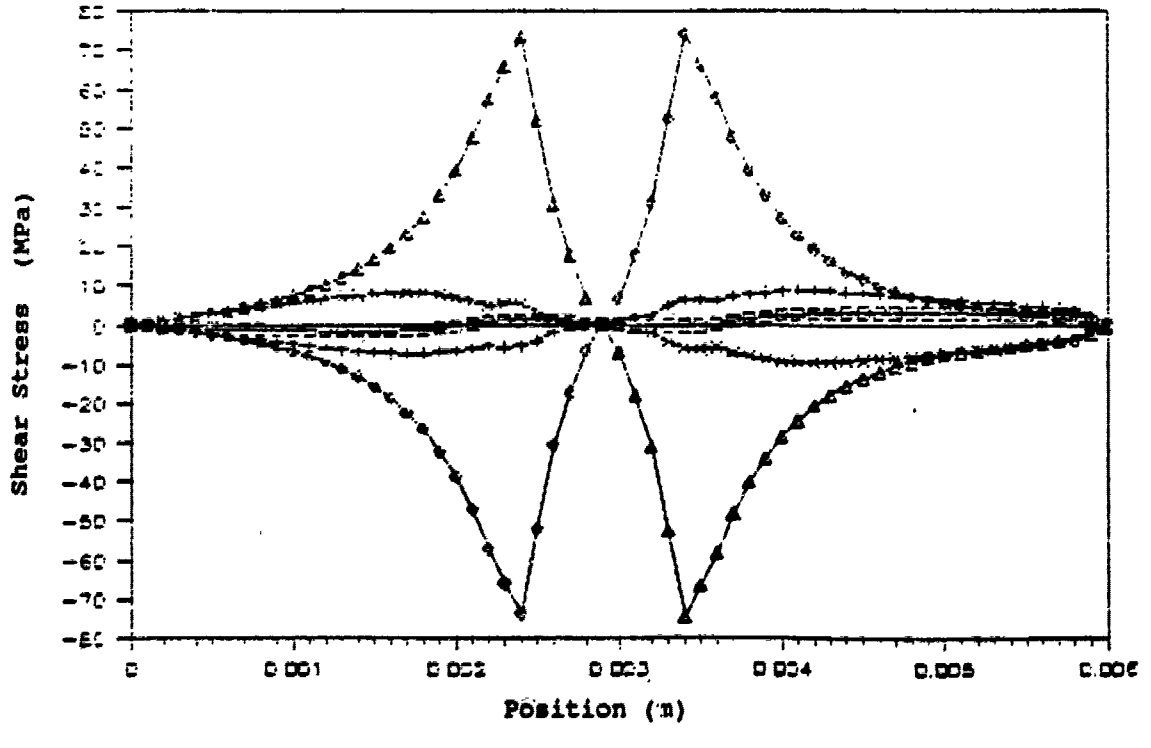

Fig. 13
Tensile and Shear Stress Distribution for Failure in Ply 4
and Delamination over 5 Elements (modulus reduction: x0.001)

a) Tensile stress concentration factor

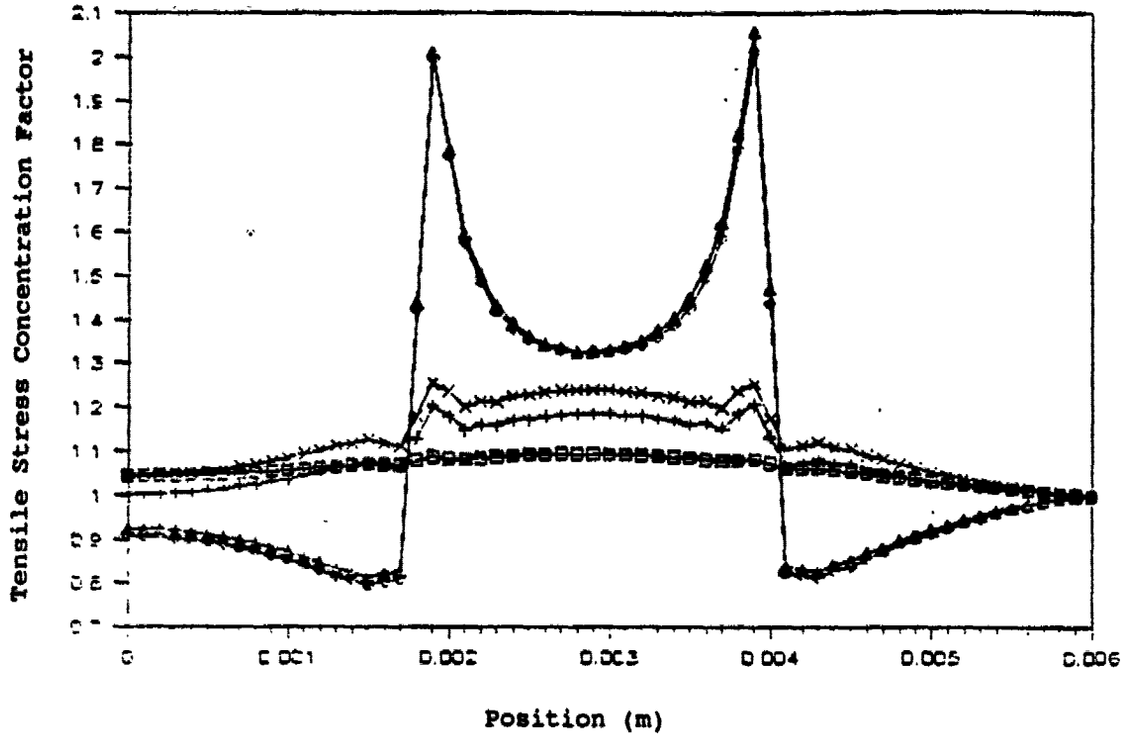

b) Interlaminar shear stress (MPa)

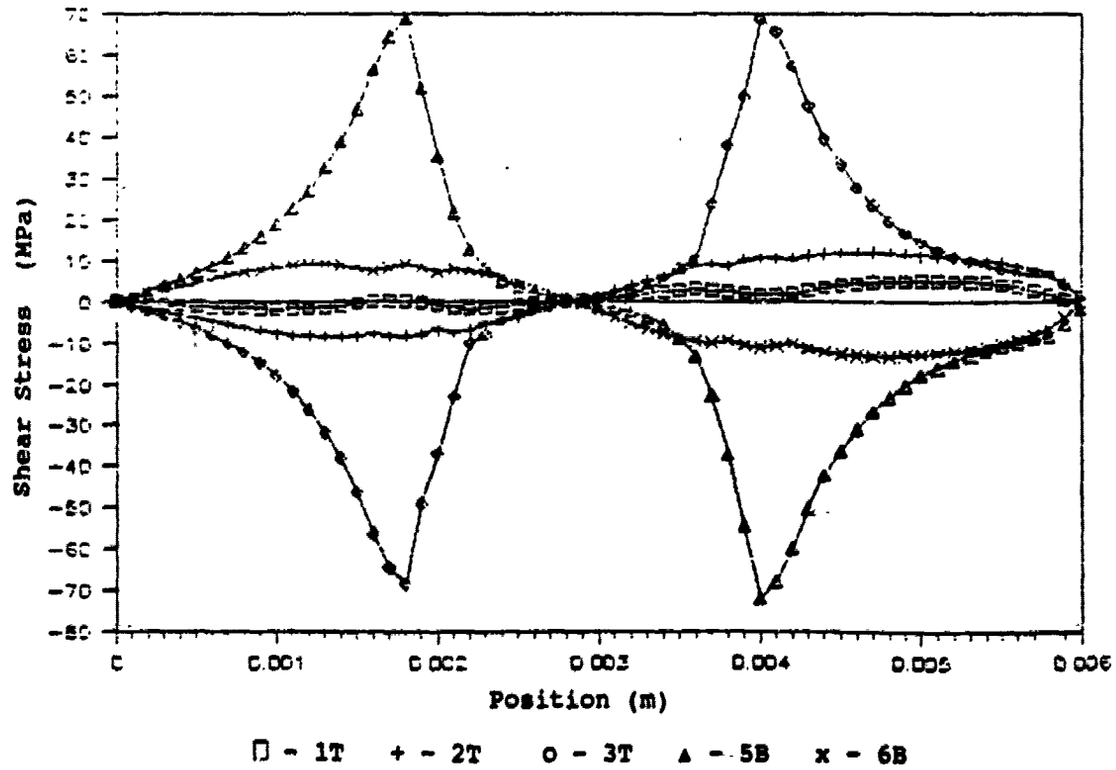

Fig. 14
Tensile and Shear Stress Distribution for Failure in Ply 4
and Delamination over 7 Elements (modulus reduction: x0.001)

a) Tensile stress concentration factor

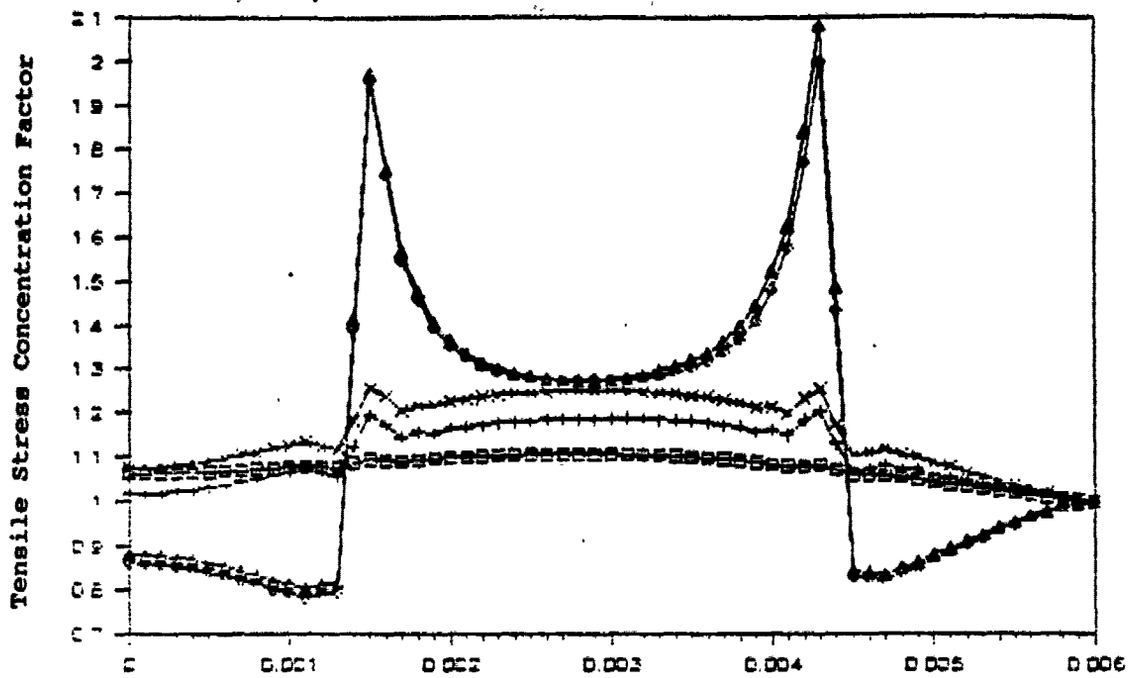

b) Interlaminar shear stress (MPa)

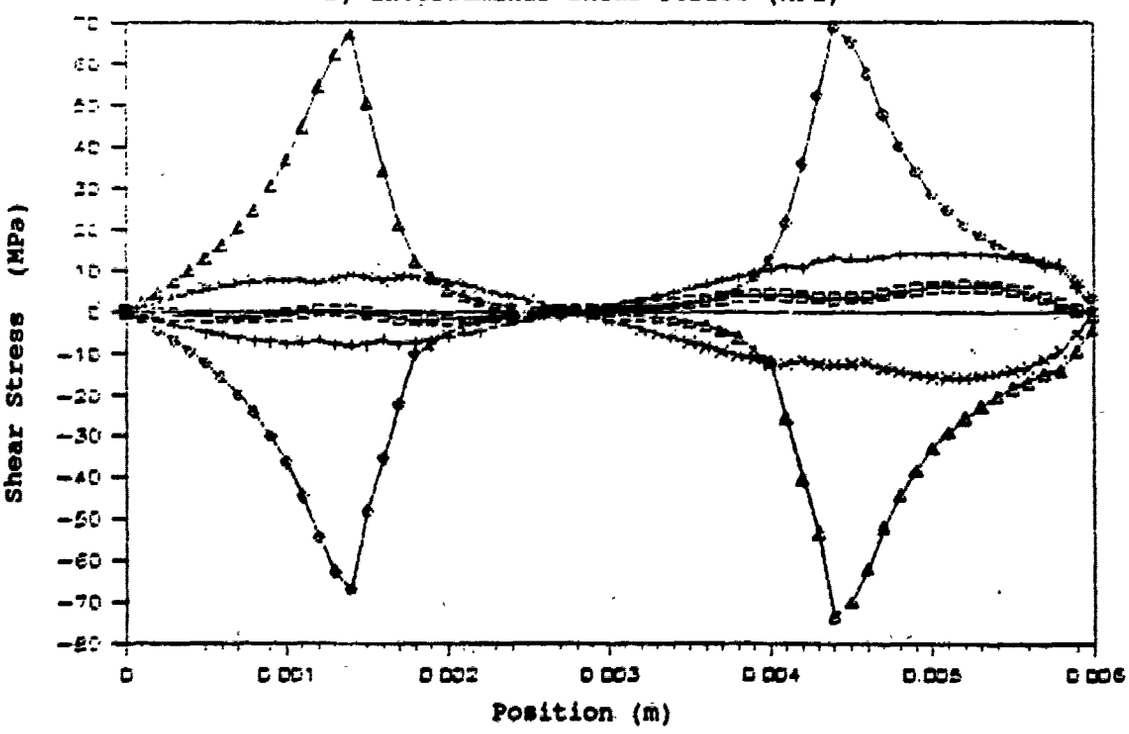

Fig. 15
Tensile and Shear Stress Distribution for Failure in Plies 3 and 4 (modulus reduction: x0.1)

a) Tensile stress concentration factor

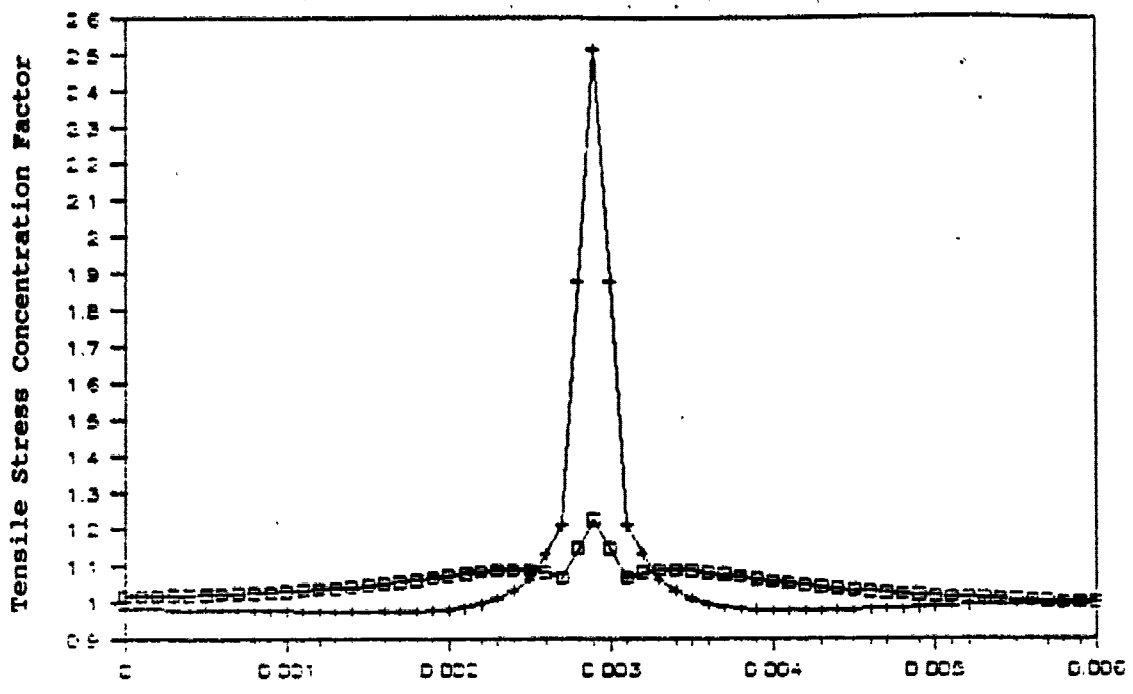

b) Interlaminar shear stress (MPa)

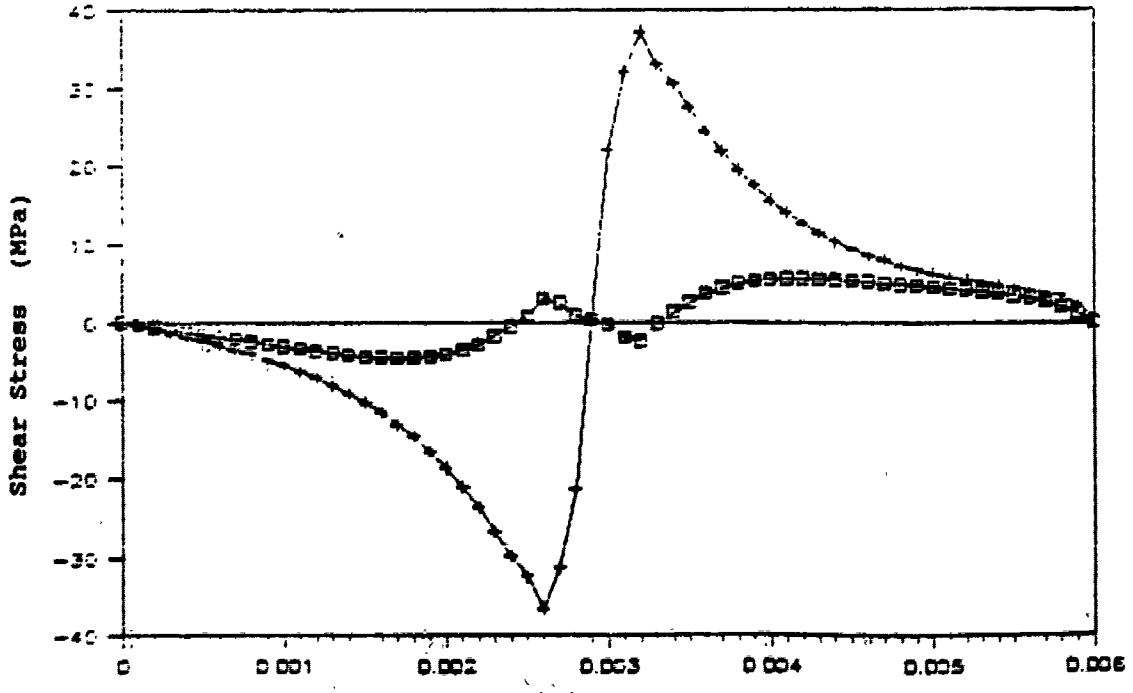

Fig. 16
Tensile and Shear Stress Distribution for Failure in Plies 3 and 4 (modulus reduction: x0.01)

a) Tensile stress concentration factor

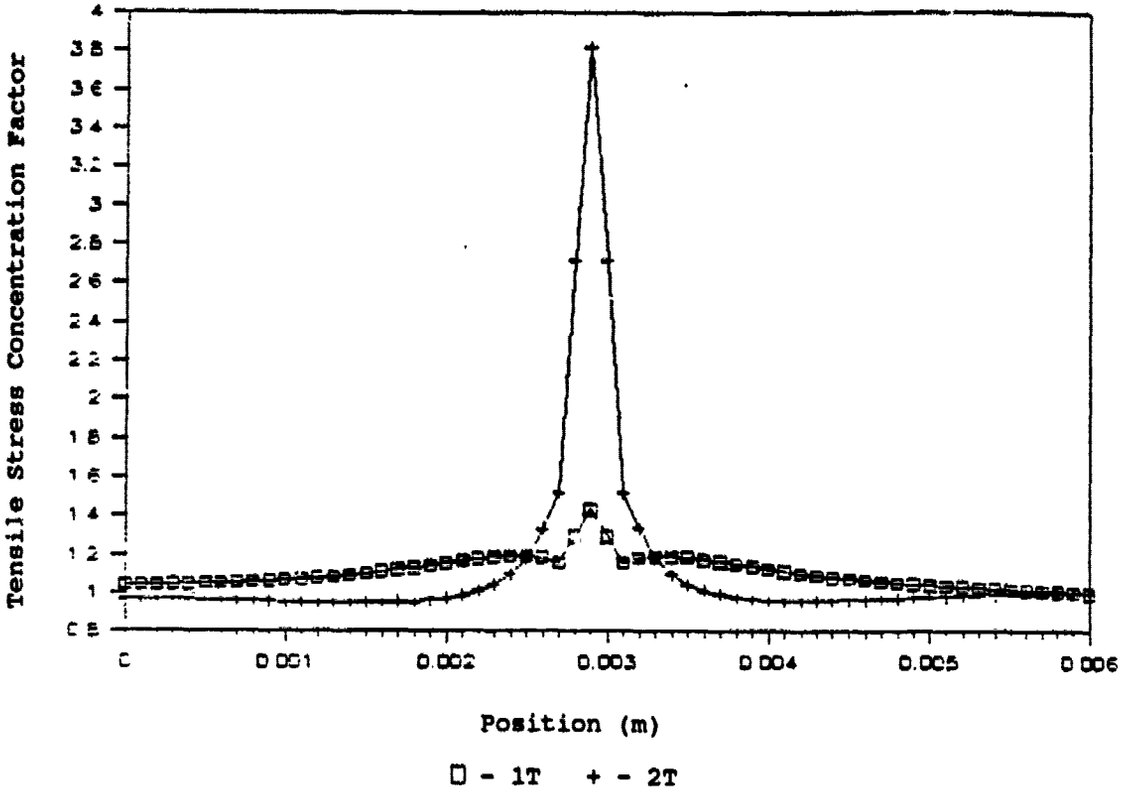

b) Interlaminar shear stress (MPa)

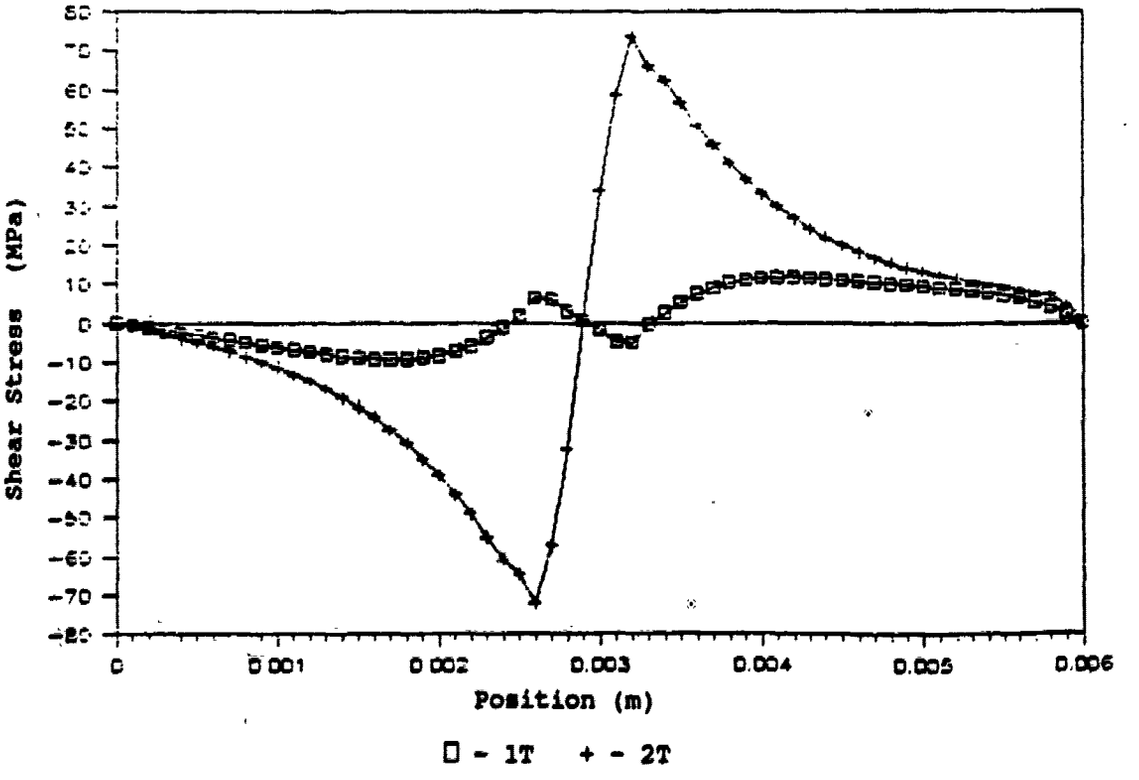

Fig. 17
Tensile and Shear Stress Distribution for Failure in Plies 3 and 4 (modulus reduction: x0.001)

a) Tensile stress concentration factor

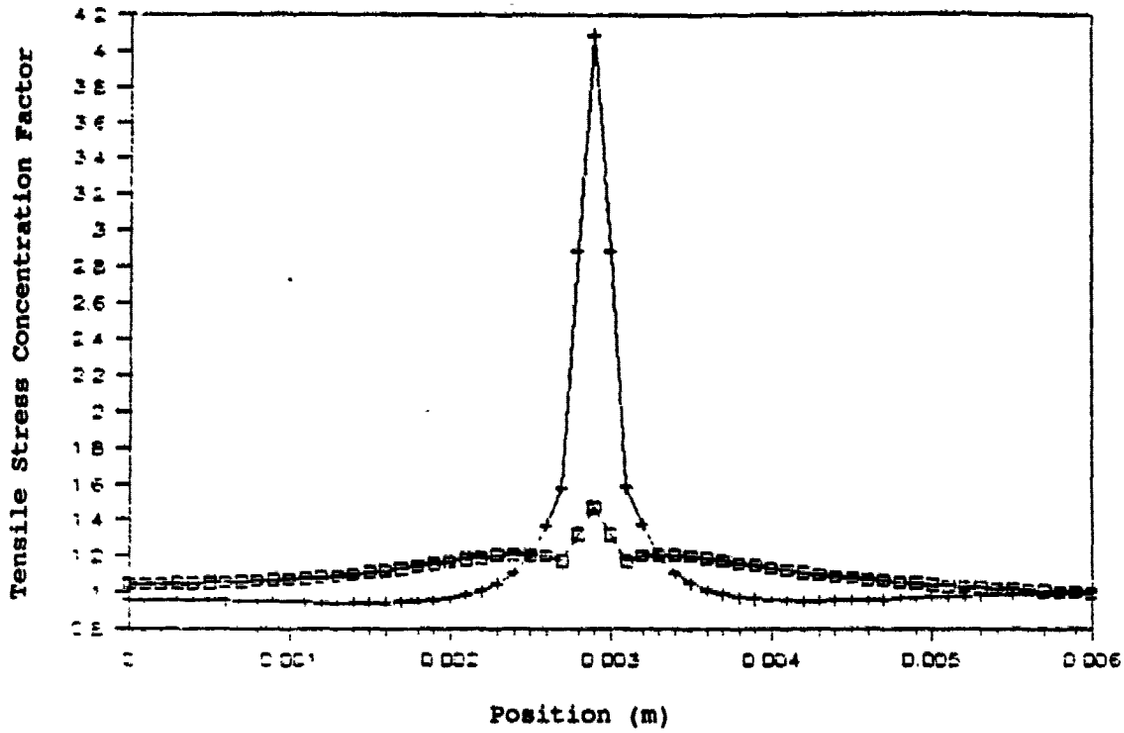

b) Interlaminar shear stress (MPa)

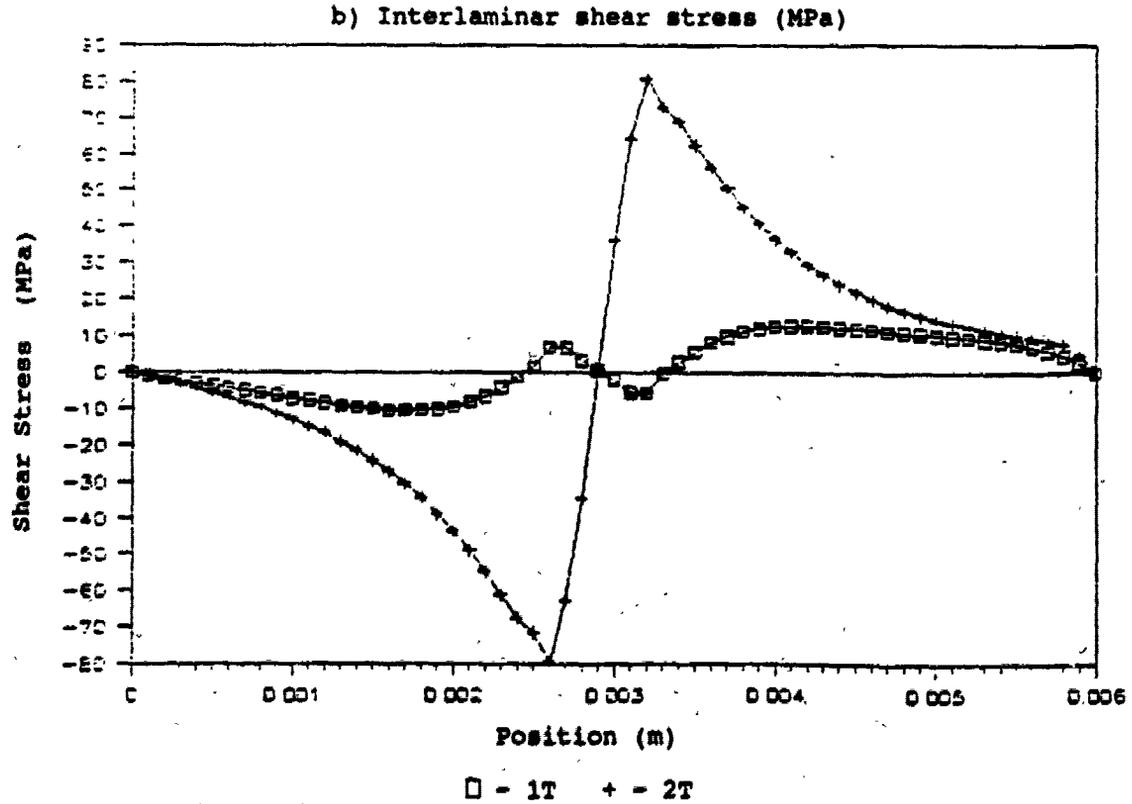

Fig. 18
Tensile and Shear Stress Distribution for Failure in Plies 4 and 5 (modulus reduction: x0.1)

a) Tensile stress concentration factor

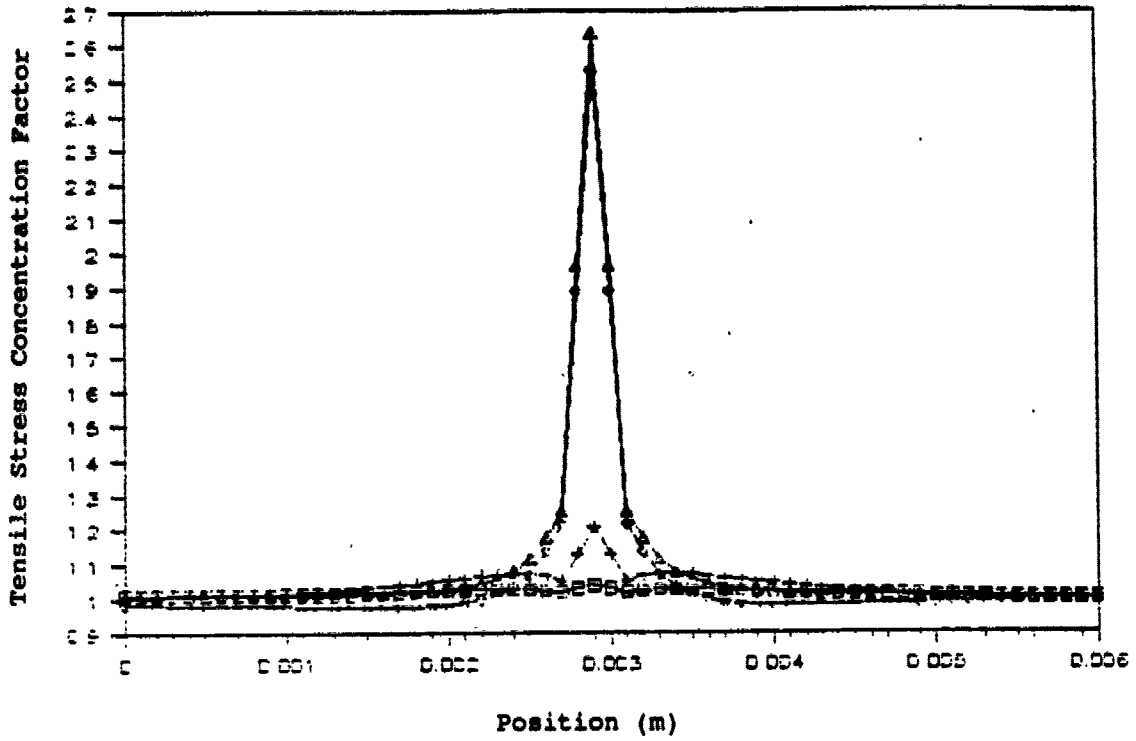

b) Interlaminar shear stress (MPa)

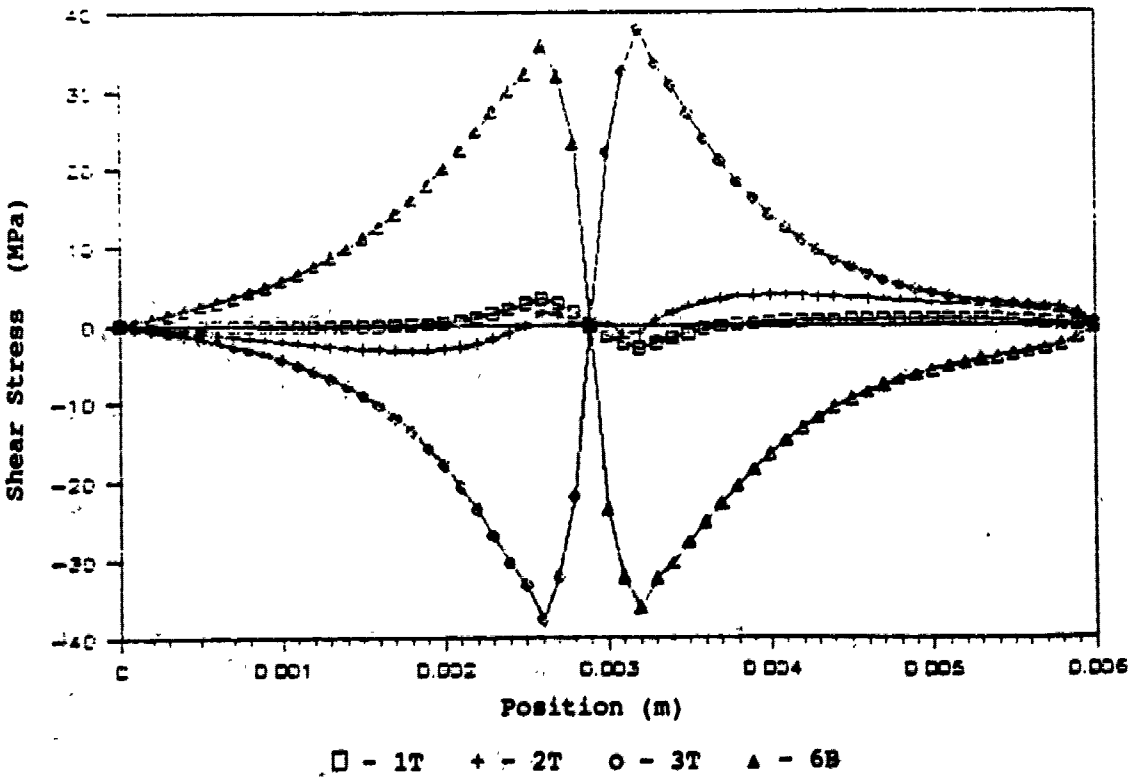

Fig. 19
Tensile and Shear Stress Distribution for Failure in Plies 4 and 5 (modulus reduction: x0.01)

a) Tensile stress concentration factor

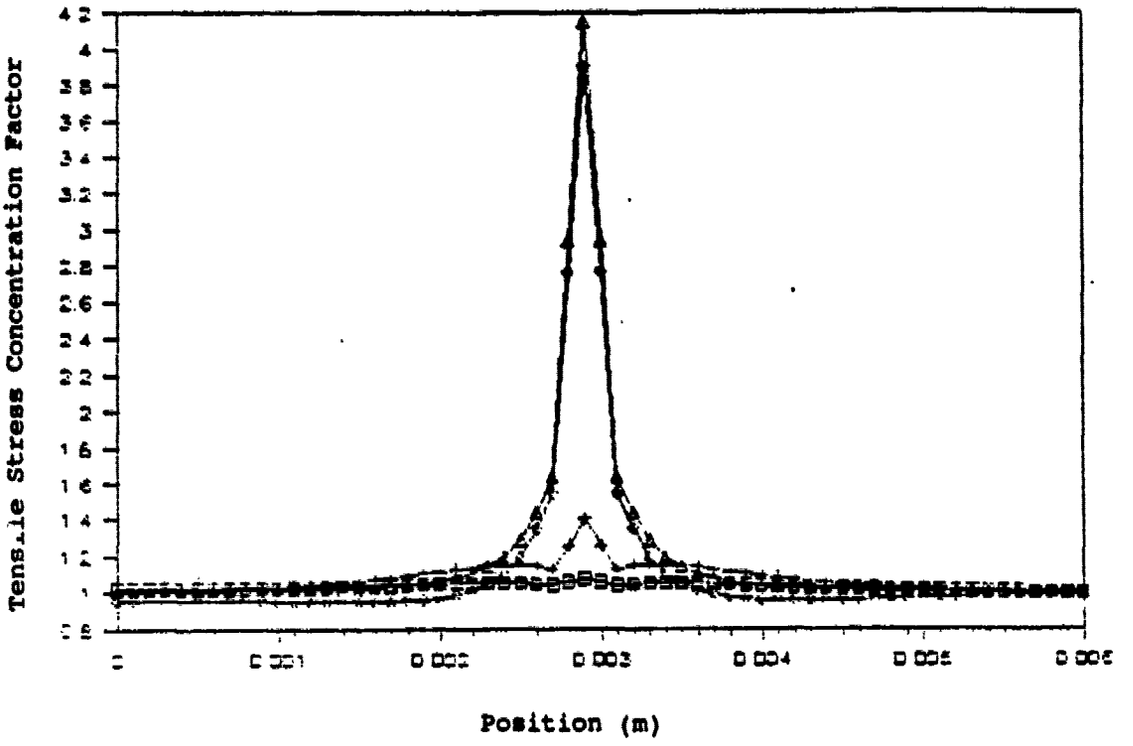

b) Interlaminar shear stress (MPa)

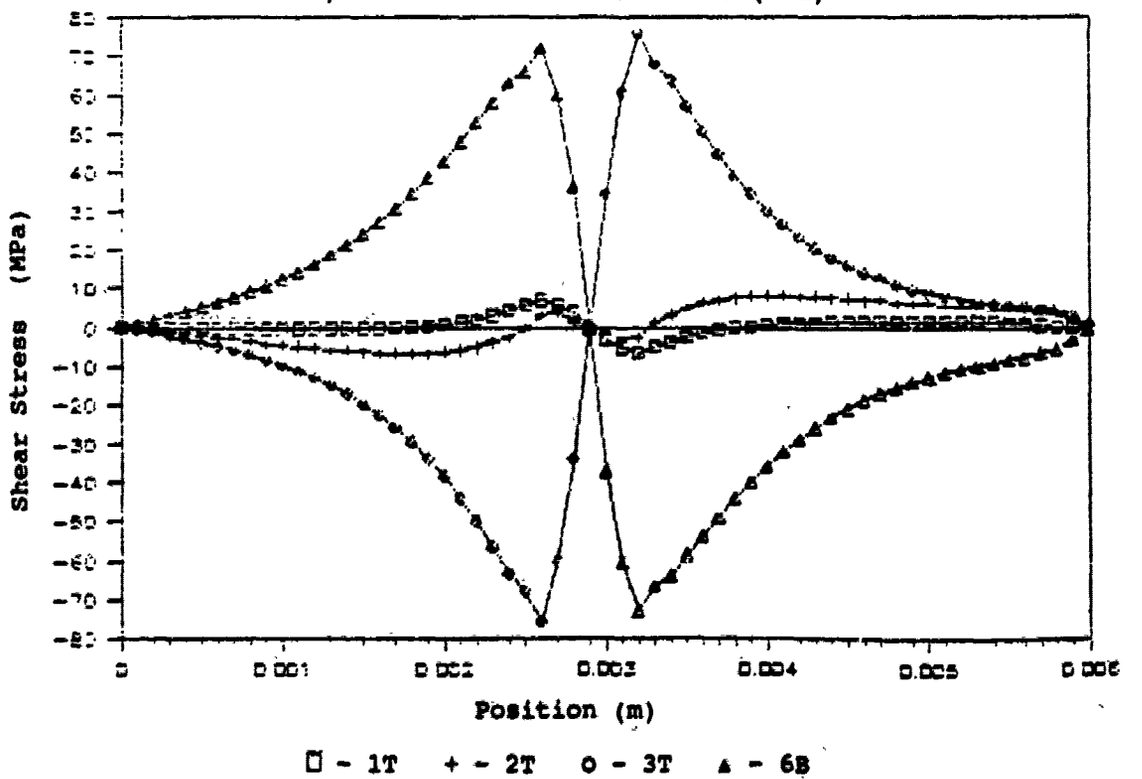

Fig. 20
Tensile and Shear Stress Distribution for Failure
in Plies 4 and 5 (modulus reduction: x0.001)

a) Tensile stress concentration factor

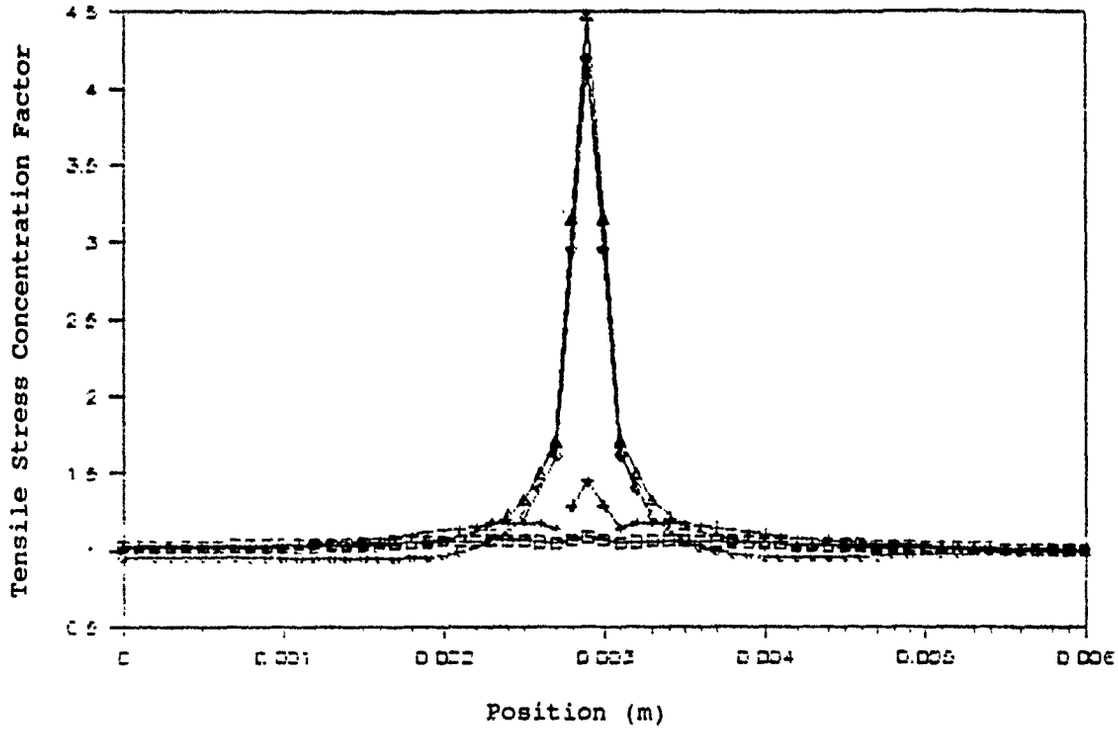

b) Interlaminar shear stress (MPa)

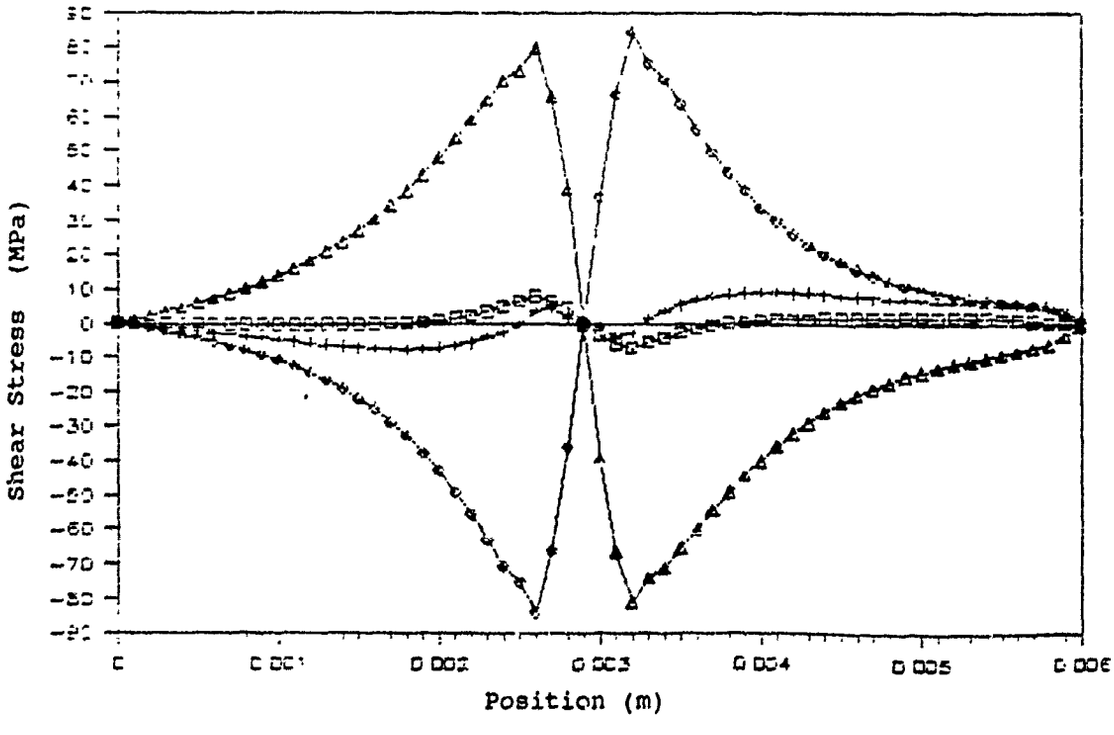

Fig. 21
Tensile and Shear Stress Distribution for Failure in Plies 3, 4 and 5 (modulus reduction: x0.1)

a) Tensile stress concentration factor

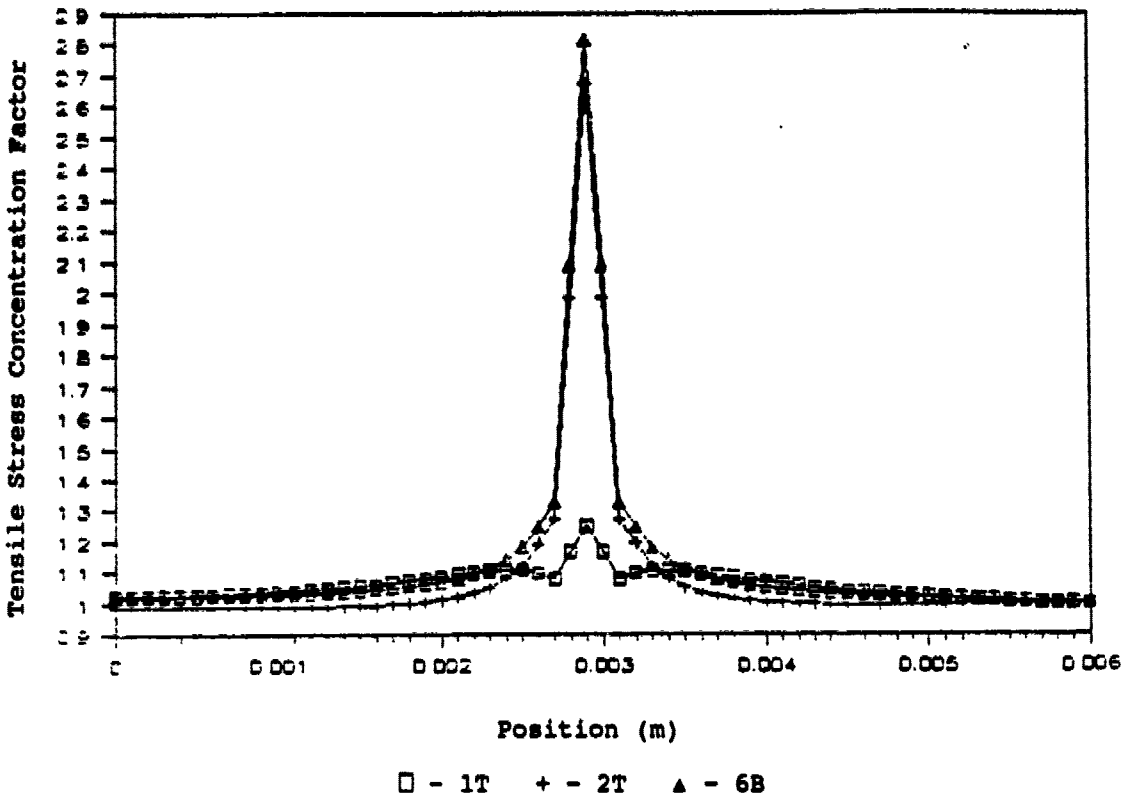

b) Interlaminar shear stress (MPa)

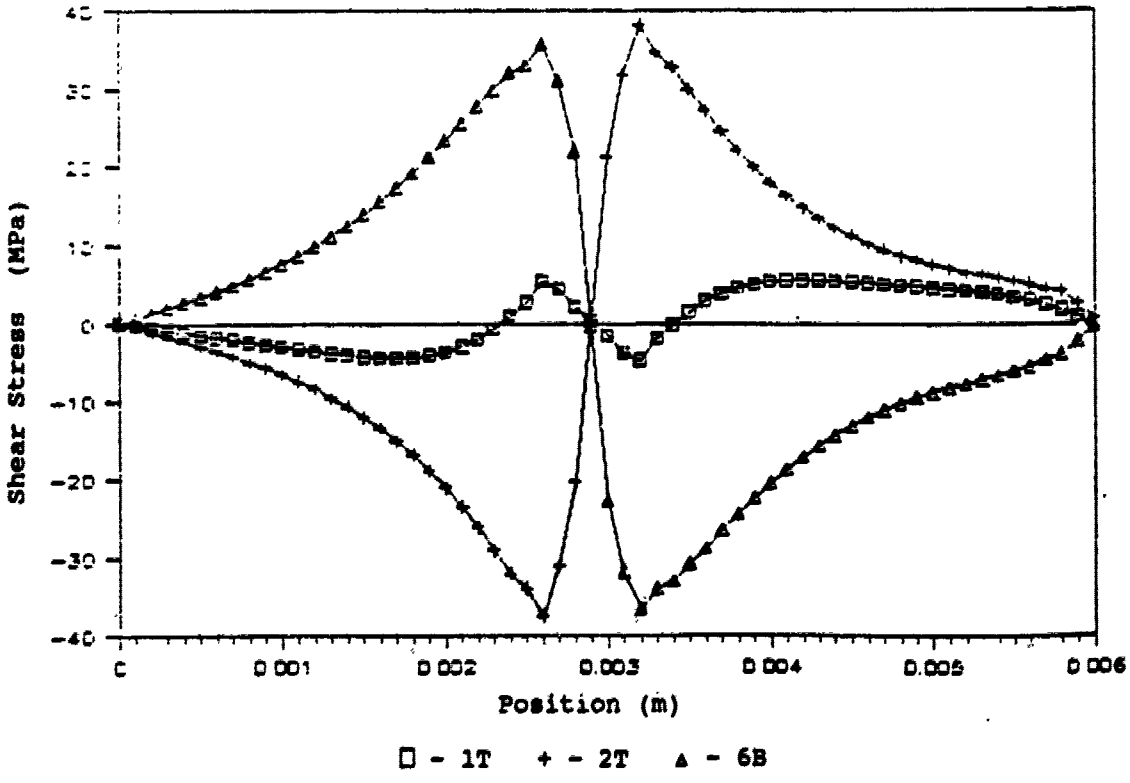

Fig. 22
Tensile and Shear Stress Distribution for Failure in Plies 3, 4 and 5 (modulus reduction: x0.01)

a) Tensile stress concentration factor

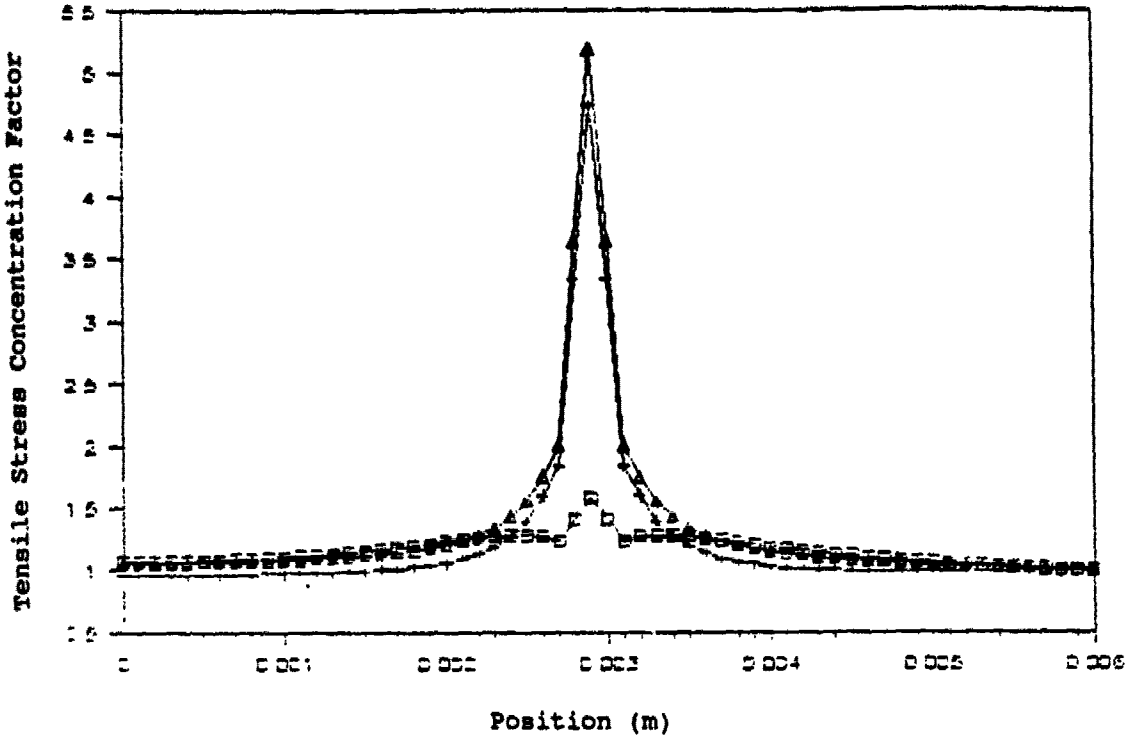

□ - 1T + - 2T ▲ - 6B

b) Interlaminar shear stress (MPa)

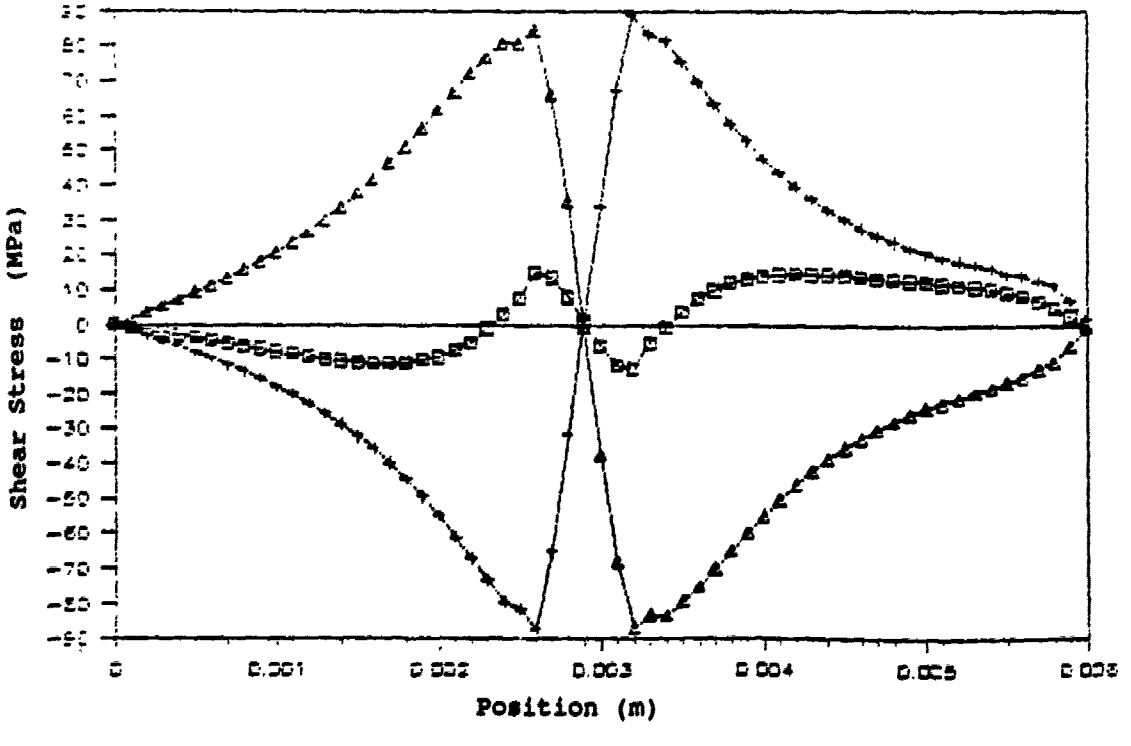

□ - 1T + - 2T ▲ - 6B

Fig. 23
Tensile and Shear Stress Distribution for Failure in Plies 3, 4 and 5 (modulus reduction: x0.001)

a) Tensile stress concentration factor

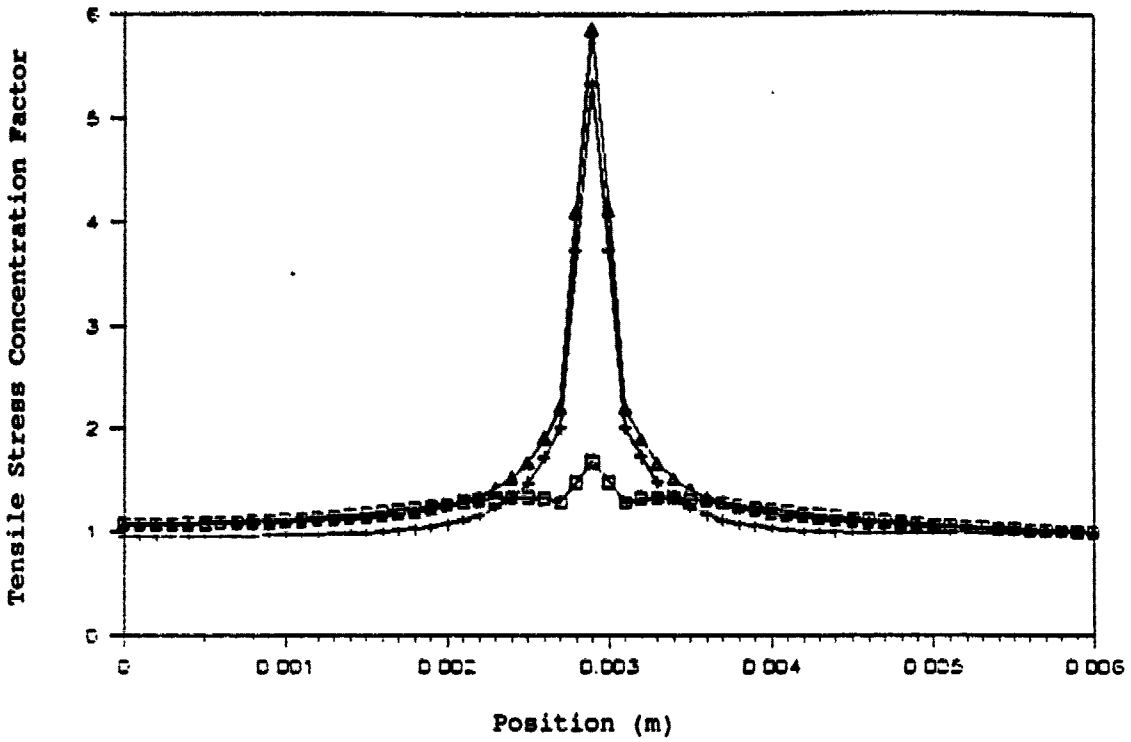

b) Interlaminar shear stress (MPa)

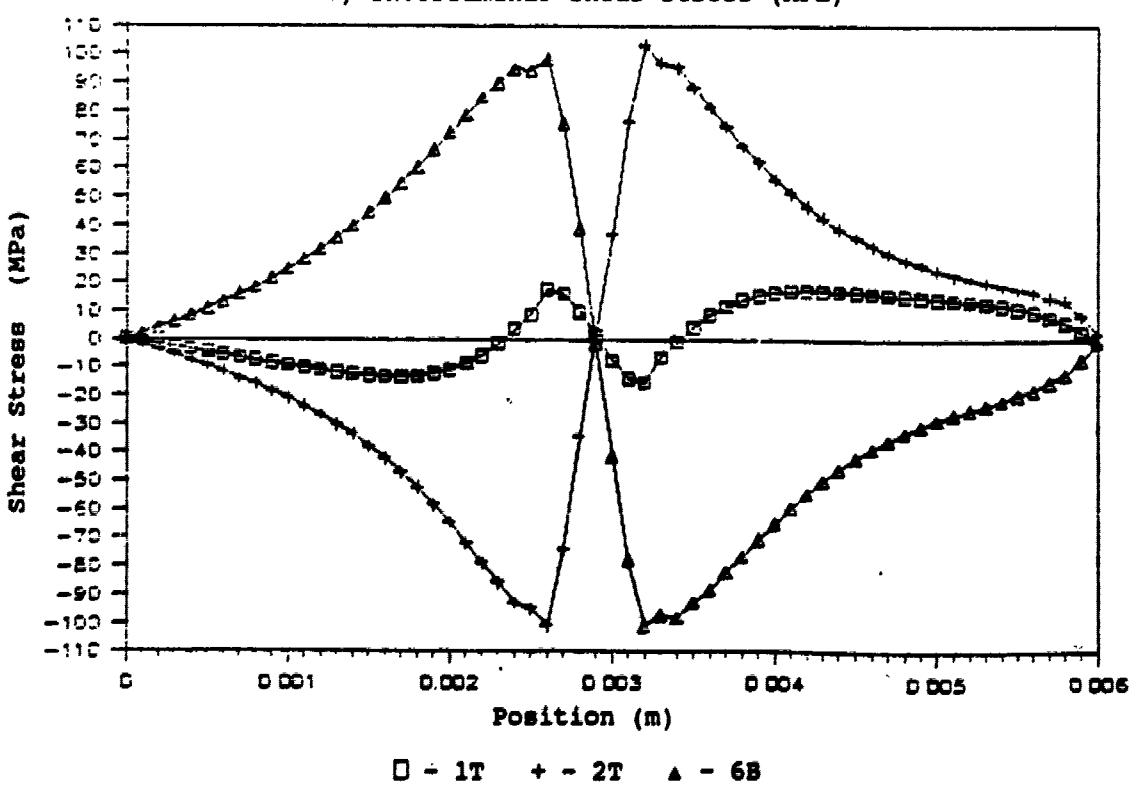

Fig. 24
Tensile and Shear Stress Distribution for Failure in Plies 4 + 5 and Delamination over 7 Elements (modulus reduction: x0.1)

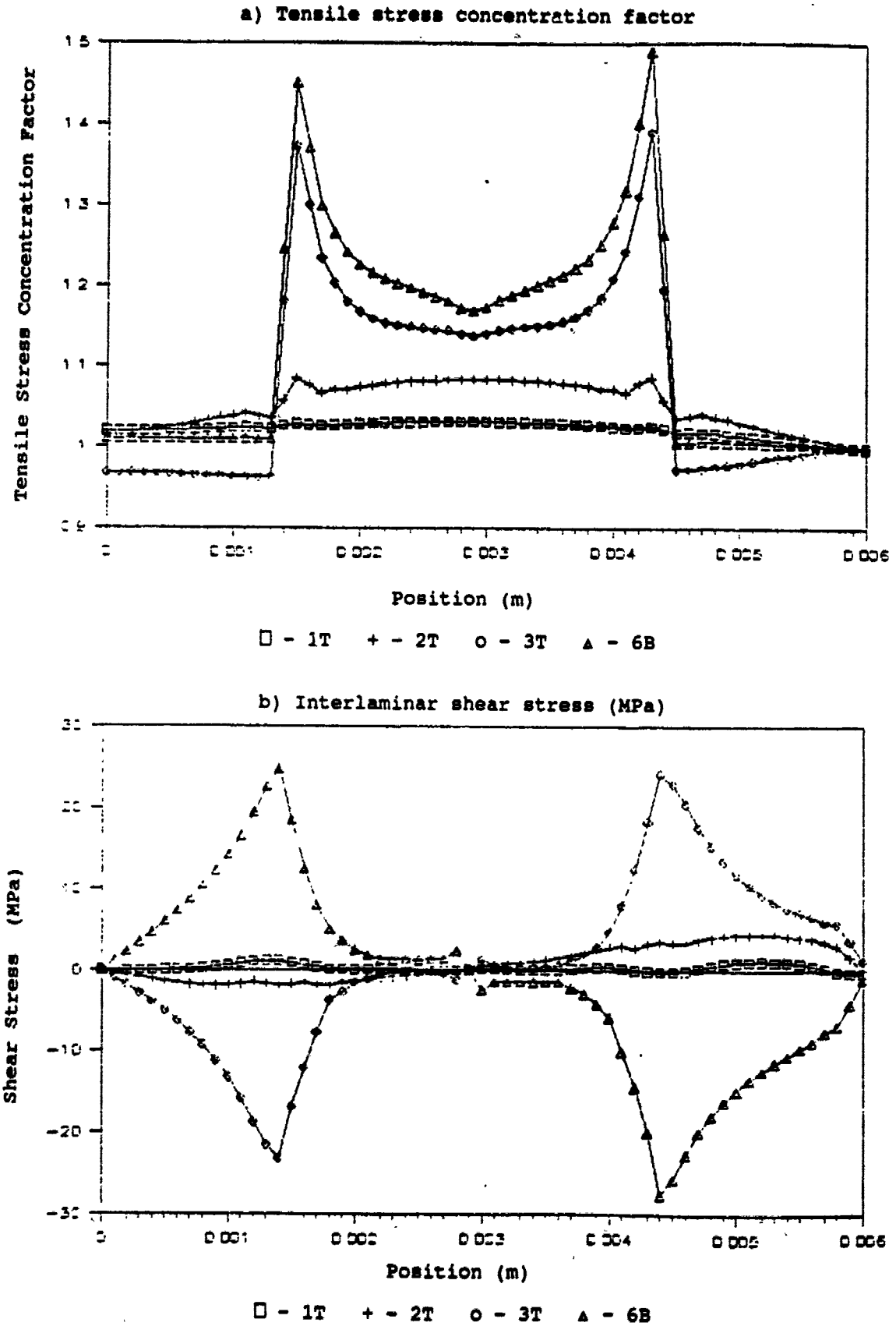

Fig. 25
Tensile and Shear Stress Distribution for Failure in Plies 4 + 5 and Delamination over 7 Elements (modulus reduction: x0.01)

a) Tensile stress concentration factor

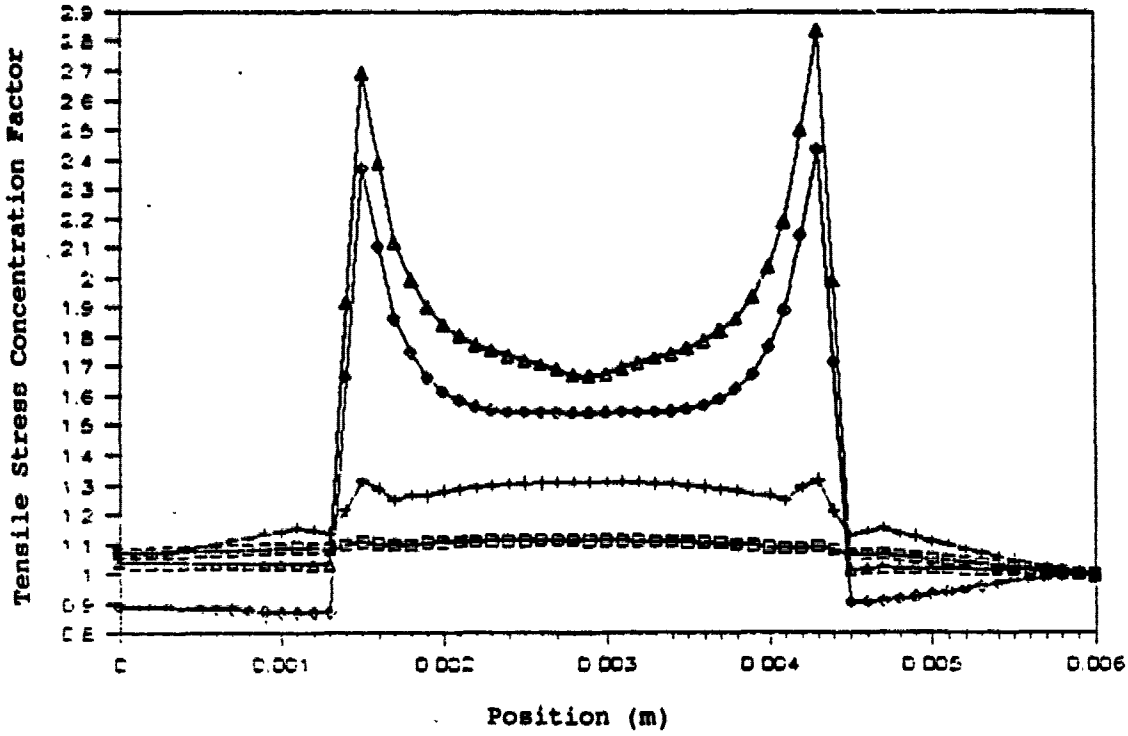

□ - 1T + - 2T o - 3T ▲ - 6B

b) Interlaminar shear stress (MPa)

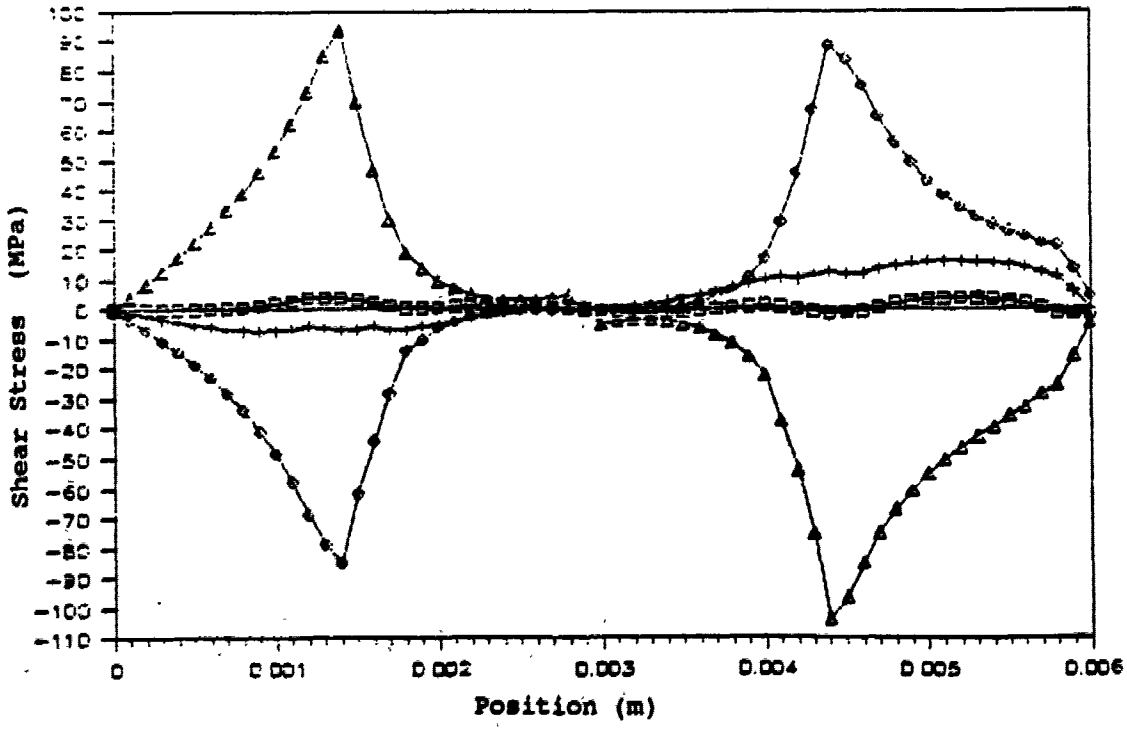

□ - 1T + - 2T o - 3T ▲ - 6B

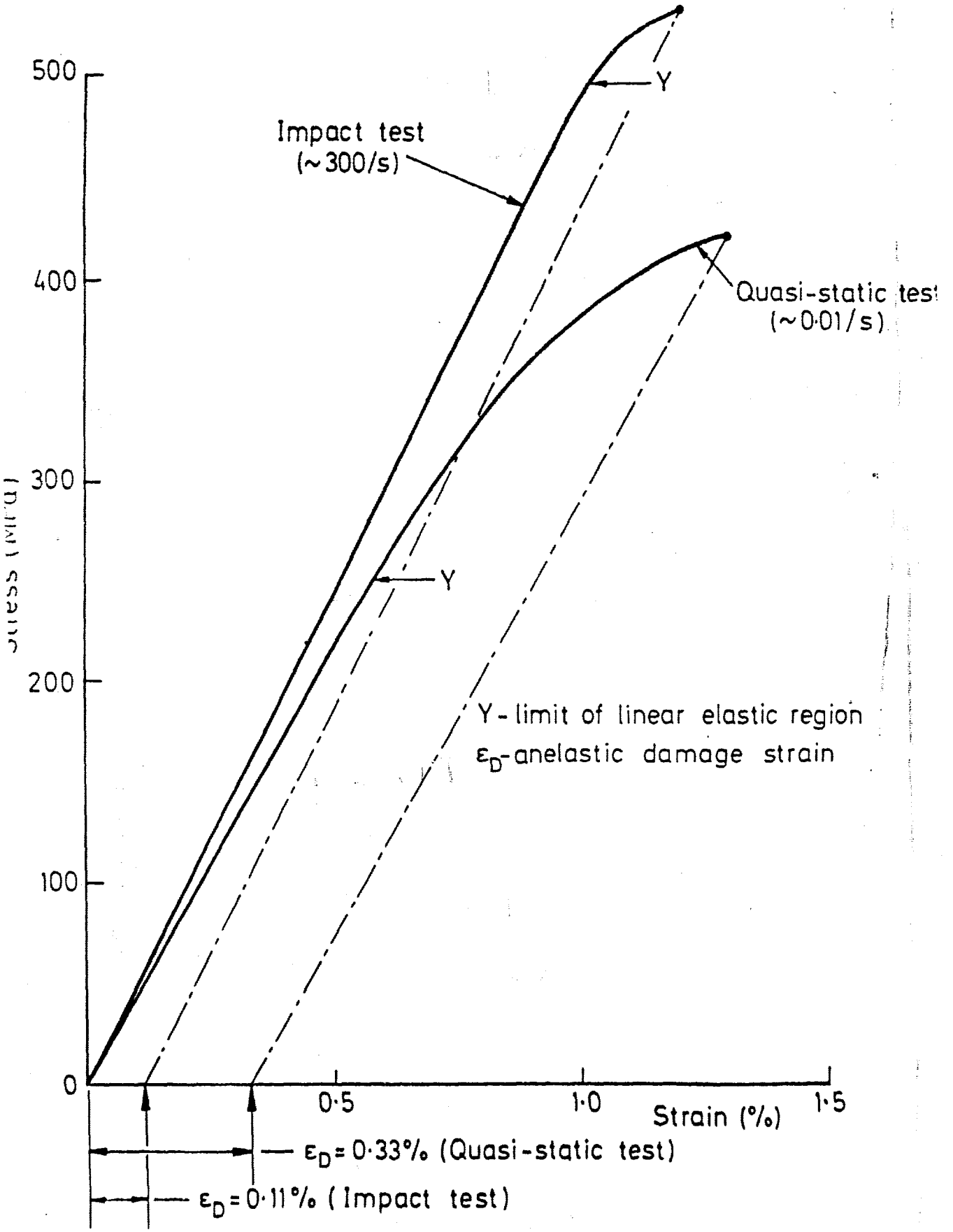

Fig. 26
Mean Experimental Stress-Strain Curves
for Woven Carbon-Reinforced Laminates

APPENDIX V

Stress Wave Propagation in Hybrid Composite Materials

Y.L.Li*, C.Ruiz and J.Harding
Department of Engineering Science
University of Oxford

Abstract

In this report, the dynamic response, in particular, the interlaminar shear stress, in three-layer symmetrical hybrid composites is studied using the shear lag model. Theoretical solutions for four different types of loading are obtained. Numerical examples are given for the step loading case and the results obtained show good agreement with those determined using the finite element method. The interlaminar shear stress is composed of static and dynamic parts and the peak interlaminar shear stress, which occurs at the loading end under the step uniform pressure loading, is dominated by the static stress and is dependent on the stiffness ratio between the centre and the outer plies. This agrees with the solution for the infinite length case, see reference[1].

1 Introduction

When a composite structure is loaded impulsively, stress waves propagate in the constituent phases. For hybrid laminates in which the modulus of each layer is different, axial stress waves propagate at different speeds in each layer, creating dynamic shear stresses at the interface. This dynamic shear stress may cause delamination. In reference[1], two semi-infinite layers with uniform cross section but different elastic properties bonded together to form a composite structure are subjected to a pressure step loading over the end. The shear stress at the interface is given in the form of a integral solution. The results show that the peak interlaminar shear stress occurs at the loading end. No reflection of the axial stress wave was considered since the only case treated was for infinitely long members.

In the present work, a composite bar consisting three plies is studied. The two outer plies have the same properties, different from those of the central ply. The

*on leave from the Northwestern Polytechnical University, Xi'an, China

analysis is based on the assumption of a shear lag model[2-7]. The fibres carry only axial normal stress and the matrix transmits only shear stress.

The equations of motion are solved by using the finite Fourier and Laplace transform techniques. The axial stresses, displacements and the shear stress at the interface are obtained in series form. They consist of static and dynamic parts under a uniform pressure step loading. The peak interlaminar shear stress occurs at the loading end and is dominated by the static part . The second largest shear stress is found in the vicinity of the slower stress wave front, in agreement with the conclusion in reference[1] for the infinitely long case. If the loading ratio at the end of each layer is equal to the stiffness ratio, i.e. there is compatibility of displacements, the maximum shear stress occurs in the same position at which the second peak value occurs under the uniform pressure and is dominated by the dynamic part. The static part is equal to zero at all times. The numerical results agree with the results of the finite element code of ABAQUS .

2 Mathematical formulation

2.1 Analytical model

The analytical model is shown in Fig. 1(a). It consists of three fibre reinforced layers which are bonded together to form the symmetric composite structure. The two outer layers have the same properties and are different from the middle layer. The structure is excited by the dynamic loading $P_1\psi(t)$ over the end of the two outside layers and $P_2\psi(t)$ over the end of the middle layer, thus producing an axial elastic wave in each layer.

It is assumed that stress and strain are uniform over the cross section of each layer and act solely in the axial direction. Transverse displacements (from Poisson's effect) and bending are neglected. The analysis is simplified further by neglecting the bond inertia and assuming that the interlaminar shear stress is, therefore, proportional to the difference between the displacements of the two adjacent layers. Since only axial displacements are involved, plane sections remain plane in each individual layer. However, plane sections do not remain plane in the composite structure as a whole since relative displacements are allowed between the two layers across the bond region.

2.2 Equation of motion

An element of the composite structure is shown in Fig. 1(b). Each layer has a Young's modulus E_i, mass density ρ_i, cross sectional area A_i, displacement $u_i(x,t)$ and tensile stress σ_i. Subscripts 1 and 2 are used to identify the outside and middle layers respectively. The bond has a thickness h_m, width b and shear modulus G.

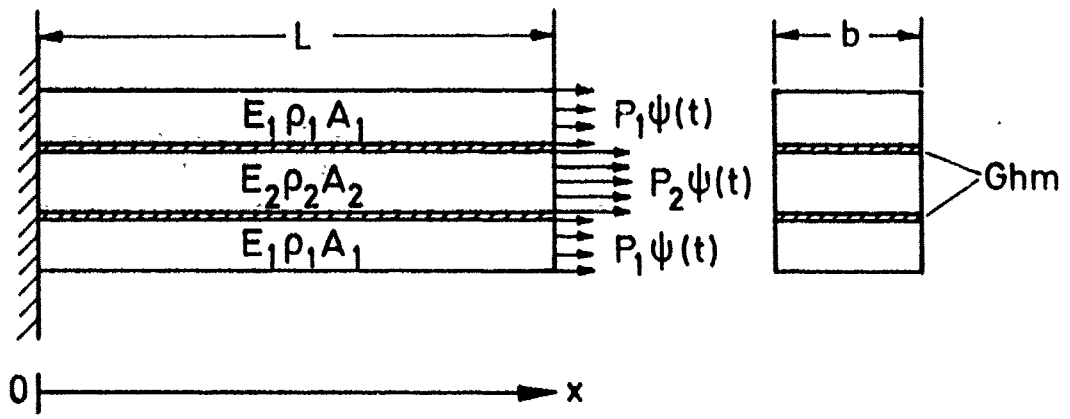

(a) Geometry of the model

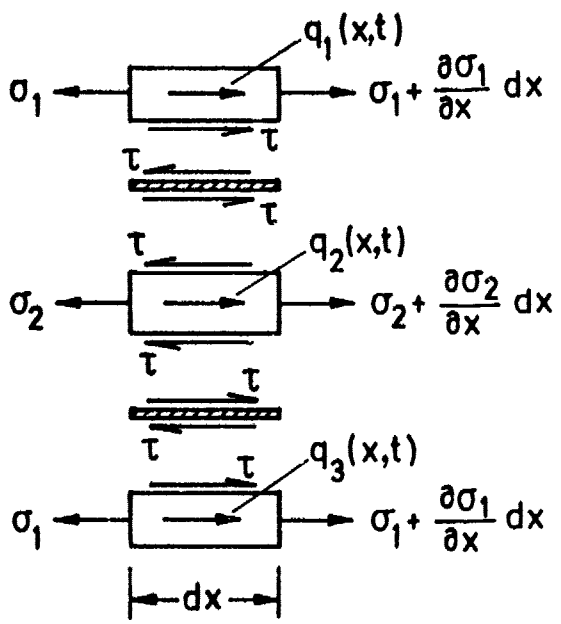

(b) Element equalibrium

Fig. 1 Analytical Model

The composite structure has a length L. In order to obtain the homogeneous boundary condition, it is assumed that the dynamic loading q(x,t) is distributed along each layer. If q(x,t) is equal to δ(x-L)$P_i\psi(t)$ (δ(x-L) is Kronecker function), the boundary conditions can be introduced into the equations of motion. Because of symmetry only the top layer and half of the central layer are considered.

From equilibrium of the element, the equations of motion are given by:

$$A_1(\sigma_1 + \frac{\partial \sigma_1}{\partial x}dx - \sigma_1) + \tau b dx + A_1 q_1(x,t)dx = \rho_1 A_1 \frac{\partial^2 u_1}{\partial t^2}dx \tag{1}$$

$$A_2(\sigma_2 + \frac{\partial \sigma_2}{\partial x}dx - \sigma_2) - 2\tau b dx + A_2 q_2(x,t)dx = \rho_2 A_2 \frac{\partial^2 u_2}{\partial t^2}dx \tag{2}$$

The axial stress and the displacement are related by:

$$\sigma_i = E_i \frac{\partial u_i}{\partial x} \tag{3}$$

while the shear stress in the bond $\tau(x,t)$ is given by :

$$\tau(x,t) = \frac{G(u_2 - u_1)}{h_m} \tag{4}$$

Substituting $q_i(x,t)$ by $\delta(x-L)P_i\psi(t)$, equations (1) and (2) can be rewritten:

$$E_1 A_1 \frac{\partial^2 u_1}{\partial x^2} + \frac{bG}{h_m}(u_2 - u_1) + A_1 \delta(x-L)P_1\psi(t) = \rho_1 A_1 \frac{\partial^2 u_1}{\partial t^2} \tag{5}$$

$$E_2 A_2 \frac{\partial^2 u_2}{\partial x^2} - 2\frac{bG}{h_m}(u_2 - u_1) + A_2 \delta(x-L)P_2\psi(t) = \rho_2 A_2 \frac{\partial^2 u_2}{\partial t^2} \tag{6}$$

To simplify equations (5) and (6), the following dimensionless parameters are introduced:

$$\xi = [\frac{Gb}{F_1 A_1 h_m}]^{\frac{1}{2}} x \qquad \zeta = [\frac{Gb}{\rho_1 A_1 h_m}]^{\frac{1}{2}} t$$

$$\alpha = \frac{E_1 A_1}{E_2 A_2} \qquad \gamma = \frac{E_1}{E_2}$$

$$c = \frac{E_2/\rho_2}{E_1/\rho_1} \qquad \beta = \frac{P_2}{P_1}$$

$$p = \frac{h_m A_1 P_1}{Gb} \qquad \phi(\zeta(t)) = \psi(t) \tag{7}$$

Thus, equations (5) and (6) are expressed as follows

$$\frac{\partial^2 u_1}{\partial \xi^2} + (u_2 - u_1) + p\delta(x-L)\phi(\zeta) = \frac{\partial^2 u_1}{\partial \zeta^2} \tag{8}$$

$$\frac{\partial^2 u_2}{\partial \xi^2} - 2\alpha(u_2 - u_1) + p\gamma\beta\delta(x - L)\phi(\zeta) = \frac{1}{c}\frac{\partial^2 u_1}{\partial \zeta^2} \tag{9}$$

2.3 Initial and boundary conditions

In order to simplify the problem, zero initial conditions are assumed:

$$u_1(\xi, 0) = \frac{\partial u_1(\xi, 0)}{\partial \zeta} = u_2(\xi, 0) = \frac{\partial u_2(\xi, 0)}{\partial \zeta} = 0 \tag{10}$$

The end loading has been introduced into the equations of motion, so the boundary conditions are homogenous:

$$u_1 = u_2 = 0 \qquad \xi = 0 \tag{11}$$

$$\frac{\partial u_1}{\partial \xi} = \frac{\partial u_2}{\partial \xi} = 0 \qquad \xi = a \tag{12}$$

where

$$a = \left[\frac{Gb}{E_1 A_1 h_m}\right]^{\frac{1}{2}} L \tag{12}$$

Although end loads have been introduced into the equations of motion by δ(x-L)$P_i\psi(t)$, the boundary conditions of the zero pressure of equation (12) at the end have also been imposed. This zero boundary conditions force the axial stress solution to be equal to zero at the end. The equilibrium at loading end can not be obtained unless the real loading pressure is added to the axial stress solutions at the loading end.

2.4 Solution

First, Laplace transform in ζ and the finite sine Fourier transform in ξ are introduced, giving

$$\bar{f}(\xi, s) = \int_0^\infty f(\xi, \zeta) e^{-s\zeta} d\zeta$$

and

$$f(\xi, \zeta) = \frac{1}{2\pi i}\int_c \bar{f}(\xi, s) e^{s\zeta} ds \tag{14}$$

and hence

$$\bar{f}^*(n, s) = \frac{1}{a}\int_0^a \bar{f}(\xi, s) sin\frac{n\pi\xi}{2a} d\xi$$

and

$$\bar{f}(\xi, s) = 2\sum_{n=1}^{\infty} \bar{f}^*(n, s) sin\frac{n\pi\xi}{2a} \qquad n = 1, 3, 5... \tag{15}$$

Equations (8) and (9) are now transformed to:

$$[(\frac{n\pi}{2a})^2 + 1 + s^2]\bar{u_1}^* - \bar{u_2}^* = P_0(-1)^{\frac{n-1}{2}}\bar{\phi}(s) \tag{16}$$

$$-2\alpha\bar{u_1}^* + [(\frac{n\pi}{2a})^2 + 2\alpha + \frac{s^2}{c}]\bar{u_2}^* = \gamma\beta P_0(-1)^{\frac{n-1}{2}}\bar{\phi}(s) \tag{17}$$

where

$$P_0 = \frac{p}{L} \tag{18}$$

The solution of equations (16) and (17) is detailed in the appendix, giving

$$\bar{u_1}^*(n,s) = P_0(-1)^{\frac{n-1}{2}}\bar{\phi}(s)(\frac{P}{s^2+X} + \frac{Q}{s^2+Y}) \tag{19}$$

$$\bar{u_2}^*(n,s) = c\gamma\beta P_0(-1)^{\frac{n-1}{2}}\bar{\phi}(s)(\frac{E}{s^2+X} + \frac{F}{s^2+Y}) \tag{20}$$

where

$$A = [(\frac{n\pi}{2a})^2 + 1] \qquad B = c[(\frac{n\pi}{2a})^2 + 2\alpha]$$

$$X = \frac{A+B}{2} + \sqrt{(\frac{A-B}{2})^2 + 2\alpha c} \qquad Y = \frac{A+B}{2} - \sqrt{(\frac{A-B}{2})^2 + 2\alpha c}$$

$$P = \frac{X - B - \gamma\beta c}{X - Y} \qquad Q = 1 - P$$

$$E = \frac{X - A - \frac{2\alpha}{\gamma}\beta}{X - Y} \qquad F = 1 - E$$

Performing the Laplace inversion and the finite sine Fourier inversion, the displacements in the structure can be given as:

$$u_1(\xi,\zeta) = 2P_0\sum_{n=1}^{\infty}(-1)^{\frac{n-1}{2}}[Pf_x + Qf_y]sin\frac{n\pi}{2a}\xi \tag{21}$$

$$u_2(\xi,\zeta) = 2c\gamma\beta P_0\sum_{n=1}^{\infty}(-1)^{\frac{n-1}{2}}[Ef_x + Ff_y]sin\frac{n\pi}{2a}\xi \tag{22}$$

where

$$f_x = \int_0^{\zeta}\phi(u)\frac{1}{\sqrt{X}}sin\sqrt{X}(\zeta - u)du \tag{23}$$

$$f_y = \int_0^{\zeta}\phi(u)\frac{1}{\sqrt{Y}}sin\sqrt{Y}(\zeta - u)du \tag{23}$$

From equations (3) and (4), the axial stresses and the shear stress in the bond region can be obtained:

$$\sigma_1 = \frac{2P_1}{a}\sum_{n=1}^{\infty}(-1)^{\frac{n-1}{2}}(\frac{n\pi}{2a})[Pf_x + Qf_y]cos\frac{n\pi}{2a}\xi + P_1\delta(\xi - a)\phi(\zeta) \qquad (25)$$

$$\sigma_2 = \frac{2P_2c}{a}\sum_{n=1}^{\infty}(-1)^{\frac{n-1}{2}}(\frac{n\pi}{2a})[Ef_x + Ff_y]cos\frac{n\pi}{2a}\xi + P_2\delta(\xi - a)\phi(\zeta) \qquad (26)$$

$$\tau = \frac{2A_1P_1}{Lb}\sum_{n=1}^{\infty}(-1)^{\frac{n-1}{2}}[(c\gamma\beta E - P)f_x + (c\gamma\beta cF - Q)f_y]sin\frac{n\pi}{2a}\xi \qquad (27)$$

In equations (25) and (26), the last term is added to satisfy the equilibrium conditions at the loading ends. If the integral of equations (23) and (24) can be completed, which depends on the loading function $\phi(\zeta)$, the analytical solution of the problem can be obtained. Four example of loading function where this is so are given below.

Example 1 Kronecker δ-function

$$\psi(t) = \delta(t) \qquad (27)$$

so

$$\phi(\zeta) = \delta(\zeta)$$

and the integral of the equations (23) and (24) can be easily completed:

$$f_x = \frac{1}{\sqrt{X}}sin\sqrt{X}\zeta \qquad (28)$$

$$f_y = \frac{1}{\sqrt{Y}}sin\sqrt{Y}\zeta \qquad (29)$$

Example 2 Step-function

$$\psi(t) = \begin{cases} 1 & t \geq 0 \\ 0 & t < 0 \end{cases} \qquad (30)$$

so

$$\phi(\zeta) = \begin{cases} 1 & \zeta \geq 0 \\ 0 & \zeta < 0 \end{cases}$$

Introducing this into equations (23) and (24) and performing the integrals the results are:

$$f_x = \frac{1}{X} - \frac{1}{X}cos\sqrt{X}\zeta \qquad (31)$$

$$f_y = \frac{1}{Y} - \frac{1}{Y} cos\sqrt{Y}\zeta \tag{32}$$

In this example, the impulse is applied as a step loading and the displacement, axial stress and shear stress in the bond region consist of static and dynamic parts. The dynamic part is similar to the solutions of example 1.

Example 3 Ramp-loading

$$\psi(t) = kt \tag{33}$$

so

$$\phi(\zeta) = k_1\zeta$$

where

$$k_1 = k[\frac{Gb}{\rho_1 A_1 h_m}]^{-\frac{1}{2}}$$

Completing the integrals of equations (23) and (24) , the following results can be obtained:

$$f_x = \frac{k_1}{X}[\zeta - \frac{1}{\sqrt{X}} sin\sqrt{X}\zeta] \tag{34}$$

$$f_y = \frac{k_1}{Y}[\zeta - \frac{1}{\sqrt{Y}} sin\sqrt{Y}\zeta] \tag{35}$$

From equations (34) and (35) it can be found that the response of the structure under ramp loading consists of two parts. One part is the ramp response and the other is vibration on the ramp.

Example 4 Triangle-function loading

$$\psi(t) = sin\omega t \tag{36}$$

so

$$\phi(\zeta) = sin\omega_1\zeta$$

where

$$\omega_1 = \omega[\frac{Gb}{\rho_1 A_1 h_m}]^{-\frac{1}{2}}$$

The following equations can be obtained from equations (23) and (24) after integrating:

$$f_x = \frac{1}{\sqrt{X}}[\frac{\omega_1 sin\sqrt{X}\zeta - \sqrt{X} sin\omega_1\zeta}{{\omega_1}^2 - X}] \tag{37}$$

$$f_y = \frac{1}{\sqrt{Y}}[\frac{\omega_1 sin\sqrt{Y}\zeta - \sqrt{Y} sin\omega_1\zeta}{{\omega_1}^2 - Y}] \tag{38}$$

3 Numerical example comparison with finite element method

For the numerical solution only the step loading case has been treated. The elastic properties of the structure were chosen to correspond to those for a woven hybrid composite consisting of a central layer reinforced with carbon fibres and outer layers reinforced with two plies of glass fibres. Two cases are considered. In the first case, the loading is a uniform pressure on all the layers, i.e.

$$P_1 = P_2 = 500.0MPa$$

which corresponds to a sudden tensile or compressive load at the end of structure. In the second case, the ratio of the loading in the different layers is equal to the ratio of the moduli of these layers, i.e.

$$\gamma = \frac{P_1}{P_2} = \frac{E_1}{E_2} = \frac{1}{\beta}$$

and

$$P_1A_1 + P_2A_2 = 500.0(A_1 + A_2)$$

This case corresponds to a uniform strain in all layers and is the one that prevails when the load is controlled by the end displacement. The geometry of the laminate is h_1=0.0002 m which is approximately equal to the thickness of two plies of woven glass reinforcement and h_2 =0.00027 m which is about the thickness of a ply of woven carbon reinforcement. The thickness of the bond region, h_m, and the overall length, L, are arbitrarily chosen to be 0.00002 and 0.02 m, respectively. The moduli in the axial direction of the carbon ply and glass plies are:

$$E_c = 45.3MPa$$

$$E_g = 16.6MPa$$

which were obtained by experimental measurement[8]. The elastic properties of the epoxy resin used for the adhesive layer and for the matrix were taken to be:

$$E_m = 1.72MPa \qquad \nu = 0.34$$

Substituting from equations (31) and (32) into equations (25), (26) and (27), the final expressions obtained for the axial stresses and for the shear stress in the bond region under the step loading are:

$$\sigma_1 = \frac{2P_{01}}{a}\sum_{n=1}^{\infty}(-1)^{\frac{n-1}{2}}(\frac{n\pi}{2a})[(\frac{P}{X}+\frac{Q}{Y})-(\frac{P}{X}cos\sqrt{X}\zeta + \frac{Q}{Y}cos\sqrt{Y}\zeta)]cos\frac{n\pi}{2a}\xi + P_1\delta(\xi-a)\phi(\zeta) \tag{39}$$

$$\sigma_2 = \frac{2P_{02}}{a}\sum_{n=1}^{\infty}(-1)^{\frac{n-1}{2}}(\frac{n\pi}{2a})[(\frac{E}{X}+\frac{F}{Y})-(\frac{E}{X}cos\sqrt{X}\zeta + \frac{F}{Y}cos\sqrt{Y}\zeta)]cos\frac{n\pi}{2a}\xi + P_{02}\delta(\xi-a)\phi(\zeta) \tag{40}$$

$$\tau = \frac{2A_1P_{01}}{Lb}\sum_{n=1}^{\infty}(-1)^{\frac{n-1}{2}}[(\frac{c\gamma\beta E-P}{X}+\frac{c\gamma\beta F-Q}{Y}) -(\frac{c\gamma\beta E-P}{X}cos\sqrt{X}\zeta + \frac{c\gamma\beta F-Q}{Y}cos\sqrt{Y}\zeta)]sin\frac{n\pi}{2a}\xi] \tag{41}$$

It is clear that all the stresses consist of a static part, the first term in equations (39), (40) and (41), and a dynamic part, i.e. the second term. So the static stress distribution under static loading can be expressed as follows:

$$\sigma_{1s} = \frac{2P_{01}}{a}\sum_{n=1}^{\infty}(-1)^{\frac{n-1}{2}}(\frac{n\pi}{2a})[\frac{P}{X}+\frac{Q}{Y}]cos\frac{n\pi}{2a}\xi + P_1\delta(\xi-a)\phi(\zeta) \tag{42}$$

$$\sigma_{2s} = \frac{2P_{02}}{a}\sum_{n=1}^{\infty}(-1)^{\frac{n-1}{2}}(\frac{n\pi}{2a})[\frac{E}{X}+\frac{F}{Y}]cos\frac{n\pi}{2a}\xi + P_2\delta(\xi-a)\phi(\zeta) \tag{43}$$

$$\tau_s = \frac{2A_1P_1}{Lb}\sum_{n=1}^{\infty}(-1)^{\frac{n-1}{2}}(\frac{c\gamma\beta E-P}{X}+\frac{c\gamma\beta F-Q}{Y})sin\frac{n\pi}{2a}\xi \tag{44}$$

If the material properties and geometrical parameters are introduced into equations (39) to (44), numerical results can be obtained with an accuracy that depends on how many terms are involved in the calculation. In the present example, a series of 1000 terms was used to calculate all the stresses.

In order to check the accuracy of this solution, the finite element method was also used to solve the same problem. Two finite element solutions were obtained,

one with a relatively coarse mesh in which half the model is divided into 300 plane strain element of eight nodes and a second where it is divided into 1000 plane strain elements, also of eight nodes, as shown in Fig. 2.

4 Numerical results

Fig. 3 compares the tensile stresses and the shear stress in the bond region obtained by the present analytical solution with that for the two finite element solutions under static uniform pressure. It is found that the shear stress in the bond reaches a peak value at the loading end and declines steeply from this maximum value to zero in a very short distance. Good agreement is found between all three solutions except at the loading end where the shear stress in the bond region has its peak value. This maximum value is 157 MPa for the present numerical solution, 125 MPa for the finite element method with a coarse mesh division and 152 MPa for the finite element method with a fine mesh division. The percentage error in terms of the analytical solution drops from 22.3 to 3.5 when the mesh is refined. This suggests that the analytical solution is very efficient and the results obtained are accurate.

Fig. 4, 5 and 6 show the axial stresses and the shear stress at 1.75 μs, 3.5 μs and 7.0 μs respectively after the uniform step pressure is applied at the loading end. In this case, the maximum shear stress still occurs at the loading end and is dominated by the static value. For each axial stress wave obtained from the analytical solution, there is an initial short period of 'noise' just ahead of the main wavefront. Corresponding to this 'noise', the shear wave shows a similar effect. Ignoring these effects, the second peak value of the shear wave is in the vicinity of the front of the slower axial wave. This peak value is totally contributed by the dynamic part. The numerical solution agrees with the finite element results for both meshes. Except at the loading end, however, where the results of the finite element method for the finer mesh are closer to the analytical solution, little difference can be seen between the two finite element solutions.

It is quite clear that, following reflection at fixed end, the shear stress in the bond region is less severe than might be expected with a peak value less than that at $1.75\mu s$ and $3.50\mu s$, i.e. before the stress wave reflection.

Fig. 7, 8 and 9 show the axial stresses and shear stress in the bond region when the ratio of the loading applied to each layer is equal to the ratio of the moduli of the layers. In this case, the static shear stress in the bond should approach zero. That this is predicted by the numerical solution can be seen from equation (41). Simplifying equation (41) further, the shear stress under step loading can be expressed in the form :

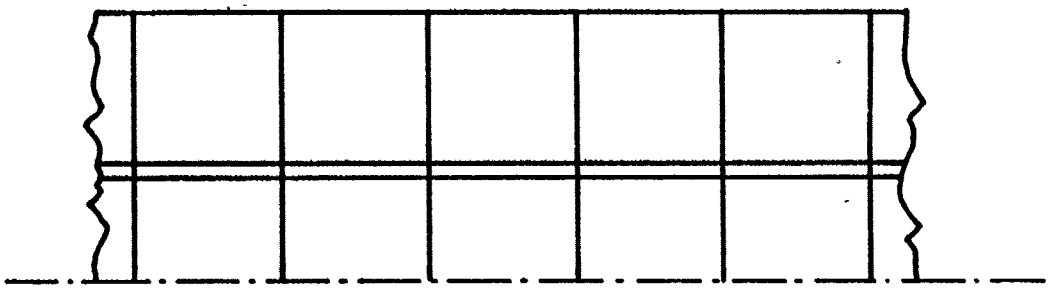

(a) Coarse mesh division

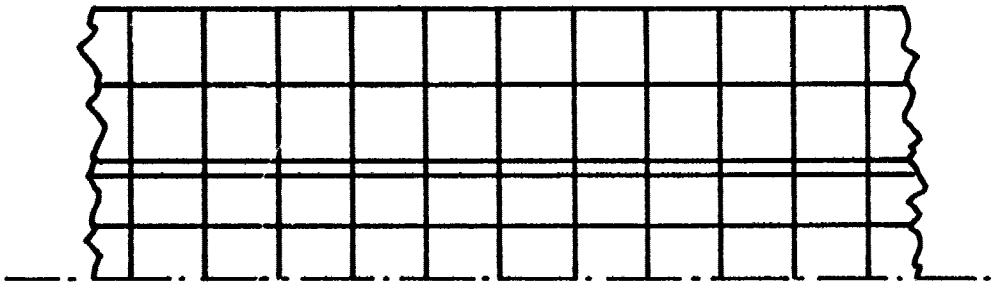

(b) Finer mesh division

Fig. 2 Finite Element Model

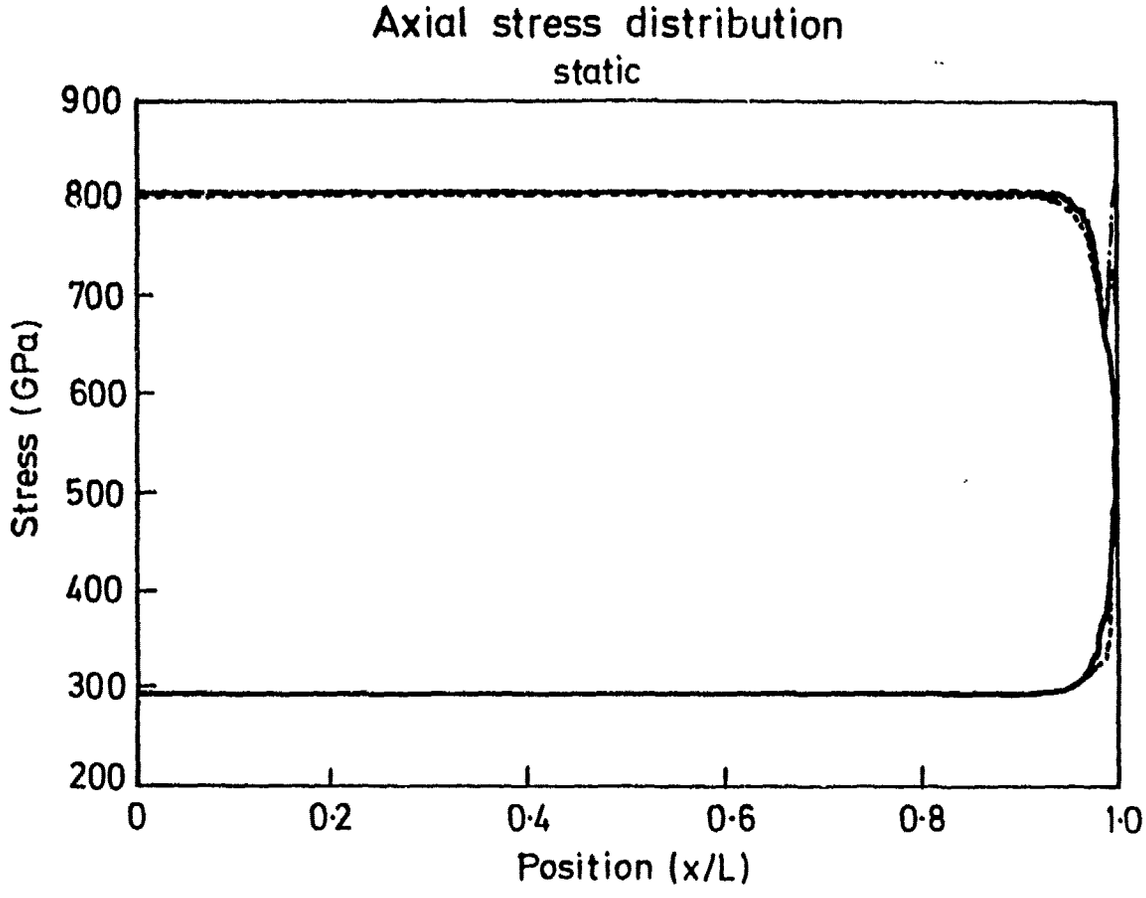
Axial stress distribution
static
900
800
700
600
500
400
300
200
Stress (GPa)
0
0·2
0·4
0·6
0·8
1·0
Position (x/L)

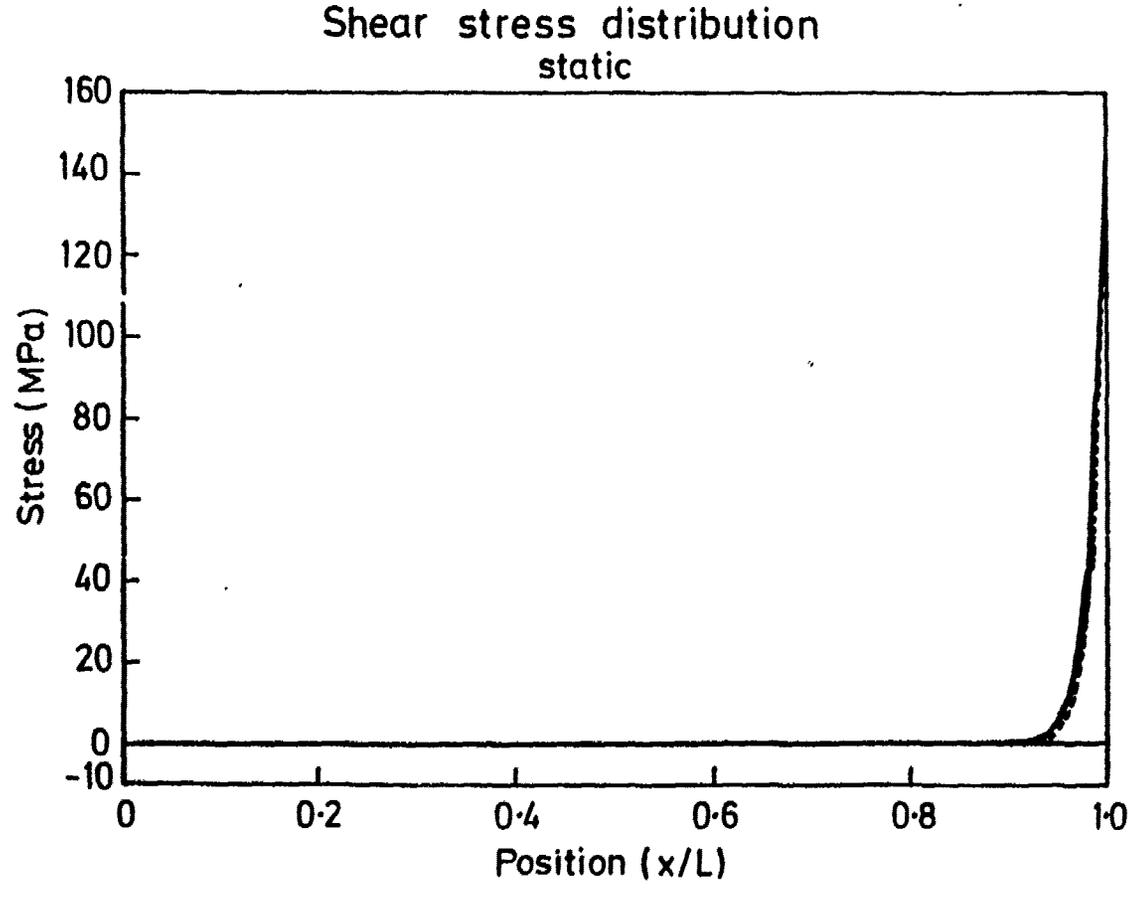
Shear stress distribution
static
160
140
120
100
80
60
40
20
0
-10
Stress (MPa)
0
0·2
0·4
0·6
0·8
1·0
Position (x/L)

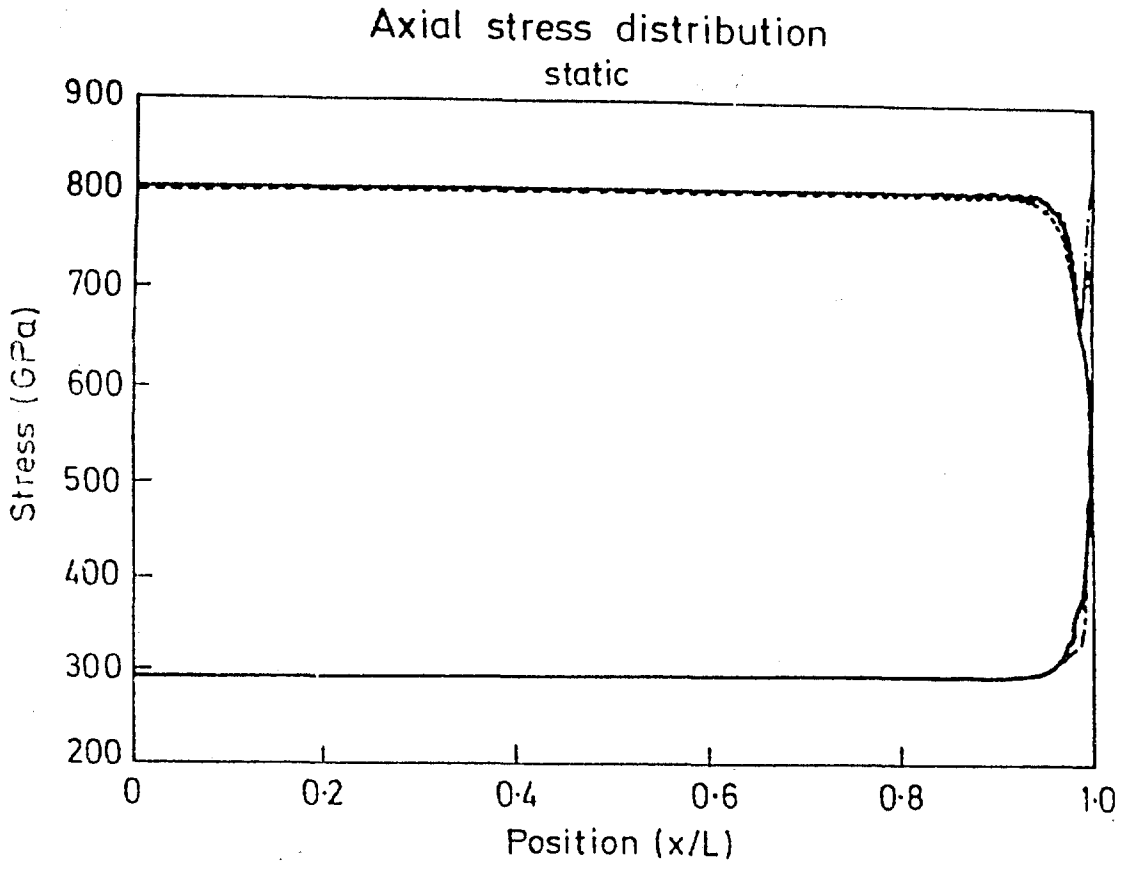

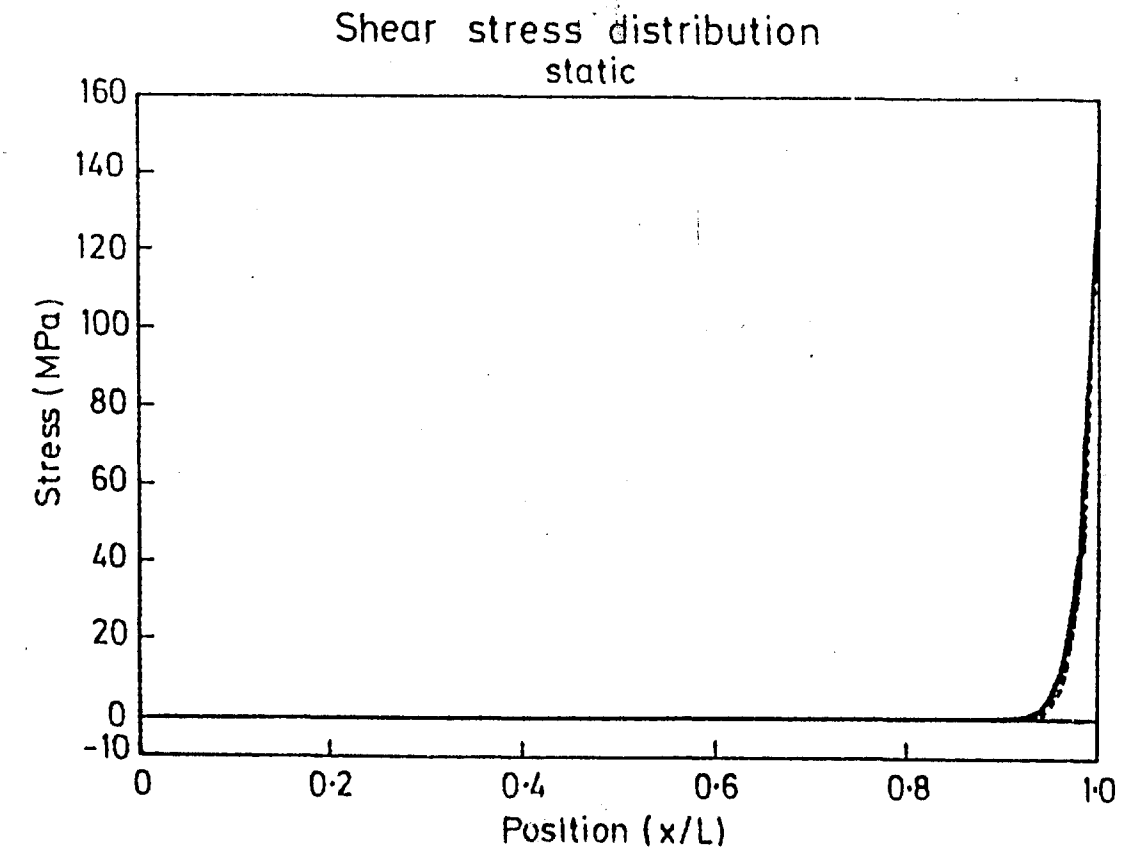

Fig. 3 Axial and Shear Stress Distribution (static loading)

Axial stress distribution

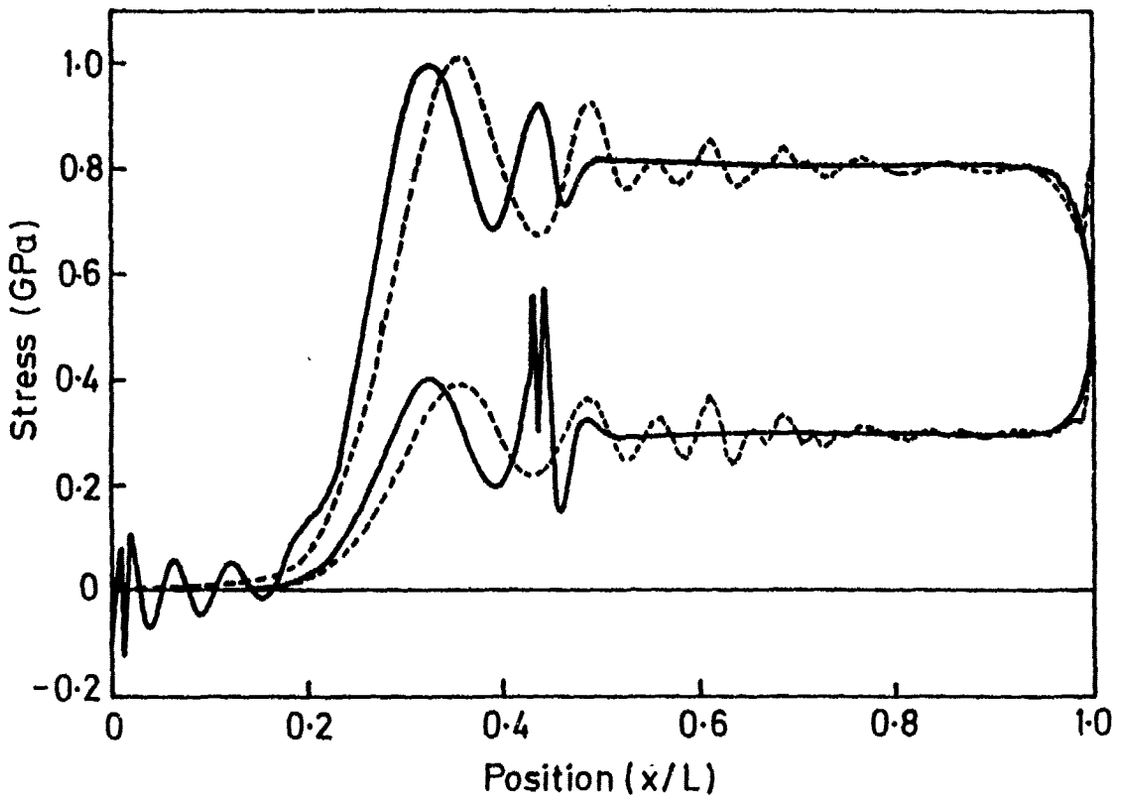

Shear stress distribution

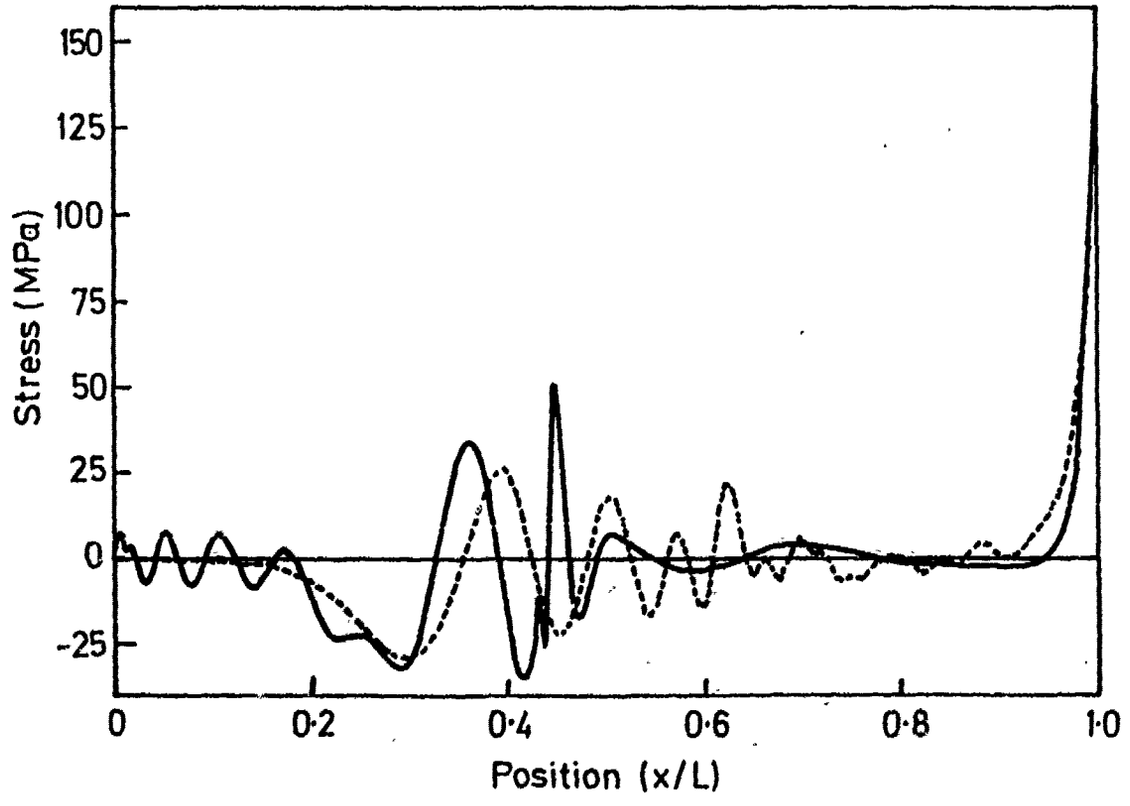

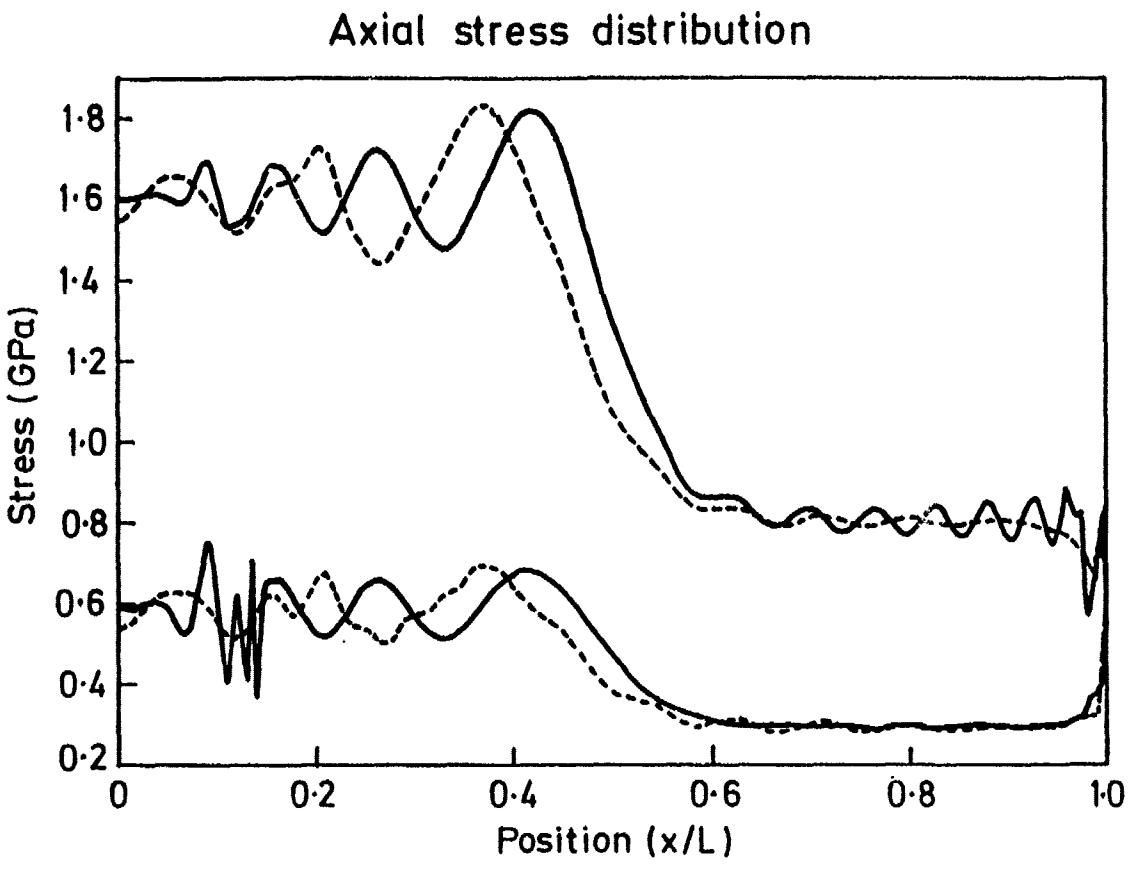
Axial stress distribution
Stress (GPa)
1·8
1·6
1·4
1·2
1·0
0·8
0·6
0·4
0·2
0
0·2
0·4
0·6
0·8
1·0
Position (x/L)

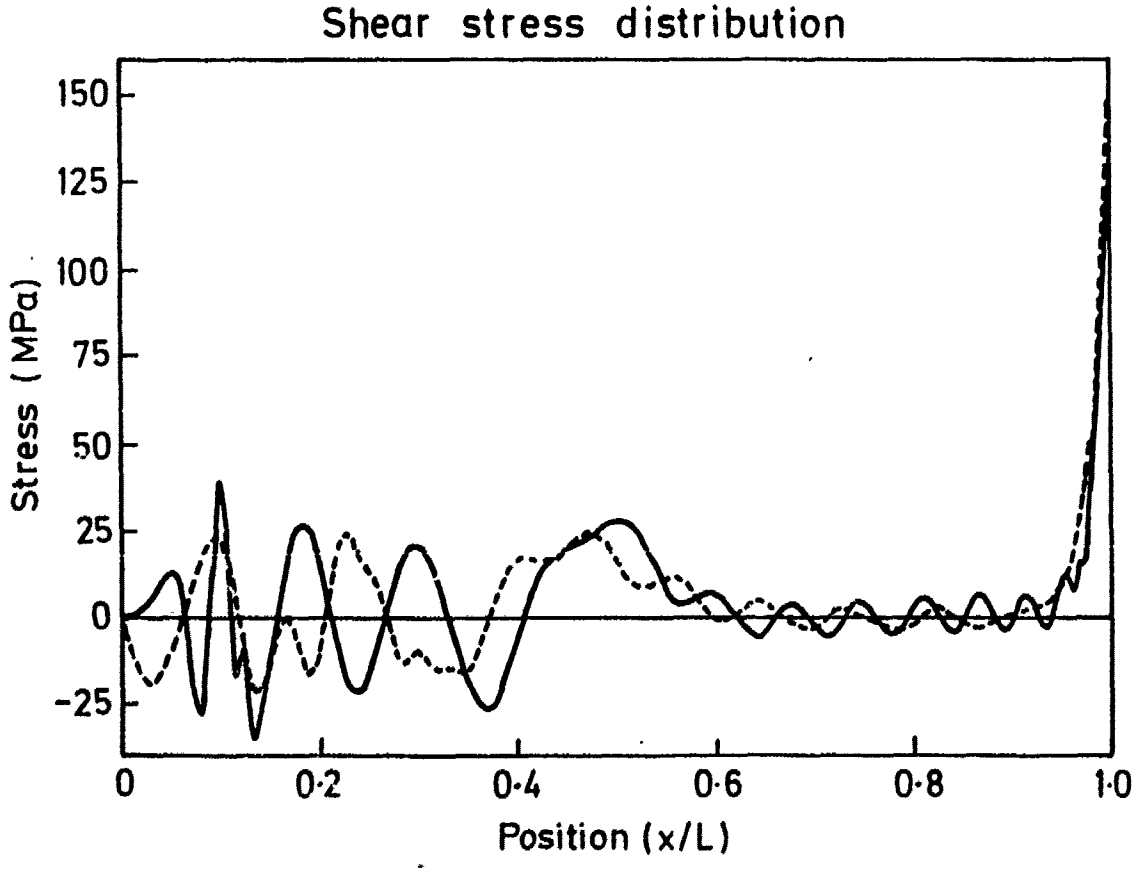
Shear stress distribution
Stress (MPa)
150
125
100
75
50
25
0
-25
0
0·2
0·4
0·6
0·8
1·0
Position (x/L)

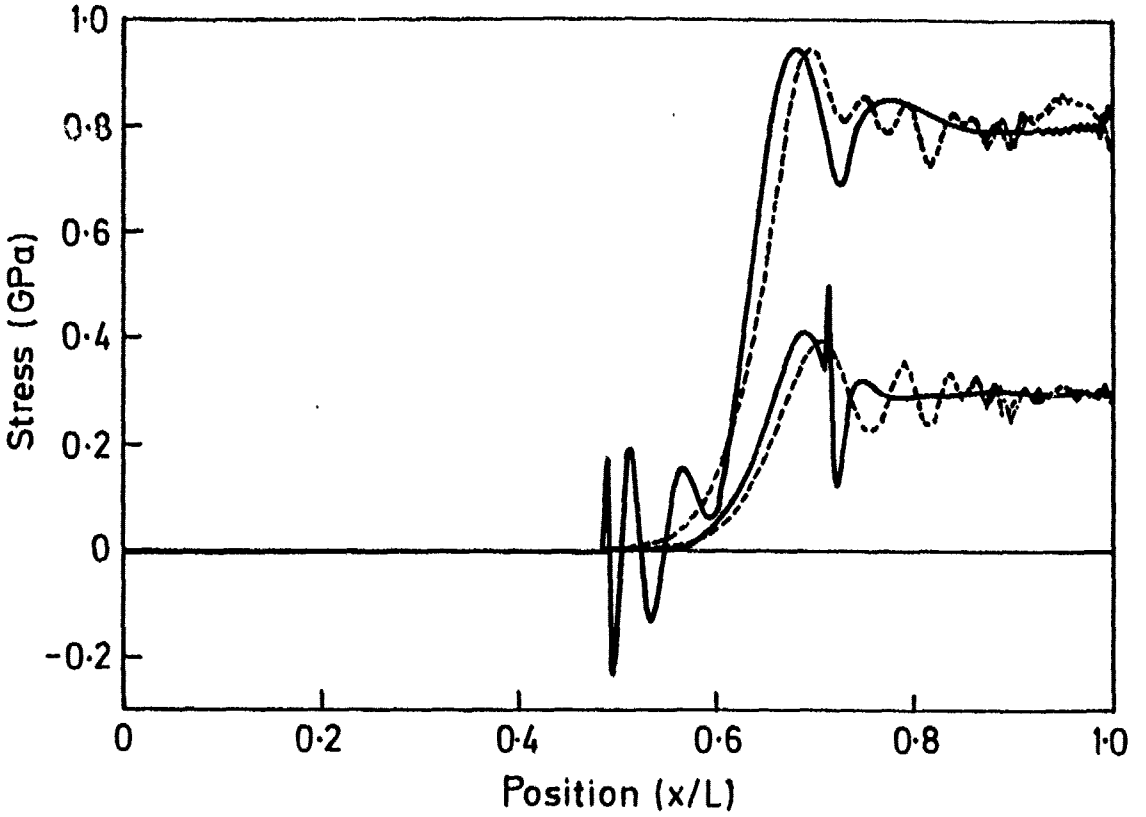
Axial stress distribution
Stress (GPa)
1·0
0·8
0·6
0·4
0·2
0
-0·2
0
0·2
0·4
0·6
0·8
1·0
Position (x/L)

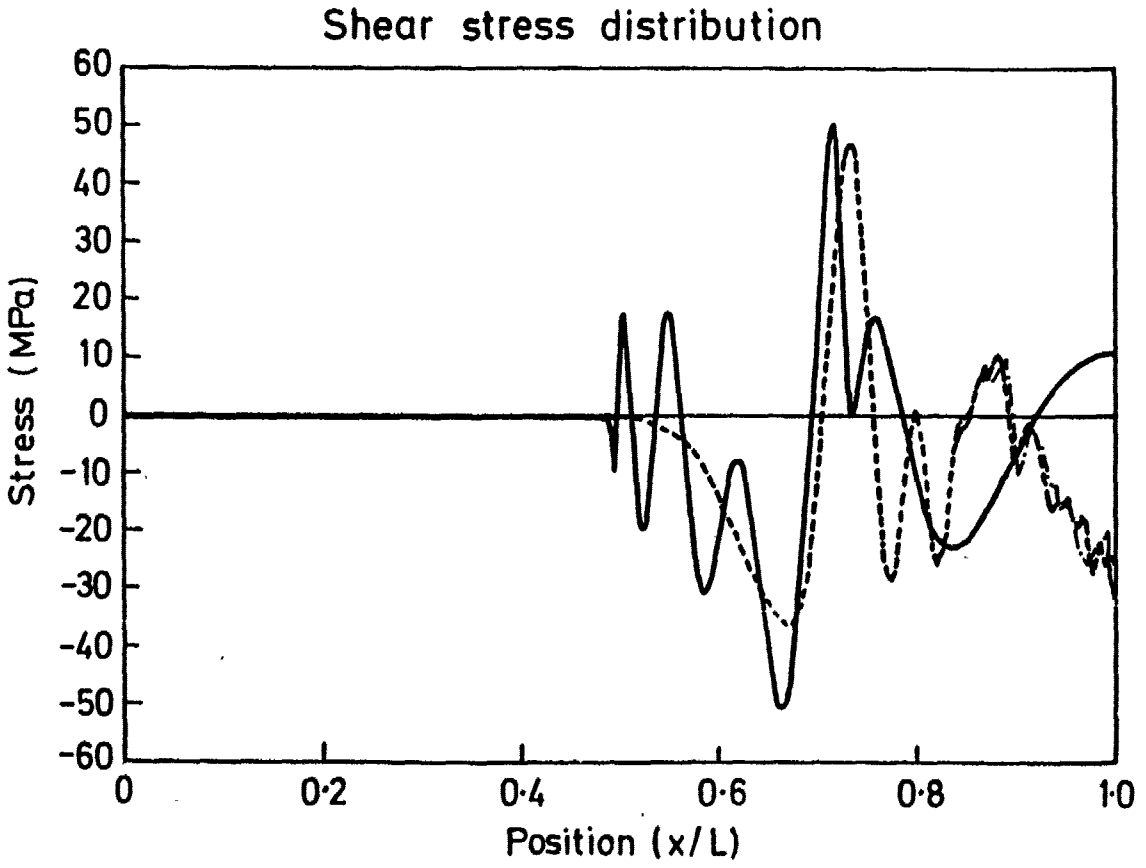
Shear stress distribution
Stress (MPa)
60
50
40
30
20
10
0
-10
-20
-30
-40
-50
-60
0
0·2
0·4
0·6
0·8
1·0
Position (x/L)

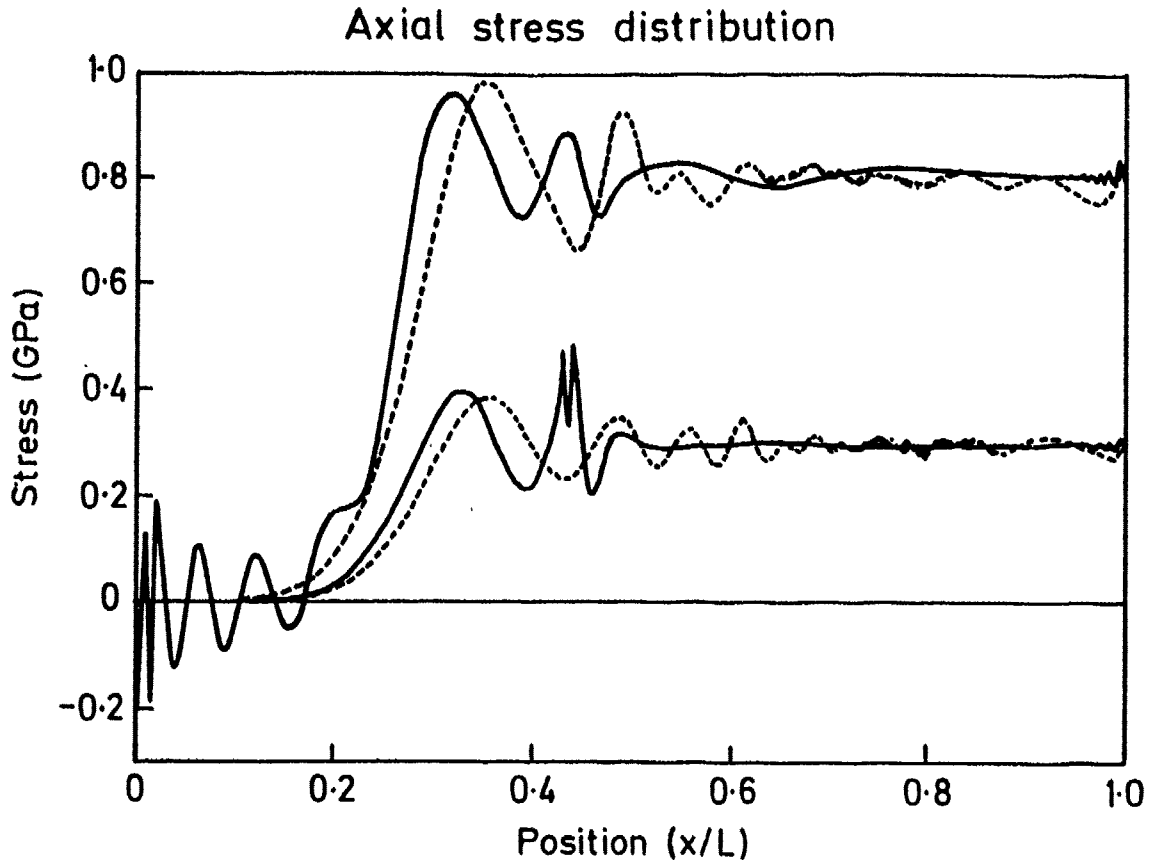
Axial stress distribution
1·0
0·8
0·6
0·4
0·2
0
-0·2
Stress (GPa)
0
0·2
0·4
0·6
0·8
1·0
Position (x/L)

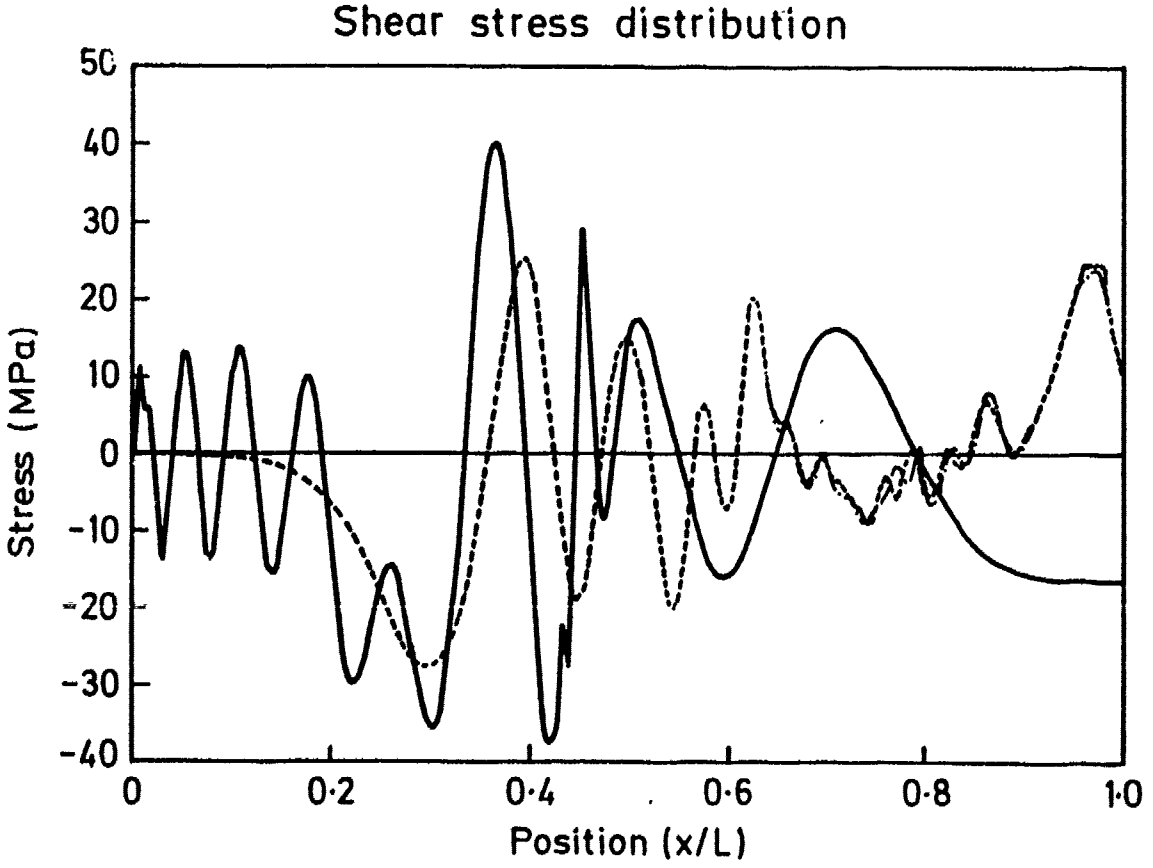
Shear stress distribution
50
40
30
20
10
0
-10
-20
-30
-40
Stress (MPa)
0
0·2
0·4
0·6
0·8
1·0
Position (x/L)

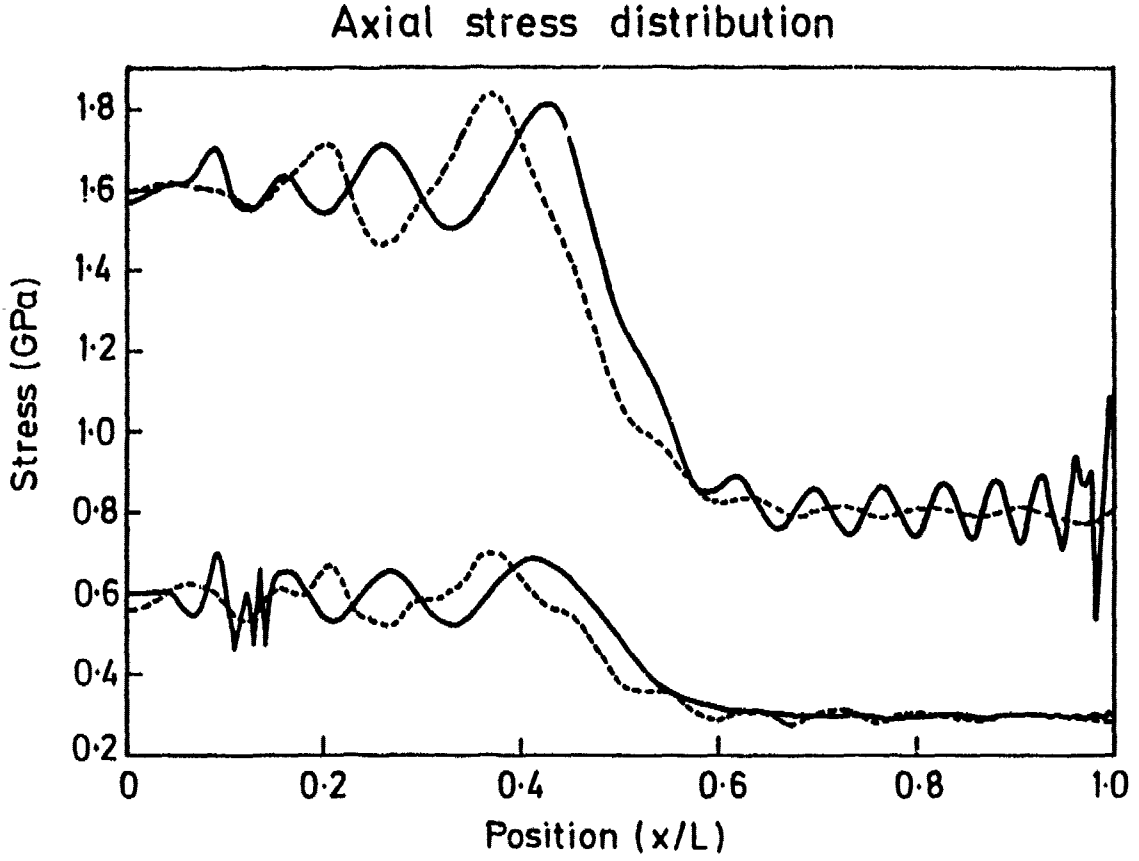
Axial stress distribution
Stress (GPa)
1·8
1·6
1·4
1·2
1·0
0·8
0·6
0·4
0·2
0
0·2
0·4
0·6
0·8
1·0
Position (x/L)

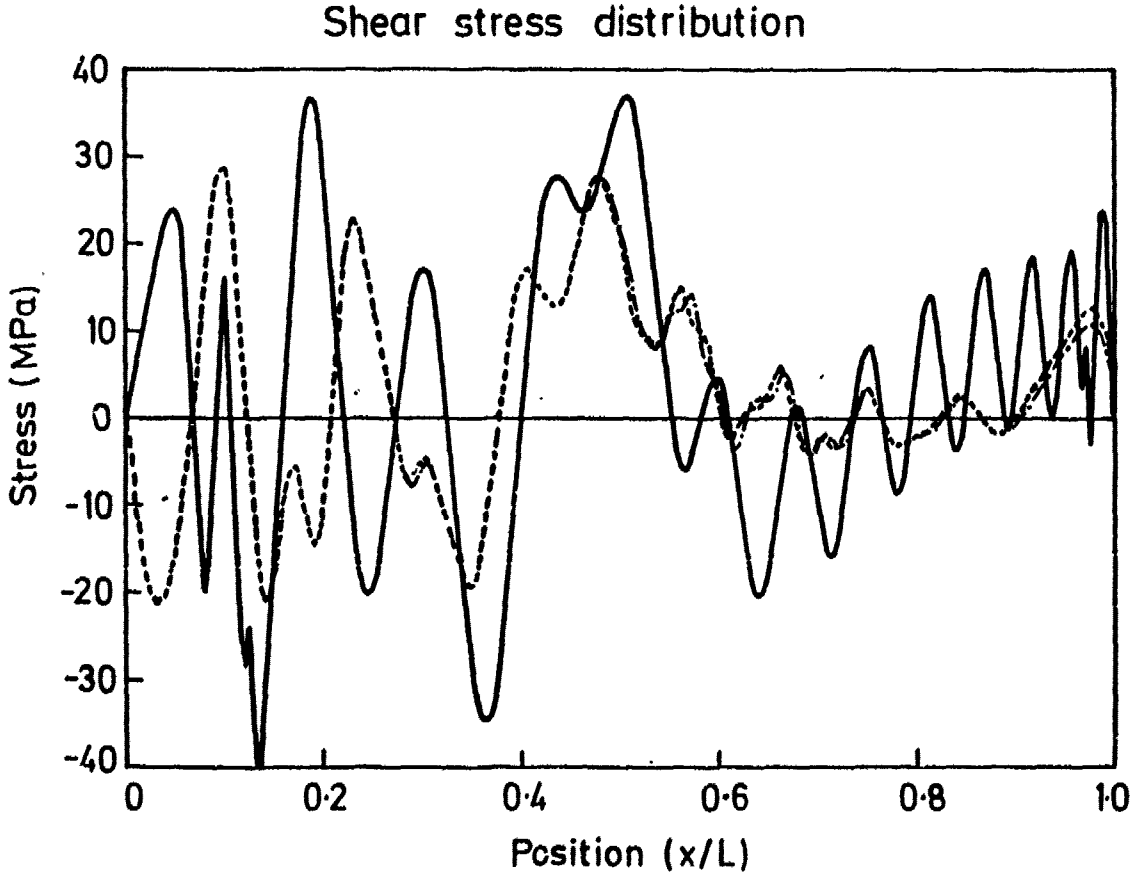
Shear stress distribution
Stress (MPa)
40
30
20
10
0
-10
-20
-30
-40
0
0·2
0·4
0·6
0·8
1·0
Position (x/L)

$$\tau = \frac{2A_1P_{01}}{Lb}\sum_{n=1}^{\infty}(-1)^{\frac{n-1}{2}}[\frac{\gamma\beta-1}{(\frac{n\pi}{2a}^2)+1+2\alpha} - (\frac{c\gamma\beta E-P}{X}cos\sqrt{X}\zeta + \frac{c\gamma\beta F-Q}{Y}cos\sqrt{Y}\zeta)sin\frac{n\pi}{2a}\xi] \quad (45)$$

The first term is the static part and, if $\gamma\beta = 1$, is identically equal to zero. So the bond shear stress is dominated by the dynamic part. Again an initial short period of 'noise' precedes the main axial wave and the main shear wave. The maximum shear stress occurs in the vicinity of the first peak on the slower axial stress wave. The maximum shear stress value is about the same as the second peak value for the uniform step pressure loading.

5 Discussion and conclusions

The analytical method of solution offers a clear advantage over the finite element approach when dealing with these simple geometries and forms of loading in that it is considerably less demanding in terms of computational time, Using a micro-computer, it requires less than 30 minutes CPU against almost 40 hours CPU for the finite element solution with 1000 elements. It is, therefore, particularly suitable for parametric studies leading to the design of composite structures. Of course, it cannot cope with a complex geometry, such as may be found in engineering practice, where only the finite element technique can solve the problem.

The shear stress has been found to reach a very high peak value under a uniform pressure loading, a case that is not likely to be of great practical importance in most thin-wall laminates where loading will tend to be governed by compatibility of displacement. Thus, under a uniform pressure, the shear stress can reach up to about 30% of the applied pressure, depending on the ratio between the elastic moduli of the layers. This may induce delamination. In contrast, under uniform displacement, the shear stress is considerably lower, although, in the typical example that has been treated, it is still quite significant. In either case, the analytical method highlights the contribution of stress wave action to the overall stress by splitting the solution into static and dynamic terms. This is not done explicitly by the finite element method where only a global solution is obtained. The static term is found to be important in the uniform pressure case and zero in the uniform strain case, where only the dynamic effect is present. Thus the difference between static and dynamic loading is made more apparent: it is possible, for example, for a laminate to develop delamination when loaded dynamically when it would not do so under static loading conditions.

. The present solution has also revealed what happens when the stress wave is reflected at a fixed end, showing that the interference between the fast and slow

waves leads to a situation that is less severe than might be expected.

6 Acknowledgments

This research was sponsored by the Force Office of Scientific Research, Air Force System Command, USAF, under Grant No. AFOSR-87-0129.

Appendix I

Solving the equations (16) and (17):

$$\Delta = \begin{vmatrix} [(\frac{n\pi}{2a})^2 + 1 + s^2] & -1 \\ -2\alpha & [(\frac{n\pi}{2a})^2 + 2\alpha + \frac{s^2}{c}] \end{vmatrix}$$

$$= \frac{1}{c}[(A + s^2)(B + s^2)] - 2\alpha$$

$$= \frac{1}{c}[s^4 + (A + B)s^2 + (AB - 2\alpha c] \qquad (I-1)$$

$$\Delta_1 = \begin{vmatrix} P_0(-1)^{\frac{n-1}{2}}\bar{\phi}(s) & -1 \\ \gamma\beta P_0(-1)^{\frac{n-1}{2}}\bar{p}(s) & [(\frac{n\pi}{2a})^2 + 2\alpha + \frac{s^2}{c}] \end{vmatrix}$$

$$= P_0(-1, \quad ^{-1}\bar{\phi}(s)\frac{1}{c}[(B + s^2) + \gamma\beta c] \qquad (I-2)$$

$$\Delta_2 = \begin{vmatrix} [(\frac{n\pi}{2a})^2 + 1 + s^2] & P_0(-1)^{\frac{n-1}{2}}\bar{\phi}(s) \\ -2\alpha & \gamma\beta P_0(-1)^{\frac{n-1}{2}}\bar{\phi}(s) \end{vmatrix}$$

$$= \gamma\beta P_0(-1)^{\frac{n-1}{2}}\bar{\phi}(s)[(A + s^2) + \frac{2\alpha}{\gamma\beta}]$$

$$= \frac{1}{c}[s^4 + (A + B)s^2 + (AB - 2\alpha c)] \qquad (I-3)$$

From the equation (I-1) to (I-3) the solution of equation (16) and (17) can be obtained:

$$\bar{u_1}^* = P_0(-1)^{\frac{n-1}{2}}\bar{\phi}(s)\frac{B + s^2 + \gamma\beta c}{s^4 + (A + B)s^2 + (AB - 2\alpha c)} \qquad (I-4)$$

$$\bar{u_1}^* = P_0(-1)^{\frac{n-1}{2}}\bar{\phi}(s)\frac{A + s^2 + \frac{2\alpha}{\gamma\beta}}{s^4 + (A + B)s^2 + (AB - 2\alpha c)} \qquad (I-5)$$

In order to perform the Laplace inversion easily the form of these solution has to be changed. Noting that we can write

$$(A + B)^2 - 4(AB - 2\alpha c) = (A - B)^2 + 2\alpha c > 0 \qquad (I-6)$$

the denominator of equations (I-4) and (I-5) can be written in the form:

$$s^4 + (A + B)s^2 + (AB - 2\alpha c) = (s^2 + X)(s^2 + Y) \qquad (I-7)$$

where

$$X = \frac{A+B}{2} - \sqrt{\left(\frac{A-B}{2}\right)^2 + 2\alpha c} \qquad (I-8)$$

$$Y = \frac{A+B}{2} + \sqrt{\left(\frac{A-B}{2}\right)^2 + 2\alpha c} \qquad (I-9)$$

It is true that:

$$\sqrt{(A+B)^2 - 4(AB - 2\alpha c)} < (A+B)$$

so X and Y are always positive. Now it is not difficult to change equations (I-4) and (I-5) into equations (19) and (20).

Reference

[1] R.G.Payton "Dynamic Bond Stress in a Composite Structure Subjected to a Sudden Pressure Rise," *J. Applied Mechanics, Vol. 32, No.3, 1965, p643-650*

[2] C.S.Chang and H.D.Conway "Bond Stress in Fibre Reinforced Composite Subjected to Uniform Tension," *J. Composite Materials, 2(1968), p168-*

[3] J.M.Hedgepeth and P.V.Dyke "Local Stress Concentrations in Imperfect Filamentary Composite Materials," *J. Composite Materials, 1(1967), p294-*

[4] H.Fukuda and Tsu-Wei Chou "An Advanced Shear-Lag Model Applicable to Discontinuous Fibre Composite," *J. Composite Materials, Vol. 15, 1(1981) p79-91*

[5] Ji Xing, G. c. Hsiao and Tsu-Wei Chou "ADynamic Explanation of The Hybrid Effect," *J. Composite Materials , Vol. 15 , 9(1981) p443-461*

[6] J.A.Nairn "Fracture Mechanics of Unidirectional Composites Using the Shear-Lag Model I: Theory," *J. Composite Materials, Vol. 22, 6(1088) p561-588*

[7] J.A.Nairn "Fracture Mechanics of Unidirectional Composites Using the Shear-Lag Model I: Experiment," *J. Composite Materials, Vol. 22, 6(1088) p589-600*

[8] J.Harding, K.Saka and M.C.Taylor "Effect of strain rate on the tensile failure of woven-reinforced carbon/glass hybrid composite," *Proc. IMPACT 87, (DGM Informationagesellschafft mbH, Oberursel), 2, (1987) p679-586*

APPENDIX VI

MECHANICAL BEHAVIOUR OF COMPOSITE MATERIALS UNDER IMPACT LOADING

by

J. Harding

Report No. OUEL 1851/90

(Presented at EXPLOMET 90, University of San Diego, California, August 1990)

University of Oxford
Department of Engineering Science
Parks Road
OXFORD
OX1 3PJ

Tel. (0865) 273000

MECHANICAL BEHAVIOUR OF COMPOSITE MATERIALS UNDER IMPACT LOADING

J. HARDING

Department of Engineering Science
University of Oxford
Parks Road, Oxford OX1-3PJ, U. K.

The problems of characterising the mechanical behaviour of composite materials under impact loading are discussed. Techniques for determining such behaviour for tensile, compressive and shear loading are described and some qualitative conclusions are drawn from the results obtained.

I. INTRODUCTION

The rate-dependence of the mechanical properties of metallic type materials may be determined using standard designs of test-piece. The macroscopic response of the bulk material, for well defined loading systems, may be related to data obtained in such tests and analytical functions, i.e. constitutive relationships, may be derived. These can then be used to describe the mechanical behaviour of structural components of different geometrical shapes and under more complex loading systems. For composite materials, however, where there are two or more phases present, several complicating factors arise. For example, the overall rate dependence of the composite will depend, to a greater or lesser extent, on the rate dependence of each of these various phases. Also of importance will be the reinforcement configuration, e.g. unidirectional, cross-ply or woven, and the type and direction of loading, e.g. tensile, shear or compressive. Thus for a unidirectionally-reinforced composite under tensile loading in the fibre direction, where fibre fracture is likely to be the process controlling the failure of the composite, the fibre properties may be expected to determine the rate dependent behaviour. In contrast, for woven reinforced mat-

erial loaded in compression in one of the principal directions of reinforcement, where a fibre buckling process is likely to control failure, the properties of the matrix will have a greater influence on the overall rate dependence.

A further complicating factor, however, for all multi-phase materials, is the presence of interfaces and hence the possibility of additional failure processes associated with the interface, for example, by deplying or interlaminar shear mechanisms. It becomes necessary, therefore, to consider whether the critical conditions under which such processes occur are also rate dependent.

In the light of these various factors it is clear that a full characterisation of the mechanical behaviour of composite materials at impact rates of straining is likely to require the use of a wider range of test configurations and test-piece designs than are commonly encountered in the testing of simpler single-phase metallic materials. The present review describes several of the techniques which have been used and discusses the results which have been obtained. Although in some of these tests it is difficult to distinguish between the various failure processes and their individual dependence on the rate of loading, so that a detailed interpretation of the results may not be possible, some general conclusions may be drawn.

II. REVIEW OF EXPERIMENTAL TECHNIQUES

Problems of data interpretation arise in all testing techniques used at impact rates of loading. For homogeneous isotropic metallic materials, however, these problems are least severe when the testing technique is based on the split Hopkinson pressure bar principle. For this reason all the experimental methods to be described here will also be based on this principle, although it is realised that for anisotropic multi-phase materials these difficulties may be greatly increased. Tensile, compressive and shear loading configurations will be considered, in each case with a design of test-piece intended to study, as far as possible, a single failure initiation process, although subsequent propagation of failure is likely to involve a complex interaction between several different failure processes.

In all Hopkinson-bar tests overall specimen dimensions need to be small, so as to minimise radial inertia and wave propagation effects within the specimen, while care has to be taken in designing the method of load transfer between the specimen and the loading bars so as to avoid the introduction of a region of significant impedance mismatch which could introduce stress wave reflections and thus invalidate the Hopkinson-bar analysis. When composite specimens are to be tested the need for small overall specimen dimensions may conflict with the requirement for a specimen which is large relative to the scale of the reinforcement while the anisotropic nature of the composite material can complicate the design of the specimen/loading bar interface.

A. *TENSILE TESTING TECHNIQUES*

A tensile version of the Hopkinson-bar apparatus for use with composite specimens is shown schematically in fig. 1. A cylindrical projectile impacts the loading block and causes an elastic tensile loading wave to propagate along the loading bar towards the specimen and output bar. The thin strip specimen is waisted in the thickness direction and has a very slow taper so as to minimise stress concentrations due to free edge effects. The state of stress within the specimen has been investigated using a two-dimensional finite element analysis. It shows the biggest stress concentrations to be at the specimen/loading bar interface and to be significantly smaller than the controlling tensile stresses in the specimen gauge region which is in a state of uniform tension.

The specimen is fixed with epoxy adhesive into parallel-sided slots in the loading bars. Strain gauge signals from two stations on the input bar and one on the output bar allow the full dynamic stress-strain curve to be derived using the standard Hopkinson-bar analysis. However, since most composites fail at low or very low strains and may show a significant rate dependence of the initial elastic deformation, for the determination of which the Hopkinson-bar analysis is not very accurate, it is usual to make, in addition, a direct determination of the specimen elongation using a fourth set of strain gauges, attached to the specimen itself. A range of fibre reinforced polymeric materials have been tested in this way and the results compared

with those obtained at lower rates of strain. Some of these results are summarised below and some tentative conclusions drawn.

Initial tests on a unidirectionally-reinforced carbon/epoxy material [1], loaded in the reinforcement direction, at mean strain rates from ~0.0001/s to ~450/s, showed no effect of strain rate, see fig. 2a, on the tensile modulus, tensile strength or strain to failure; nor was there any effect of strain rate on the fracture appearance. Such behaviour is consistent with the conclusion that the tensile properties of the composite are entirely controlled by the carbon fibres the behaviour of which is entirely independent of strain rate. In contrast similar tests [2] on a plain coarse-weave carbon/epoxy material when loaded in a principal reinforcing direction, see fig. 2b, showed a small effect of strain rate on the initial tensile modulus and a more significant effect on the tensile strength and the elongation to failure. Here, however, the woven reinforcement geometry is likely to result in a stronger interaction with the matrix so that the rate dependent properties of the matrix play a more important role in the deformation process.

The rate dependence is much more marked when glass reinforcing fibres are used. Tensile stress-strain curves for a plain fine-weave glass/epoxy material [3] are shown in fig. 2c. The initial modulus and the tensile strength both increase very significantly with strain rate while, in contrast with the behaviour shown by the woven carbon/epoxy material, the overall elongation also increases with rate of loading. Part of this increased rate sensitivity may be due to a greater interaction with the matrix when a fine weave reinforcement is used. More important, however, is likely to be the rate dependent behaviour of the glass fibres themselves, the strength of which is expected to increase quite markedly at impact rates [4]. A direct confirmation of this in tensile tests on unidirectional glass/epoxy composites loaded in the reinforcement direction, however, did not prove possible. Although under quasi-static loading a tensile failure was obtained in the central gauge section of the specimen, under impact loading failure was invariably by the pull-out of glass-fibres from the matrix in the grip-regions of the specimen, see fig. 3, [5]. This implies that the ratio of the tensile strength of the glass fibres to the interfacial shear

strength between the glass fibres and the epoxy matrix increases with increasing strain rate. This could be due either to an increase in the former or to a decrease in the latter.

Further evidence for the relative importance of the tensile to the shear strength in composite materials was obtained in tensile tests on some coarse satin-weave glass/polyester specimens, loaded in a principal reinforcement direction [6]. Here there was a continuous change in both the stress-strain response, fig. 4a, and the fracture appearance, fig. 4b, from those observed at the quasi-static rate, where a tensile failure with limited fibre tow pull-out was obtained, to the medium rate, where a tensile failure was still obtained but fibre tow pull-out was very extensive and the overall strain to failure was quite high, ~7%, up to the impact rate, where failure was dominated by shear stresses giving pull-out of the whole central section of the specimen from the two ends with only limited tensile failure of individual fibre tows and an overall strain to failure of the order of 13%.

In the light of these results it is necessary to devise a technique for determining the effect of strain rate specifically on the shear strength of the composite specimen, i.e. both the interlaminar shear strength between adjacent reinforcing plies and the interfacial shear strength between fibre tows and the matrix.

B. SHEAR TESTING TECHNIQUES

Several techniques for determining the rate dependence of the interlaminar shear strength in composite materials have been devised. In two of these [7,8], both based on the torsional Hopkinson-bar, a very significant increase in shear strength with strain rate was observed for both woven and cross-ply glass/epoxy specimens. In contrast, a study of both the interlaminar and the transverse shear strength of a plain-weave carbon/epoxy laminate [9], using a test based on the double-notch shear version of the split Hopkinson-bar apparatus, showed no significant rate dependence. Unlike the previously described tensile tests, however, in none of these various shear tests was the specimen subjected to a well-defined stress system.

This problem has been tackled in a more recently developed test [10] which uses the "double-lap" shear specimen shown in fig. 5a. In this specimen, which has to be especially laid-up and cannot be cut from existing laminates, failure occurs on pre-determined interlaminar planes, fig. 5b. The strain distribution along one of these planes, as derived from a two-dimensional finite element analysis, gives the results shown in fig. 5c. It is clear that the shear strain on the interlaminar failure plane is very far from uniform. This is a problem common to most designs of shear specimen. It means that, although we may be able to determine the effect of strain rate on the critical load at which interlaminar shear failure occurs in the double-lap specimen, the corresponding shear stresses as estimated from the area of the interlaminar failure planes will only be representative values.

With this proviso it may be reported that all such measurements so far made, for a satin weave carbon/epoxy, a plain weave carbon/epoxy, a unidirectionally reinforced carbon/epoxy, a plain weave glass/epoxy and at the interface between plies of plain weave glass and a plain weave carbon in a hybrid carbon/glass/epoxy lay-up, showed a significant increase in the interlaminar shear strength at impact rates of loading. While these results clearly establish the general trend, the wide variations in shear stress and shear strain along the interlaminar plane at failure make it difficult to determine from these tests a critical value of interlaminar shear stress for use in modelling damage accumulation processes in composites under impact loading.

C. COMPRESSIVE TESTING TECHNIQUES

The question of specimen design arises again when compressive impact testing of composite materials is considered. The standard design of specimen for use with the compression Hopkinson-bar is a short cylinder of diameter slightly less than that of the loading bars. Most of the work on composite materials in the compression SHPB [11,12] has in fact used this design of specimen even though it is far from ideal for this type of material. In tests on a woven glass/epoxy laminate loaded in a principal reinforcing direction for specimens with different length to diameter ratio Parry [13] showed a significant increase in the ultimate compressive strength under impact loading, see fig. 6a. In the quasi-static tests failure was by a combination of

shear and longitudinal splitting, see fig. 6b, with the possibility that failure was initiated at the ends of the specimen. In the impact tests the specimens completely disintegrated preventing any conclusions from being drawn.

Some evidence that the initiation of compressive failure in woven glass/epoxy composites, at both quasi-static and impact rates, was by a shearing process was obtained in tests on cylindrical specimens reinforced with a single woven glass ply on a diametral plane [14]. The first sign of damage was a sudden drop in load on the stress-strain curve, see fig. 7a, corresponding to a shear failure across the axially-aligned fibre tow near the centre of the specimen, see fig. 7b. Nevertheless doubts clearly remain regarding the validity of data obtained using this design of specimen in the Hopkinson bar test.

However, since the specimen will only be subjected to transient loading, provided the loading bars are well aligned there is no reason why the waisted thin-strip tensile specimen of fig. 1b should not also be used in compression. It is close to the design recommended for the quasi-static compression testing of unidirectional carbon/epoxy specimens [15] and has the major advantage that failure is unlikely to be initiated by end effects at the specimen/loading bar interfaces.

Using this specimen design very marked increases in the compressive strength and the strain to failure under impact loading have been found [16] for both woven carbon and woven glass/epoxy specimens loaded in a principal reinforcing direction, see fig. 8. Failure initiates by shear across the central parallel region of the specimen on a plane inclined at ~45° to both the loading and the thickness directions, see fig. 9 for the glass/epoxy specimen. The damage zone is more extensive in the impacted specimens, corresponding to the much greater strain to failure.

III. DISCUSSION

Although considerable data are now becoming available on the impact mechanical response of fibre-reinforced composites, most of which show that there are quite significant effects which need to be taken into account, no clear picture is yet

emerging on which to base a general approach, e.g. the development of some form of "constitutive relationship", which might be used to describe this behaviour. This may be for many reasons but perhaps primarily because the deformation of fibre reinforced polymers is essentially a damage accumulation process involving a large number of different possible damage mechanisms. The testing techniques described above make some attempt to isolate and study some of these mechanisms. In other cases, e.g. in compression, the complex interaction between the fibres and the matrix make a detailed interpretation of the test data extremely difficult.

An attempt has been made [17] to apply finite element methods to the modelling of the tensile impact response of hybrid woven carbon/glass/epoxy laminates. Failure is assumed to initiate at an arbitrarily chosen site by the tensile fracture of an axially-aligned carbon tow and to be followed by limited delamination on adjacent interlaminar planes. The results obtained showed qualitative agreement with experiment but the technique cannot yet give a quantitative prediction of the hybrid impact behaviour.

IV. CONCLUSIONS

Testing techniques have been developed for studying the impact response of fibre-reinforced composites and for obtaining reliable data on their mechanical behaviour at high rates of strain. Care is required, however, in evaluating the data obtained if true "material properties" are to be derived and more work is needed if particular damage processes are to be isolated and their individual rate dependence determined.

V. ACKNOWLEDGMENT

Grateful acknowledgment is made to the Air Force Office of Scientific Research (AFSC), United States Air Force, from whom financial support was received, under Grant No. AFOSR-87-0129, during which much of the work reviewed above was performed.

REFERENCES

1. J. Harding and L. M. Welsh, in Proc ICCM IV, Fourth Int. Conf. on Composite Materials, Japan Soc. for Composite Materials, Tokyo, 1982, 845-852.
2. J. Harding, K. Saka and M. E. C. Taylor, Oxford University Engineering Laboratory Report No. 1654/1986
3. J. Harding and L. M. Welsh, J. Mater. Sci., 18, 1810-1826 (1983).
4. A. Rotem and J. M. Lifshitz, in Proc. 26th. Annual Tech. Conf. SPI, Reinforced Plastics/Composites Division, Society of Plastics Industry, New York, 1971, paper 10-G
5. L. M. Welsh and J. Harding, in Proc ICCM V, Fifth Int. Conf. on Composite Materials, TMS-AIME, 1985, 1517-1531.
6. L. M. Welsh and J. Harding, in Proc DYMAT 85, Mechanical and Physical Behaviour of Materials under Dynamic Loading, Jour. de Physique, Colloque C5, 1985, 405-414.
7. T. Parry and J. Harding, Colloque Int. du CNRS No. 319, Plastic Behaviour of Anistropic Solids, CNRS, Paris 1988, 271-288.
8. C. Y. Chiem and Z. G. Liu, in Proc IMPACT 87, Impact Loading and Dynamic Behaviour of Materials, DGM Informationsgesellschafft mbH, Oberursel, 1988, 2, 579-586.
9. S. M. Werner and C. K. H. Dharan, J. Comp. Mater., 20, 365-374 (1986)
10. J. Harding, Y. L. Li, K. Saka and M. E. C. Taylor, in Proc. 4th. Oxford Int. Conf. on Mech. Properties of materials at High Rates of Strain, Inst. of Phys. Conf. Series No. 102, Inst. of Physics, London and Bristol, 1989, 403-410.
11. L. J. Griffiths and D. J. Martin, J. Phys. D. Appl. Phys., 7, 2329-2341 (1974)
12. R. L. Sierakowski, G. E. Nevill, C. A. Ross and E. R. Jones, J. Comp. Mater., 5, 362-377 (1971)
13. T. Parry, Oxford University Engineering Laboratory (unpublished work)
14. Y. Bai and J. Harding, in Proc. Int. Conf. on Structural Impact and Crashworthiness, Elsevier Applied Science, London and New York, 1984, 2, 482-493
15. P. D. Ewins, RAE Technical Report No. 71217, 1971.
16. S. Shah, R. K. Y. Li and J. Harding, Oxford University Engineering Laboratory Report No. OUEL 1730/1988.
17. Y. L. Li, C. Ruiz and J. Harding, to appear in Composites Science and Technology.

Fig. 1 Tensile version of split Hopkinson bar (a) general assembly (schematic) (b) specimen design (dimensions in mm)

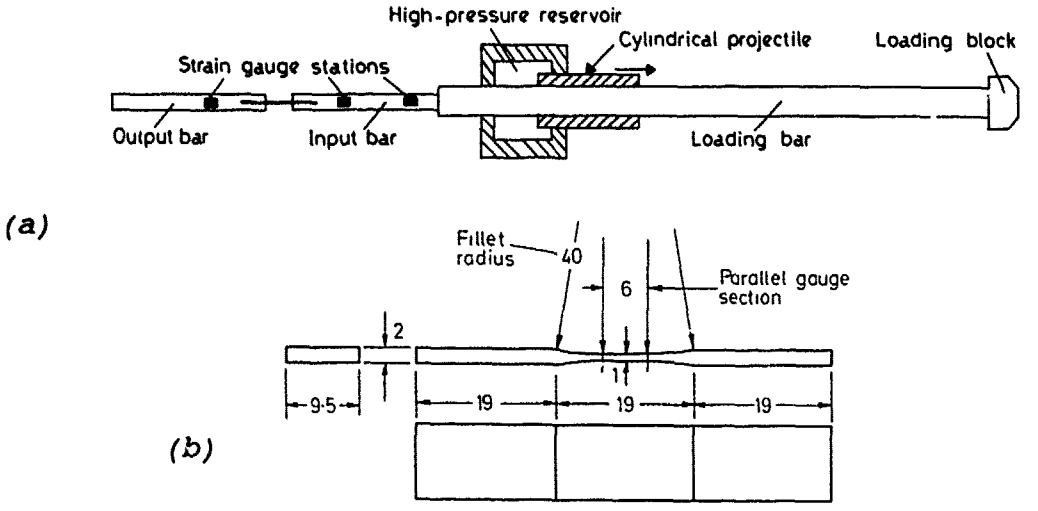

Fig. 2 Effect of strain rate on tensile stress-strain curves for composite materials

(a) unidirectional carbon/epoxy
[mean strain rate (/s): a) - 0.0001; b) - 10; c) - 450;]

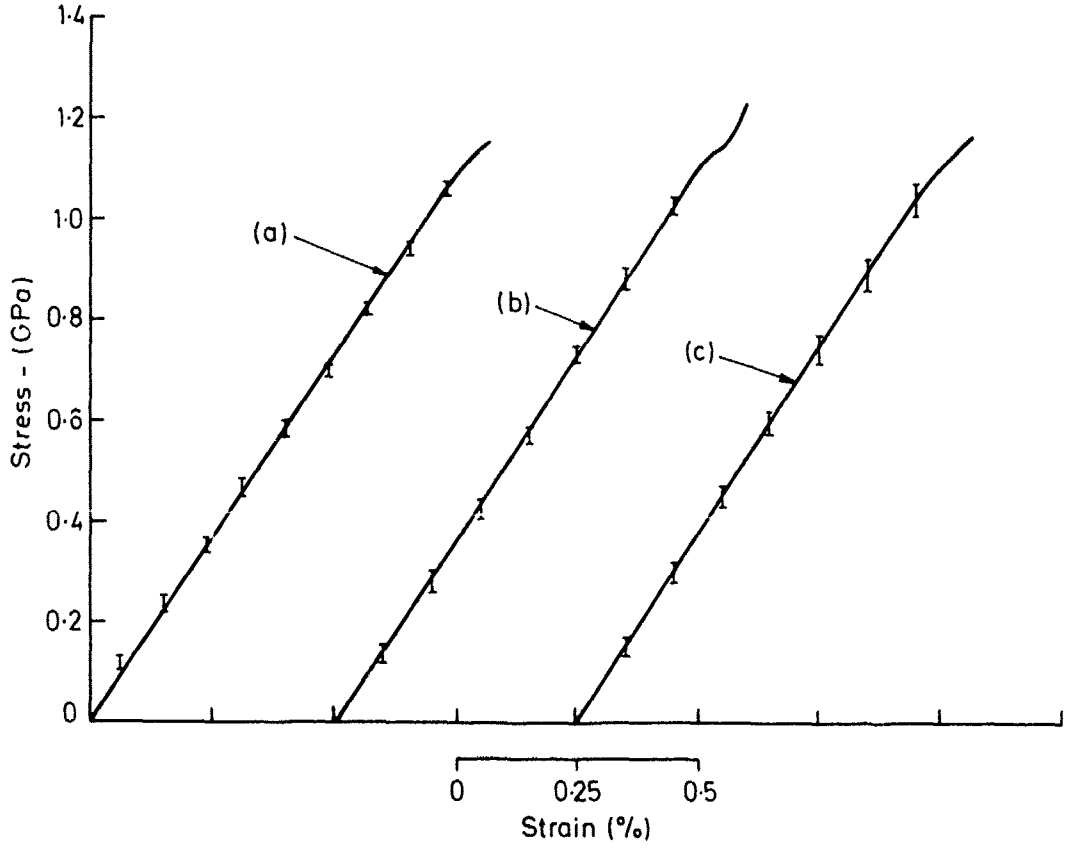

(b) woven carbon/epoxy

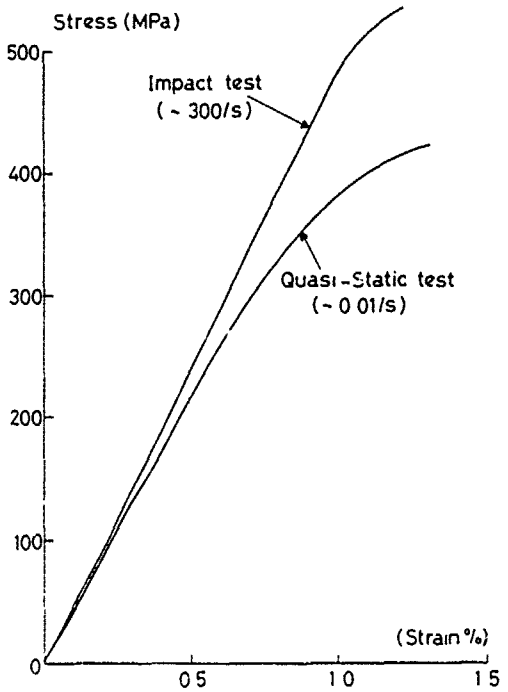

(c) woven glass/epoxy
[mean strain rate (/s): a) - 0.0001; b) - 10; (c) - 900;]

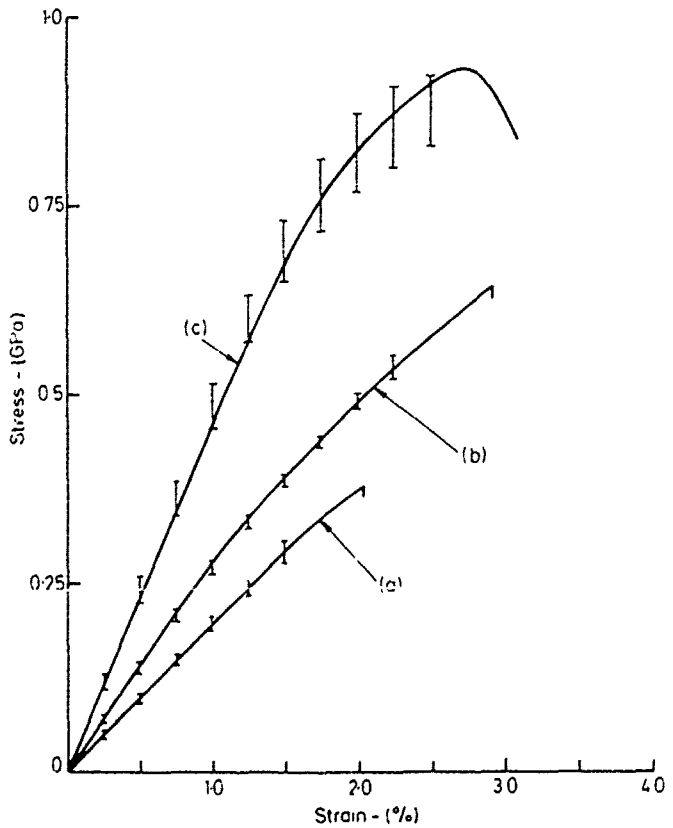

b) Fine-weave glass/epoxy specimens
mean strain rate (sec^{-1}): (a) - 10^{-4}; (b) - 10; (c) - 900)

Fig. 8 Effect of strain rate on the compressive stress-strain curves for thin strip specimens of (a) woven carbon/epoxy and (b) woven glass/epoxy

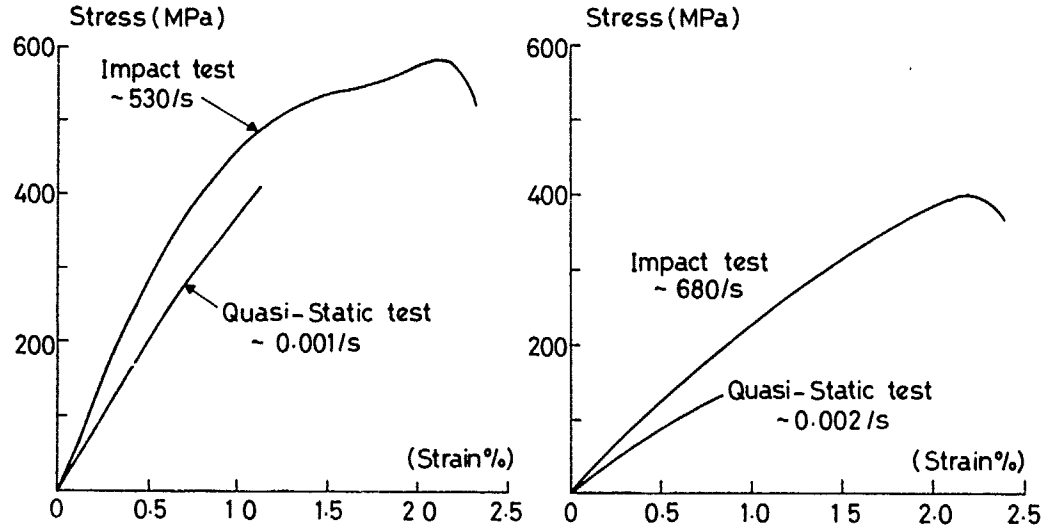

(a) *(b)*

Fig. 9 Effect of strain rate on compressive failure mode in thin strips specimens of woven glass/epoxy under (a) quasi-static and (b) impact loading

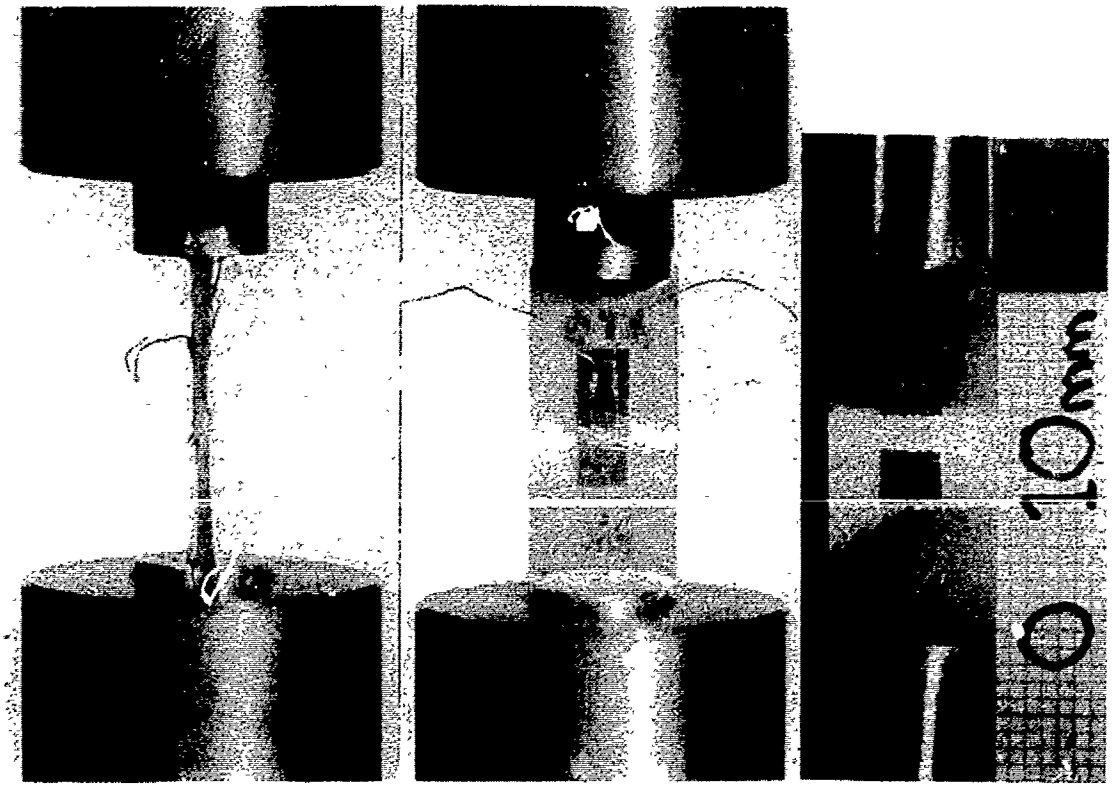

(a) *(b)*